5-2014

Structure and Multi-Center Bonding: From Atomic Clusters to Solid Phase Materials

Timur R. Galeev
Utah State University

STRUCTURE AND MULTI-CENTER BONDING: FROM ATOMIC CLUSTERS TO SOLID PHASE MATERIALS

by

Timur R. Galeev

A dissertation submitted in partial fulfillment
of the requirements for the degree

of

DOCTOR OF PHILOSOPHY

in

Chemistry

Approved:

_____	_____
Alexander I. Boldyrev Major Professor	D. Mark Riffe Committee Member
_____	_____
Lisa M. Berreau Committee Member	Steve Scheiner Committee Member
_____	_____
David Farrelly Committee Member	Mark R. McLellan Vice President for Research and Dean of the School of Graduate Studies

UTAH STATE UNIVERSITY
Logan, Utah

2014

ABSTRACT

Structure and Multi-Center Bonding: From Atomic Clusters

to Solid Phase Materials

by

Timur R. Galeev, Doctor of Philosophy

Utah State University, 2014

Major Professor: Dr. Alexander I. Boldyrev
Department: Chemistry and Biochemistry

The work presented in this dissertation has been focused on structure, stability, electronic properties, and chemical bonding of atomic clusters and solid-state compounds. The common thread was development of chemically intuitive models and theoretical methods capable of describing and interpreting bonding and hence, structures of these compounds. Understanding how interactions between atoms in sub-nano clusters and solid-state compounds of certain compositions determine their structures, physical properties, and reactivities is essential for rational design of new materials, catalysts, and molecular devices. A significant part of this work presents joint experimental and theoretical studies of doped boron clusters. Several projects on carbon- and aluminum-substituted boron clusters were aimed at establishing their structures, energetic and electronic properties, and understanding bonding interactions. The dissertation introduces a series of peculiar clusters containing transition metal atoms inside perfectly

symmetrical boron rings. These clusters, featuring planar octa-, nona-, and decacoordinated transition metal atoms, were designed based on a simple chemical bonding model governing stabilities of such species. One of the most important parts of this dissertation deals with chemical bonding in the solid state. The Adaptive Natural Density Partitioning method previously developed by the Boldyrev group at Utah State University has proven very efficient for understanding chemical bonding in clusters and complex molecules. In this work, a periodic implementation of this method has been developed, yielding a new theoretical tool capable of interpretation of bonding in solid state in chemically intuitive terms of localized and multi-center bonds.

(431 pages)

PUBLIC ABSTRACT

Structure and Multi-Center Bonding: From Atomic Clusters

to Solid Phase Materials

by

Timur R. Galeev, Doctor of Philosophy

Utah State University, 2014

Major Professor: Dr. Alexander I. Boldyrev
Department: Chemistry and Biochemistry

The work presented in this dissertation has been focused on structure, stability, and chemical bonding of atomic clusters and solid-state compounds. The common thread was development of theoretical models and methods capable of interpreting bonding and hence, structures of these species. A major part of this work presents joint experimental and theoretical studies of a large series of doped boron clusters. The dissertation introduces a new theoretical tool for interpretation of bonding of solid phase materials in chemically intuitive terms of localized and multi-center bonds. Understanding how interactions between atoms in sub-nano clusters and solid-state compounds determine their structures, physical properties, and reactivities is essential for rational design of new materials, catalysts, and molecular devices.

(431 pages)

ACKNOWLEDGMENTS

First of all, I would like to express my sincere gratitude to my Ph.D. advisor, Prof. Alexander I. Boldyrev, for all I have learned from him throughout my four years at Utah State University. He helped me to master the methodology of scientific research, to develop my skills in theoretical chemistry, and has always been very helpful and supportive, all of which were indespensable for my progress and professional growth.

I would like to thank all of our collaborators who contributed to the manuscripts included in this dissertation, especially, Prof. Lai-Sheng Wang (Brown University) and Prof. JR Schmidt (University of Wisconsin-Madison), as well as their group members. Much of the work presented here was only possible due to their invaluable contributions.

I thank all of the members of my supervisory committee: Prof. Lisa M. Berreau, Prof. David Farrelly, Prof. D. Mark Riffe, and Prof. Steve Scheiner. I appreciate their support, encouragement and openness for questions and discussion.

Most importantly, I want to thank my family, the source of who I am: my parents, younger sister, grandparents, and uncle for … everything (with their support during the last four years being an important part of 'everything'). They, with contributions from friends and teachers, shaped the person I am today. There is just no way to give sufficient thanks to them…

During the four years at Utah State University, I have been supported by the National Science Foundation (CHE-1057746 grant to Prof. Alexander I. Boldyrev), Vice President for Research Graduate Fellowship (Utah State University), School of Graduate Studies Dissertation Fellowship (Office of Research and Graduate Studies, Utah State

University), and Teaching Assistanships (Department of Chemistry and Biochemistry, Utah State University).

Compute, storage, and other resources from the Division of Research Computing in the Office of Research and Graduate Studies at Utah State University as well as an allocation of computer time from the Center for High Performance Computing at the University of Utah are gratefully acknowledged.

Timur R. Galeev

CONTENTS

LIST OF TABLES

LIST OF FIGURES

CHAPTER 1

INTRODUCTION AND PRIOR WORK

1-1. Atomic Clusters

Atomic clusters – groups or aggregates of atoms, which may consist of as few as two atoms to as many as thousands of atoms – are sometimes called an intermediate form of matter[1] or a bridge between isolated molecules and bulk materials.[2] Cluster science, a relatively new discipline at the interface of chemistry, physics, materials science, biology and atmospheric science,[1,3–5] provides insight into the early stages of growth of matter and on evolution of properties towards the bulk. In general, cluster structures and properties evolve very nonmonotonically with size,[6] so that addition of an atom or an electron may lead to completely new bonding and often unpredictable structures. Clusters may serve as building blocks of solid state materials or ligands in complex compounds.[7,8] Development of bonding models capable of explaining and predicting cluster structures and properties based on their composition is a considerable challenge,[2] which could allow rational design of new compounds, materials, and catalysts.

The major difficulty with studying atomic clusters is due to the fact they are metastable and cannot be isolated and characterized at ambient conditions. Although, experimentally, clusters can be produced in the gas phase as molecular beam, little (Chapter 11, for example, provides an explanation how certain structural and bonding features, such as high symmetry and stability of clusters can be recognized from their photoelectron spectra) or no structural information can be obtained solely from available experimental techniques. Current theoretical quantum chemistry approaches can provide

very accurate information on structures and properties of atomic clusters. Joint theoretical and experimental studies have been critical in the development of cluster science.[1,9]

Most of the cluster projects (Chapters 2–11) of this dissertation were performed in collaboration with experimentalists: Prof. Lai-Sheng Wang's group at Brown University. Experimentally, the clusters were obtained and their photoelectron spectra were recorded using a magnetic-bottle photoelectron spectroscopy apparatus equipped with a laser vaporization cluster source.[10] Theoretical studies usually involved several steps. First, for a given stoichiometrical composition, global minimum structure and low-lying isomers were established using the Coalescence Kick program written by Dr. Boris B. Averkiev[11,12] coupled with *ab initio* calculations. Then, theoretical vertical detachment energies were calculated for the lowest-energy structures and compared with the experimentally observed PES peaks in order to confirm the proposed global minima. Finally, chemical bonding analyses were performed to understand cluster geometries, stabilities and electronic properties. Adaptive Natural Density Partitioning (AdNDP)[13,14] method developed by Dr. Dmitry Yu. Zubarev and Prof. Alexander I. Boldyrev has proven a very powerful and indispensable tool for interpreting chemical bonding in clusters. In AdNDP terms, chemical bonding in clusters is usually represented as a set of localized (lone pairs and 2-center – 2-electron, 2c-2e, bonds) and delocalized (multi-center) bonds and often described involving the concepts of aromaticity, antiaromaticity, or conflicting aromaticity.[9,15–20]

1-1.1. Carbon-doped boron clusters

Small carbon-boron mixed clusters of different stoichiometries have been studied quite extensively.[21–28] In particular, some of these works proposed viability of hypercoordinate carbon atoms centered in boron rings: carbon-doped boron clusters containing pentacoordinate,[23] hexacoordinate,[22,25] heptacoordinate,[25] and even octacoordinate[24] carbon were found to be minima on the potential energy surfaces. More recent *ab initio* and photoelectron spectroscopy studies showed, however, that structures with the carbon atoms occupying a peripheral rather than the central positions are significantly more stable.[26,29] A planar-to-linear structural transition has been found in the $C_xB_{5-x}^-$ (x = 1–5) series: boron-rich members of the series were shown to be planar, whereas, the carbon rich clusters are linear.

A similar, synergetic theoretical and photoelectron spectroscopy, approach has been utilized to investigate structural transformations in two other mixed carbon-boron cluster series. Chapter 2 reports an observation of a new type of structural transition, a wheel-to-ring transition in the $C_xB_{8-x}^-$ series. In Chapter 3, structural changes caused by substitution of one and two boron atoms in B_{10}^- by carbon atoms are investigated. The chapters provide a detailed interpretation of photoelectron spectra and the global minimum geometries established for all of the studied carbon-boron mixed clusters.

1-1.2. Aluminum-doped boron clusters

Chapter 4 reports unusual umbrella-like structures established for the AlB_7^- and AlB_8^- global minimum isomers. It is shown that in these clusters, Al cations are ionically bound to negatively charged doubly (σ and π) aromatic B_7 and B_8 fragments. Structures

and bonding of two other clusters, AlB_9^- and AlB_{10}^-, are discussed in Chapter 5. Prior studies of aluminum-doped boron clusters include combined theoretical and experimental studies of the $Al_nB_m^-$ (m+n=3–8, m=1–2)[30] and $Al_{n-m}B_m^-$ ($n \geqslant 5$ for m=1, $n \geqslant 10$ for m=2)[31] series, the AlB_6^- and AlB_{11}^- clusters,[32] and several theoretical works.[33–36] Two of the latter studies[34,35] proposed hypercoordinate aluminum atom in the neutral D_{9h} AlB_9 cluster. Chapter 5 explains why addition of an electron to this cluster leads to significant destabiliziation of the wheel-type isomer in the anionic AlB_9^- cluster.

1-1.3. Transition metal-centered boron sub-nano wheels, M©B_n^{q-}

The quest for anionic clusters containing hypercoordinate main-group elements enclosed in planar boron rings (including some of the works of carbon- and aluminum-doped boron clusters mentioned in Sections 1-1.1 and 1-1.2) was inspired by an unprecedented structure of the B_9^- cluster: the cluster is a planar highly-symmetric molecular wheel with an octacoordinate boron atom in its center.[37] After it was realized that the main group elements are not favorable candidates to form D_{nh} wheel-type structures, a number of transition metal-containing boron wheels were probed theoretically,[38–41] including closed-shell CoB_8^- (D_{8h}), FeB_8^{2-} (D_{8h}), and FeB_9^- (D_{9h}) clusters, which were predicted[38,40] to be the lowest-energy isomers on their potential energy surfaces.

We have performed a large series of joint photoelectron spectroscopy and theoretical studies of transition metal-centered boron wheels, M©B_n^{q-}. Chapter 6 reports the first experimental observation of two such wheels. By comparison of the experimental photoelectron spectroscopic features with theoretically calculated vertical

detachment energies for the wheel-type isomer of CoB_8^-, it was confirmed that the perfectly symmetric $Co©B_8^-$ wheel is indeed the global minimum isomer (the © sign was introduced to denote a hypercoordinate atom centered in a planar ring). Another wheel-type cluster, $Ru©B_9^-$, was newly introduced. Based on chemical bonding analyses of the two clusters, Chapter 6 proposes the so called 'electronic fit' principle – a simple electron-counting rule governing stabilities and enabling rational design of $M©B_n^{q-}$. Chapters 7 – 10 report other transition metal-centered boron wheels, including $Nb©B_{10}^-$ and $Ta©B_{10}^-$ (Chapter 8), where Nb and Ta have the highest coordination number known for planar structures. Chapter 11 overviews this new class of borometallic compounds.

1-1.4. Structural studies of the $C_xH_xP_{6-x}$ (x = 0-6) species

The P_6 cluster is valence isoelectronic with benzene and its global minimum isomer is known[42] to have a benzvalene-like structure. Benzvalene is a relatively high-energy[43] isomer of benzene. The planar D_{6h} isomer of P_6 is unstable towards out-of-plane distortion, which is caused by the pseudo Jahn-Teller effect.[44,45] Chapter 12 represents a systematic computational study of the $C_xH_xP_{6-x}$ (x = 0-6) series, aimed to trace the effect of isolobal substituion both on structural (non-planar benzvalene-like to planar benzene-like) transitions of global minima and on the suppression of the pseudo Jahn-Teller effect responsible for the distortion of the cyclic isomers along the series.

1-2. Localized and multi-center bonding: from clusters to solids

Bonding between atoms in isolated molecules, ions, clusters or bulk materials determines their structures and properties. The concepts and theories developed by physicists and chemists to rationalize chemical bonding and electronic structure often

remained within the discipline where they originated.[46] Solid state physics usually involves the language of maximally delocalized bands, whereas the chemists' perception is often local.[47–49] The former approach is widely used in materials science owing to its wide applicability and capability to interpret physical properties. The latter approach can contribute intuitive chemical knowledge gained from empirical experience,[47–49] indispensable for understanding reactivities of solid state compounds and surfaces and for rational design and synthesis of new materials.

The Lewis model,[50] albeit widely used and taught in chemistry to describe covalent bonding in molecules (and applicable to some covalent network crystals, such as diamond or quartz), often cannot satisfactorily describe delocalized bonding, such as interactions in non-stoichiometric clusters and a multitude of solid state compounds. The AdNDP[13,14] scheme utilizes Lewis' concept of electron pair as the primary element of a chemical bond, but involves not only Lewis lone pairs (1c-2e) and bonds (2c-2e), but also multi-center bonding elements. This generalization yielding *n*c-2e bonds (with *n* ranging from one to the total number of atoms in the species) has proven instrumental for the method's significantly wider applicability to molecular[51–53] and cluster[29,51,54,55] species.

The remaining part of this dissertation deals with bonding in periodic structures. Our study of chemical bonding in all-boron α-sheet using cluster models shows importance of multi-center bonding for rationalization of its structure. Finally, we developed a periodic implementation of the AdNDP method – Solid State AdNDP – a new theoretical tool to elucidate chemical bonding in bulk solids, surfaces and nanostructures.

1-2.1. Chemical bonding in all-boron α-sheet

A number of structures for one atom thick boron sheets and boron nanotubes have been proposed theoretically.[56–61] The most stable planar structure, the so-called all-boron α-sheet,[61–63] contains triagonal and hexagonal motifs – symmetrically arranged filled and vacant hexagons. Chapter 13 investigates chemical bonding in α-sheet and explains its peculiar structure by applying the AdNDP method to fragments (cluster models) of the periodic structure.

1-2.2. Development of the Solid State Adaptive Natural Density Partitioning method

AdNDP[14] is an extension of Natural Bond Orbital (NBO) analysis.[64–67] NBO provides Lewis-like representation of chemical bonding based on an underlying electronic structure calculation. AdNDP generalizes this approach to multi-center bonding operating with *n*c-2e bonding elements, with *n* ranging from 1 to the total number of atoms in a system. A periodic implementation of the NBO analysis was recently developed by Dunnington and Schmidt.[68] Chapter 14 describes extension of AdNDP to structures with translational symmetry yielding Solid State Adaptive Natural Density Partitioning (SSAdNDP) and its application to all-boron α-sheet, magnesium diboride, and the Na_8BaSn_6 Zintl phase.

References

(1) Castleman, A. W.; Jena, P. *Proc. Natl. Acad. Sci.* **2006**, *103*, 10552–10553.

(2) Alonso, J. A. *Structure and Properties of Atomic Nanoclusters*; Imperial College Press: London, 2012.

(3) Jena, P.; Castleman, A. W. *Nanoclusters: A Bridge Across Disciplines*; Science and technology of atomic, molecular, condensed matter & biological systems; Elsevier: Oxford, 2010.

(4) Castleman, A. W.; Jena, P. *Proc. Natl. Acad. Sci.* **2006**, *103*, 10554–10559.

(5) Jena, P.; Castleman, A. W. *Proc. Natl. Acad. Sci.* **2006**, *103*, 10560–10569.

(6) Jena, P.; Khanna, S.; Rao, B. K. *Physics and Chemistry of Finite Systems: From Clusters to Crystals*; Kluwer Academic Publishers: Dordreght, 1992; Vol. 1.

(7) Alexandrova, A. N.; Boldyrev, A. I.; Zhai, H. J.; Wang, L. S. *Coord. Chem. Rev.* **2006**, *250*, 2811–2866.

(8) Fokwa, B. P. T.; Hermus, M. *Angew. Chem. Int. Ed.*, **2012**, *51*, 1702–1705.

(9) Boldyrev, A. I.; Wang, L.-S. *Chem. Rev.* **2005**, *105*, 3716–3757.

(10) Wang, L.-S.; Cheng, H.-S.; Fan, J. *J. Chem. Phys.* **1995**, *102*, 9480–9493.

(11) Averkiev, B. B. Geometry and Electronic Structure of Doped Clusters via the Coalescence Kick Method. PhD Dissertation, Utah State University, Logan, UT, 2009.

(12) Sergeeva, A. P.; Averkiev, B. B.; Zhai, H.-J.; Boldyrev, A. I.; Wang, L. S. *J. Chem. Phys.* **2011**, *134*, 224304–224304.

(13) Zubarev D. Yu. Analysis of Chemical Bonding in Clusters by Means of The Adaptive Natural Density Partitioning. PhD Dissertation, Utah State University: Logan, UT, 2008.

(14) Zubarev, D. Y.; Boldyrev, A. I. *Phys. Chem. Chem. Phys.* **2008**, *10*, 5207–5217.

(15) Li, X.; Kuznetsov, A. E.; Zhang, H.-F.; Boldyrev, A. I.; Wang, L.-S. *Science* **2001**, *291*, 859–861.

(16) Kuznetsov, A. E.; Birch, K. A.; Boldyrev, A. I.; Li, X.; Zhai, H.-J.; Wang, L.-S. *Science* **2003**, *300*, 622–625.

(17) Zubarev, D. Y.; Averkiev, B. B.; Zhai, H.-J.; Wang, L.-S.; Boldyrev, A. I. *Phys. Chem. Chem. Phys.* **2007**, *10*, 257–267.

(18) Sergeeva, A. P.; Averkiev, B. B.; Boldyrev, A. I. All-Transition Metal Aromaticity and Antiaromaticity. In *Metal-Metal Bonding*; Parkin, G., Ed.; Structure and Bonding; Springer: Berlin Heidelberg, 2010; Vol. 136, pp. 275–305.

(19) Galeev, T. R.; Boldyrev, A. I. *Annu. Rep. Sect. C Phys. Chem.* **2011**, *107*, 124–147.

(20) Galeev, T. R.; Boldyrev, A. I. Aromaticity and Antiaromaticity in Inorganic Chemistry. In *Comprehensive Inorganic Chemistry II (Second Edition)*; Reedijk, J.; Poeppelmeier, K., Eds.; Elsevier: Amsterdam, 2013; pp. 245–275.

(21) Shao, J.; He, C.; Shi, R.; Wang, C.; Zhu, X.; Lu, X. *J. Mol. Struct. THEOCHEM* **2010**, *961*, 17–28 and references cited therein.

(22) Exner, K.; Schleyer, P. v. R. *Science* **2000**, *290*, 1937–1940.

(23) Wang, Z.-X.; Schleyer, P. v. R. *Science* **2001**, *292*, 2465–2469.

(24) Minyaev, R. M.; Gribanova, T. N.; Starikov, A. G.; Minkin, V. I. *Mendeleev Commun.* **2001**, *11*, 213–214.

(25) Islas, R.; Heine, T.; Ito, K.; Schleyer, P. v. R.; Merino, G. *J. Am. Chem. Soc.* **2007**, *129*, 14767–14774.

(26) Wang, L.-M.; Huang, W.; Averkiev, B. B.; Boldyrev, A. I.; Wang, L.-S. *Angew. Chem. Int. Ed.* **2007**, *46*, 4550–4553.

(27) Averkiev, B. B.; Wang, L.-M.; Huang, W.; Wang, L. S.; Boldyrev, A. I. *Phys. Chem. Chem. Phys.* **2009**, *11*, 9840–9849.

(28) Wang, L.-M.; Averkiev, B. B.; Ramilowski, J. A.; Huang, W.; Wang, L. S.; Boldyrev, A. I. *J. Am. Chem. Soc.* **2010**, *132*, 14104–14112.

(29) Averkiev, B. B.; Wang, L.-M.; Huang, W.; Wang, L.-S.; Boldyrev, A. I. *Phys. Chem. Chem. Phys.* **2009**, *11*, 9840.

(30) Jiang, Z.-Y.; Luo, X.-M.; Li, S.-T.; Chu, S.-Y. *Int. J. Mass Spectrom.* **2006**, *252*, 197–203.

(31) Kawamata, H.; Negishi, Y.; Nakajima, A.; Kaya, K. *Chem. Phys. Lett.* **2001**, *337*, 255–262.

(32) Romanescu, C.; Sergeeva, A. P.; Li, W.-L.; Boldyrev, A. I.; Wang, L. S. *J. Am. Chem. Soc.* **2011**, *133*, 8646–8653.

(33) Feng, X.-J.; Luo, Y.-H. *J. Phys. Chem. A* **2007**, *111*, 2420–2425.

(34) Averkiev, B. B.; Boldyrev, A. I. *Russ. J. Gen. Chem.* **2008**, *78*, 769–773.

(35) Guo, J.; Yao, W.; Li, Z.; Li, S. *Sci. China Ser. B Chem.* **2009**, *52*, 566–570.

(36) Böyükata, M.; Güvenç, Z. B. *J. Alloys Compd.* **2011**, *509*, 4214–4234.

(37) Zhai, H.-J.; Alexandrova, A. N.; Birch, K. A.; Boldyrev, A. I.; Wang, L.-S. *Angew. Chem. Int. Ed.* **2003**, *42*, 6004–6008.

(38) Ito, K.; Pu, Z.; Li, Q.-S.; Schleyer, P. von R. *Inorg. Chem.* **2008**, *47*, 10906–10910.

(39) Luo, Q. *Sci. China Ser. B Chem.* **2008**, *51*, 607–613.

(40) Pu, Z.; Ito, K.; Schleyer, P. v. R.; Li, Q.-S. *Inorg. Chem.* **2009**, *48*, 10679–10686.

(41) Miao, C.; Guo, J.; Li, S. *Sci. China Ser. B Chem.* **2009**, *52*, 900–904.

(42) Hiberty, P. C.; Volatron, F. *Heteroat. Chem.* **2007**, *18*, 129–134.

(43) Dinadayalane, T. C.; Priyakumar, U. D.; Sastry, G. N. *J. Phys. Chem. A* **2004**, *108*, 11433–11448.

(44) Pearson, R. G. *Proc. Natl. Acad. Sci.* **1975**, *72*, 2104–2106.

(45) Bersuker, I. B. *Chem. Rev.* **2001**, *101*, 1067–1114.

(46) Burdett, J. K. *Chemical Bonding in Solids (Topics in Inorganic Chemistry)*; Oxford University Press: New York, 1995.

(47) Hoffmann, R. *Angew. Chem. Int. Ed. Engl.* **1987**, *26*, 846–878.

(48) Hoffmann, R. *Rev. Mod. Phys.* **1988**, *60*, 601–628.

(49) Hoffmann, R. *Solids and Surfaces: A Chemist's View of Bonding in Extended Structures*; Wiley-VCH: New York, 1989.

(50) Lewis, G. N. *J. Am. Chem. Soc.* **1916**, *38*, 762–785.

(51) Zubarev, D. Y.; Boldyrev, A. I. *J. Org. Chem.* **2008**, *73*, 9251–9258.

(52) Sergeeva, A. P.; Boldyrev, A. I. *Phys. Chem. Chem. Phys.* **2010**, *12*, 12050–12054.

(53) Sergeeva, A. P.; Boldyrev, A. I. *Comments Inorg. Chem.* **2010**, *31*, 2–12.

(54) Sergeeva, A. P.; Zubarev, D. Y.; Zhai, H. J.; Boldyrev, A. I.; Wang, L. S. *J. Am. Chem. Soc.* **2008**, *130*, 7244–7246.

(55) Zubarev, D. Y.; Boldyrev, A. I. *J. Phys. Chem. A* **2009**, *113*, 866–868.

(56) Boustani, I.; Quandt, A.; Hernández, E.; Rubio, A. *J. Chem. Phys.* **1999**, *110*, 3176.

(57) Evans, M. H.; Joannopoulos, J. D.; Pantelides, S. T. *Phys. Rev. B* **2005**, *72*, 045434.

(58) Kunstmann, J.; Quandt, A. *Phys. Rev. B* **2006**, *74*, 035413.

(59) Lau, K. C.; Pandey, R. *J. Phys. Chem. C* **2007**, *111*, 2906–2912.

(60) Tang, H.; Ismail-Beigi, S. *Phys. Rev. Lett.* **2007**, *99*, 115501.

(61) Yang, X.; Ding, Y.; Ni, J. *Phys. Rev. B* **2008**, *77*, 041402.

(62) Tang, H.; Ismail-Beigi, S. *Phys. Rev. Lett.* **2007**, *99*, 115501.

(63) Tang, H.; Ismail-Beigi, S. *Phys. Rev. B* **2009**, *80*, 134113.

(64) Foster, J. P.; Weinhold, F. *J. Am. Chem. Soc.* **1980**, *102*, 7211–7218.

(65) Reed, A. E.; Weinhold, F. *J. Chem. Phys.* **1985**, *83*, 1736–1740.

(66) Reed, A. E.; Curtiss, L. A.; Weinhold, F. *Chem. Rev.* **1988**, *88*, 899–926.

(67) Weinhold, F.; Landis, C. R. *Valency and Bonding: A Natural Bond Orbital Donor-Acceptor Perspective*; Cambridge University Press: Cambridge, UK, 2005.

(68) Dunnington, B. D.; Schmidt, J. R. *J. Chem. Theory Comput.* **2012**, *8*, 1902–1911.

CHAPTER 2

MOLECULAR WHEEL TO MONOCYCLIC RING TRANSITION IN BORON–CARBON MIXED CLUSTERS $C_2B_6^-$ AND $C_3B_5^-$ *

Abstract

In this joint experimental and theoretical work we present a novel type of structural transition occurring in the series of $C_xB_{8-x}^-$ (x = 1–8) mixed clusters upon increase of the carbon content from x = 2 to x = 3. The wheel-to-ring transition is surprising because it is rather planar-to-linear type of transition to be expected in the series since B_8, B_8^-, B_8^{2-} and CB_7^- are known to possess wheel-type global minimum structures while C_8 is linear.

Carbon and boron being neighbors in the Periodic Table have very different geometric structures of their small clusters. Small carbon clusters are either linear or cyclic,[1] whereas, those of boron are either planar or quasi-planar.[2] Thus, one can expect peculiar transitions from planar to linear structures upon increasing the number of carbon atoms in mixed boron-carbon clusters. An example of such planar-to-linear structural transition as a function of the number of carbon atoms has been found to occur in the mixed boron-carbon clusters, $C_xB_{5-x}^-$ (x = 1–5) between x = 2 and 3.[3] Larger boron-carbon mixed clusters have been computationally proposed to exemplify unusual hexa-, hepta and octa-coordinated planar carbon species (CB_6^{2-},[4] CB_7^-,[5] and CB_8[6]).

* Coauthored by Timur R. Galeev, Alexander S. Ivanov, Constantin Romanescu, Wei-Li Li, Konstantin V. Bozhenko, Lai-Sheng Wang, and Alexander I. Boldyrev. Reproduced from *Phys. Chem. Chem. Phys*. **2011**, *13*, 8805-8810 with permission from the PCCP Owner Societies.

However, it was shown later in joint experimental and theoretical works[7–9] that carbon avoids the central position in those wheel-type global minimum geometries and occupies the peripheral position instead. It is known that the B_8, B_8^- and B_8^{2-} clusters[10–14] and the CB_7^- cluster[8] have wheel-type heptagon structures with one boron atom in the center. The C_8 cluster has a linear global minimum structure with the cyclic isomer being about 10 kcal mol^{-1} higher.[1,15,16] Therefore, a planar-to-linear transition could be expected in the $C_xB_{8-x}^-$ (x = 1–8) series upon increasing the carbon content in the clusters. Surprisingly, we found a novel structural transition that has never been observed before – wheel-to-ring transition between $C_2B_6^-$ and $C_3B_5^-$ structures of the series. We would like to point out that ring-like structures have been previously reported in a theoretical study by Shao *et al.*[17] for the neutral C_nB_3 (n = 4–8) clusters.

The $C_2B_6^-$ and $C_3B_5^-$ clusters were investigated by photoelectron spectroscopy (PES) and *ab initio* calculations. The experiment was performed with a laser-vaporization cluster source and a magnetic-bottle photoelectron spectrometer (Experimental section).[18]

The photoelectron spectra of the $C_2B_6^-$ cluster are presented in Fig. 2-1 and the photoelectron spectra of $C_3B_5^-$ are shown in Fig. 2-2. The experimentally observed vertical detachment energies (VDEs) for the clusters are given in Tables 2-1 and 2-2 and are compared to the theoretically calculated data.

Fig. 2-1 shows the PES spectra of $C_2B_6^-$ at three photon energies. The 193 nm spectrum of $C_2B_6^-$ reveals six well-resolved features labelled A–F (Fig. 2-1b). At the low binding energy side, we observe a very broad feature (X, X′) corresponding to

photodetachment from the two lowest lying isomers of $C_2B_6^-$. The ninth band (G) can be tentatively identified, but the signal-to-noise ratios are poor at the high binding energy side. The spectra recorded at 266 nm (Fig. 2-1a) reveal fine vibrational features for the A and B electronic bands. For the A band we measured a vibrational spacing of 330 ± 30 cm^{-1} using the PES measured at 355 nm (see the inset of Fig. 2-1a). The B band shows a fine structure both at 193 nm and 266 nm, however, the measurement of the vibrational spacing is complicated by the existence of two nearly isoenergetic photodetachment channels.

The spectra of $C_3B_5^-$ are shown in Fig. 2-2. The VDE of the X band was measured to be 3.94 ± 0.03 eV. The intensity change between the X and the A bands confirms that there are two features rather than a vibrational progression. The X band shows a short vibrational progression with a spacing of 380 ± 30 cm^{-1}.

Computationally, we first performed the global minimum structure search for the $C_2B_6^-$ ion using the Coalescence Kick (CK)[19–21] program written by Averkiev. The CK method subjects large populations of randomly generated structures to a coalescence procedure in which all atoms are pushed gradually to the molecular center of mass to avoid generation of fragmented structures and then optimized to the nearest local minima. The CK calculations were performed at the B3LYP/3-21G level of theory. All the low-lying (ΔE < 25 kcal mol^{-1}) isomers revealed were reoptimized with follow up frequency calculations at the B3LYP/6-311+G* level of theory. Single point calculations for the lowest energy structures were performed at the RCCSD(T)/6-311+G(2df) level of theory

using the B3LYP/6-311+G* optimized geometries. The relative energies of a series of representative isomers are given in Fig. 2-3.

The CK search revealed that the cyclic structure I.6 is the lowest isomer with the structures I.1–I.5 being 12–25 kcal mol^{-1} higher at the B3LYP/3-21G level of theory. However, when we reoptimized all the low-lying structures at the B3LYP/6-311+G* level of theory we found a significantly different order of the isomers with the wheel-type structure I.1 being the lowest isomer and the cyclic structure I.6 lying 9.1 kcal mol^{-1} higher (Fig. 2-3). Therefore, the set of isomers for subsequent investigation should be formed of all the structures lying in the range of about 20 kcal mol^{-1} relative energies at this level of theory as it was done in the current work. Moreover, the B3LYP/6-311+G* calculated results were further corrected by the single point calculations at the RCCSD(T)/6-311+G(2df)//B3LYP/6-311+G* level of theory (Fig. 2-3). Thus, according to our most accurate calculations, the wheel-type structure I.1 is the global minimum for the $C_2B_6^-$ cluster. In order to verify this theoretical prediction we calculated theoretical VDEs for the global minimum structure I.1 at three levels of theory: TD-B3LYP/6-311+G(2df), UOVGF/6-311+G(2df) and R(U)CCSD(T)/6-311+G(2df), all at the B3LYP/6-311+G* optimized geometries. We also calculated VDEs for the second lowest structure I.2 at the same three levels of theory and found out that it also contributes to the experimental PES of $C_2B_6^-$. Results of the VDEs calculations are summarized in Table 2-1.

The broad feature X(X′) in the experimental spectrum of $C_2B_6^-$ (Fig. 2-1) can be assigned to the electron detachment from the singly-occupied HOMO $7a_1$ of the global

minimum structure I.1. The broad shape of the peak is an indication of a large geometry change upon the electron detachment, which was confirmed by geometry optimization of the neutral C_2B_6 cluster (see Fig. 2-4). The electron detachment from the singly occupied HOMO 11a′ of the I.2 isomer can also contribute to this peak since the first VDE is very close to that of I.1. None of the calculated VDEs of I.1 could be assigned to the experimental feature at ~3.2 eV. This peak confirms the presence of the second-lowest isomer I.2 of $C_2B_6^-$ in the molecular beam since it can be clearly explained by the electron detachment from 3a″ of I.2 leading to the final ^{3}A″ state. Electron detachment processes with final triplet states are expected to be more prominent in the experimental spectra, therefore, we discuss only the transitions leading to the final triplet states. The feature at 3.54 eV in the experimental PES is due to the electron detachment from HOMO − 1 $2b_1$ with the final state $^3B_1$. The next feature (4.35 eV) corresponds to the electron detachment from HOMO − 2 $1a_2$ to the final $^3A_2$ state. Both of these detachment channels are of isomer I.1. The features at 4.68 and 4.77 eV can be explained only by the electron detachment from 2a″ and 10a′ of I.2 corresponding to two final states: ^{3}A′ and ^{3}A″. The sharp peak at 4.96 eV is due to the detachment from HOMO − 3 $6a_1$ leading to the $^3A_1$ state of I.1. The broad feature at about 6 eV can be assigned to two detachments of electrons from HOMO − 4 $4b_2$ of I.1 and from HOMO − 4 9a′ of I.2 with the final states $^3B_2$ and ^{3}A′, respectively. The excellent agreement between the experimentally observed and the theoretically calculated VDEs confirms the predicted structures of the two lowest-lying isomers I.1 and I.2 contributing to the experimental PES of $C_2B_6^-$.

According to the CK search, the global minimum structure of the $C_3B_5^-$cluster is a cyclic isomer II.1 with the lowest wheel-type structure II.5 being 62.1 kcal mol^{-1} higher at the B3LYP/3-21G level of theory (Fig. 2-5).

Geometry optimization for the low-lying isomers (ΔE < 25 kcal mol^{-1}) and the lowest-found wheel-type structure II.5 at the B3LYP/6-311+G* level of theory with subsequent single point calculations at the RCCSD(T)/6-311+G(2df)//B3LYP/6-311+G* level revealed the presented (Fig. 2-5) order. Thus, according to our calculations the global minimum is the cyclic isomer II.1 and the structural transition from the wheel-type structure to the monocyclic ring occurs between $C_2B_6^-$ and $C_3B_5^-$. The lowest wheel-type structure II.5 is 28.8 kcal mol^{-1} higher than the global minimum (RCCSD(T)/6-311+G(2df)//B3LYP/6-311+G*).

Again, we calculated VDEs of the proposed structure II.1 to compare those with the experimental PES. Only the isomer II.1 is expected to contribute to the experimental PES of the $C_3B_5^-$cluster, since the lowest alternative isomer II.2 is 13 kcal mol^{-1} higher than II.1. The VDE calculations were performed at the same three levels of theory: TD-B3LYP/6-311+G(2df), ROVGF/6-311+G(2df) and RCCSD(T)/6-311+G(2df), all at the B3LYP/6-311+G* optimized geometry. The VDEs calculated are summarized in Table 2-2. Our calculations revealed two very close transitions corresponding to the electron detachments from HOMO ($5b_2$) and HOMO − 1 ($1a_2$). The first VDE is 0.1–0.2 eV lower than that assigned to the detachment from HOMO − 1 according to all the three theory levels. These two transitions are responsible for the features X and A in the experimental spectra of the $C_3B_5^-$ cluster (Fig. 2-2). There is a big gap between these two

transitions and the transition corresponding to electron detachment from HOMO − 2 ($2b_1$) which varies from 1.0 eV (TD-DFT) to 1.3 eV (RCCSD(T)). This computational prediction is confirmed by the experimental spectra, showing the gap of 1.2 eV between feature A and feature B. The fourth electron detachment occurs from HOMO − 3 ($6a_1$) and the calculated VDE agrees well with the experimental value (5.47 eV). The sharp shape of the first peak in the PES spectra of the $C_3B_5^-$ cluster is consistent with the calculated small geometry change upon the electron detachment (see Fig. 2-4). The perfect agreement between the experimental and the theoretical VDEs confirms the global minimum structure II.1 for the $C_3B_5^-$ cluster.

In order to trace structural change from the wheel-type structure to the monocyclic ring structure we calculated the monocyclic structure for the cluster CB_7^-. The calculated relative energy of the wheel-type global minimum structure with respect to the monocyclic ring structure is presented in Fig. 2-6 as well as the corresponding relative energies of the monocyclic ring and wheel-type structures for the $C_2B_6^-$ and $C_3B_5^-$clusters.

One can see that the energy difference between the wheel-type and monocyclic ring isomers dropped from 79.0 to 20.5 kcal mol^{-1} (at RCCSD(T)/6-311+G(2df)//B3LYP/6-311+G*) upon transition from CB_7^- to $C_2B_6^-$. The substitution of another boron by a carbon atom in $C_3B_5^-$ leads to the inversion of the wheel-type and monocyclic structures with the monocyclic structure being now the global minimum. It was proposed by Zubarev and Boldyrev[22] that the wheel-type structures appear in boron clusters beginning from B_8 since the dangling electron density at the center of the

monocyclic cluster cannot be supported by the valence charge of the boron atoms. Migration of one of the boron atoms into the center of the ring provides the necessary electrostatic field stabilization in the wheel-type structures and that is the reason why those structures are the global minima. The substitution of boron atoms in the peripheral ring by carbon atoms provided additional electrostatic field stabilization at the center of the ring due to the higher valence charge of carbon, which eventually leads to the higher stability of the monocyclic structures over the wheel-type structures in the mixed carbon–boron clusters.

It was previously shown[7] that the global minimum wheel-type structure of CB_7^- is doubly aromatic. The CB_7^- monocyclic structure has a conflicting aromaticity. The chemical bonding is consistent with the higher stability of the doubly aromatic wheel-type structure relative to the monocyclic structure with the conflicting aromaticity.

We performed chemical bonding analysis of the studied clusters using the Adaptive Natural Density Partitioning method (AdNDP) developed by Zubarev and Boldyrev.[23] Results of the AdNDP analysis are summarized in Fig. 2-7 and 2-8. According to our AdNDP analysis, chemical bonding in the wheel-type structure of the $C_2B_6^-$ cluster (Fig. 2-7) can be described as a combination of three 2c–2e σ B–B bonds, four 2c–2e σ C–B bonds, three delocalized π-bonds (responsible for π-aromaticity), three delocalized doubly-occupied σ-bonds and one delocalized singly-occupied σ-bond. Here and elsewhere the terms delocalized σ-bonds and delocalized π-bonds mean that those bonds cannot be reduced to 2c–2e bonds by the AdNDP method. It was previously proposed[24] to name cases like the one we have here with an odd number of electrons for

σ-delocalized bonds as ½-σ-antiaromatic. "½" is used as a label and means that the σ-system with singly occupied delocalized bond is half way down to being σ-antiaromatic in the wheel-type structure of the doubly-charged $C_2B_6^{2-}$ ion. The ½-σ-antiaromatic nature of the global minimum structure I.1 of the $C_2B_6^-$cluster is consistent with relatively low first VDE of the cluster. When the extra electron in the $C_2B_6^-$cluster is removed from the singly-occupied orbital, the resulting neutral C_2B_6 species becomes a doubly-aromatic system which is consistent with the round structure of the neutral species (Fig. 2-7).

The chemical bonding in the monocyclic structure I.6 of the $C_2B_6^-$cluster can be described as follows. There are four 2c–2e σ B–B bonds, four 2c–2e σ C–B bonds, three delocalized π-bonds (responsible for π-aromaticity), two delocalized doubly-occupied σ-bonds and one delocalized singly-occupied σ-bond. Thus, the structure I.6 is ½-σ-aromatic since the singly occupied delocalized bond is half way down to being σ-aromatic in the monocyclic ring-type structure of the doubly-charged $C_2B_6^{2-}$ ion (see Fig. 2-7). The presence of ½-σ-antiaromaticity in the wheel-type structure and of the ½-σ-aromaticity in the monocyclic structure explains the relatively low energy difference compared to that of the CB_7^- structures (Fig. 2-6).

The global minimum monocyclic structure II.1 of the $C_3B_5^-$cluster (Fig. 2-8) is doubly-aromatic with two 2c–2e σ B–B bonds, six 2c–2e σ C–B bonds, three delocalized π-bonds (responsible for π-aromaticity), three delocalized σ-bonds (responsible for σ-aromaticity). The doubly-aromatic nature of the global minimum structure $C_3B_5^-$ is consistent with the rather high first VDE of this cluster.

Chemical bonding analysis of the lowest-lying wheel-type isomer II.5 (Fig. 2-8) revealed one 2c–2e σ B–B bond, six 2c–2e σ C–B bonds, three delocalized π-bonds (responsible for π-aromaticity) and four delocalized σ-bonds (responsible for σ-antiaromaticity). The σ-antiaromaticity leads to deformation of the heptagon structure into the hexagon structure with one carbon atom coordinated to the edge of the hexagon. As a result of that we have three σ-bonds delocalized over the hexagon and one 3c–2e σ-bond delocalized over the external carbon atom and the two edge boron atoms (see Fig. 2-8). The structure II.5 possessing conflicting aromaticity is higher in energy than the doubly-aromatic global minimum structure II.1.

In the above discussion we presented chemical bonding explanation for different stabilities of the wheel-type and monocyclic ring-type structures. With the chemical bonding analysis we can explain why the $C_2B_6^-$cluster has relatively low first VDE compared to that of the $C_3B_5^-$cluster. However we would like to stress that we believe that the transition from the wheel-type to the ring-type structures in the series occurs due to the increase of the stabilizing electrostatic field at the center of the cluster as a result of the increased number of carbon atoms in $C_3B_5^-$, which makes the presence of the central boron atom unnecessary.

2-1. Experimental section

The experiment was performed using a magnetic-bottle PES apparatus equipped with a laser vaporization cluster source, details of which have been published elsewhere.[25,26] Briefly, the carbon-doped boron clusters were produced by laser vaporization of a disk target made of isotopically enriched ^{10}B (~6% wt), C (~0.6% wt),

and Bi. The clusters were entrained by the helium carrier gas supplied by two pulsed Jordan valves and underwent a supersonic expansion to form a collimated molecular beam. The cluster composition and the cooling were controlled by the time delay between the pulsed beam valves and the vaporization laser. The negatively charged clusters were extracted from the cluster beam and analyzed with a time-of-flight mass spectrometer. The clusters of interest were mass selected and decelerated before being intercepted by the probe photodetachment laser beam: 193 nm (6.424 eV) from an ArF excimer laser and 355 nm (3.496 eV) or 266 nm (4.661 eV) from a Nd:YAG laser. Photoelectrons were collected at nearly 100% efficiency by a magnetic bottle and analyzed in a 3.5 m long electron flight tube. The cluster PE spectra were calibrated using the known spectra of Bi^-. The kinetic energy resolution of the magnetic bottle apparatus, $\Delta E/E$, was typically better than 2.5%, *i.e.* ~25 meV for 1 eV electrons.

2-2. Theoretical section

We searched for the global minimum of the $C_2B_6^-$ and $C_3B_5^-$clusters using the Coalescence Kick (CK) program[19–21] with the B3LYP/3-21G method for energy and gradient calculations. Then we reoptimized the geometries and performed frequency calculations for the lowest isomers (E < 25 kcal mol^{-1}) at the B3LYP/6-311+G* level of theory and recalculated total energies of the isomers at the RCCSD(T)/6-311+G(2df)//B3LYP/6-311+G* level of theory. The VDEs for the global minima I.1 and II.1 and the low-lying isomer I.2 were calculated using the R(U)CCSD(T)/6-311+G(2df) method, the outer-valence Green Function method (R(U)OVGF/6-311+G(2df)) and the time-dependent DFT method (TD B3LYP/6-311+G(2df) at the B3LYP/6-311+G*

geometries. The calculations were performed with the Gaussian 03[27] and Molpro[28] software. Molecular orbitals were visualized with the MOLDEN 3.4[29] and Molekel 5.4.0.8[30] programs.

Notes and references

1 A. V. Orden and R. J. Saykally, *Chem. Rev.*, 1998, **98**, 2313.

2 A. N. Alexandrova, A. I. Boldyrev, H.-J. Zhai and L. S. Wang, *Coord. Chem. Rev.*, 2006, **250**, 2811.

3 L. M. Wang, B. B. Averkiev, J. A. Ramilowski, W. Huang, L. S. Wang and A. I. Boldyrev, *J. Am. Chem. Soc.*, 2010, **132**, 14104.

4 K. Exner and P. v. R. Schleyer, *Science*, 2000, **290**, 1937.

5 Z. X. Wang and P. v. R. Schleyer, *Science*, 2001, **292**, 2456.

6 R. M. Minyaev, T. N. Gribanova, A. G. Starikov and V. I. Minkin, *Mendeleev Commun.*, 2001, **11**, 213.

7 B. B. Averkiev, D. Yu. Zubarev, L. M. Wang, W. Huang, L. S. Wang and A. I. Boldyrev, *J. Am. Chem. Soc.*, 2008, **120**, 9248.

8 L. M. Wang, W. Huang, B. B. Averkiev, A. I. Boldyrev and L. S. Wang, *Angew. Chem., Int. Ed.*, 2007, **46**, 4550.

9 B. B. Averkiev, L. M. Wang, W. Huang, L. S. Wang and A. I. Boldyrev, *Phys. Chem. Chem. Phys.*, 2009 **11**, 9840.

10 I. Boustani, *Phys. Rev. B: Condens. Matter*, 1997, **55**, 233.

11 V. Bonacic-Koutecky, P. Fantucci and J. Koutecky, *Chem. Rev.*, 1991, **91**, 1035.

12 H.-J. Zhai, A. N. Alexandrova, K. A. Birch, A. I. Boldyrev and L. S. Wang, *Angew. Chem., Int. Ed.*, 2003, **42**, 6004.

13 A. N. Alexandrova, H.-J. Zhai, L. S. Wang and A. I. Boldyrev, *Inorg. Chem.*, 2004, **43**, 3552.

14 Q. S. Li, Y. Zhao, W. Xu and N. Li, *Int. J. Quantum Chem.*, 2005, **101**, 219.

15 J. M. L. Martin and P. R. J. Taylor, *J. Phys. Chem.*, 1996, **100**, 6047.

16 Yu. Shlyakhter and S. Sokolova, *J. Chem. Phys.*, 1999, **110**, 10725.

17 J. Shao, C. He, R. Shi, C. Wang, X. Zhu and X. Lu, *THEOCHEM*, 2010, **961**, 17.

18 L. S. Wang, H. S. Cheng and J. Fan, *J. Chem. Phys.*, 1995, **102**, 9480.

19 B. B. Averkiev, *PhD thesis*, Utah State University, USA, 2009.

20 W. Huang, A. P. Sergeeva, H.-J. Zhai, B. B. Averkiev, L. S. Wang and A. I. Boldyrev, *Nat. Chem.*, 2010, **2**, 202.

21 M. Saunders, *J. Comput. Chem.*, 2004, **25**, 621.

22 D. Yu. Zubarev and A. I. Boldyrev, *J. Comput. Chem.*, 2007, **28**, 251.

23 D. Yu. Zubarev and A. I. Boldyrev, *Phys. Chem. Chem. Phys.*, 2008, **10**, 5207.

24 D. Yu. Zubarev, A. P. Sergeeva and A. I. Boldyrev, in *Chemical Reactivity Theory. A Density Functional View*, ed. P. K. Chattaraj, CRC Press. Taylor & Francis Group, New York, 2009, pp. 439–452.

25 J. W. Fan and L. S. Wang, *J. Chem. Phys.*, 1995, **102**, 8714–8717.

26 L. S. Wang and X. Li, in *Proc. Int. Symp. on Clusters and Nanostructure Interfaces*, Oct. 25–28, 1999, Richmond, VA, ed. P. Jena, S. N. Khanna and B. K. Rao, World Scientific, River Edge, New Jersey, 2000, pp. 293–300.

27 M. J. Frisch, G. W. Trucks, H. B. Schlegel, G. E. Scuseria, M. A. Robb, J. R. Cheeseman, J. A. Montgomery, Jr., T. Vreven, K. N. Kudin, J. C. Burant, J. M. Millam, S. S. Iyengar, J. Tomasi, V. Barone, B. Mennucci, M. Cossi, G. Scalmani, N. Rega, G. A. Petersson, H. Nakatsuji, M. Hada, M. Ehara, K. Toyota, R. Fukuda, J. Hasegawa, M. Ishida, T. Nakajima, Y. Honda, O. Kitao, H. Nakai, M. Klene, X. Li, J. E. Knox, H. P. Hratchian, J. B. Cross, V. Bakken, C. Adamo, J. Jaramillo, R. Gomperts, R. E. Stratmann, O. Yazyev, A. J. Austin, R. Cammi, C. Pomelli, J. W. Ochterski, P. Y. Ayala, K. Morokuma, G. A. Voth, P. Salvador, J. J. Dannenberg, V. G. Zakrzewski, S. Dapprich, A. D. Daniels, M. C. Strain, O. Farkas, D. K. Malick, A. D. Rabuck, K. Raghavachari, J. B. Foresman, J. V. Ortiz, Q. Cui, A. G. Baboul, S. Clifford, J. Cioslowski, B. B. Stefanov, G. Liu, A. Liashenko, P. Piskorz, I. Komaromi, R. L. Martin, D. J. Fox, T. Keith, M. A. Al-Laham, C. Y. Peng, A. Nanayakkara, M. Challacombe, P. M. W. Gill, B. Johnson, W. Chen, M. W. Wong, C. Gonzalez, J. A. Pople, *Gaussian 03, Revision D.01*. Gaussian, Inc., Wallingford, CT, 2004.

28 H.-J. Werner, P. J. Knowles, F. R. Manby, M. Schütz, P. Celani, G. Knizia, T. Korona, R. Lindh, A. Mitrushenkov, G. Rauhut, T. B. Adler, R. D. Amos, A. Bernhardsson, A. Berning, D. L. Cooper, M. J. O. Deegan, A. J. Dobbyn, F. Eckert, E. Goll, C. Hampel, A. Hesselmann, G. Hetzer, T. Hrenar, G. Jansen, C. Köppl, Y. Liu, A. W. Lloyd, R. A. Mata, A. J. May, S. J. McNicholas, W. Meyer, M. E. Mura, A. Nicklaß, P. Palmieri, K. Pflüger, R. Pitzer, M. Reiher, T.

Shiozaki, H. Stoll, A. J. Stone, R. Tarroni, T. Thorsteinsson, M. Wang, A. Wolf, *MOLPRO, version 2006.1*.

29 G. Schaftenaar, *MOLDEN 4.3*, CAOS/CAMM Center, The Netherlands, 1998.

30 U. Varetto, *Molekel 5.4.0.8*, Swiss National Supercomputing Centre, Manno, Switzerland, 2009.

Table 2-1 Comparison of the experimental VDEs with calculated values for the structures I.1 C_{2v} ($^2A_1$) and I.2 C_s ($^2A'$) of the $C_2B_6^-$ cluster. All energies are in eV

			VDE (theor.)		
Feature	VDE (exp)[a]	Final state and electronic configuration	TD-B3LYP[b]	UOVGF[c]	R(U)CCSD(T)[d]
I.1 C_{2v} ($^2A_1$)					
X′	2.3(1)	$^1A_1$, {…$5a_1^{(2)}4b_2^{(2)}6a_1^{(2)}1a_2^{(2)}2b_1^{(2)}7a_1^{(0)}$}	2.26	2.59 (0.89)	2.17
B	3.54(3)	$^3B_1$, {…$5a_1^{(2)}4b_2^{(2)}6a_1^{(2)}1a_2^{(2)}2b_1^{(1)}7a_1^{(1)}$}	3.51	3.54 (0.89)	3.64
		$^1B_1$, {…$5a_1^{(2)}4b_2^{(2)}6a_1^{(2)}1a_2^{(2)}2b_1^{(1)}7a_1^{(1)}$}	3.91	—[e]	—[e]
C	4.35(5)	$^3A_2$, {…$5a_1^{(2)}4b_2^{(2)}6a_1^{(2)}1a_2^{(1)}2b_1^{(2)}7a_1^{(1)}$}	4.25	4.25 (0.88)	4.41
		$^1A_2$, {…$5a_1^{(2)}4b_2^{(2)}6a_1^{(2)}1a_2^{(1)}2b_1^{(2)}7a_1^{(1)}$}	4.46	—[e]	—[e]
F	4.96(5)	$^3A_1$, {…$5a_1^{(2)}4b_2^{(2)}6a_1^{(1)}1a_2^{(2)}2b_1^{(2)}7a_1^{(1)}$}	4.93	4.88 (0.89)	5.06
G	5.7(2)	$^3B_2$, {…$5a_1^{(2)}4b_2^{(1)}6a_1^{(2)}1a_2^{(2)}2b_1^{(2)}7a_1^{(1)}$}	5.58	5.72 (0.89)	5.79
		$^1A_1$, {…$5a_1^{(2)}4b_2^{(2)}6a_1^{(1)}1a_2^{(2)}2b_1^{(2)}7a_1^{(1)}$}	5.66	—[e]	—[e]
		$^1B_2$, {…$5a_1^{(2)}4b_2^{(1)}6a_1^{(2)}1a_2^{(2)}2b_1^{(2)}7a_1^{(1)}$}	5.93	—[e]	—[e]
I.2 C_s ($^2A'$)					
X	2.2(1)	$^1A'$, {…$9a'^{(2)}10a'^{(2)}2a''^{(2)}3a''^{(2)}11a'^{(0)}$}	2.19	—[f]	2.09
A	3.23(2)	$^3A''$, {…$9a'^{(2)}10a'^{(2)}2a''^{(2)}3a''^{(1)}11a'^{(1)}$}	3.12	—[f]	3.28
		$^1A''$, {…$9a'^{(2)}10a'^{(2)}2a''^{(2)}3a''^{(1)}11a'^{(1)}$}	3.52	—[f]	—[e]
D	4.68(5)	$^3A'$, {…$9a'^{(2)}10a'^{(1)}2a''^{(2)}3a''^{(2)}11a'^{(1)}$}	4.62	—[f]	4.81
E	4.77(5)	$^3A''$, {…$9a'^{(2)}10a'^{(2)}2a''^{(1)}3a''^{(2)}11a'^{(1)}$}	4.69	—[f]	—[e]
		$^1A''$, {…$9a'^{(2)}10a'^{(2)}2a''^{(1)}3a''^{(2)}11a'^{(1)}$}	4.91	—[f]	—[e]
		$^1A'$, {…$9a'^{(2)}10a'^{(1)}2a''^{(2)}3a''^{(2)}11a'^{(1)}$}	5.31	—[f]	—[e]
G	5.7(2)	$^3A'$, {…$9a'^{(1)}10a'^{(2)}2a''^{(2)}3a''^{(2)}11a'^{(1)}$}	5.90	—[f]	—[e]

[a] Numbers in parentheses represent the uncertainty in the last digit. [b] VDEs were calculated at the TD-B3LYP/6-311+G(2df)//B3LYP/6-311+G* level of theory. [c] VDEs were calculated at the UOVGF/6-311+G(2df)//B3LYP/6-311+G* level of theory. Values in parentheses represent the pole strength of the OVGF calculation. [d] VDEs were calculated at the R(U)CCSD(T)/6-311+G(2df)//B3LYP/6-311+G* level of theory. [e] VDE value cannot be calculated at this level of theory. [f] These VDEs are not presented because of large spin contamination at the UHF/6-311+G(2df) level of theory.

Table 2-2 Comparison of the experimental VDEs with calculated values for the structure II.1 C_{2v} ($^1A_1$) of the $C_3B_5^-$ cluster. All energies are in eV

			VDE (theor.)		
Feature	VDE (exp)[a]	Final state and electronic configuration	TD-B3LYP[b]	ROVGF[c]	RCCSD(T)[d]
X	3.94(3)	$^2B_2$ {…$5a_1^{(2)}1b_1^{(2)}6a_1^{(2)}2b_1^{(2)}1a_2^{(2)}5b_2^{(1)}$}	3.82	3.99 (0.87)	3.94
A	4.04(3)	$^2A_2$ {…$5a_1^{(2)}1b_1^{(2)}6a_1^{(2)}2b_1^{(2)}1a_2^{(1)}5b_2^{(2)}$}	4.03	4.09 (0.88)	4.11
B	5.26(5)	$^2B_1$ {…$5a_1^{(2)}1b_1^{(2)}6a_1^{(2)}2b_1^{(1)}1a_2^{(2)}5b_2^{(2)}$}	5.06	5.26 (0.87)	5.38
C	5.47(5)	$^2A_1$ {…$5a_1^{(2)}1b_1^{(2)}6a_1^{(1)}2b_1^{(2)}1a_2^{(2)}5b_2^{(2)}$}	5.41	5.55 (0.85)	5.53

[a] Numbers in parentheses represent the uncertainty in the last digit. [b] VDEs were calculated at the TD-B3LYP/6-311+G(2df)//B3LYP/6-311+G* level of theory. [c] VDEs were calculated at the ROVGF/6-311+G(2df)//B3LYP/6-311+G* level of theory. Values in parentheses represent the pole strength of the OVGF calculation. [d] VDEs were calculated at the RCCSD(T)/6-311+G(2df)//B3LYP/6-311+G* level of theory.

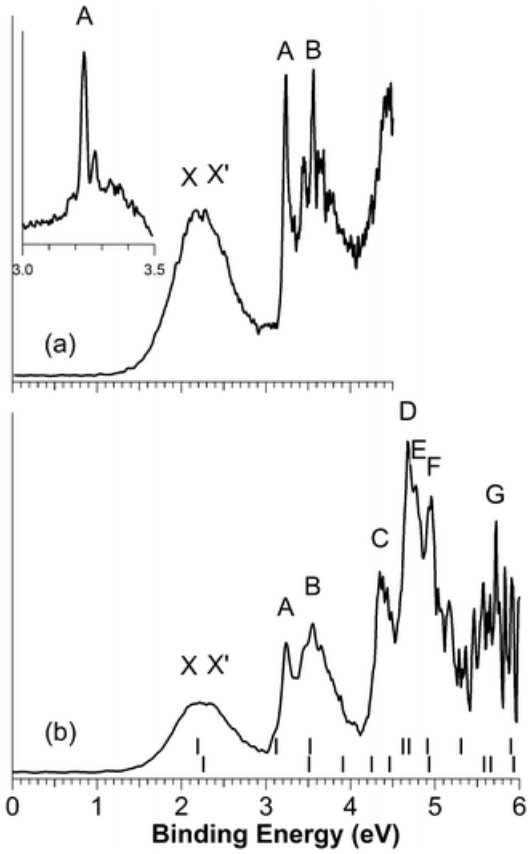

Fig. 2-1 Photoelectron spectra of $C_2B_6^-$ at (a) 266 nm (4.661 eV) and (b) 193 nm (6.424 eV). The inset shows a partial PES at 355 nm (3.496 eV). The short vertical lines represent the TD-B3LYP values of VDE for structures I.1 (bottom) and I.2 (top).

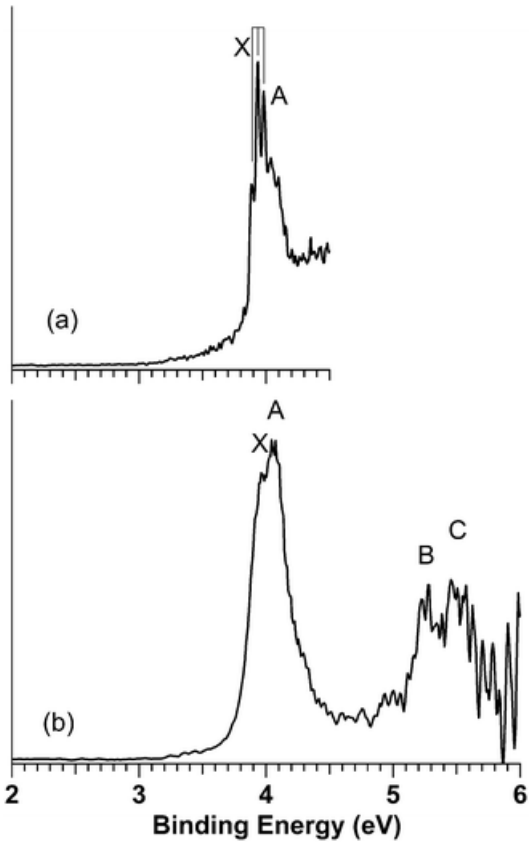

Fig. 2-2 Photoelectron spectra of $C_3B_5^-$ at (a) 266 nm (4.661 eV) and (b) 193 nm (6.424 eV).

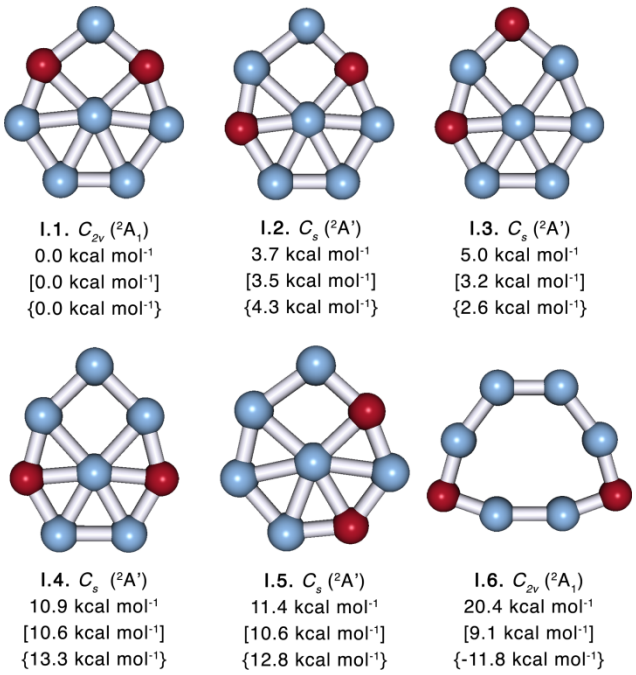

Fig. 2-3 Representative optimized isomers of the $C_2B_6^-$ cluster, their point group symmetries, spectroscopic states and relative energies. The ZPE corrected energies are given at the RCCSD(T)/6-311+G(2df)//B3LYP/6-311+G*, B3LYP/6-311+G* (in square brackets), and B3LYP/3-21G (in curly brackets) levels of theory.

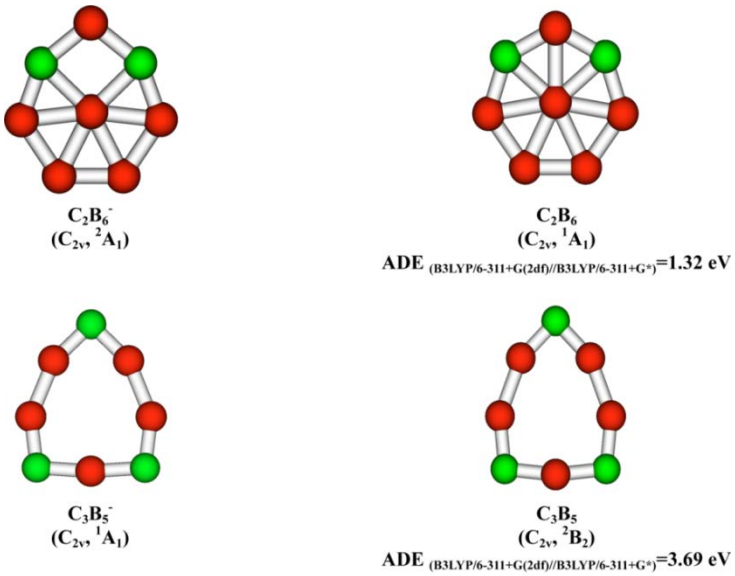

Fig. 2-4 Adiabatic Detachment Energies (ADE) of the $C_2B_6^-$ and $C_3B_5^-$ clusters

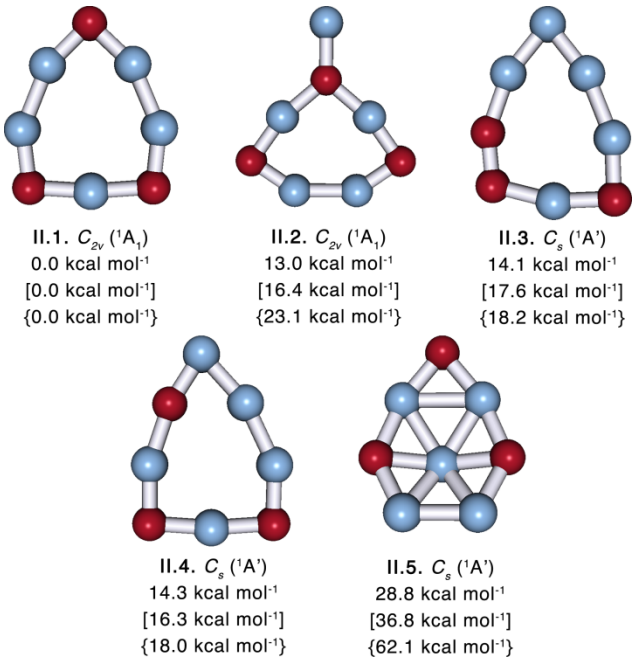

Fig. 2-5 Optimized isomers of the $C_3B_5^-$ cluster, their point group symmetries, spectroscopic states and relative energies. The ZPE corrected energies are given at the RCCSD(T)/6-311+G(2df)//B3LYP/6-311+G*, B3LYP/6-311+G* (in square brackets), and B3LYP/3-21G (in curly brackets) levels of theory.

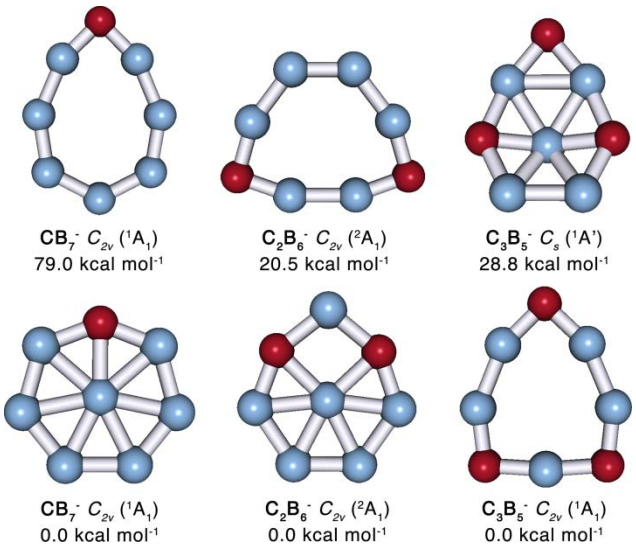

Fig. 2-6 Wheel-type to monocyclic ring structural transition in the series of the $C_xB_{8-x}^-$ (x = 1–3) clusters. Relative energies are given at RCCSD(T)/6-311+G(2df)//B3LYP/6-311+G*.

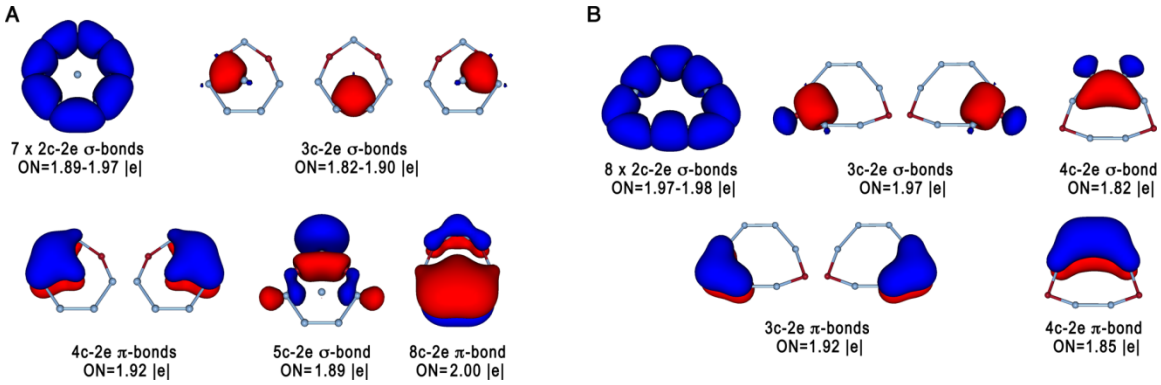

Fig. 2-7 The chemical bonding patterns revealed by the AdNDP analysis for the $C_2B_6^{2-}$ cluster at the optimized geometries of the global minimum wheel-type structure I.1 (**A**) and lowest ring isomer I.6 (**B**) of the $C_2B_6^-$ cluster. The extra electron was added in order to avoid complications of the chemical bonding picture caused by spin polarization in the open-shell $C_2B_6^-$ cluster. The 2c-2e C-B and B-B bonds of both isomers are superimposed on a single molecular framework.

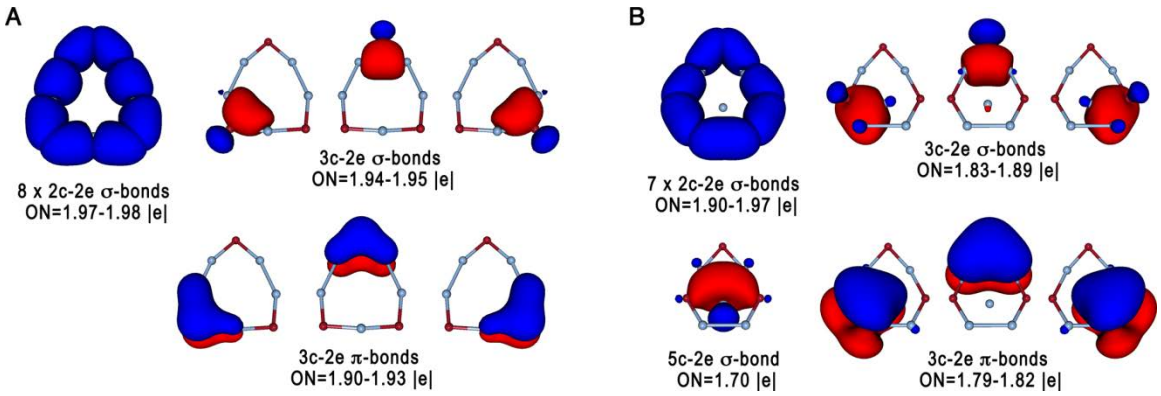

Fig. 2-8 The chemical bonding patterns revealed by the AdNDP analysis for the global minimum ring isomer II.1 (**A**) and the lowest wheel-type isomer II.5 (**B**) of the $C_3B_5^-$ cluster. The 2c-2e C-B and B-B bonds of both isomers are superimposed on a single molecular framework.

CHAPTER 3

PHOTOELECTRON SPECTROSCOPY AND AB INITIO STUDY OF BORON-CARBON MIXED CLUSTERS: CB_9^- AND $C_2B_8^-$ *

Abstract

We performed a joint photoelectron spectroscopy and *ab initio* study of two carbon-doped boron clusters, CB_9^- and $C_2B_8^-$. Unbiased computational searches revealed similar global minimum structures for both clusters. The comparison of the experimentally observed and theoretically calculated vertical detachment energies revealed that only the global minimum structure is responsible for the experimental spectra of CB_9^-, whereas the two lowest-lying isomers of $C_2B_8^-$ contribute to the experimental spectra. The planar "distorted wheel" type structures with a single inner boron atom found for CB_9^- and $C_2B_8^-$ are different from the quasi-planar structure of B_{10}^-, which consists of two inner atoms and eight peripheral boron atoms. The adaptive natural density partitioning chemical bonding analysis revealed that CB_9^- and C_2B_8 clusters exhibit π aromaticity and σ antiaromaticity, which is consistent with their planar distorted structures.

3-1. Introduction

Experimental and theoretical studies over the last decade showed that anionic boron clusters are planar or quasi-planar at least up to B_{23}^-.[1–14] Neutral boron clusters have been reported to have planar structures up to B_{20},[15–17] except for B_{14}, for which a

* Coauthored by Timur R. Galeev, Wei-Li Li, Constantin Romanescu, Ivan Černušák, Lai-Sheng Wang, and Alexander I. Boldyrev. Reprinted with permission from *J. Chem. Phys*. **2012**, *137*, 234306.

three-dimensional global minimum structure was proposed.[18] Boron cationic clusters are planar up to B_{16}^+.[19] The exceptional stability of the icosahedral B_{12} cage found in bulk boron allotropes and boranes led to suggestions in early experimental studies that 3D cage structures might occur for small boron clusters.[20–22] However, subsequent computational studies showed that icosahedral cage structures for B_{12} and B_{13} were unstable.[23–30]

Chemical bonding analyses revealed that the concepts of aromaticity, multiple aromaticity/antiaromaticity, and conflicting aromaticity could nicely explain the geometries and stabilities of these quasi-planar boron clusters.[1–13,31–34] The following chemical bonding model was developed for planar boron clusters: all peripheral boron atoms are bonded to their neighbors by two-center two-electron (2c–2e) σ bonds, while the central atoms are bonded via delocalized multi-center σ and π bonds with the peripheral atoms. If the number of delocalized σ or π electrons satisfies the $4n$+2 Hückel rule, the cluster exhibits σ or π aromaticity. The planarity, stability, and high symmetry of some of the boron clusters suggested that they may serve as ligands or building blocks.[13] A planar cyclic B_6 building block has recently been observed in a tertiary boride compound, $Ti_7Rh_4Ir_2B_8$, showing that planar boron clusters can indeed exist in solid compounds.[35]

Doping boron clusters with other elements widens the range of potential ligands and building blocks. The CB_6^{2-}, CB_7^-, and CB_8 clusters have been suggested theoretically to be hexa-, hepta-, and octacoordinated planar carbon species, respectively, though they are only local minima, not global minima.[36–38] In joint experimental and theoretical

investigations, we have shown that the wheel-type structures are indeed global minima for the CB_6^{2-}, CB_7^-, and CB_8 clusters,[39–41] but carbon avoids hypercoordination in these species and occupies a peripheral position instead. Theoretical investigations on planar tetra-, penta-, hexa-, hepta-, and octacoordinated structures of boron-carbon mixed clusters showed that boron-centered isomers are generally more stable than the ones with carbon in the center.[42] Carbon being more electronegative than boron prefers localized bonding, which is only possible on the periphery of the cluster, and avoids the central position since the central atoms participate only in delocalized bonding. We have also studied a series of AlB_x^- clusters and found that the Al atom also avoids hypercoordination in the anionic clusters.[43–45] A variety of elements have been tested computationally for the central position in high symmetry wheel-type structures.[38,46–52] In recent joint experimental and theoretical works, we discovered a series of transition metal-centered boron wheels.[53–56] In particular, we have shown[55] that Ta in $Ta©B_{10}^-$ and Nb in $Nb©B_{10}^-$ have the highest coordination number for an atom in two-dimensional environment.[57] All of these wheel-type clusters belong to a new class of aromatic borometallic compounds and may be viable for condensed phase synthesis.

A few systematic studies of the influence of elemental substitution in clusters on their geometries and electronic properties have been reported. For the $C_xB_{5-x}^-$ series, a planar-to-linear structural transition was observed:[58] the global minimum structures of the boron-rich clusters CB_4^- and $C_2B_3^-$, are planar, similar to B_5^-, and those of the carbon-rich clusters, $C_3B_2^-$ and C_4B^-, are linear, similar to C_5^-. A wheel-to-ring structural transition was reported[59] for the $C_xB_{8-x}^-$ series between $x = 2$ and 3. In the $B_nAl_{6-n}^{2-}$ and

$LiB_nAl_{6-n}^-$ cluster series, 3D to 2D transitions in both series occur between $n = 2$ and 3.[60] Computational studies of the $C_xH_xP_{6-x}$ ($x = 0–6$)[61] and $C_xH_xP_{4-x}$ ($x = 0–4$)[62] series showed that the global minima become planar at $x = 4$ and $x = 3$, respectively. A 3D to 2D transition in the $Si_{6-n}C_nH_6$ ($n = 0−6$) series occurs between $n = 4$ and 5.[63] Finally, a 3D to linear transition in the $Si_{6-n}C_n$ series was observed between $n = 3$ and 4 in a joint experimental and theoretical study.[64]

In the current work, we report a joint photoelectron spectroscopic and *ab initio* study of the CB_9^- and $C_2B_8^-$ clusters. It was previously found that B_{10}^- has a quasi-planar structure (Figure 3-1), which could be described as an eight-membered outer ring enclosing two inner atoms.[14] Substitution of one and two boron atoms in the B_{10}^- cluster by carbon results in planar global minima in CB_9^- and $C_2B_8^-$, as presented in Figure 3-1. The carbon atoms not only occupy peripheral positions, as expected, but they also induce significant structural changes to the boron networks: one of the inner boron atoms is pushed to a peripheral position, resulting in the "distorted wheel" structures.

3-2. Experimental and Computational Methods

3-2.1. Experimental Method

The experiment was performed using a magnetic-bottle PES apparatus equipped with a laser vaporization cluster source, details of which have been published in Ref. 65. Briefly, the CB_9^- and $C_2B_8^-$ clusters were produced by laser vaporization of composite targets made with isotopically enriched ^{10}B containing about 0.1% C. Clusters formed in the source were entrained by a helium carrier and underwent a supersonic expansion to produce a cold cluster beam. Negatively charged clusters were extracted from the cluster

beam and analyzed using a time-of-flight mass spectrometer. The CB_9^- and $C_2B_8^-$ clusters of interest were mass selected and decelerated before being intercepted by a 193 nm (6.424 eV) laser beam from an ArF excimer laser or 355 nm (3.496 eV) and 266 nm (4.661 eV) from a Nd:YAG laser for photodetachment. Photoelectron time-of-flight spectra were measured and calibrated using the known spectra of Bi^- at 193, 266, and 355 nm and converted to the binding energy spectra by subtracting the kinetic energy spectra from the corresponding photon energies. The energy resolution of the magnetic-bottle PES spectrometer is $\Delta E/E \approx 2.5\%$, i.e., about 25 meV for 1 eV electrons.

3-2.2. Computational Methods

We first performed global minimum searches for CB_9^- and $C_2B_8^-$ using the Coalescence Kick (CK) program.[10,66] Low energy structures within 50 kcal/mol of the global minimum structure at the PBE0/6-31G level[67–69] were reoptimized with follow-up frequency calculations at the PBE0/6-311+G(*d*) level[70] of theory (see Figs. 3-2 and 3-3).[71] Single point coupled cluster including single, double and non-iterative triple excitations (CCSD(T)),[72–74] CCSD(T)/6-311+G(2*df*), calculations were performed for the 10 lowest energy isomers of both clusters. Vertical detachment energies (VDEs) were calculated at the time dependent density functional theory (TD-DFT),[75,76] TD-PBE0/6-311+G(*d*), outer-valence Green's Function method (OVGF),[77–80] OVGF/6-311+G(2*df*), and CCSD(T)/6-311+G(2*df*), all at the PBE0/6-311+G(*d*) geometries. At the TD-DFT, the first VDEs for CB_9^- and $C_2B_8^-$ were calculated as the lowest transitions from the anions into the final lowest state of the neutral species at the geometry optimized for the anions. Then, the vertical excitation energies of the neutral species calculated at the anion

geometry were added to the first VDE to obtain the second and higher VDEs. The OVGF/6-311+G(2*df*) energies are presented only for CB_9^-, since high spin contamination was observed for $C_2B_8^-$. Chemical bonding analysis was performed using the adaptive natural density partitioning method (AdNDP)[81] at PBE0/6-31G.

All calculations were performed using the GAUSSIAN09[82] and MOLPRO[83] software packages, Molekel 5.4.0.8[84] and Chemcraft[85] programs were used for visualizations.

3-3. Experimental Results

The photoelectron spectra of CB_9^- and $C_2B_8^-$ at different photon energies are shown in Figs. 3-4 and 3-5, respectively. The PES bands are labeled with letters (X, A, B, …) and the measured VDEs are given in Tables 3-1 and 3-2, where they are also compared with computational results. In each spectrum, the X band represents the transition from the anionic ground state to the neutral ground state. The A, B, … bands denote transitions to the excited states of the neutrals.

3-3.1. Photoelectron spectra of CB_9^-

The 266 nm spectrum of CB_9^- (Fig. 3-4(a)) shows a vibrationally resolved ground state band with a VDE of 3.61 eV. The inset of Fig. 3-4(a) displays more clearly the vibrational progression with an average spacing of 340 ± 50 cm^{-1}. The adiabatic detachment energy (ADE) or the electron affinity of the corresponding neutral CB_9 is defined by the 0-0 vibrational peak, which is 3.61 ± 0.03 eV, the same as the VDE. Following an energy gap of ~0.8 eV, a relatively broad band A is observed with a VDE of 4.49 eV. Two more bands are observed in the 193 nm spectrum with VDEs of 4.88 eV

for band B and 5.74 eV for band C. There is discernible signal beyond 6 eV and a band D with a VDE of ~6.2 eV is tentatively identified.

The weak feature labeled as "*" in the low binding energy range comes from the B_{10}^- cluster, which has a first VDE of 3.06 eV.[14] The mass of B_{10}^- is very close to that of CB_9^- and its intensity was very high in the mass spectrum, making it difficult to be completely eliminated when the CB_9^- mass peak was selected during the PES experiment. In fact, contributions from the B_{10}^- contamination can be identified in other parts of the CB_9^- spectra, namely, around 3.8 eV and between 5 and 5.6 eV by comparing with the previously reported PES spectra of B_{10}^-.[14]

3-3.2. Photoelectron spectra of $C_2B_8^-$

The 355 nm spectrum (Fig. 3-5(a)) displays two relatively sharp and vibrationally resolved bands. The band labeled as X′ has the same ADE and VDE of 2.39 ± 0.03 eV. The sharp onset of band X′ suggests a minimal geometry change upon photodetachment. Two vibrational progressions are observed in band X′ with frequencies of 390 ± 50 cm^{-1} and 1330 ± 50 cm^{-1}. The band labeled as X has an ADE and VDE of 2.67 ± 0.03 eV. There are also two vibrational progressions associated with band X with frequencies of 510 ± 50 cm^{-1} and 1480 ± 50 cm^{-1}. As will be shown later, the X′ and X bands come from two different isomers with close energies.

The 266 nm spectrum (Fig. 3-5(b)) shows two sharp bands (A′, A) at 4.05 eV and 4.14 eV and one broad band B at 4.52 eV. The 193 nm spectrum (Fig. 3-5(c)) has poor signal-to-noise ratio and three bands (C, D, and E) are tentatively identified with VDEs of 4.92 eV, 5.30 eV, and 5.58 eV, respectively. The weak peak labeled with "*" around 3.6

eV is likely due to contributions from CB_9^-, because these two clusters also have very close masses.

3-4. Theoretical Results

3-4.1. CB_9^-

The lowest energy isomers ($\Delta E < 50$ kcal/mol) revealed by the unbiased global minimum search at PBE0/6-31G were reoptimized with frequency calculations at the PBE0/6-311+G(d) level of theory (Fig. 3-2).[71] Single point CCSD(T)/6-311+G(2df) calculations were performed for the 10 lowest in energy isomers of CB_9^-, as shown in Fig. 3-2. All these structures are planar or quasi-planar and mostly are permutational isomers of either the global minimum structure or the structure analogous to the global minimum of B_{10}^-.[14] The lowest energy isomer **I.1** is a distorted wheel-type structure with the carbon atom occupying a peripheral position. The isomers **I.3**, **I.5**, **I.9**, and **I.10** are isostructural with the global minimum structure of B_{10}^- (Fig. 3-2), but are appreciably higher in energy. The structure **I.9**, which has a carbon atom in the central position, is 22.5 kcal/mol higher in energy than the global minimum. The preference for the peripheral position of the carbon atom is consistent with the previous findings for the CB_6^{2-}, CB_7^-, and CB_8 clusters.[39–

3-4.2. $C_2B_8^-$

The global minimum structure search for $C_2B_8^-$ at PBE0/6-31G(d) revealed 35 isomers within $\Delta E < 50$ kcal/mol. The isomers were reoptimized with frequency calculations at the PBE0/6-311+G(d) level of theory (Fig. 3-3).[71] Single point

CCSD(T)/6-311+G(2df) calculations were performed for the 10 lowest in energy isomers, as shown in Fig. 3-3. The global minimum structure **II.1** of $C_2B_8^-$ is very similar to the global minimum structure **I.1** of CB_9^-. The next 4 isomers (**II.2-II.5**), as well as the isomers **II.7-II.9**, are simply permutational isomers of the global minimum structure with the two carbon atoms occupying different peripheral positions. Interestingly, all structures with two neighboring carbon atoms are appreciably higher in energy (Fig. 3-3).[71]

3-5. Interpretation of the Photoelectron Spectra

3-5.1. CB_9^-

According to the theoretical calculations, only the lowest in energy isomer **I.1** of CB_9^- is expected to contribute to the experimental photoelectron spectra because the second lowest energy isomer is significantly higher in energy (by 9.9 kcal/mol). The calculated VDEs, at TD-PBE0, OVGF, and CCSD(T) levels, all with the 6-311+G(2df) basis set and at the PBE0/6-311+G(d) geometry, are compared with the experimental features in Table 3-1. The first peak X in the experimental spectrum of CB_9^- (Fig. 3-4) comes from electron detachment from the HOMO ($1a_2$) of the global minimum structure **I.1**, leading to the final doublet state $^2A_2$ (see Fig. 3-6 for the valence molecular orbital plots).[71] The three theoretical values for the first VDE, 3.53 eV (TD-PBE0), 3.54 eV (ROVGF), and 3.62 eV (CCSD(T)) are all in good agreement with the experimental value of 3.61 ± 0.03 eV. The observed vibrational frequency of 340 cm^{-1} agrees well with the totally symmetric mode ω_1 of the neutral ground state with a calculated frequency of 346 cm^{-1} (Table 3-3).[71] The band A corresponds to electron detachment

from HOMO-1 ($8a_1$) with the final doublet state $^2A_1$. Again, all three theoretical VDEs, 4.64, 4.49, and 4.57 eV at TD-PBE0, ROVGF, and CCSD(T), respectively, are in excellent agreement with each other and the experimental value of 4.49 ± 0.03 eV. Similarly, the bands B, C, and D can be assigned to electron detachments from HOMO-2 ($5b_2$), HOMO-3 ($2b_1$), and HOMO-4 ($7a_1$), respectively, resulting in the final $^2B_2$, $^2B_1$, and $^2A_1$ states. The corresponding theoretical VDEs also agree well with the experimental values (Table 3-1). The overall excellent agreement between the experimentally observed and the theoretically calculated VDEs confirms unequivocally the predicted global minimum structure **I.1** for CB_9^-.

3-5.2. $C_2B_8^-$

According to our calculations, the second lowest energy isomer of $C_2B_8^-$ (**II.2**) is only 1.6 kcal/mol higher than the global minimum structure **II.1**, and thus is anticipated to contribute to the experimental spectra. The VDEs calculated for both isomers are compared with the experimental data in Table 3-2. The valence canonical molecular orbitals for the global minimum of $C_2B_8^-$ are shown in Fig. 3-6. The first VDE of $C_2B_8^-$ **II.1** corresponds to the detachment from the singly occupied HOMO ($4a''$) to produce the ground state neutral C_2B_8 ($^1A'$). The VDE is calculated to be 2.78 eV (TD-PBE0) and 2.66 eV (CCSD(T)), which agree well with band X at 2.67 ± 0.03 eV. The observed vibrational structures with frequencies of 510 and 1480 cm^{-1} can be assigned to the ω_4 mode (553 cm^{-1}) and the ω_{14} mode (1465 cm^{-1}) and/or the ω_{15} mode (1483 cm^{-1}), respectively, as given in Table 3-4.[71] The next detachment channel from the doubly occupied HOMO-1 ($3a''$) yields a $^3A'$ final state with a VDE of 4.12 eV (TD-PBE0) and

4.21 eV (CCSD(T)), in good agreement with band A at 4.14 ± 0.03 eV in the spectra. Thus, neutral C_2B_8 is closed with a large HOMO-LUMO gap (1.47 eV), as defined by the X-A bands. The corresponding singlet final state ($^1A''$) from the HOMO-1 ($3a''$) state has a VDE of 5.11 eV at TD-PBE0, falling in the congested region D. The detachment from the HOMO-2 ($13a'$) gives rise to triplet ($3A''$) and singlet ($1A''$) final states with calculated VDEs of 4.52 and 4.89 eV at TD-PBE0, in excellent agreement with the observed bands B and C (Table 3-2).

The first VDE of the $C_2B_8^-$ low-lying isomer **II.2** is calculated to be 2.49 eV (TD-PBE0) and 2.38 eV (CCSD(T)), in excellent agreement with band X′ at 2.39 ± 0.03 eV; it corresponds to electron detachment from the singly occupied HOMO ($4a''$) to the lowest singlet state $^1A'$ of neutral **II.2**. The observed vibrational structures with frequencies of 390 and 1330 cm^{-1} can be assigned to the ω_2 mode (355 cm^{-1}) and the ω_{13} mode (1304 cm^{-1}), respectively, as given in Table 3-5.[71] The next detachment channel from HOMO-1 ($3a''$) of **II.2** is calculated to be 4.00 eV (TD-PBE0) and 4.10 eV (CCSD(T)), corresponding to band A′ at 4.05 eV. This detachment channel leads to the lowest triplet state ($^3A'$) of **II.2**. Thus, the X′ and A′ bands define a large HOMO-LUMO gap (1.66 eV) for the neutral of **II.2**. The higher detachment channels of isomer **II.2** and those of the global minimum start to overlap, leading to the congested spectral features in the higher binding energy range. The relatively lower intensities of bands X′ and A′ compared to the X and A bands, respectively, are consistent with the higher energy of isomer **II.2**. The good agreement between experimental and theoretical VDEs for both isomers **II.1** and **II.2** confirms firmly their structures and their energetic ordering.

3-6. Chemical Bonding

A single carbon substitution induces a major structural change to the B_{10}^- structure, giving rise to a rather peculiar global minimum for CB_9^-. Clearly, carbon prefers the lowest possible coordination site by bonding only to two boron atoms in a CB_2 triangle. The second carbon in $C_2B_8^-$ also prefers the low coordination peripheral sites, yielding two close-lying structures **II.1** and **II.2**. Neutral C_2B_8 is isoelectronic with CB_9^- and both isomers possess large HOMO-LUMO gaps, suggesting that the neutral C_2B_8 structures are both highly stable closed-shell electronic systems.

We performed chemical bonding analysis for the two clusters using the AdNDP. AdNDP analysis was performed for CB_9^- and for neutral C_2B_8 at the geometry of the lowest energy structure of $C_2B_8^-$. The chemical bonding in the CB_9^- cluster (Fig. 3-7(a)) can be described as a combination of seven 2c–2e B–B σ bonds and two 2c–2e C–B σ bonds (shown superimposed on a single molecular framework) responsible for the peripheral bonding in the cluster, four 3c–2e σ bonds responsible for the bonding between the central and peripheral atoms, and one 3c–2e and two 4c–2e π bonds also responsible for bonding between the central atom and the peripheral atoms. The AdNDP analysis for C_2B_8 (Fig. 3-7(b)) is nearly identical to that of CB_9^-. The presence of the eight delocalized σ electrons in both clusters makes them σ antiaromatic,[86] consistent with their in-plane distortions. Both clusters have six π electrons, rendering them π aromatic. Overall, the two clusters can be characterized as systems with conflicting aromaticity.

3-7. Summary

We performed a joint photoelectron spectroscopy and ab initio study of two carbon-boron mixed clusters, CB_9^- and $C_2B_8^-$. Computational global minimum searches revealed that both clusters have similar global minimum structures, which can be described as distorted wheel structures. Carbon atoms are found to occupy the peripheral positions in both cases, in agreement with previous findings for the CB_6^{2-}, CB_7^-, and CB_8 clusters.[39–41] The comparison of the experimental and theoretical VDEs for both clusters revealed that only the global minimum structure is responsible for the experimental spectra of CB_9^-, while two low-lying structures contribute to the experimental spectra for $C_2B_8^-$. The structural transition from B_{10}^- with two inner atoms to distorted wheel-like structures with a single inner atom in CB_9^- and $C_2B_8^-$ occurs in part because of the preference of carbon to form localized bonds. The AdNDP chemical bonding analyses revealed that CB_9^- and C_2B_8 are both π aromatic, but σ antiaromatic, consistent with their planar distorted structures.

References

[1]H. J. Zhai, L. S. Wang, A. N. Alexandrova, and A. I. Boldyrev, J. Chem. Phys. **117**, 7917 (2002).

[2]A. N. Alexandrova, A. I. Boldyrev, H. J. Zhai, L. S. Wang, E. Steiner, and P. W. Fowler, J. Phys. Chem. A **107**, 1359 (2003).

[3]A. N. Alexandrova, A. I. Boldyrev, H. J. Zhai, and L. S. Wang, J. Phys. Chem. A **108**, 3509 (2004).

[4]A. N. Alexandrova, A. I. Boldyrev, H. J. Zhai, and L. S. Wang, J. Chem. Phys. **122**, 054313 (2005).

[5]L. L. Pan, J. Li, and L. S. Wang, J. Chem. Phys. **129**, 024302 (2008).

[6]H. J. Zhai, A. N. Alexandrova, K. A. Birch, A. I. Boldyrev, and L. S. Wang, Angew. Chem., Int. Ed. **42**, 6004 (2003).

[7]A. N. Alexandrova, H. J. Zhai, L. S. Wang, and A. I. Boldyrev, Inorg. Chem. **43**, 3552 (2004).

[8]A. P. Sergeeva, D. Y. Zubarev, H. J. Zhai, A. I. Boldyrev, and L. S. Wang, J. Am. Chem. Soc. **130**, 7244 (2008).

[9]W. Huang, A. P. Sergeeva, H. J. Zhai, B. B. Averkiev, L. S. Wang, and A. I. Boldyrev, Nat. Chem. **2**, 202 (2010).

[10]A. P. Sergeeva, B. B. Averkiev, H. J. Zhai, A. I. Boldyrev, and L. S. Wang, J. Chem. Phys. **134**, 224304 (2011).

[11]Z. A. Piazza, W. L. Li, C. Romanescu, A. P. Sergeeva, L. S. Wang, and A. I. Boldyrev, J. Chem. Phys. **136**, 104310 (2012).

[12]A. P. Sergeeva, Z. A. Piazza, C. Romanescu, W. L. Li, A. I. Boldyrev, and L. S. Wang, J. Am. Chem. Soc. **134**, 18065 (2012).

[13]A. N. Alexandrova, A. I. Boldyrev, H. J. Zhai, and L. S. Wang, Coord. Chem. Rev. **250**, 2811 (2006).

[14]H. J. Zhai, B. Kiran, J. Li, and L. S. Wang, Nat. Mater. **2**, 827 (2003).

[15]B. Kiran, S. Bulusu, H. J. Zhai, S. Yoo, X. C. Zeng, and L. S. Wang, Proc. Natl. Acad. Sci. U.S.A. **102**, 961 (2005).

[16]C. Romanescu, D. J. Harding, A. Fielicke, and L. S. Wang, J. Chem. Phys. **137**, 014317 (2012).

[17]T. B. Tai, N. M. Tam, and M. T. Nguyen, Chem. Phys. Lett. **530**, 71 (2012).

[18]L. Cheng, J. Chem. Phys. **136**, 104301 (2012).

[19]E. Oger, N. R. M. Crawford, R. Kelting, P. Weis, M. M. Kappes, and R. Ahlrichs, Angew. Chem., Int. Ed. **46**, 8503 (2007).

[20]L. Hanley, J. L. Whitten, and S. L. Anderson, J. Phys. Chem. **92**, 5803 (1988).

[21]P. A. Hintz, S. A. Ruatta, and S. L. Anderson, J. Chem. Phys. **92**, 292 (1990).

[22]S. A. Ruatta, P. A. Hintz, and S. L. Anderson, J. Chem. Phys. **94**, 2833 (1991).

[23]R. Kawai and J. H. Weare, J. Chem. Phys. **95**, 1151 (1991).

[24]R. Kawai and J. H. Weare, Chem. Phys. Lett. **191**, 311 (1992).

[25]I. Boustani, Int. J. Quantum Chem. **52**, 1081 (1994).

[26]I. Boustani, Chem. Phys. Lett. **233**, 273 (1995).

[27]I. Boustani, Chem. Phys. Lett. **240**, 135 (1995).

[28]A. Ricca and C. W. Bauschlicher Jr., Chem. Phys. **208**, 233 (1996).

[29]I. Boustani, Surf. Sci. **370**, 355 (1997).

[30]F. L. Gu, X. Yang, A.-C. Tang, H. Jiao, and P. v. R. Schleyer, J. Comput. Chem. **19**, 203 (1998).

[31]J. E. Fowler and J. M. Ugalde, J. Phys. Chem. A **104**, 397 (1999).

[32]J. Aihara, J. Phys. Chem. A **105**, 5486 (2001).

[33]D. Y. Zubarev and A. I. Boldyrev, J. Comput. Chem. **28**, 251 (2007).

[34]P. W. Fowler and B. R. Gray, Inorg. Chem. **46**, 2892 (2007).

[35]B. P. T. Fokwa and M. Hermus, Angew. Chem., Int. Ed. **51**, 1702 (2012).

[36]K. Exner and P. v. R. Schleyer, Science **290**, 1937 (2000).

[37]Z.-X. Wang and P. v. R. Schleyer, Science **292**, 2465 (2001).

[38]R. M. Minyaev, T. N. Gribanova, A. G. Starikov, and V. I. Minkin, Mendeleev Commun. **11**, 213 (2001).

[39]L. M. Wang, W. Huang, B. B. Averkiev, A. I. Boldyrev, and L. S. Wang, Angew. Chem., Int. Ed. **46**, 4550 (2007).

[40]B. B. Averkiev, D. Y. Zubarev, L. M. Wang, W. Huang, L. S. Wang, and A. I. Boldyrev, J. Am. Chem. Soc. **130**, 9248 (2008).

[41]B. B. Averkiev, L. M. Wang, W. Huang, L. S. Wang, and A. I. Boldyrev, Phys. Chem. Chem. Phys. **11**, 9840 (2009).

[42]Y. Pei and X. C. Zeng, J. Am. Chem. Soc. **130**, 2580 (2008).

[43]C. Romanescu, A. P. Sergeeva, W. L. Li, A. I. Boldyrev, and L. S. Wang, J. Am. Chem. Soc. **133**, 8646 (2011).

[44]T. R. Galeev, C. Romanescu, W. L. Li, L. S. Wang, and A. I. Boldyrev, J. Chem. Phys. **135**, 104301 (2011).

[45]W. L. Li, C. Romanescu, T. R. Galeev, L. S. Wang, and A. I. Boldyrev, J. Phys. Chem. A **115**, 10391 (2011).

[46]R. Islas, T. Heine, K. Ito, P. v. R. Schleyer, and G. Merino, J. Am. Chem. Soc. **129**, 14767 (2007).

[47]B. B. Averkiev and A. I. Boldyrev, Russ. J. Gen. Chem. **78**, 769 (2008).

[48]K. Ito, Z. Pu, Q.-S. Li, and P. v. R. Schleyer, Inorg. Chem. **47**, 10906 (2008).

[49]J. Guo, W. Yao, Z. Li, and S. Li, Sci. China Ser. B: Chem. **52**, 566 (2009).

[50]C. Miao, J. Guo, and S. Li, Sci. China Ser. B: Chem. **52**, 900 (2009).

[51]Z. Pu, K. Ito, P. v. R. Schleyer, and Q.-S. Li, Inorg. Chem. **48**, 10679 (2009).

[52]Y. Liao, C. L. Cruz, P. v. R. Schleyer, and Z. Chen, Phys. Chem. Chem. Phys. **14**, 14898 (2012).

[53]W. L. Li, C. Romanescu, T. R. Galeev, Z. A. Piazza, A. I. Boldyrev, and L. S. Wang, J. Am. Chem. Soc. **134**, 165 (2011).

[54]C. Romanescu, T. R. Galeev, W. L. Li, A. I. Boldyrev, and L. S. Wang, Angew. Chem., Int. Ed. **50**, 9334 (2011).

[55]T. R. Galeev, C. Romanescu, W. L. Li, L. S. Wang, and A. I. Boldyrev, Angew. Chem., Int. Ed. **51**, 2101 (2012).

[56]C. Romanescu, T. R. Galeev, A. P. Sergeeva, W. L. Li, L. S. Wang, and A. I. Boldyrev, J. Organomet. Chem. **721–722**, 148 (2012).

[57]T. Heine and G. Merino, Angew. Chem., Int. Ed. **51**, 4275 (2012).

[58]L. M. Wang, B. B. Averkiev, J. A. Ramilowski, W. Huang, L. S. Wang, and A. I. Boldyrev, J. Am. Chem. Soc. **132**, 14104 (2010).

[59]T. R. Galeev, A. S. Ivanov, C. Romanescu, W. L. Li, K. V. Bozhenko, L. S. Wang, and A. I. Boldyrev, Phys. Chem. Chem. Phys. **13**, 8805 (2011).

[60]M. T. Huynh and A. N. Alexandrova, J. Phys. Chem. Lett. **2**, 2046 (2011).

[61]T. R. Galeev and A. I. Boldyrev, Phys. Chem. Chem. Phys. **13**, 20549 (2011).

[62]A. S. Ivanov, K. V. Bozhenko, and A. I. Boldyrev, J. Chem. Theory Comput. **8**, 135 (2012).

[63]A. S. Ivanov and A. I. Boldyrev, J. Phys. Chem. A **116**, 9591 (2012).

[64]M. Savoca, A. Lagutschenkov, J. Langer, D. J. Harding, A. Fielicke, and O. Dopfer, J. Phys. Chem. A, **117**, 1158 (2013).

[65]J. Fan and L. S. Wang, J. Chem. Phys. **102**, 8714 (1995).

[66]B. B. Averkiev, Ph.D. thesis, Utah State University, Logan, UT (2009).

[67]J. P. Perdew, K. Burke, and M. Ernzerhof, Phys. Rev. Lett. **77**, 3865 (1996).

[68]C. Adamo and V. Barone, J. Chem. Phys. **110**, 6158 (1999).

[69]W. J. Hehre, R. Ditchfield, and J. A. Pople, J. Chem. Phys. **56**, 2257 (1972).

[70]R. Krishnan, J. S. Binkley, R. Seeger, and J. A. Pople, J. Chem. Phys. **72**, 650 (1980).

[71]See supplementary material at http://dx.doi.org/10.1063/1.4770231 for optimized isomers of CB_9^- and $C_2B_8^-$, valence canonical molecular orbital plots for the lowest energy structures of CB_9^- and $C_2B_8^-$, and vibrational frequencies for the neutral CB_9 and C_2B_8.

[72]G. D. Purvis and R. J. Bartlett, J. Chem. Phys. **76**, 1910 (1982).

[73]K. Raghavachari, G. W. Trucks, J. A. Pople, and M. Head-Gordon, Chem. Phys. Lett. **157**, 479 (1989).

[74]J. Čížek, in Advances in Chemical Physics (Wiley, 2007), pp. 35–89.

[75]R. Bauernschmitt and R. Ahlrichs, Chem. Phys. Lett. **256**, 454 (1996).

[76]M. E. Casida, C. Jamorski, K. C. Casida, and D. R. Salahub, J. Chem. Phys. **108**, 4439 (1998).

[77]L. S. Cederbaum, J. Phys. B **8**, 290 (1975).

[78]J. V. Ortiz, Int. J. Quantum Chem. **36**(S23), 321 (1989).

[79]J.-S. Lin and J. V. Ortiz, Chem. Phys. Lett. **171**, 197 (1990).

[80]V. G. Zakrzewski, J. V. Ortiz, J. A. Nichols, D. Heryadi, D. L. Yeager, and J. T. Golab, Int. J. Quantum Chem. **60**, 29 (1996)

[81]D. Y. Zubarev and A. I. Boldyrev, Phys. Chem. Chem. Phys. **10**, 5207 (2008).

[82]M. J. Frisch, G. W. Trucks, H. B. Schlegel et al., GAUSSIAN 09, Revision B.01, Gaussian, Inc., Wallingford, CT, 2009.

[83]H.-J. Werner, P. J. Knowles, G. Knizia, F. R. Manby, M. Schutz et al., MOLPRO, version 2010.1, a package of ab initio programs, 2010, see http://www.molpro.net.

[84]M. U. Varetto, Swiss National Supercomputing Centre, Manno, Switzerland, 2009.

[85]See http://www.chemcraftprog.com for information about the Chemcraft program.

[86]J. Chandrasekhar, E. D. Jemmis, and P. v. R. Schleyer, Tetrahedron Lett. **20**, 3707 (1979)

TABLE 3-1. Observed vertical electron detachment energies (VDEs) of **I.1** CB_9^- compared with the theoretically calculated values for the lowest isomer of CB_9^-. All energies are in eV.

Observed features	VDE (exp)[a]	Final State and Electronic Configuration	VDE (theoretical)		
			TD-PBE0[b]	ROVGF[c]	CCSD(T)[d]
I.1 CB_9^- (C_{2v}, $^1A_1$)					
X	3.61 (3)	$^2A_2 \ldots 7a_1^{(2)}\ 2b_1^{(2)}\ 5b_2^{(2)}\ 8a_1^{(2)}\ 1a_2^{(1)}$	3.53	3.54 (0.88)	3.62
A	4.49 (3)	$^2A_1 \ldots 7a_1^{(2)}\ 2b_1^{(2)}\ 5b_2^{(2)}\ 8a_1^{(1)}\ 1a_2^{(2)}$	4.64	4.49 (0.88)	4.57
B	4.88 (4)	$^2B_2 \ldots 7a_1^{(2)}\ 2b_1^{(2)}\ 5b_2^{(1)}\ 8a_1^{(2)}\ 1a_2^{(2)}$	4.88	4.88 (0.88)	4.93
C	5.74 (4)	$^2B_1 \ldots 7a_1^{(2)}\ 2b_1^{(1)}\ 5b_2^{(2)}\ 8a_1^{(2)}\ 1a_2^{(2)}$	5.67	5.73 (0.87)	5.74
D	6.2 (1)	$^2A_1 \ldots 7a_1^{(1)}\ 2b_1^{(2)}\ 5b_2^{(2)}\ 8a_1^{(2)}\ 1a_2^{(2)}$	5.96	6.05 (0.84)	

[a] Numbers in parentheses represent the uncertainty in the last digit.
[b] VDEs were calculated at TD-PBE0/6-311+G(2*df*)//PBE0/6-311+G(*d*).
[c] VDEs were calculated at ROVGF/6-311+G(2*df*)//PBE0/6-311+G(*d*). Values in parentheses represent the pole strength of the OVGF calculation.
[d] VDEs were calculated at CCSD(T)/6-311+G(2*df*)//PBE0/6-311+G(*d*).

TABLE 3-2. Observed vertical detachment energies (VDEs) of $C_2B_8^-$ compared with the calculated values for the two lowest energy isomers of $C_2B_8^-$. All energies are in eV.

Observed Features	VDE (exp)[a]	Final State and Electronic Configuration	VDE (theoretical)[b]	
			TD-PBE0[c]	CCSD(T)[d]
II.1 $C_2B_8^-$ (C_s, ^{2}A“)				
X	2.67 (3)	^{1}A‘ … 11a‘$^{(2)}$ 12a‘$^{(2)}$ 2a“$^{(2)}$ 13a‘$^{(2)}$ 3a“$^{(2)}$ 4a“$^{(0)}$	2.78	2.66
A	4.14 (3)	^{3}A‘ … 11a‘$^{(2)}$ 12a‘$^{(2)}$ 2a“$^{(2)}$ 13a‘$^{(2)}$ 3a“$^{(1)}$ 4a“$^{(1)}$	4.12	4.21
B	4.52 (3)	^{3}A“ … 11a‘$^{(2)}$ 12a‘$^{(2)}$ 2a“$^{(2)}$ 13a‘$^{(1)}$ 3a“$^{(2)}$ 4a“$^{(1)}$	4.52	4.51
C	4.92 (5)	^{1}A“ … 11a‘$^{(2)}$ 12a‘$^{(2)}$ 2a“$^{(2)}$ 13a‘$^{(1)}$ 3a“$^{(2)}$ 4a“$^{(1)}$	4.89	
D	5.30 (5)	^{1}A“ … 11a‘$^{(2)}$ 12a‘$^{(2)}$ 2a“$^{(2)}$ 13a‘$^{(2)}$ 3a“$^{(1)}$ 4a“$^{(1)}$	5.11	
		^{3}A‘ … 11a‘$^{(2)}$ 12a‘$^{(2)}$ 2a“$^{(1)}$ 13a‘$^{(2)}$ 3a“$^{(2)}$ 4a“$^{(1)}$	5.23	
E	5.58 (5)	^{3}A“ … 11a‘$^{(2)}$ 12a‘$^{(1)}$ 2a“$^{(2)}$ 13a‘$^{(2)}$ 3a“$^{(2)}$ 4a“$^{(1)}$	5.58	
		^{3}A“ … 11a‘$^{(1)}$ 12a‘$^{(2)}$ 2a“$^{(2)}$ 13a‘$^{(2)}$ 3a“$^{(2)}$ 4a“$^{(1)}$	5.83	
II.2 $C_2B_8^-$ (C_s, ^{2}A“)				
X’	2.39 (3)	^{1}A' … 11a'$^{(2)}$ 2a”$^{(2)}$ 12a'$^{(2)}$ 13a'$^{(2)}$ 3a”$^{(2)}$ 4a”$^{(0)}$	2.49	2.38
A’	4.05 (3)	^{3}A' … 11a'$^{(2)}$ 2a”$^{(2)}$ 12a'$^{(2)}$ 13a'$^{(2)}$ 3a”$^{(1)}$ 4a”$^{(1)}$	4.00	4.10
		^{3}A“ … 11a'$^{(2)}$ 2a”$^{(2)}$ 12a'$^{(2)}$ 13a'$^{(1)}$ 3a”$^{(2)}$ 4a”$^{(1)}$	4.61	4.57
		^{1}A' … 11a'$^{(2)}$ 2a”$^{(2)}$ 12a'$^{(2)}$ 13a'$^{(2)}$ 3a”$^{(1)}$ 4a”$^{(1)}$	4.90	
		^{1}A“ … 11a'$^{(2)}$ 2a”$^{(2)}$ 12a'$^{(2)}$ 13a'$^{(1)}$ 3a”$^{(2)}$ 4a”$^{(1)}$	4.96	
		^{3}A“ … 11a'$^{(2)}$ 2a”$^{(2)}$ 12a'$^{(1)}$ 13a'$^{(2)}$ 3a”$^{(2)}$ 4a”$^{(1)}$	5.29	
		^{1}A“ … 11a'$^{(2)}$ 2a”$^{(2)}$ 12a'$^{(1)}$ 13a'$^{(2)}$ 3a”$^{(2)}$ 4a”$^{(1)}$	5.54	
		^{3}A“ … 11a'$^{(2)}$ 2a”$^{(1)}$ 12a'$^{(2)}$ 13a'$^{(2)}$ 3a”$^{(2)}$ 4a”$^{(1)}$	5.63	
		^{3}A“ … 11a'$^{(1)}$ 2a”$^{(2)}$ 12a'$^{(2)}$ 13a'$^{(2)}$ 3a”$^{(2)}$ 4a”$^{(1)}$	6.08	

[a] Numbers in parentheses represent the uncertainty in the last digit.
[b] OVGF/6-311+G(2*df*) energies are not reported for $C_2B_8^-$ due to high spin contamination observed in the calculation.
[c] VDEs were calculated at TD-PBE0/6-311+G(2*df*)//PBE0/6-311+G(*d*).
[d] VDEs were calculated at CCSD(T)/6-311+G(2*df*)//PBE0/6-311+G(*d*).

TABLE 3-3. Vibrational frequencies for the neutral I.1A CB_9 (C_{2v}, $^2A_2$) at PBE0/6-311+G(*d*)

	ω (a_1), cm^{-1}		ω (a_2), cm^{-1}		ω (b_1), cm^{-1}		ω (b_2), cm^{-1}
1	346	**10**	161	**13**	132	**17**	318
2	514	**11**	378	**14**	274	**18**	423
3	631	**12**	492	**15**	334	**19**	595
4	671			**16**	488	**20**	623
5	778					**21**	839
6	958					**22**	1068
7	1267					**23**	1345
8	1448					**24**	1623
9	1556						

TABLE 3-4. Vibrational frequencies for the neutral II.1A C_2B_8 (C_s, $^1A'$) at PBE0/6-311+G(*d*)

	ω (a'), cm^{-1}		ω (a'), cm^{-1}		ω (a"), cm^{-1}
1	334	**10**	859	**18**	140
2	390	**11**	958	**19**	187
3	444	**12**	1116	**20**	296
4	553	**13**	1284	**21**	409
5	600	**14**	1465	**22**	426
6	648	**15**	1483	**23**	486
7	653	**16**	1615	**24**	519
8	683	**17**	1743		
9	786				

TABLE 3-5. Vibrational frequencies for the neutral II.2A C_2B_8 (C_s, $^1A'$) at PBE0/6-311+G(*d*)

	ω (a'), cm^{-1}		ω (a'), cm^{-1}		ω (a"), cm^{-1}
1	311	**10**	893	**18**	132
2	355	**11**	1001	**19**	192
3	467	**12**	1174	**20**	314
4	552	**13**	1304	**21**	368
5	619	**14**	1412	**22**	445
6	638	**15**	1527	**23**	492
7	658	**16**	1590	**24**	510
8	683	**17**	1727		
9	801				

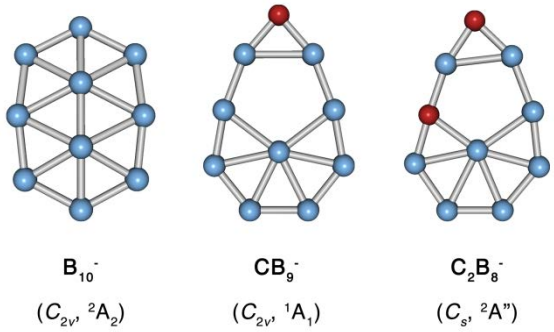

FIG. 3-1. Global minima structures of B_{10}^- (Ref. 14), CB_9^-, and $C_2B_8^-$.

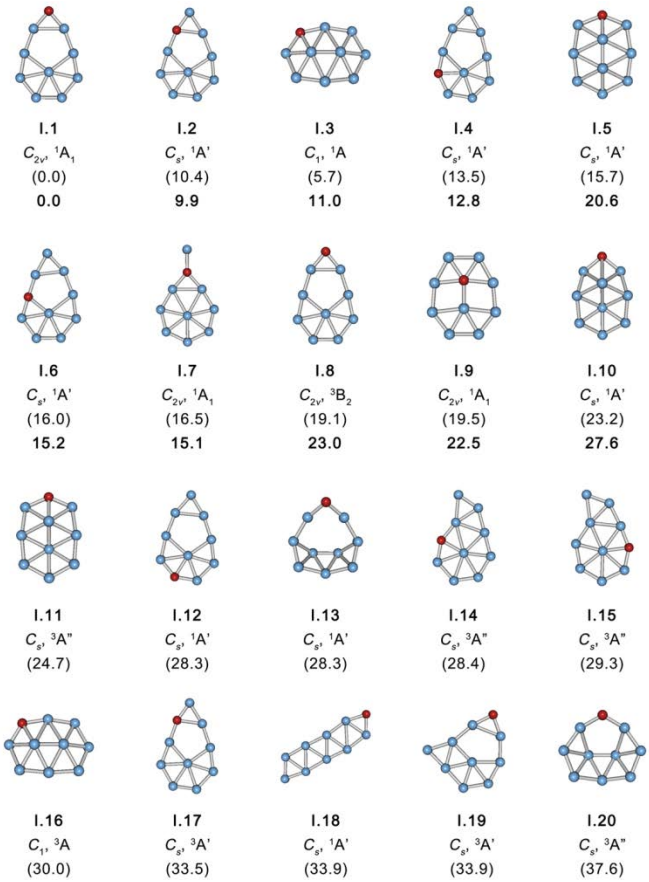

FIG. 3-2. Structures of the lowest found isomers of CB_9^-, their point group symmetries and spectroscopic states. ZPE corrected relative energies are given at PBE0/6-311+G(*d*) in parentheses. CCSD(T)/6-311+G(2*df*)//PBE0/6-311+G(*d*) energies (ZPE PBE0/6-311+G(*d*)) are given for the 10 lowest found isomers (bold). All energies are in kcal/mol.

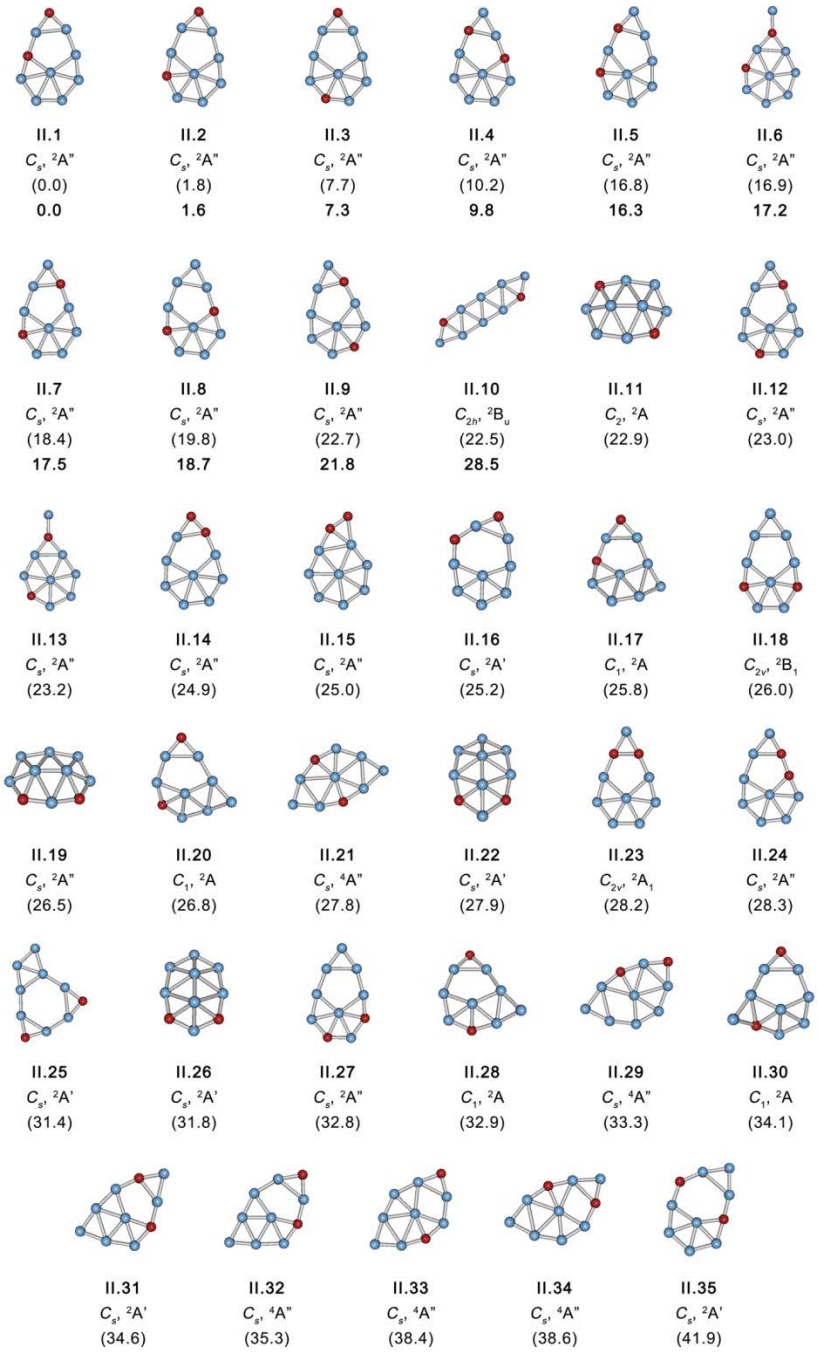

FIG. 3-3. Structures of the lowest found isomers of $C_2B_9^-$, their point group symmetries and spectroscopic states. ZPE corrected relative energies are given at PBE0/6-311+G(*d*) in parentheses. CCSD(T)/6-311+G(2*df*)//PBE0/6-311+G(*d*) energies (ZPE PBE0/6-311+G(*d*)) are given for the 10 lowest found isomers (bold). All energies are in kcal/mol.

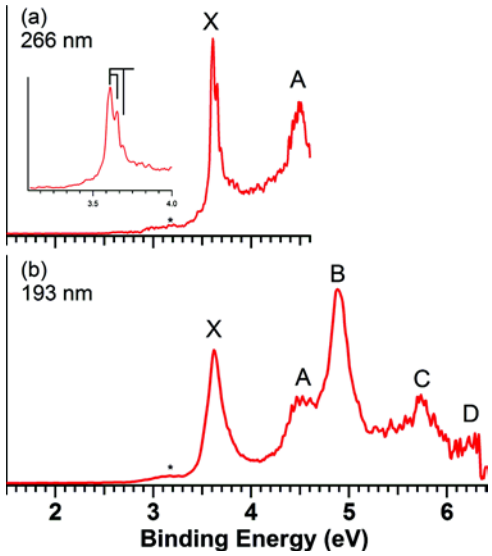

FIG. 3-4. Photoelectron spectra of CB_9^- at (a) 266 nm (4.661 eV) and (b) 193 nm (6.424 eV). The inset in (a) shows the resolved vibrational structures in band X.

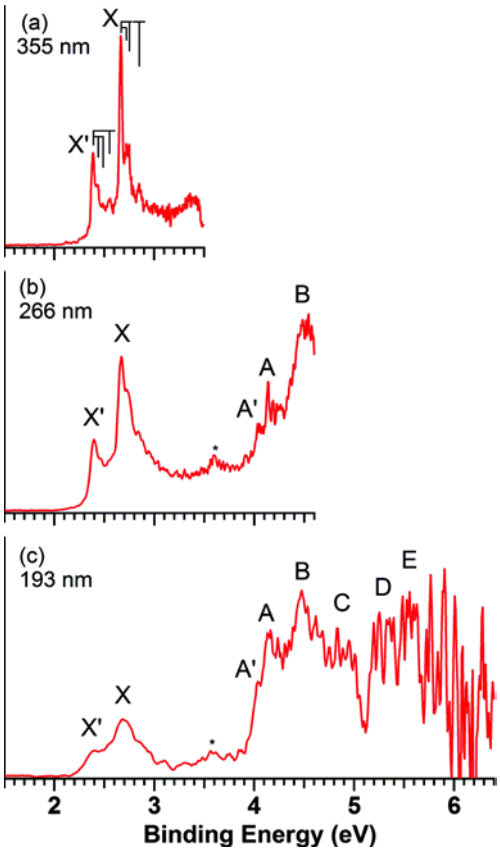

FIG. 3-5. Photoelectron spectra of $C_2B_9^-$ at (a) 355 nm (3.496 eV), (b) 266 nm, and (c) 193 nm. The vertical lines in (a) show the resolved vibrational structures

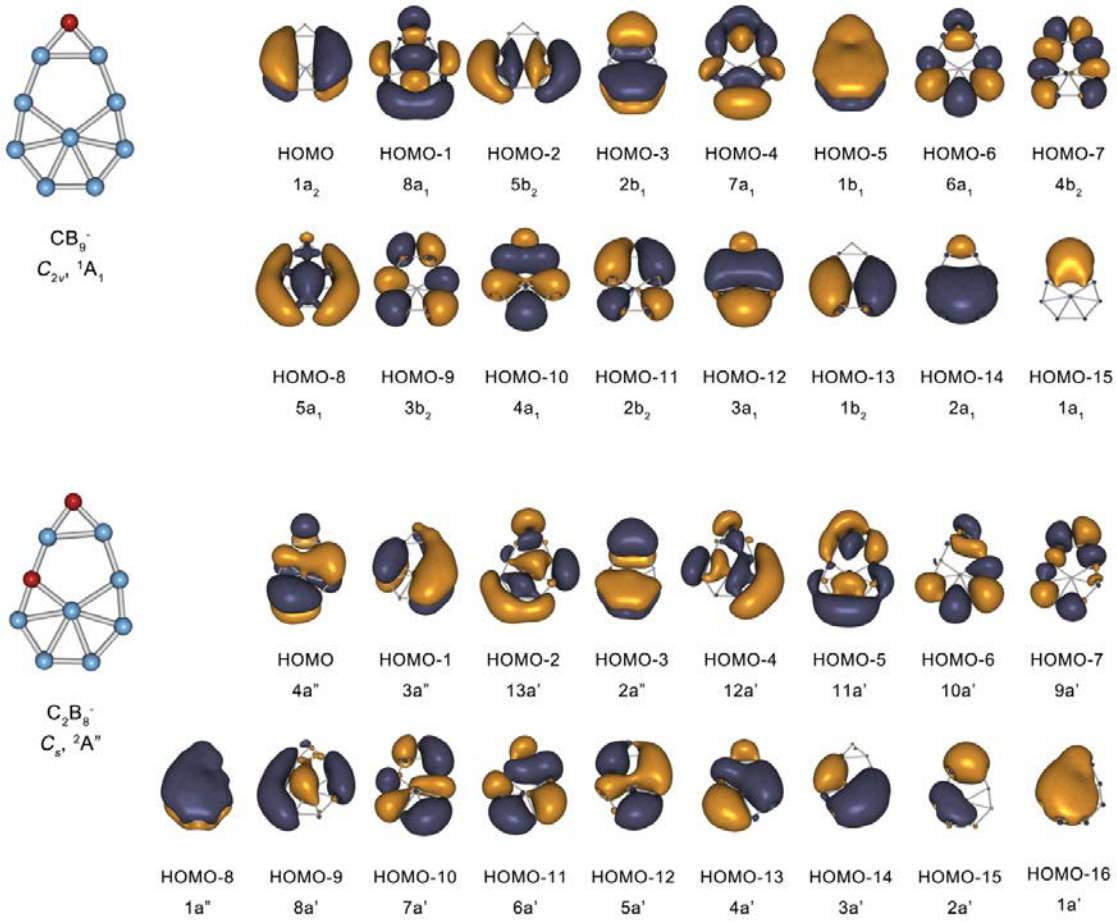

FIG. 3-6. Valence CMOs of CB_9^- and $C_2B_9^-$ global minima

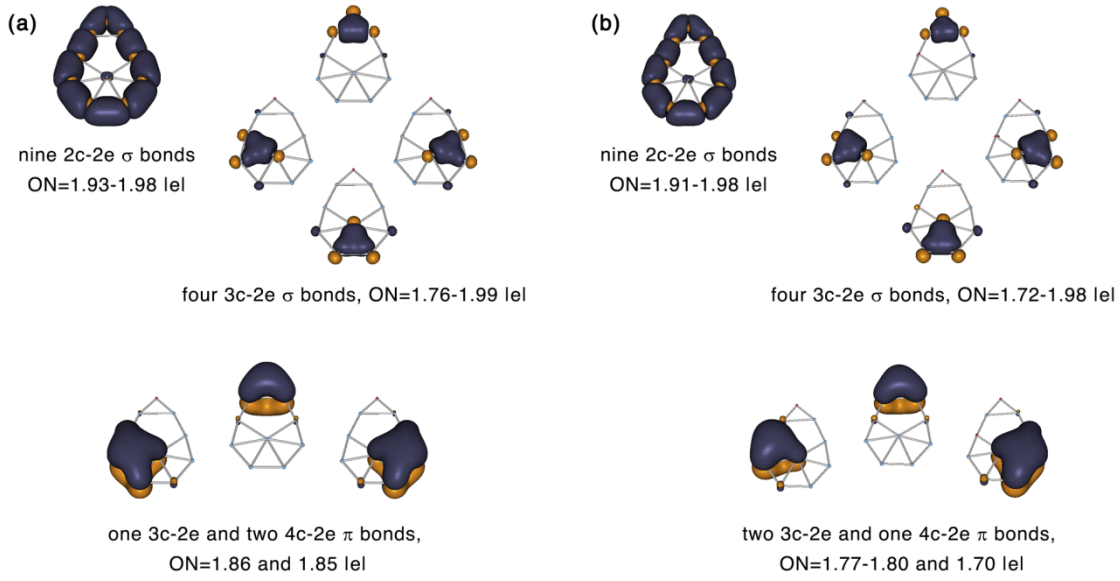

FIG. 3-7. Adaptive natural density partitioning chemical bonding analysis for (a) CB_9^- and (b) C_2B_8 at the geometry optimized for $C_2B_8^-$

CHAPTER 4

VALENCE ISOELECTRONIC SUBSTITUTION IN THE B_8^- AND B_9^- MOLECULAR WHEELS BY AN Al DOPANT ATOM: UMBRELLA-LIKE STRUCTURES OF AlB_7^- AND AlB_8^- *

Abstract

The structures and the electronic properties of two aluminum-doped boron clusters, AlB_7^- and AlB_8^-, were investigated using photoelectron spectroscopy and *ab initio* calculations. The photoelectron spectra of AlB_7^- and AlB_8^- are both broad, suggesting significant geometry changes between the ground states of the anions and the neutrals. Unbiased global minimum searches were carried out and the calculated vertical electron detachment energies were used to compare with the experimental data. We found that the Al atom does not simply replace a B atom in the parent B_8^- and B_9^- planar clusters in AlB_7^- and AlB_8^-. Instead, the global minima of the two doped-clusters are of umbrella shapes, featuring an Al atom interacting ionically with a hexagonal and heptagonal pyramidal B_7 (C_{6v}) and B_8 (C_{7v}) fragment, respectively. These unique umbrella-type structures are understood on the basis of the special stability of the quasi-planar B_7^{3-} and planar B_8^{2-} molecular wheels derived from double aromaticity.

---

* Coauthored by Timur R. Galeev, Constantin Romanescu, Wei-Li Li, Lai-Sheng Wang, and Alexander I. Boldyrev. Reprinted with permission from *J. Chem. Phys*. **2011**, *135*, 104301. Copyright 2011, AIP Publishing LLC

4-1. Introduction

The eight- and nine-atom anionic clusters of boron form beautiful molecular wheels with a central B atom and a monocyclic B_7 and B_8 ring, respectively.[1] The chemical bonding in these molecular wheels is interesting. The peripheral B_7 and B_8 rings are bonded by classical two-center-two-electron (2c–2e) bonds, whereas the central B atom is bonded with the outer ring via three delocalized σ and three delocalized π bonds. Thus, the negatively charged nine-atom (B_9^-) cluster with 28 valence electrons is closed shell with a perfect D_{8h} symmetry. Among its 28 valence electrons, 16 are used to form 8 classical 2c–2e peripheral bonds, 6 are used to form three delocalized σ bonds, and the remaining 6 electrons form three delocalized π bonds. The delocalized σ and π bonding each conform with the (4n + 2) Hückel rule for aromaticity, giving rise to double aromaticity and high electronic stability for the B_9^- molecular wheel. To fulfill the double aromaticity, the eight-atom cluster requires 26 valence electrons: 14 for the seven classical peripheral 2c–2c B–B bonds, 6 delocalized σ electrons, and 6 delocalized π electrons. Thus, the B_8^{2-} cluster is a closed shell system with a perfect D_{7h} symmetry, whereas the B_8^- cluster with 25 valence electrons possesses a planar C_{2v} structure slightly distorted from the D_{7h} structure due to the Jahn-Teller effect because the highest occupied molecular orbital (HOMO) is a doubly degenerate orbital ($1e_1''$). The neutral B_8 cluster possesses a perfect D_{7h} structure with a half-filled HOMO ($1e_1''^2$) and a triplet ground electronic state ($^3A_2$). In the present article, we address the issue of valence isoelectronic substitution by an Al atom in the B_8 and B_9 molecular wheels. Understanding the

structures of the doped clusters, AlB_7^- and AlB_8^-, will provide further insight into the bonding and stability of the planar boron clusters.[2,3]

Despite recent advances in the spectroscopy of boron clusters,[2] relatively little is known about metal-doped boron clusters. There are only two prior joint experimental and theoretical studies characterizing metal-doped boron clusters, namely $Au_2B_7^-$ and AuB_{10}^-.[4,5] It was found that in the global minimum structures gold mimics the behavior of H atoms,[6] i.e., the gold atoms are covalently bonded to the corresponding boron clusters. Mass spectra of $Al_nB_m^-$ clusters have been reported,[7] as well as photoelectron spectra of one or two B atoms doped aluminum clusters.[8] A number of theoretical calculations on Al–B mixed clusters have also been reported.[9–12] Theoretical studies on neutral AlB_9, suggest a D_{9h} global minimum with Al in the center of a B_9 ring.[9,12]

Recently, we reported a joint PES and computational study of two Al doped boron clusters, AlB_6^- and AlB_{11}^-, aimed at investigating the structural effects of valence isoelectronic substitution on two quasi-planar boron clusters: B_7^- ($^3A_1$, C_{6v}) and B_{12}^- ($^2A'$, C_s).[13] We showed that the Al atom replaces a peripheral B atom. Such substitution slightly expands the circumferences of the clusters and induces planarization in AlB_6^- and AlB_{11}^- relative to the quasi-planar parent boron clusters. In the current article, we expand the scope of our initial study and examine the structural changes of the molecular wheels (B_8^- and B_9^-) upon B-atom substitution by Al. We have obtained photoelectron spectra of AlB_7^- and AlB_8^- at two photodetachment laser energies, 6.424 and 4.661 eV. Unbiased global minimum searches were used to find the lowest energy isomers. One should not expect that geometries of the aluminum-doped clusters are the same as the

global minimum structures of unsubstituted ones. Indeed, in this work, we found that AlB_7^- and AlB_8^- have different geometries compared to B_8^- and B_9^-. We show that in both cases the Al atom is ionically bonded to a quasi-planar boron cluster, C_{6v} B_7 and C_{7v} B_8, respectively, similar to the LiB_8^- cluster reported earlier.[14] We would like to mention two recent comprehensive reviews[15,16] on negative molecular ions where various theoretical techniques and applications were discussed.

4-2. Experimental Method

The experiment was performed using a magnetic-bottle PES apparatus equipped with a laser vaporization cluster source, details of which have been published Refs. 17 and 18. Briefly, the aluminum-doped boron clusters were produced by laser vaporization of a disk target made of isotopically enriched ^{10}B (~10wt. %), Al (~2.5wt. %), balanced by Bi. The ^{11}B to ^{10}B ratio is 1:24. The clusters entrained in the helium carrier gas underwent a supersonic expansion to form a collimated molecular beam. The cluster composition and temperature to some degree were controlled by the time delay between the pulsed He carrier gas and the vaporization laser.[19,20] To achieve an even higher degree of vibrational cooling of the clusters some experiments were carried out using a mixture of 5% Ar in He as a carrier gas. The last approach was previously shown to produce cold gold cluster anions via the observation of Ar-tagged gold clusters.[21] The negatively charged clusters were extracted from the cluster beam and analyzed with a time-of-flight mass spectrometer. The clusters of interest were mass-selected and decelerated before being intercepted by the probe photodetachment laser beam: 193 nm (6.424 eV) from an ArF excimer laser and 266 nm (4.661 eV) from an Nd:YAG laser. Photoelectrons were

collected at nearly 100% efficiency by a magnetic bottle and analyzed in a 3.5 m long electron flight tube. The photoelectron spectra were calibrated using the known spectra of Bi^-. The kinetic energy resolution of the magnetic bottle apparatus, $\Delta E/E$, was typically better than 2.5%, i.e., ~25 meV for 1 eV electrons.

4-3. Theoretical Methods

The computational search for the global minima of the AlB_7^- and AlB_8^- clusters was performed using the Coalescence Kick (CK) program written by Averkiev.[22] The CK method subjects large populations of randomly generated structures to a coalescence procedure in which all atoms are pushed gradually to the molecular center of mass to avoid generation of fragmented structures and then optimized to the nearest local minima. The CK calculations were performed using the B3LYP (Refs. 23–25) hybrid method with the small split-valence basis set 3–21G.[26] The low-lying isomers revealed by the search were reoptimized with follow-up frequency calculations at the B3LYP level of theory using the 6–311+G* basis set.[27–30] To avoid high spin contaminations, single point calculations for the lowest energy structures of AlB_7^- (doublet ground state) were performed using the restricted coupled cluster [RCCSD(T)] method[31–33] with the 6–311+G(2*df*) basis set at the B3LYP/6–311+G* optimized geometries. Single-point calculations for the lowest energy structures of AlB_8^- (singlet ground state) were done using the coupled cluster [RCCSD(T)] method with the 6–311+G(2*df*) basis set at the B3LYP/6–311+G* optimized geometries.

The vertical electron detachment energies (VDEs) were calculated using the UCCSD(T)/6–311+G(2df) method, the outer valence Green function method[34–37]

[R(U)OVGF/6–311+G(2*df*)] and the time-dependent DFT method,[36,37] TD-B3LYP/6–311+G(2*df*),[38,39] and TD-PBE1PBE/6–311+G(2*df*),[40,41] all at the B3LYP/6–311+G* optimized geometries. In the last approach, for AlB_8^-, the first VDE was calculated as the lowest transition from the singlet state of the AlB_8^- anion into the final lowest doublet state of the neutral AlB_8 species at the geometry optimized for the anion. Then, the vertical excitation energies of the neutral species calculated at the anion geometry were added to the first VDE to obtain the second and higher VDEs. For AlB_7^-, the first two VDEs were calculated as the lowest transition from the doublet ground state of the anion into the final lowest singlet and triplet states of the neutral species at the anion geometry at the geometry optimized for the anion. Then, in order to obtain higher VDEs, the vertical excitation energies of the neutral species at the anion geometry calculated for the singlet and triplet states were added to the two lowest VDEs with the singlet and triplet final states, respectively. Core electrons were frozen in treating the electron correlation at the CCSD(T) and OVGF levels of theory.

Chemical bonding analysis was performed using the natural bond orbital (NBO) (Refs. 42–44) analysis. The B3LYP, UCCSD(T), R(U)OVGF, and TD-B3LYP calculations were performed using the GAUSSIAN 03 software[45] and RCCSD(T) calculations were performed using the MOLPRO program.[46] The MOLDEN 3.4 (Ref. 47) and MOLEKEL 5.4.0.8 (Ref. 48) programs were used for molecular structure visualizations.

4-4. Experimental Results

The photoelectron spectra of AlB_7^- and AlB_8^- at 266 and 193 nm are shown in Figs. 4-1 and 4-2, respectively. The major detachment features are labeled with letters and the measured vertical detachment energies are given in Tables 4-1 and 4-2, where they are compared with theoretical calculations at various levels (*vide infra*). Commonly, the peak marked as X represents the transition between the ground electronic states of the anion and the neutral species, while the higher binding energy peaks (A, B…) denote transitions to excited electronic states of the neutral cluster.

4-4.1. AlB_7^-

A single broad band is observed in the 266 nm spectrum of AlB_7^- (Fig. 4-1(a)) with a VDE of 3.3 ± 0.1 eV. There seems to be a shoulder on the higher binding energy side, suggesting that the band may contain multiple electronic transitions.

Under our experimental conditions, the clusters were fairly cold, as shown, recently, in our studies of AlB_6^- and AlB_{11}^-.[13] Thus, the broad PES band observed suggests a large geometry change between the ground states of the AlB_7^- anion and that of AlB_7 neutral. The broad band and the long tail on the lower binding energy side prevent us from accurately measuring the adiabatic detachment energy. Only a detachment threshold can be estimated to be ~2.8 eV. The 193 nm spectrum reveals two additional strong PES bands, A and B. The A band with a VDE of 4.89 ± 0.06 eV is broad and contains shoulder in both the lower and higher binding energy sides, suggesting that it contains multiply detachment transitions. The weak sharp band at ~4.5 eV in the 266 nm spectrum becomes part of the low binding energy shoulder on the A

band. The B band with a VDE of 5.98 ± 0.03 eV is relatively sharp and well defined and it should correspond to a singly electronic transition.

4-4.2. AlB_8^-

The 266 nm spectrum of AlB_8^- displays two well-resolved detachment bands (Fig. 4-2(a)). The X band with a VDE of 3.66 ± 0.05 eV is again very broad with a long tail on the lower binding energy side, suggesting a large geometry change from the ground state of AlB_8^- to that of the corresponding AlB_8 neutral structure. A detachment threshold is estimated to be ~3.1 eV. The A band with a VDE of 4.07 ± 0.04 eV is relatively sharp, but it seems to contain a shoulder on the higher binding energy side. In the 193 nm spectrum (Fig. 4-2(b)), a higher binding energy band (B) with a VDE of 5.12 ± 0.05 eV is observed. No other spectral transitions are observed beyond 5.5 eV in the 193 nm spectrum.

4-5. Theoretical Results

4-5.1. AlB_7^-

The initial CK search for the global minimum of AlB_7^- was performed at the B3LYP/3–21G level of theory. The low-lying isomers revealed by the search ($\Delta E < 20$ kcal/mol) are presented in Fig. 4-3. The geometries of all the low-lying isomers I.1 to I.5 were reoptimized with follow up frequency calculations at the B3LYP/6–311+G* level of theory. Single point calculations were performed at the RCCSD(T)/6–311+G(2*df*) level at the B3LYP/6–311+G* optimized geometries. At the B3LYP/6–311+G* level the structures I.2 and I.3 were found to be only 2.0 and 2.4 kcal/mol higher in energy than the

global minimum isomer I.1 (C_{6v}, $^2A_1$). However, the structure I.2 is a first order saddle point with an imaginary frequency of 70 cm^{-1}. Geometry optimization following the imaginary frequency mode led to a slightly non-planar structure, which is only 0.01 kcal/mol lower in energy than the structure I.2. With zero-point energy (ZPE) correction the planar structure is actually 0.1 kcal/mol lower in energy. Thus, the planar structure I.2 (C_{2v}, $^2B_1$) should be considered as the second-lowest isomer. According to our highest level of theory, RCCSD(T)/6–311+G(2df), the relative energies of the I.2 and I.3 structures are 13.6 and 20.9 kcal/mol, respectively. Thus, only isomer I.1 is expected to be present in the cluster beam.

The valence isoelectronic B_8^- cluster was shown previously to possess a slightly distorted heptagonal wheel-type planar global minimum structure (C_{2v}, $^2B_1$),[2] which can be compared with the isomer I.2 of AlB_7^-. The umbrella-type isomer for B_8^- (D_{6h}, $^2A_{1g}$), similar to the structure I.1 of AlB_7^- cluster, was found to be 25.0 kcal/mol (B3LYP/6–311+G*) higher in energy than the global minimum planar structure of B_8^-. Clearly, the substitution of one B atom by an Al atom led to an inversion of the relative stabilities of the wheel-type versus the umbrella-type structures between B_8^- and AlB_7^-.

4-5.2. AlB_8^-

The CK search for the global minimum structure of AlB_8^- at the B3LYP/3–21G level of theory revealed only three structures with relative energies $\Delta E < 30$ kcal/mol. The structures were reoptimized at the B3LYP/6–311+G* level of theory and single point RCCSD(T) calculations were performed on these geometries. The results are summarized in Fig. 4-4. The highly symmetrical planar structure II.3 (D_{8h}, $^1A_{1g}$) with the

octacoordinated Al atom is 31.0 kcal/mol (RCCSD(T)/6–311+G(2*df*)//B3LYP/6–311+G*) higher in energy than the global minimum structure II.1 (C_{7v}, $^1A_1$). Moreover, this structure is a first order saddle point. Geometry optimization following the imaginary frequency mode led to the structure II.2 with the Al atom being 0.53 Å above the plane. Thus, the B_8 ring is clearly too small to host an Al atom in the center. The barrier for planarization is only 1.6 kcal/mol (RCCSD(T)/6–311+G(2*df*)//B3LYP/6–311+G*). The second lowest isomer II.2 (C_{8v}, $^1A_1$) is 29.4 kcal/mol higher in energy at RCCSD(T)/6–311+G(2*df*)//B3LYP/6–311+G* level than the global minimum isomer II.1. Thus, only isomer II.1 is expected to be present in the cluster beam.

The global minimum of the valence isoelectronic B_9^- cluster was shown previously to be a perfect molecular wheel (D_{8v}, $^1A_{1g}$).[1] The umbrella-type isomer (D_{7h}, $^1A_1'$), which is similar to the structure II.1 (C_{7v}, $^1A_1$) of the AlB_8^- cluster, is 31.1 kcal/mol (B3LYP/6—311+G*) higher in energy than the global minimum planar structure of B_9^-. Moreover, this structure was found to be a second order saddle point. Geometry optimization following the imaginary frequency mode led to a distorted umbrella-type structure, which is 23.0 kcal/mol (B3LYP/6–311+G*) or 6.3 kcal/mol (RCCSD(T)/cc-pvTZ) (Ref. 49) higher in energy than the global minimum. Again, the substitution of one B atom by an Al atom led to significant structural changes in the AlB_8^- cluster.

4-6. Interpretation of the Photoelectronic Spectra

4-6.1. AlB_7^-

The calculated VDEs for the global minimum isomer I.1 are compared with the experimental data in Table 4-1.

The first calculated VDE corresponds to the electron detachment channel from the HOMO-1 ($3e_1$) leading to the final triplet state $^3E_1$. Although the calculated VDE at B3LYP (3.02 eV) is somewhat lower than the experimental value, the calculated values at PBE1PBE (3.28 eV), UOVGF (3.30 eV), and UCCSD(T) (3.27 eV) are in excellent agreement with the experimental VDE of 3.3 eV. In this particular case, we found very little spin contamination in unrestricted Hartree-Fock UHF (also UOVGF and UCCSD(T)) for the ground doublet state and two triplet states, $^3E_1$ and $^3B_1$. The triplet nature of the final state of the first VDE is consistent with the high intensity of the experimental feature X. The second VDE corresponds to the transition into the $^1E_1$ final state with the electron detachment from HOMO-1 ($3e_1$). We were not able to calculate VDE for this transition at B3LYP but our VDE of 3.42 eV at PBE1PBE could be responsible for the weak shoulder in the 266 nm spectrum. The next transition into the final singlet state according to our calculations corresponds to the electron detachment from HOMO ($4a_1$) with calculated VDEs of 4.48 eV (UCCSD(T)), 4.62 eV (UOVGF), 4.39 eV (B3LYP), and 4.49 eV (PBE1PBE). However, there is no any prominent feature in this part of the experimental spectrum at 193 nm, though a small peak is present in the spectrum at 266 nm. Since transitions to final triplet states are much more prominent in the experimental spectra, we will further consider those transitions only. The next transition to the final triplet state with the electron detachment from HOMO-2 ($2e_1$) was calculated to be at 4.90 eV (UOVGF), 4.96 eV (B3LYP), and 4.92 eV (PBE1PBE). These numbers are in excellent agreement with the experimental feature A at 4.89 eV. According to our calculations, there is another transition from HOMO-3 ($3b_1$) into the

final triplet state $^3B_1$ with the calculated VDEs 5.29 eV (UCCSD(T)), 5.46 eV (UOVGF), 5.42 eV (B3LYP), and 5.37 eV (PBE1PBE). There is no any prominent feature in this part of the spectrum, but the broad right shoulder of the feature A could be due to this transition. Finally, there is a prominent feature B in the experimental spectrum at 5.98 eV. According to our calculations that could be a transition to the final triplet state with the electron detachment from HOMO-4 ($3a_1$). Calculated VDEs at all levels of theory are way off from the experimental value, again because of the multi-configurational nature of the final state.

We optimized the neutral AlB_7 structure obtained by the detachment of an electron from the HOMO-1 ($3e_1$) of AlB_7^-, as shown in Fig. 4-5. We found that there is an appreciable geometry change from AlB_7^- (C_{2v}, $^2A_1$) to AlB_7 (C_{2v}, $^3B_1$). This structural relaxation is consistent with broad X band observed in the PES spectra. Overall, the theoretical results are in good agreement with the experimental data, confirming isomer I.1 as the global minimum for AlB_7^-.

4-6.2. AlB_8^-

The calculated VDEs from the global minimum of AlB_8^- are compared with the experimental data in Table 4-2.

Since the AlB_8^- anion is a closed-shell system, one-electron detachments lead only to doublet final states. The first calculated VDE corresponds to electron detachment from HOMO ($4a_1$). The theoretical values 3.70 eV (UCCSD(T)), 3.80 eV (UOVGF), 3.78 eV (B3LYP), and 3.71 (PBE1PBE) are all in excellent agreement with the experimental feature X at 3.66 eV. The second VDE can be assigned to an electron detachment from

HOMO-1 ($3e_1$). The calculated values 3.93 eV (PBE1PBE), 4.05 eV (UCCSD(T)), and 4.02 eV (UOVGF) are congruous to the experimental feature A at 4.07 eV. Though, the calculated VDE at B3LYP (3.73 eV) is appreciably lower than the experimental value. The B band in the experimental spectrum (VDE = 5.12 eV) is assigned to photo-detachment from HOMO-2 ($2e_1$) and the corresponding theoretical VDEs are 4.78 eV (B3LYP), 5.02 eV (PBE1PBE), and 4.97 (UOVGF). The photodetachment from HOMO-3 and HOMO-4 have VDE values that are too high in energy to be probed at 193 nm.

We also optimized the structure of the neutral C_{7v} AlB_8 upon removal of an electron from the HOMO of AlB_8^-, as shown in Fig.4-5. We found a very large increase in the interaction between the Al atom and the B_8 fragment. The Al–B distances with the peripheral B atoms are reduced from 2.37 Å in the anion AlB_8^- (C_{7v}, $^1A_1$) to 2.12 Å in the neutral AlB_8 (C_{7v}, $^2A_1$). Such a large structural change is consistent with the broad X band observed in the PES spectra of AlB_8^-. Overall, the theoretical results are in excellent agreement with the experimental observations, confirming unequivocally the umbrella-type structure II.1 as the global minimum for AlB_8^-.

4-7. Chemical Bonding

4-7.1. AlB_7^-

Chemical bonding in the global minimum structure I.1 of the AlB_7^- cluster can be formally described as the Al^{2+} cation coordinated to the B_7^{3-} anion in the ionic limit. NBO analysis of I.1 revealed that the effective atomic charges on aluminum and B_7 are +0.94|e| and –1.94|e|, respectively, which are significantly off from the ionic limit, though, this kind of deviation is expected. This charge distribution is consistent with the

suggested bonding model for the AlB_7^- cluster. It was previously shown[50] that the B_7^- cluster has a pyramidal (C_{6v}, $^3A_2$) global minimum structure. Chemical bonding analysis[3,50] performed for the planar B_7^- (D_{6h}, $^3A_{2g}$) structure revealed six peripheral 2c–2e bonds, three delocalized σ B–B bonds with six σ-electrons responsible for its σ-aromaticity (the 4n + 2 rule for singlet coupled electrons), and three delocalized π-bonds with four π-electrons responsible for its π-aromaticity (the 4n rule for triplet coupled electrons). Although the σ- and π-MOs in the pyramidal structure are mixed, the bonding picture developed for the planar structure is still believed to be qualitatively valid and can explain why the B_7^- cluster adopts the high symmetry C_{6v} structure.

Two extra electrons occupy the semi-occupied $3e_1$ orbital of B_7^- when we proceed to the B_7^{3-} anion making the orbital completely occupied and the cluster doubly aromatic with six delocalized σ-electrons and six delocalized π-electrons. Since formal charge on the aluminum atom is +2|e|, one electron is located primarily on the aluminum atom. This electron occupies the HOMO in AlB_7^-, and it was revealed by the NBO analysis that 95% of its density is located on the aluminum atom. Valence canonical molecular orbitals of the global minimum I.1 isomer of AlB_7^- are presented on Fig. 4-6. As it was shown before[3,50–52] the set of six MOs (HOMO-8, HOMO-7, HOMO-7′, HOMO-5, HOMO-5′, and HOMO-3) is responsible for the peripheral bonding and can be localized into six 2c–2e σ B–B bonds. HOMO-6, HOMO-2, and HOMO-2′ can be approximately assigned to delocalized π-bonds and thus, the system is formally "π-aromatic." HOMO-4, HOMO-1, and HOMO-1′ can be approximately assigned to delocalized σ-bonds and the system is

formally "σ-aromatic". The singly-occupied HOMO being primarily the 3s AO of aluminum is consistent with NBO analysis results (Fig. 4-6).

4-7.2. AlB_8^-

Taking a similar approach to the one we used for AlB_7^-, the global minimum II.1 of the AlB_8^- cluster can be considered as the Al^+ cation coordinated to the B_8^{2-} anion in the ionic limit. The model is consistent with the charge distribution revealed by the NBO analysis (+0.48|e| on aluminum and −1.48|e| on B_8), though, again the charges are expectedly lower than the ionic limit. The B_8^{2-} anion has a wheel-type (D_{7h}, $^1A_1'$) structure.[3,14] With the total of 26 valence electrons, 14 form seven 2c–2e peripheral σ B–B bonds, six electrons are responsible for the delocalized π-bonding and the six left are responsible for the delocalized σ-bonding. Thus, the B_8^{2-} anion is doubly (σ- and π-) aromatic. As it was shown in a joint experimental and theoretical study,[14] the LiB_8^- anion has a "half-sandwich" structure with the Li^+ cation bound to the almost unperturbed B_8^{2-} dianion. We have a similar bonding pattern for the AlB_8^- cluster with about the same perturbation from Al^+ cation on the B_8^{2-} dianion (the central boron atom is pushed out plane of the boron cycle by 0.32 Å compared to the 0.29 Å in LiB_8^-).

Valence canonical molecular orbitals of the global minimum II.1 isomer of AlB_8^- are presented in Fig. 4-7.

As it was shown before[2,3] the set of seven MOs (HOMO-8, HOMO-7, HOMO-7′, HOMO-6, HOMO-6′, HOMO-3, and HOMO-3′) form the peripheral bonding and can be localized into seven 2c–2e σ B–B bonds. HOMO-5 and HOMO-1 and HOMO-1′ can be approximately assigned to delocalized π-bonds and thus, the system is formally "π-

aromatic." HOMO-4, HOMO-2 and HOMO-2′ can be approximately assigned to delocalized σ-bonds and thus, the system is formally "σ-aromatic." The doubly-occupied HOMO is primarily the 3s AO of aluminum as one can see from Fig. 4-7.

With this chemical model for two umbrella-type isomers I.1 (AlB_7^-) and II.1 (AlB_8^-), we can explain why the distance between aluminum and the central boron atom is shorter in AlB_7^- than in AlB_8^- (2.14 and 2.37 Å, respectively). Indeed, since the formal charge of aluminum is +2|e| and that of B_7 is –3|e| compared to the formal charge of aluminum +1|e| and that of B_8 –2|e|, one would expect a stronger bonding between aluminum atom and boron fragment in the first case. Though, the multiply charged B_7^{3-} and B_8^{2-} are not electronically stable in the isolated state, the overall stability is achieved in AlB_7^- and AlB_8^- due to the external field of Al^{2+} and Al^+ cations, respectively. Our chemical bonding model can also explain why, upon electron detachment, the Al-B bond gets longer in AlB_7^- and shortens in AlB_8^-. In AlB_7^- the extra electron goes from the B_7^{3-} anion making the charge distribution Al^{2+} and B_7^{2-}, while in AlB_8^- the extra electron leaves the Al atom leading to the charge distribution Al^{2+} and B_8^{2-}.

4-8. Summary

We investigated the AlB_7^- and AlB_8^- clusters in a combined photoelectron spectroscopy and ab initio study and established the global minimum umbrella-type structures for these clusters. Chemical bonding in the umbrella-type structure of the AlB_7^- cluster can be viewed as an Al^{2+} cation coordinated to a B_7^{3-} anion and the AlB_8^- cluster can be described as an Al^+ cation coordinated to a B_8^{2-} anion. The B_7^{3-} anion in the AlB_7^- cluster has six peripheral 2c–2e σ-bonds, three delocalized π-bonds responsible

for the formal "π-aromaticity" and three delocalized σ-bonds (formal "σ-aromaticity"). Similarly, the B_8^{2-} anion in the AlB_8^- cluster is formally "σ- and π-aromatic" with seven peripheral 2c–2e σ–bonds, three delocalized π-bonds, and three delocalized σ-bonds. Apparently, the high stability of the umbrella type structures is due to the high stabilities of the quasiplanar B_7^{3-} and B_8^{2-} fragments derived from their doubly aromatic nature. The current study provides additional evidence for the robustness of the molecular wheel boron clusters and the importance of aromaticity in their stability.

References

[1]H. J. Zhai, A. N. Alexandrova, K. A. Birch, A. I. Boldyrev, and L. S. Wang, Angew. Chem. Int. Ed. **42**, 6004 (2003).

[2]A. N. Alexandrova, A. I. Boldyrev, H. J. Zhai, and L. S. Wang, Coord. Chem. Rev. **250**, 2811 (2006).

[3]D. Y. Zubarev and A. I. Boldyrev, J. Comput. Chem. **28**, 251 (2007).

[4]H. J. Zhai, L. S. Wang, D. Y. Zubarev, and A. I. Boldyrev, J. Phys. Chem. A **110**, 1689 (2006).

[5]H. J. Zhai, C. Q. Miao, S. D. Li, and L. S. Wang, J. Phys. Chem. A **114**, 12155 (2010).

[6]B. Kiran, X. Li, H. J. Zhai, L. F. Cui, and L. S. Wang, Angew. Chem. Int. Ed. **43**, 2125 (2004).

[7]Z. Y. Jiang, X. M. Luo, S. T. Li, and S. Y. Chu, Int. J. Mass Spectrom. **252**, 197 (2006).

[8]H. Kawamata, Y. Negishi, A. Nakajima, and K. Kaya, Chem. Phys. Lett. **337**, 255 (2001).

[9]B. B. Averkiev and A. I. Boldyrev, Russ. J. Gen. Chem. **78**, 769 (2008).

[10]B. B. Averkiev, L. M. Wang, W. Huang, L. S. Wang, and A. I. Boldyrev, Phys. Chem. Chem. Phys. **11**, 9840 (2009).

[11]X. J. Feng and Y. H. Luo, J. Phys. Chem. A **111**, 2420 (2007).

[12]J. C. Guo, W. Z. Yao, Z. Li, and S. D. Li, Sci. China Ser. B: Chem. **52**, 566 (2009).

[13]C. Romanescu, A. Sergeeva, W.-L. Li, A. I. Boldyrev, and L. S. Wang, J. Am. Chem. Soc. **113**, 8646 (2011).

[14]A. N. Alexandrova, H. J. Zhai, L. S. Wang, and A. I. Boldyrev, Inorg. Chem. **43**, 3552 (2004).

[15]J. Simons, J. Phys. Chem. A **112**, 6401 (2008).

[16]J. Simons, Annu. Rev. Phys. Chem. **62**, 107 (2011).

[17]L. S. Wang, H. S. Cheng, and J. W. Fan, J. Chem. Phys. **102**, 9480 (1995).

[18]L. S. Wang and H. Wu, in *Advances in Metal and Semiconductor Clusters*, edited by M. A. Duncan (JAI, Greenwich, CT, 1998), Vol. 4, pp. 299–343.

[19]J. Akola, M. Manninen, H. Hakkinen, U. Landman, X. Li, and L. S. Wang, Phys. Rev. B **60**, 11297 (1999).

[20]L. S. Wang and X. Li, in *Proceedings International Symposium on Clusters and Nanostructure Interfaces, Richmond, VA, 25–28 October 1999*, edited by P. Jena, S. N. Khanna, and B. K. Rao (World Scientific, River Edge, New Jersey, 2000), pp. 293–300.

[21]W. Huang and L. S. Wang, Phys. Rev. Lett. **102**, 153401 (2009).

[22]A. P. Sergeeva, B. B. Averkiev, H. J. Zhai, A. I. Boldyrev, and L. S. Wang, J. Chem. Phys. **134**, 224304 (2011)

[23]A. D. Becke, J. Chem. Phys. **98**, 5648 (1993).

[24]S. H. Vosko, L. Wilk, and M. Nusair, Can. J. Phys. **58**, 1200 (1980).

[25]C. T. Lee, W. T. Yang, and R. G. Parr, Phys. Rev. B **37**, 785 (1988).

[26]J. Binkley, J. A. Pople, and W. J. Hehre, J. Am. Chem. Soc. **102**, 939 (1980)

[27]M. S. Gordon, J. S. Binkley, J. A. Pople, W. J. Pietro, and W. J. Hehre, J. Am. Chem. Soc. **104**, 2797 (1982).

[28]A. D. McLean and G. S. Chandler, J. Chem. Phys. **72**, 5639 (1980).

[29]W. J. Pietro, M. M. Francl, W. J. Hehre, D. J. Defrees, J. A. Pople, and J. S. Binkley, J. Am. Chem. Soc. **104**, 5039 (1982).

[30]T. Clark, J. Chandrasekhar, G. W. Spitznagel, and P. v. R. Schleyer, J. Comput. Chem. **4**, 294 (1983).

[31]J. Cizek, Adv. Chem. Phys. **14**, 35 (1969).

[32]G. D. Purvis and R. J. Bartlett, J. Chem. Phys. **76**, 1910 (1982).

[33]K. Raghavachari, G. W. Trucks, J. A. Pople, and M. Head-Gordon, Chem. Phys. Lett. **157**, 479 (1989).

[34]L. S. Cederbaum, J. Phys. B **8**, 290 (1975).

[35]J. V. Ortiz, Int. J. Quantum Chem. **36**(S23), 321 (1989).

[36]J. S. Lin and J. V. Ortiz, Chem. Phys. Lett. **171**, 197 (1990).

[37]V. G. Zakrzewski, J. V. Ortiz, J. A. Nichols, D. Heryadi, D. L. Yeager, and J. T. Golab, Int. J. Quantum Chem. **60**, 29 (1996).

[38]R. Bauernschmitt and R. Ahlrichs, Chem. Phys. Lett. **256**, 454 (1996).

[39]M. E. Casida, C. Jamorski, K. C. Casida, and D. R. Salahub, J. Chem. Phys. **108**, 4439 (1998).

[40]J. P. Perdew, K. Burke, and M. Ernzerhof, Phys. Rev. Lett. **77**, 3865 (1996).

[41]J. P. Perdew, K. Burke, and M. Ernzerhof, Phys. Rev. Lett. **78**, 1396 (1997).

[42]J. P. Foster and F. Weinhold, J. Am. Chem. Soc. **102**, 7211 (1980).

[43]A. E. Reed, L. A. Curtiss, and F. Weinhold, Chem. Rev. **88**, 899 (1988).

[44]F. Weinhold and C. R. Landis, *Valency and Bonding: A Natural Bond Orbital Donor-Acceptor Perspective* (Cambridge University Press, Cambridge, England, 2005).

[45]M. J. Frisch, G. W. Trucks, and H. B. Schlegel et al., Gaussian 03, revision D.01; Gaussian, Inc., Wallingford, CT, 2004.

[46]H.-J. Werner, P. J. Knowles, G. Knizia, F. R. Manby, M. Schütz et al.; MOLPRO, a package of ab initio programs, version 2006.1, see http://www.molpro.net.

[47]G. Schaftnenaar, molden3.4, CAOS/CAMM Center, The Netherlands (1998).

[48]U. Varetto, MOLEKEL 5.4.0.8, Swiss National Supercomputing Centre: Manno (Switzerland) (2009).

[49]L. L. Pan, J. Li, and L. S. Wang, J. Chem. Phys. **129**, 024302 (2008).

[50]A. N. Alexandrova, A. I. Boldyrev, H. J. Zhai, and L. S. Wang, J. Phys. Chem. A **108**, 3509 (2004).

[51]P. W. Fowler and B. R. Gray, Inorg. Chem. **46**, 2892 (2007).

[52]D. Y. Zubarev and A. I. Boldyrev, Phys. Chem. Chem. Phys. **10**, 5207 (2008).

TABLE 4-1. Experimentally observed and theoretically calculated VDEs for the isomer I.1 (C_{6v}, $^2A_1$) of AlB_7^-. All energies are in eV.

Feature	VDE (exp.)[a]	Final State and Electronic Configuration	VDE (theoretical)			
			TD-B3LYP[b]	TD-PBE1PBE[c]	UOVGF[d]	UCCSD(T)[e]
X	3.3(1)	$^3E_1$, {...$3a_1^2 1b_1^2 2e_1^4 3e_1^3 4a_1^1$}	3.02	3.28	3.30 (0.88)	3.27
		$^1E_1$, {...$3a_1^2 1b_1^2 2e_1^4 3e_1^3 4a_1^1$}	[f]	3.42	[g]	[g]
	4.45(5)	$^1A_1$, {...$3a_1^2 1b_1^2 2e_1^4 3e_1^4 4a_1^0$}	4.39	4.49	4.62 (0.91)	4.48
A	4.89(5)	$^3E_1$, {...$3a_1^2 1b_1^2 2e_1^3 3e_1^4 4a_1^1$}	4.96	4.92	4.90 (0.89)	[g]
		$^3B_1$, {...$3a_1^2 1b_1^1 2e_1^4 3e_1^4 4a_1^1$}	5.42	5.37	5.46 (0.88)	5.29
		$^1E_1$, {...$3a_1^2 1b_1^2 2e_1^3 3e_1^4 4a_1^1$}	[f]	5.43	[g]	[g]
		$^1B_1$, {...$3a_1^2 1b_1^1 2e_1^4 3e_1^4 4a_1^1$}	[f]	5.59	[g]	[g]
B	5.9	$^3A_1$, {...$3a_1^1 1b_1^2 2e_1^4 3e_1^4 4a_1^1$}	5.83	5.70	6.52 (0.81)	[g]

[a] Numbers in parentheses represent the uncertainty in the last digit.
[b] VDEs were calculated at TD-B3LYP/6-311+G(2*df*)//B3LYP/6-311+G*.
[c] VDEs were calculated at TD-PBE1PBE/6-311+G(2*df*)//B3LYP/6-311+G*.
[d] VDEs were calculated at UOVGF/6-311+G(2*df*)//B3LYP/6-311+G*. Values in parentheses represent the pole strength of the OVGF calculation.
[e] VDEs were calculated at UCCSD(T)/6-311+G(2*df*)//B3LYP/6-311+G*.
[f] We were not able to calculate these VDEs at the TD-B3LYP/6-311+G(2*df*)//B3LYP/6-311+G* level. (the calculations terminate with the 'Fatal Problem: The smallest alpha delta epsilon is -0.94992484D-02')
[g] VDE value cannot be calculated due to limitation of the theory.

TABLE 4-2. Experimentally observed and theoretically calculated VDEs for the isomer II.1 (C_{7v}, $^1A_1$) of AlB_8^-. All energies are in eV.

Feature	VDE (exp.)[a]	Final State and Electronic Configuration	VDE (theo.)			
			TD-B3LYP[b]	TD-PBE1PBE[c]	ROVGF[d]	UCCSD(T)[e]
X	3.66(5)	$^2A_1$, {...$3a_1^2 1e_3^4 2e_1^4 3e_1^4 4a_1^1$}	3.78	3.71	3.80 (0.89)	3.83
A	4.07(4)	$^2E_1$, {...$3a_1^2 1e_3^4 2e_1^4 3e_1^3 4a_1^2$}	3.73	3.93	4.02 (0.88)	4.05
B	5.12(5)	$^2E_1$, {...$3a_1^2 1e_3^4 2e_1^3 3e_1^4 4a_1^2$}	4.78	5.02	4.97 (0.89)	[f]
		$^2E_3$, {...$3a_1^2 1e_3^3 2e_1^4 3e_1^4 4a_1^2$}	6.18	6.41	6.65 (0.87)	[f]

[a] Numbers in parentheses represent the uncertainty in the last digit.
[b] VDEs were calculated at TD-B3LYP/6-311+G(2*df*)//B3LYP/6-311+G*.
[c] VDEs were calculated at TD-PBE1PBE/6-311+G(2*df*)//B3LYP/6-311+G*.
[d] VDEs were calculated at ROVGF/6-311+G(2*df*)//B3LYP/6-311+G*. Values in parentheses represent the pole strength of the OVGF calculation.
[e] VDEs were calculated at UCCSD(T)/6-311+G(2*df*)//B3LYP/6-311+G*.
[f] VDE value cannot be calculated due to limitation of the theory.

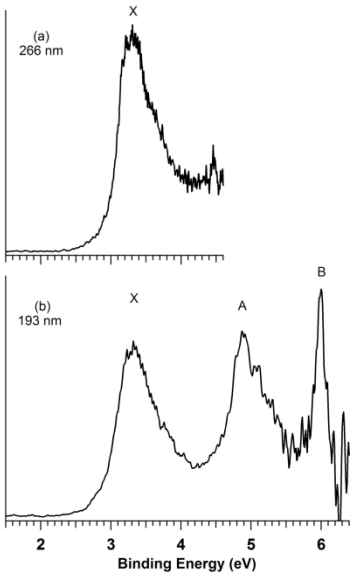

FIG. 4-1. Photoelectron spectra of AlB_7^- at (a) 266 nm and (b) 193 nm photodetachment wavelengths.

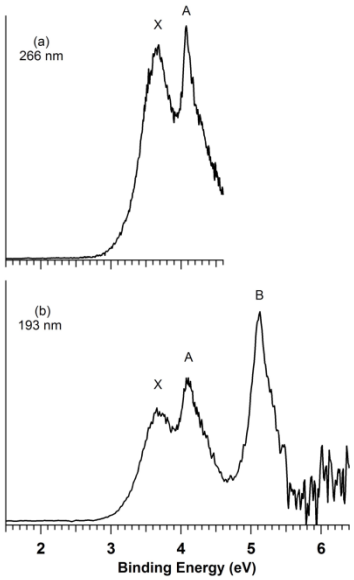

FIG. 4-2. Photoelectron spectra of AlB_8^- at (a) 266 nm and (b) 193 nm photodetachment wavelengths.

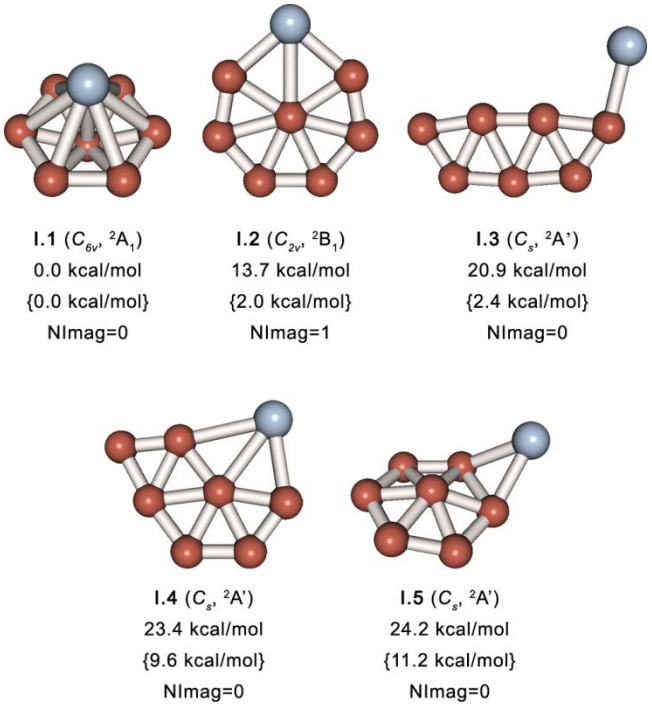

FIG. 4-3. Optimized structures of the AlB_7^- cluster, their point group symmetries, spectroscopic states, and relative energies. Relative energies are given at the RCCSD(T)/6–311+G(2*df*)//B3LYP/6–311+G* and the B3LYP/6–311+G* (in squiggle brackets) levels of theory. All the relative energies are ZPE corrected. NImag is the number of imaginary frequencies at B3LYP/6–311+G*.

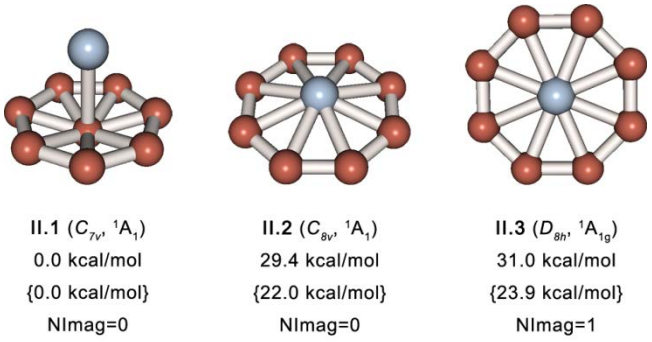

FIG. 4-4. Optimized structures of the AlB_8^- cluster, their point group symmetries, spectroscopic states, and relative energies. Relative energies are given at the RCCSD(T)/6–311+G(2*df*)//B3LYP/6–311+G* and the B3LYP/6–311+G* (in squiggle brackets) levels of theory. All the relative energies are ZPE corrected. NImag is the number of imaginary frequencies at B3LYP/6–311+G*.

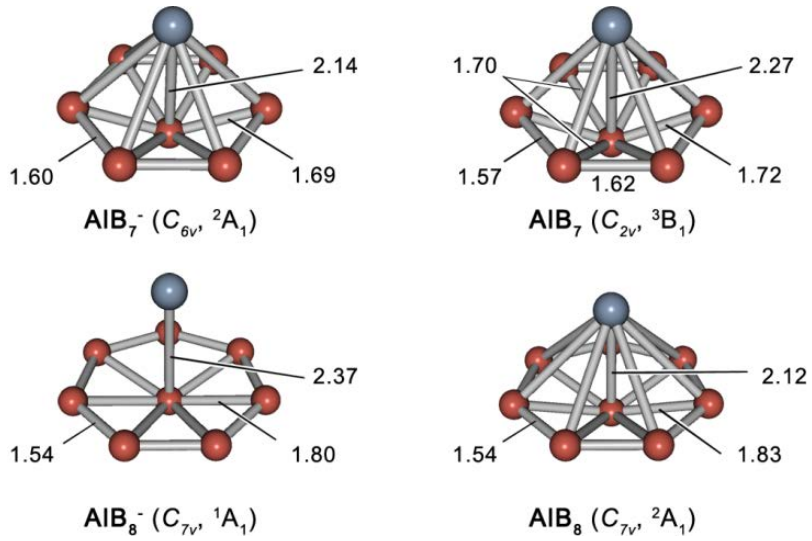

FIG. 4-5. Optimized structures (B3LYP/6–311+G*) of AlB_7^- (C_{6v}, $^2A_1$), AlB_8^- (C_{7v}, $^1A_1$), AlB_7 (C_{2v}, $^3B_1$), and AlB_8 (C_{7v}, $^2A_1$). Bond lengths are given in Å.

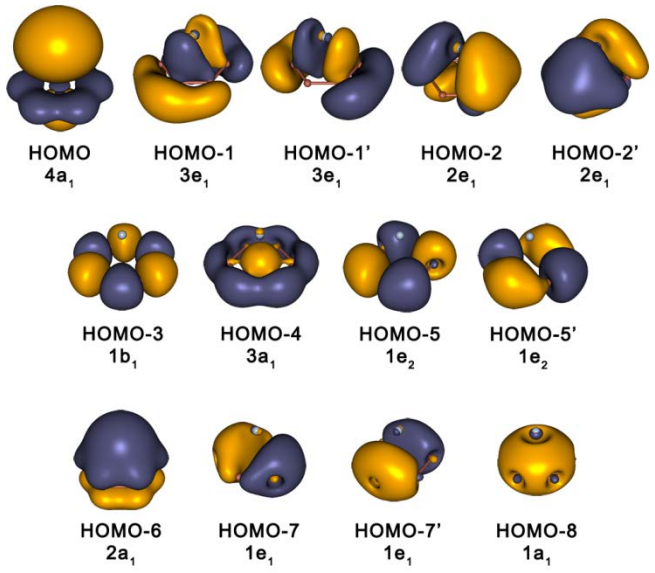

FIG. 4-6. Valence canonical molecular orbitals of the global minimum I.1 isomer of AlB_7^- (B3LYP/6–311+G*).

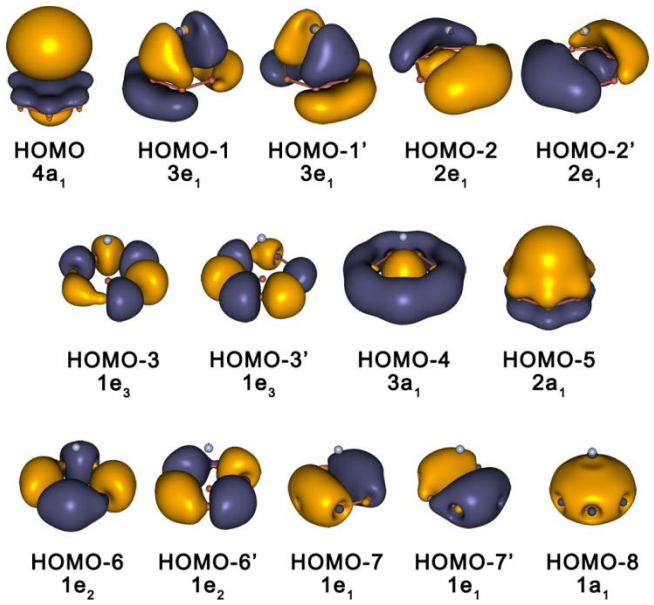

FIG. 4-7. Valence canonical molecular orbitals of the global minimum II.1 isomer of AlB_8^- (B3LYP/6–311 +G*).

CHAPTER 5

ALUMINUM AVOIDS THE CENTRAL POSITION IN AlB_9^- AND AlB_{10}^-: PHOTOELECTRON SPECTROSCOPY AND AB INITIO STUDY *

Abstract

The structures and the electronic properties of two Al-doped boron clusters, AlB_9^- and AlB_{10}^-, were investigated via joint photoelectron spectroscopy and high-level ab initio study. The photoelectron spectra of both anions are relatively broad and have no vibrational structure. The geometrical structures were established by unbiased global minimum searches using the Coalescence Kick method and comparison between the experimental and calculated vertical electron detachment energies. The results show that both clusters have quasi-planar structures and that the Al atom is located at the periphery. Chemical bonding analysis revealed that the global minimum structures of both anions can be described as doubly (σ- and π-) aromatic systems. The nona-coordinated wheel-type structure of AlB_9^- was found to be a relatively high-lying isomer, while a similar structure for the neutral AlB_9 cluster was previously shown to be either a global minimum or a low-lying isomer.

5.1. Introduction

Boron possesses peculiar chemical bonding.[1,2] Due to its small covalent radius and electron deficiency compared to carbon (boron has four valence atomic orbitals and

* Coauthored by Wei-Li Li, Constantin Romanescu, Timur R. Galeev, Lai-Sheng Wang, and Alexander I. Boldyrev. Reprinted with permission from *J. Phys. Chem. A* **2011**, *115*, 10391-10397. Copyright 2011 American Chemical Society

only three valence electrons), boron forms planar or quasi-planar anionic structures, at least up to 20 atoms. Over the past decade, we have performed combined photoelectron spectroscopy (PES) and theoretical calculations on small boron clusters to investigate their structures and bonding properties.[3-16] All of these small boron clusters show strong peripheral two-center-two-electron (2c-2e) B–B σ-bonds and two-dimensional delocalized σ- and/or π-bonds between inner and peripheral boron atoms, giving rise to σ- and π-aromaticity, σ- and π-antiaromaticity or conflicting aromaticity-antiaromaticity. [3-18] It was concluded that the perfectly planar clusters feature multiple aromaticity (σ, π) and the optimum circumference and inner group sizes. One question arises: how do the electronic structure and the bonding change upon doping of the boron clusters with an isoelectronic aluminum atom?

In a previous work, we have shown that Al-doping enhances the planarity of B_7^- and B_{12}^- in AlB_6^- and AlB_{11}^-, by slightly expanding the size of the outer rings.[19] For the perfectly planar AlB_{11}^- cluster, we found that two nearly degenerate isomers compete for the global minimum structure and that the second lowest-lying isomer is a coordination complex between the Al atom and B_{11}^- anion. Subsequent studies of AlB_7^- and AlB_8^- have shown that the global minima are umbrella-type structures featuring positively charged Al atoms bonded ionically to the negatively charged B_n (n = 7, 8) counterions.[20] Although the multiply charged B_7^{3-} and B_8^{2-}anions are not electronically stable in the isolated state, the overall stability is achieved in AlB_7^- and AlB_8^- due to the external field of Al^{2+} and Al^+ cations, respectively. As a comparison, the isoelectronic boron clusters

are planar (B_8^-, C_{2v} – slightly distorted from D_{7h}) and perfect octagon (B_9^-, D_{8h}) structures.

Previous experimental studies of mixed Al–B clusters include a mass spectrometry investigation[21] and a photoelectron spectroscopy study[22] of aluminum clusters doped with one or two boron atoms. A number of theoretical calculations on Al-doped boron clusters have also been reported, mostly on neutral clusters.[23-27] We would like to point out two recent comprehensive reviews[28,29] on negative molecular ions where various theoretical techniques and applications were discussed.

In the present work, we set out to investigate the chemical bonding in the two intermediate sized Al-doped boron clusters: AlB_9^- and AlB_{10}^-. One should not expect that geometries of the aluminum-doped clusters are the same as the global minimum structures of unsubstituted ones. Although in this work we found that AlB_9^- has a similar geometry as that of B_{10}^- with one peripheral boron atom substituted by an aluminum atom, whereas AlB_{10}^- has a different geometry compared to B_{11}^-. The geometrical structures of anionic clusters were established by unbiased global minimum searches and comparison of the experimental (photoelectron spectroscopy) and theoretical photodetachment energies

5-2. Experimental Section

The experiment was performed using a magnetic-bottle PES apparatus equipped with a laser vaporization cluster source, details of which have been published elsewhere.[30,31] Briefly, AlB_x^- (x = 9, 10) were produced by means of laser ablation (532 nm) of a disk target made of isotopically enriched ^{10}B (10%), Al (2.5%), balanced by Bi

which acted as a target binder and, also, provided calibration for the photoelectron spectra. The clusters were entrained by a 5% Ar in He carrier gas and underwent a supersonic expansion to form a collimated molecular beam. The composition and the cooling of the clusters were controlled by the time delay between the carrier gas pulse and the ablation laser.[32,33] The negatively charged clusters were extracted and analyzed with a Time-of-Flight Mass Spectrometer. The species of interest were mass-selected and decelerated before being photodetached by a pulsed laser beams at 193 nm (6.424 eV) or 266 nm (4.661 eV). Photoelectrons were collected at nearly 100% efficiency by a magnetic bottle and analyzed in a 3.5 m long electron flight tube. The resolution of the apparatus, $\Delta E/E$, was better than 2.5%, i.e., 25 meV for 1 eV electron.

5-3. Theoretical Methods

The search for the global minima structures of the AlB_9^- and AlB_{10}^- clusters was performed using the Coalescence Kick (CK) program, written by Averkiev.[34] The program randomly generates a large number of structures which undergo a coalescence procedure during which all atoms are gradually pushed to the molecular center of mass to avoid generation of fragmented structures and then optimized to the nearest local minima. All CK calculations were performed using the B3LYP[35-37] hybrid method with the 3-21G[38] basis set. The low-lying isomers were reoptimized with follow up frequency calculations at the B3LYP/6-311+G* level of theory.[39-42] In order to avoid high spin contamination at the UCCSD(T) method, single point energy calculations for the lowest isomers of AlB_9^- were performed using the restricted coupled cluster [RCCSD(T)] method[43-45] with the 6-311+G(2df) basis set at the B3LYP/6-311+G* optimized

geometries. These calculations were performed with the Molpro program.[46] Single point calculations for the lowest energy structures for AlB_{10}^- were done with the Gaussian 03 software[47] using coupled cluster [RCCSD(T)] method and the 6-311+G(2df) basis set at the B3LYP/6-311+G* optimized geometries.

The VDEs were calculated using the RCCSD(T)/6-311+G(2df) method, the restricted outer valence Green Function method [ROVGF/6-311+ G(2df)][48-51] (for AlB_{10}^- only) and the time-dependent DFT method[52,53] TD-B3LYP/6-311+G(2df) and TD-PBE1PBE/6-311+G(2df),[54,55] all at B3LYP/6-311+G* optimized geometries. The first two VDEs for the AlB_9^- were calculated at the B3LYP and PBE1PBE levels of theory as the transitions from the doublet ground state of the anion into the final lowest singlet and triplet states of the neutral species at the anion geometry. Then the vertical excitation energies of the neutral species (at the TD-B3LYP and TD-PBE1PBE levels) calculated for the singlet and triplet states were added to the two lowest VDEs with the singlet and triplet final states, respectively, to obtain the second and higher VDEs. Similarly, the first VDE for the AlB_{10}^- cluster was calculated at the B3LYP and PBE1PBE levels of theory as the lowest transition from the singlet state of the anion into the final lowest doublet state of the neutral AlB_{10} species at the AlB_{10}^- optimized geometry. Then the vertical excitation energies of the neutral species (at the TD-B3LYP and PBE1PBE levels) were added to the first VDE to obtain the second and higher VDEs. Core electrons were frozen in treating the electron correlation at the CCSD(T) and ROVGF levels of theory.

Chemical bonding analysis was performed using the Adaptive Natural Density Partitioning (AdNDP) method recently developed by Zubarev and Boldyrev. [56-59] AdNDP

is based on the concept of an electron pair as the main element of chemical bonding models. Thus, it represents the electronic structure in terms of *n*c-2e bonds. With *n* spanning the interval from one to the total amount of atoms in the particular atomic assembly, AdNDP recovers both Lewis bonding elements (1c-2e and 2c-2e objects, corresponding to the core electrons and lone pairs, and two-center two-electron bonds) and delocalized bonding elements, which are associated with the concepts of aromaticity and antiaromaticity. From this point of view, AdNDP achieves seamless description of systems featuring both localized and delocalized bonding without invoking the concept of resonance. Molecular structure visualization was done with the MOLDEN 3.4[60] and Molekel 5.4.0.8[61] programs.

5-4. Experimental Results

The photoelectron spectra of AlB_9^- and AlB_{10}^- are shown in Figures 5-1 and 5-2, respectively, each at 266 and 193 nm. Since better spectral resolution is obtained for low kinetic energy photoelectrons, i.e., near the excitation threshold of an electronic transition, we employ multiple photodetachment conditions to achieve spectra with enhanced electronic and vibrational resolution. The spectral bands were labeled with letters (X, A, B, C, ...) and VDEs were given in Table 5-1 and 5-2. The X band represents the transition between the ground states of the anion and the neutral species, while the higher binding energy bands (A, B, ...) denote transitions to electronically excited states of the neutral.

5-4.1. AlB_9^-

The 266 nm spectrum of AlB_9^- displays three well-resolved electronic bands (X, A, B), with no apparent vibrational structure. The measured VDEs of the first two bands are closely spaced in values, 3.15 ± 0.05 eV (X band) and 3.36 ± 0.04 eV (A band), which indicate possible electronic transitions from a ground doublet anionic state to singlet and triplet neutral ground state. For the third band, B, we measured a VDE of 4.40 ± 0.04 eV. In addition to the features revealed by the 266 nm spectrum, three more features are identified in the 193 nm PES (C-E). The VDEs values are summarized in Table 5-1. All spectral features identified in the PES (X, A-E) are slightly broad, indicating some degree of geometry change between the ground state of AlB_9^- and respective states of the AlB_9. The absence of any resolved vibrational structure, especially for the near-threshold bands, B at 266 nm and E at 193 nm, suggests that low energy vibrational modes might be active in the photodetachment transitions. No spectral features were observed beyond 5.5 eV.

5-4.2. AlB_{10}^-

At 266 nm, the PES shows also three peaks without resolved vibrational structures. The first two peaks, with VDEs of 3.61 ± 0.05 eV (X) and 3.78 ± 0.05 eV (A) are not well resolved. The third peak, B, is broader and has a measured VDE value of 4.26 ± 0.05 eV. In addition to these features, we note the presence of a small feature at the low binding energy side of the X peak. The presence of this feature prevents us from measuring the ADE value for the X transition, for which we estimate a threshold value of 3.4 ± 0.1 eV. Since the expansion conditions were identical to those used to create the

AlB_6^- and AlB_{11}^- clusters, which were shown to be vibrationally cold,[19] we believe that this feature should be attributed to higher energy metastable isomers of AlB_{10}^- rather than vibrational hot bands. Another two electronic transitions, C and D, are identified in the 193 nm spectrum. The VDEs values are summarized in Table 5-2. Similarly to the AlB_9^- spectrum, no spectral features were observed beyond 5.5 eV.

5-5. Theoretical Results

5-5.1. AlB_9^-

The lowest-lying isomers of AlB_9^- (ΔE < 20 kcal/mol) revealed by the CK global minimum search at the B3LYP/3-21G level of theory were then reoptimized at B3LYP/6-311+G* and single point energy calculations were performed for the isomers at RCCSD(T)/6-311+G(2df) on the B3LYP/6-311+G* geometries. The global minimum structure and four lowest isomers are presented in Figure 5-3.

According to the computational results at our highest level of theory (RCCSD(T)/6-311+G(2df)//B3LYP/6-311+G*), structure I.1 is the global minimum and the other low-lying isomers I.2, I.3, I.4, and I.5 are 8.3, 10.6, 11.7, and 16.7 kcal/mol higher in energy, respectively. It is interesting to compare these results with those obtained at the same level of theory for the neutral AlB_9 cluster.[24] The structures of the five low-lying isomers of AlB_9 are similar to those found for the AlB_9^- anion, however, the order of the isomers is different. Two almost degenerate isomers were found for the neutral AlB_9 cluster: one similar to the global minimum I.1 of AlB_9^- and another similar to the wheel-type isomer I.5 of AlB_9^-, whereas, the global minimum isomer I.1 of AlB_9^- is significantly lower in energy than the wheel-type structure I.5. Thus, addition of an

extra electron substantially altered the relative stability of one of the two practically degenerate lowest isomers.

5-5.2. AlB_{10}^-

We applied a similar global minimum search approach for AlB_{10}^-, which revealed the presented (Figure 5-4) order of isomers with the structure II.1 being significantly lower in energy than other isomers. The second lowest-lying isomer II.2 was found to be 7.7 kcal/mol higher in energy than the global minimum II.1.

5-6. Interpretation of the Photoelectronic Spectra

5-6.1. AlB_9^-

The global minimum isomer I.1 is significantly lower in energy than the other isomers, therefore, only isomer I.1 contributes to the experimental PES of AlB_9^-. The calculated VDEs for I.1 at three levels of theory compared with the experimental results are presented in Table 5-1. We do not report here VDEs calculated at UOVGF/6-311+G(2df)//B3LYP/6-311+G* due to high spin contamination.

The first calculated VDE corresponds to the electron detachment channel from HOMO leading to the final singlet state. The calculated VDEs of 3.01 eV (RCCSD(T)), 3.08 eV (B3LYP), and 3.21 eV (PBE1PBE) correspond to the experimental feature X at 3.15 eV. The second VDE can be assigned to the detachment channel from HOMO-1 leading to the final triplet state. Again, all three theoretically calculated values: 3.43 eV (RCCSD(T)), 3.28 eV (B3LYP), and 3.33 eV (PBE1PBE) are in agreement with the experimental VDE of 3.36 eV (feature A). Higher intensity of the feature A compared to

the feature X is consistent with the triplet nature of the second final state since transitions into triplet states are usually more prominent in the experimental photoelectron spectra than those for singlet final state. Therefore, we will further discuss only transitions leading to the final triplet states. The next transition into the second triplet state can be calculated only with TD-DFT methods and the theoretical values of 4.21 eV (B3LYP) and 4.35 eV (PBE1PBE) are consistent with the experimental feature B at 4.40 eV. The third and fourth transitions into the triplet states at 4.70 and 4.82 eV (B3LYP) and 4.78 and 4.93 eV (PBE1PBE) correspond to the features C and D in the experimental spectrum. Finally, two other transitions into the triplet states at 5.36 and 5.42 eV (B3LYP) are responsible for the experimental feature E.

Overall, the experimental data are in excellent agreement with the detachment transitions theoretically calculated for the isomer I.1, clearly confirming that this isomer is the global minimum for the AlB_9^- cluster.

5-6.2. AlB_{10}^-

The global minimum isomer II.1 was found to be significantly more stable than any other isomer of AlB_{10}^- and thus, only II.1 is responsible for the experimental PES. The theoretical and experimental data are summarized in Table 5-2.

Since the AlB_{10}^- anion is a closed-shell system single electron detachments lead only to doublet final states. The first calculated VDE corresponds to electron detachment from HOMO (7a"). The theoretical values 3.67 eV (RCCSD(T)), 3.52 eV (ROVGF), 3.51 eV (B3LYP), and 3.61 eV (PBE1PBE) are all congruent to the experimental feature X at 3.61 eV. The second VDE can be assigned to an electron detachment from HOMO-1

(10a'). Although the calculated values at B3LYP (3.55 eV) and PBE1PBE (3.55 eV) are appreciably lower than the experimental value of 3.78 eV (feature A), the VDEs at RCCSD(T) (3.80 eV) and ROVGF (3.79 eV) are in excellent agreement with it. The next feature B at 4.26 eV can be explained by the detachment of an electron from HOMO-2 (9a′). Indeed, the theoretical results at all three levels B3LYP (4.09 eV), PBE1PBE (4.19 eV), ROVGF (4.24 eV) are very close to the experimental value. The feature C at 4.91 eV can be assigned to the electron transition from HOMO-3 (6a″). Theoretically calculated values 5.11 eV (ROVGF) and 5.0 eV (PBE1PBE) are in a good agreement with the experimental value while the VDE B3LYP (4.74 eV) is somewhat lower in energy. The calculated VDE values for transition from HOMO-4 (8a′) of 5.51 eV (ROVGF) and 5.44 eV (PBE1PBE) are congruent with the experimental VDE feature D at 5.31 eV. The calculated VDE at B3LYP (5.23 eV) is again lower than the experimental value. One can see that application of several theoretical methods is required in order to make a solid assignment of the experimental peaks in the AlB_{10}^- PES. One method would not be reliable enough to get a clear picture. The global minimum II.1 for the AlB_{10}^- cluster was confirmed by the overall agreement between the experimental data and the calculated VDEs.

5-7. Chemical Bonding Analysis

5-7.1. AlB_9^-

Let us first analyze chemical bonding in the global minimum structure I.1. In order to avoid complications due to spin polarization we performed the AdNDP analysis (at B3LYP/6-311+G*) for the doubly charged anion AlB_9^{2-} (C_1, ^1A) at the geometry

optimized (B3LYP/6-311+G*) for AlB_9^-. Results of the AdNDP analysis are presented in Figure 5-5. Six B–B and one Al–B 2c-2e σ-bonds with ONs ranging from 1.70 |e| (Al–B) to 1.96 |e| were revealed by AdNDP. There are also five delocalized "σ-bonds," which are responsible for its "σ-aromaticity" and three delocalized "π-bonds," which are responsible for its "π-aromaticity." We would like to stress here that the cluster is not planar, therefore, our assignment of delocalized bonds to σ- and π-types is approximate, yet, we believe that recognizing its σ- and π-aromaticity is a useful tool for the explanation of chemical bonding and stability of this cluster. Finally, the AdNDP analysis revealed a lone pair on the aluminum atom with ON of 1.77 |e|. Although we consider this global minimum structure as doubly aromatic, it is not a planar structure. We believe that the reason for the nonplanarity of I.1 is of a mechanical nature: the cavity inside of the eight member external ring is two small to comfortably accommodate two boron atoms. Our analysis was performed for the doubly charged anion AlB_9^{2-}, but the assessment of aromaticity is valid for AlB_9^- too because the electron is removed from the aluminum lone pair.

It was mentioned above that the isomers found before[24,26] for the neutral AlB_9 cluster similar to I.1 and I.5 of the AlB_9^- anion are nearly degenerate and yet for the anion we observe that the wheel-type structure I.5 is significantly less stable than the global minimum structure I.1. In order to explain the higher energy difference between the anions compared to the neutral clusters we performed the AdNDP analysis of the wheel-type isomer I.5. Again, in order to avoid spin-polarization we analyzed the doubly

charged anion AlB_9^{2-} (C_{2v}, $^1A_1$) at the geometry optimized for the wheel-type isomer I.5 of AlB_9^-. The bonding pattern revealed is shown in Figure 5-6.

According to this analysis, AlB_9^{2-} has nine peripheral 2c-2e B–B σ-bonds and four delocalized σ-bonds, making this cluster σ-antiaromatic and three delocalized π-bonds responsible for π-aromaticity in this cluster. Thus, the doubly charged anion exhibits conflicting aromaticity. The neutral AlB_9 (D_{9h}, $^1A_1'$) cluster is a doubly aromatic system with six delocalized σ- and six delocalized π-electrons,[24,26] therefore, the AlB_9^- cluster with five delocalized σ-electrons and six delocalized π-electrons is 1/2-σ-antiaromatic[62] and π-aromatic. However, the AdNDP analysis of the neutral AlB_9 C_1 isomer revealed a bonding pattern similar to that of the doubly charged anion, but without the sp-LP on aluminum. Thus, the addition of two extra electrons does not disturb the σ- and π-aromaticity, but leads to the formation of a lone pair on aluminum atom. We believe that the increase in energy difference between the I.1 and I.5 anionic structures is due to the fact that the addition of an extra electron to the neutral double aromatic C_1 structure does not disturb its doubly aromatic nature (the electron is localized on the aluminum atom), whereas, the electron added to neutral wheel-type structure leads to the formation of π-aromatic but 1/2-σ-antiaromatic AlB_9^- anion.

5-7.2. AlB_{10}^-

AdNDP for the AlB_{10}^- global minimum structure II.1 (Figure 5-7) revealed a lone pair on aluminum atom with ON=1.87 |e|, eight peripheral 2c-2e B–B σ-bonds with ON = 1.80–1.94 |e|, five delocalized 'σ-bonds' responsible for 'σ-aromaticity' and three delocalized "π-bonds" responsible for "π-aromaticity." Again, since the cluster is not

planar, the assignment of delocalized bonds to σ- and π- can be done only approximately, though, we believe that recognizing its σ- and π-aromaticity is a useful tool for explanation of chemical bonding and stability of this cluster. Thus, the global minimum structure of the AlB_{10}^- cluster is approximately a doubly (σ- and π-) aromatic system. Again, we believe that the reason for nonplanarity is mechanical, since the external ring of eight boron atoms is not large enough to accommodate two internal boron atoms

5-8. Conclusions

In this joint photoelectron and ab initio work, we probed the structures and the chemical bonding of the AlB_9^- and AlB_{10}^- clusters. Well-resolved photoelectron spectra were recorded and compared with the theoretically calculated VDEs. Global minimum structures of both anions were established through CK search at B3LYP/3-21G with follow up geometry optimization of the lowest isomers at B3LYP/6-311+G*. The final conclusion on the global minimum structures was based on CCSD(T)/6-311+G(2df)//B3LYP/6-311+G* calculations. VDEs were calculated at the RCCSD(T)/6-311+G(2df), ROVGF/6-311+G(2df), TD-B3LYP/6-311+G(2df), and TD-PBE1PBE/6-311+G(2df), all at the B3LYP/6-311+G* optimized geometries. Good agreement between theoretical and experimental VDEs confirmed the computationally predicted global minimum structures. We found that the nona-coordinated wheel-type structure for AlB_9^- is not a global minimum and it is not even a low-lying isomer as was previously found for the neutral AlB_9 cluster. We have shown that this is due to the 1/2-σ-antiaromatic nature of the anionic wheel-type structure. However, addition of an extra electron to the C_1 global minimum structure of the neutral AlB_9 cluster does not disturb

its double (σ- and π-) aromaticity since the electron is localized on aluminum atom. Thus, the similar C_1 isomer I.1 is the global minimum of the anionic AlB_9^- cluster. The global minimum of the AlB_{10}^- cluster was also shown to represent a doubly (σ- and π-) "aromatic" system.

References

(1) Cotton, F. A. *Advanced Inorganic Chemistry*; Wiley: New York, **1999**.

(2) Greenwood, N. N. and Earnshaw, A. *Chemistry of the Elements*; Pergamon Press:Elmsford, NY, **1984**.

(3) Zhai, H. J.; Wang, L. S.; Alexandrova, A. N.; Boldyrev, A. I. *J. Chem. Phys.* **2002**, 117, 7917.

(4) Alexandrova, A. N.; Boldyrev, A. I.; Zhai, H. J.; Wang, L. S.; Steiner, E.; Fowler, P. W. *J. Phys. Chem. A* **2003**, 107, 1359.

(5) Zhai, H. J.; Alexandrova, A. N.; Birch, K. A.; Boldyrev, A. I.; Wang, L. S. *Angew. Chem., Int. Ed. Engl.* **2003**, 42, 6004.

(6) Zhai, H. J.; Kiran, B.; Li, J.; Wang, L. S. *Nat. Mater.* **2003**, 2, 827.

(7) Zhai, H. J.; Wang, L. S.; Alexandrova, A. N.; Boldyrev, A. I.; Zakrzewski, V. G. *J. Phys. Chem. A* **2003**, 107, 9319.

(8) Zhai, H. J.; Kiran, B.; Li, J.; Wang, L. S. *Nat. Mater.* **2003**, 2, 827.

(9) Alexandrova, A. N.; Zhai, H. J.; Wang, L. S.; Boldyrev, A. I. *Inorg. Chem.* **2004**, 43, 3552.

(10) Alexandrova, A. N.; Boldyrev, A. I.; Zhai, H.-J.; Wang, L. S. *J. Phys. Chem. A* **2004**,108, 3509.

(11) Kiran, B.; Bulusu, S.; Zhai, H. J.; Yoo, S.; Zeng, X. C.; Wang, L. S. *Proc. Natl. Acad. Sci. U. S. A.* **2005**, 102, 961.

(12) Alexandrova, A. N.; Boldyrev, A. I.; Zhai, H. J.; Wang, L. S. *J. Chem. Phys.* **2005**, 122, 054313.

(13) Alexandrova, A. N.; Boldyrev, A. I.; Zhai, H. J.; Wang, L. S. *Coord. Chem. Rev.* **2006**,250, 2811.

(14) Sergeeva, A. P.; Zubarev, D. Y.; Zhai, H. J.; Boldyrev, A. I.; Wang, L. S. *J. Am. Chem. Soc.* **2008**, 130, 7244.

(15) Pan, L. L.; Li, J.; Wang, L. S. *J. Chem. Phys.* **2008**, 129, 024302.

(16) Huang, W.; Sergeeva, A. P.; Zhai, H. J.; Averkiev, B. B.; Wang, L. S.; Boldyrev, A. I. *Nat. Chem.* **2010**, 2, 202.

(17) Alexandrova, A. N.; Boldyrev, A. I.; Zhai, H. J.; Wang, L. S. *Coord. Chem. Rev.* **2006**, 250, 2811.

(18) Zubarev, D. Y.; Boldyrev, A. I. *J. Comput. Chem.* **2007**, 28, 251.

(19) Romanescu, C.; Sergeeva, A. P.; Li, W.-L.; Boldyrev, A. I.; Wang, L. S. *J. Am. Chem. Soc.* **2011**, 113, 8646.

(20) Galeev, T. R.; Romanescu, C.; Li, W.-L.; Wang, L. S.; Boldyrev, A. I. *J. Chem. Phys.***2011**, 135, 140301.

(21) Jiang, Z. Y.; Luo, X. M.; Li, S. T.; Chu, S. Y. *Int. J. Mass Spectrom.* **2006**, 252, 197.

(22) Kawamata, H.; Negishi, Y.; Nakajima, A.; Kaya, K. *Chem. Phys. Lett.* **2001**, 337, 255.

(23) Feng, X. J.; Luo, Y. H. *J. Phys. Chem. A* **2007**, 111, 2420.

(24) Averkiev, B. B.; Boldyrev, A. I. *Russ. J. Gen. Chem.* **2008**, 78, 769.

(25) Averkiev, B. B.; Wang, L. M.; Huang, W.; Wang, L. S.; Boldyrev, A. I. *Phys. Chem. Chem. Phys.* **2009**, 11, 9840.

(26) Guo, J. C.; Yao, W. Z.; Li, Z.; Li, S. D. *Sci. China, Ser. B-Chem.* **2009**, 52, 566.

(27) Boyukata, M.; Guvenc, Z. B. *J. Alloy. Compd.* **2011**, 509, 4214.

(28) Simons, J. *J. Phys. Chem. A* **2008**, 112, 6401.

(29) Simons, J. *Annu. Rev. Phys. Chem.* **2011**, 62, 107.

(30) Wang, L. S.; Cheng, H. S.; Fan, J. W. *J. Chem. Phys.* **1995**, 102, 9480.

(31) Wang, L.-S.; Wu, H. In *Advances in Metal and Semiconductor Clusters*; Duncan, M. A., Ed.; JAI Press: Greenwich, CT, **1998**; Vol. 4; pp 299– 343.

(32) Akola, J.; Manninen, M.; Hakkinen, H.; Landman, U.; Li, X.; Wang, L. S. *Phys. Rev. B***1999**, 60, 11297.

(33) Wang, L.-S.; Li, X. In *Proc. Int. Symp. on Clusters and Nanostructure Interfaces* (Oct. 25–28, 1999, Richmond, VA); Jena, P.; Khanna, S. N.; Rao, B. K., Eds.; World Scientific:River Edge, NJ, **2000**; pp 293– 300.

(34) Sergeeva, A. P.; Averkiev, B. B.; Zhai, H.-J.; Boldyrev, A. I.; Wang, L. S *J. Chem. Phys.***2011**, 134, 224304.

(35) Becke, A. D. *J. Chem. Phys.* **1993**, 98, 5648.

(36) Vosko, S. H.; Wilk, L.; Nusair, M. *Can. J. Phys.* **1980**, 58, 1200.

(37) Lee, C.; Yang, W.; Parr, R. G. *Phys. Rev. B* **1988**, 37, 785.

(38) Binkley, J. S.; Pople, J. A.; Hehre, W. J. *J. Am. Chem. Soc.* **1980**, 102, 939.

(39) Gordon, M. S.; Binkley, J. S.; Pople, J. A.; Pietro, W. J.; Hehre, W. J. *J. Am. Chem. Soc.* **1982**, 104, 2797.

(40) Pietro, W. J.; Francl, M. M.; Hehre, W. J.; Defrees, D. J.; Pople, J. A.; Binkley, J. S. *J. Am. Chem. Soc.* **1982**, 104, 5039.

(41) McLean, A. D.; Chandler, G. S. *J. Chem. Phys.* **1980**, 72, 5639.

(42) Clark, T.; Chandrasekhar, J.; Spitznagel, G. W.; Schleyer, P. v. R. *J. Comput. Chem.***1983**, 4, 294.

(43) Cizek, J. *Adv. Chem. Phys.* **1969**, 14, 35.

(44) Purvis, G.; Bartlett, R. J. *J. Chem. Phys.* **1982**, 76, 1910.

(45) Raghavachari, K.; Trucks, G. W.; Pople, J. A.; Head-Gordon, M. *Chem. Phys. Lett.***1989**, 157, 479.

(46) Werner, H.-J.; Knowles, P. J.; Lindh, R.MOLPRO, version 2006.1, a package of ab initio programs.

(47) Frisch, M. J.; Trucks, G. W.; Schlegel, H. B. Gaussian 03, revision D.01; Gaussian, Inc.:Wallingford, CT, **2004**.

(48) Cederbaum, L. S. *J. Phys. B* **1975**, 8, 290.

(49) Ortiz, J. V. *Int. J. Quantum Chem., Quantum Chem. Symp.* **1989**, 23, 321.

(50) Lin, J. S.; Ortiz, J. V. *Chem. Phys. Lett.* **1990**, 171, 197.

(51) Zakrzewski, V. G.; Ortiz, J. V.; Nichols, J. A.; Heryadi, D.; Yeager, D. L.; Golab, J. T. *Int. J. Quantum Chem.* **1996**, 60, 29.

(52) Bauernschmitt, R.; Alrichs, R. *Chem. Phys. Lett.* **1996**, 256, 454.

(53) Casida, M. E.; Jamorski, C.; Casida, K. C.; Salahub, D. R. *J. Chem. Phys.* **1998**, 108,4439.

(54) Perdew, J. P.; Burke, K.; Ernzerhof, M. *Phys. Rev. Lett.* **1996**, 77, 3865.

(55) Perdew, J. P.; Burke, K.; Ernzerhof, M. *Phys. Rev. Lett. M* **1997**, 78, 1396.

(56) Zubarev, D. Yu.; Boldyrev, A. I. *Phys. Chem. Chem. Phys.* **2008**, 10, 5207.

(57) Zubarev, D. Yu.; Boldyrev, A. I. *J. Org. Chem.* **2008**, 73, 9251.

(58) Zubarev, D. Yu.; Boldyrev, A. I. *J. Phys. Chem. A* **2009**, 113, 866.

(59) Zubarev, D. Yu.; Robertson, N.; Domin, D.; McClean, J.; Wang, J. H.; Lester, W. A.; Whitesides, R.; You, X. Q.; Frenklach, M. *J. Phys. Chem. C* **2010**, 114, 5429.

(60) MOLDEN 3.4. Schaftenaar, G., *CAOS/CAMM Center*, The Netherlands, **1998**.

(61) Varetto, U. Molekel 5.4.0.8, Swiss National Supercomputing Centre: Manno, *Switzerland* **2009**.

(62) Zubarev, D. Yu.; Sergeeva, A. P.; Boldyrev, A. I. In *Chemical Reactivity Theory: A Density Functional View*; Chattaraj, P. K., Ed.; CRC Press, Taylor & Francis Group: New York, **2009**, pp 439– 452.

Table 5-1. Experimentally observed and theoretically calculated VDEs for the I.1 isomer (C_1, ^{2}A) of AlB_9^-.[a]

feature	VDE (exp.)[b]	final state and electronic configuration	VDE (theoretical)		
			TD-B3LYP[c]	TD-PBE1PBE[d]	RCCSD(T)[e]
X	3.15(5)	^{1}**A,** ...9a$^{(2)}$10a$^{(2)}$11a$^{(2)}$12a$^{(2)}$13a$^{(2)}$14a$^{(2)}$15a$^{(2)}$16a$^{(0)}$	3.08	3.21	3.01
A	3.36(4)	^{3}**A,** ...9a$^{(2)}$10a$^{(2)}$11a$^{(2)}$12a$^{(2)}$13a$^{(2)}$14a$^{(2)}$15a$^{(1)}$16a$^{(1)}$	3.28	3.33	3.43
		^{1}**A,** ...9a$^{(2)}$10a$^{(2)}$11a$^{(2)}$12a$^{(2)}$13a$^{(2)}$14a$^{(2)}$15a$^{(1)}$16a$^{(1)}$	3.88	4.01	[g]
B	4.40(4)	^{3}**A,** ...9a$^{(2)}$10a$^{(2)}$11a$^{(2)}$12a$^{(2)}$13a$^{(2)}$14a$^{(1)}$15a$^{(2)}$16a$^{(1)}$	4.21	4.35	[g]
		^{1}**A,** ...9a$^{(2)}$10a$^{(2)}$11a$^{(2)}$12a$^{(2)}$13a$^{(2)}$14a$^{(1)}$15a$^{(2)}$16a$^{(1)}$	4.59	4.79	[g]
C	4.79(5)	^{3}**A,** ...9a$^{(2)}$10a$^{(2)}$11a$^{(2)}$12a$^{(2)}$13a$^{(1)}$14a$^{(2)}$15a$^{(2)}$16a$^{(1)}$	4.70	4.78	[g]
D	4.91(5)	^{3}**A,** ...9a$^{(2)}$10a$^{(2)}$11a$^{(2)}$12a$^{(1)}$13a$^{(2)}$14a$^{(2)}$15a$^{(2)}$16a$^{(1)}$	4.82	4.93	[g]
		^{1}**A,** ...9a$^{(2)}$10a$^{(2)}$11a$^{(2)}$12a$^{(2)}$13a$^{(1)}$14a$^{(2)}$15a$^{(2)}$16a$^{(1)}$	5.02	5.20	[g]
		^{1}**A,** ...9a$^{(2)}$10a$^{(2)}$11a$^{(2)}$12a$^{(1)}$13a$^{(2)}$14a$^{(2)}$15a$^{(2)}$16a$^{(1)}$	5.32	5.47	[g]
E	5.36(5)	^{3}**A,** ...9a$^{(2)}$10a$^{(2)}$11a$^{(1)}$12a$^{(2)}$13a$^{(2)}$14a$^{(2)}$15a$^{(2)}$16a$^{(1)}$	5.36	[f]	[g]
		^{3}**A,** ...9a$^{(2)}$10a$^{(1)}$11a$^{(2)}$12a$^{(2)}$13a$^{(2)}$14a$^{(2)}$15a$^{(2)}$16a$^{(1)}$	5.42	[f]	[g]
		^{1}**A,** ...9a$^{(2)}$10a$^{(2)}$11a$^{(1)}$12a$^{(2)}$13a$^{(2)}$14a$^{(2)}$15a$^{(2)}$16a$^{(1)}$	5.78	5.96	[g]
		^{1}**A,** ...9a$^{(2)}$10a$^{(1)}$11a$^{(2)}$12a$^{(2)}$13a$^{(2)}$14a$^{(2)}$15a$^{(2)}$16a$^{(1)}$	5.95	[f]	[g]

[a]All energies are in eV. [b]Numbers in parentheses represent the uncertainty in the last digit. [c]VDEs were calculated at TD-B3LYP/6-311+G(2df)//B3LYP/6-311+G*.[d]VDEs were calculated at TD-PBE1PBE/6-311+G(2df)//B3LYP/6-311+G*. [e]VDEs were calculated at RCCSD(T)/6-311+G(2df)//B3LYP/6-311+G*. [f]We were not able to calculate these VDE at the TD-PBE1PBE/6-311+G(2df)//B3LYP/6-311+G*. [g]VDE value cannot be calculated at this level of theory.

Table 5-2. Experimentally observed and theoretically calculated VDEs for II.1 isomer (C_s, ^{1}A') of AlB_{10}^-.[a]

feature	VDE (exp.)[b]	final state and electronic configuration	VDE (theoretical)			
			TD-B3LYP[c]	TD-PBE1PBE[d]	ROVGF[e]	RCCSD(T)[f]
X	3.61(5)	^{2}**A''**, ... $5a''^{(2)}8a'^{(2)}6a''^{(2)}9a'^{(2)}10a'^{(2)}7a''^{(1)}$	3.51	3.61	3.52 (0.88)	3.67
A	3.78(5)	^{2}**A'**, ... $5a''^{(2)}8a'^{(2)}6a''^{(2)}9a'^{(2)}10a'^{(1)}7a''^{(2)}$	3.55	3.55	3.79 (0.88)	3.80
B	4.26(5)	^{2}**A'**, ... $5a''^{(2)}8a'^{(2)}6a''^{(2)}9a'^{(1)}10a'^{(2)}7a''^{(2)}$	4.09	4.19	4.24 (0.88)	[g]
C	4.91(5)	^{2}**A''**, ... $5a''^{(2)}8a'^{(2)}6a''^{(1)}9a'^{(2)}10a'^{(2)}7a''^{(2)}$	4.74	5.00	5.11 (0.88)	[g]
D	5.31(5)	^{2}**A'**, ... $5a''^{(2)}8a'^{(1)}6a''^{(2)}9a'^{(2)}10a'^{(2)}7a''^{(2)}$	5.23	5.44	5.51 (0.86)	[g]
		^{2}**A''**, ... $5a''^{(1)}8a'^{(2)}6a''^{(2)}9a'^{(2)}10a'^{(2)}7a''^{(2)}$	5.89	5.96	6.29 (0.83)	[g]

[a]All energies are in eV. [b]Numbers in parentheses represent the uncertainty in the last digit. [c]VDEs were calculated at TD-B3LYP/6-311+G(2df)//B3LYP/6-311+G*. [d]VDEs were calculated at TD-PBE1PBE/6-311+G(2df)//B3LYP/6-311+G*. [e]VDEs were calculated at ROVGF/6-311+G(2df)//B3LYP/6-311+G*. Values in parentheses represent the pole strength of the OVGF calculation. [f]VDEs were calculated at RCCSD(T)/6-311+G(2df)//B3LYP/6-311+G*.[g]VDE value cannot be calculated at this level of theory.

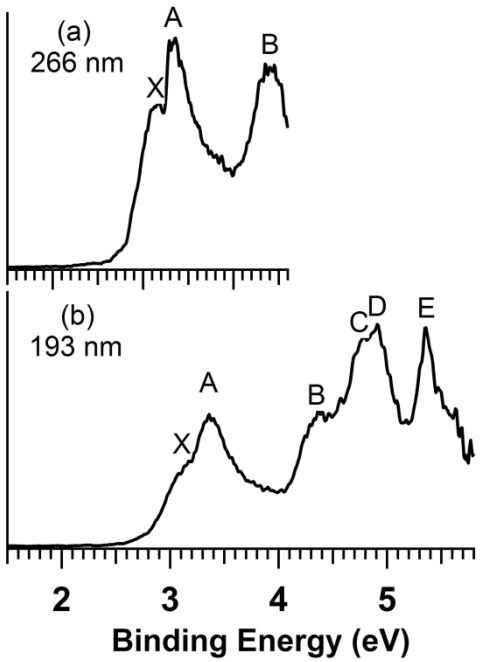

Figure 5-1. Photoelectron spectra of AlB_9^- at (a) 266 nm, and (b) 193 nm photodetachment wavelengths.

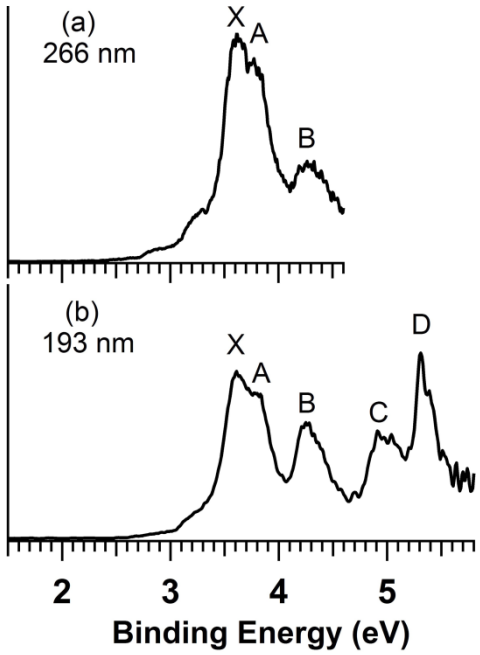

Figure 5-2. Photoelectron spectra of AlB_{10}^- at (a) 266 nm, and (b) 193 nm photodetachment wavelengths.

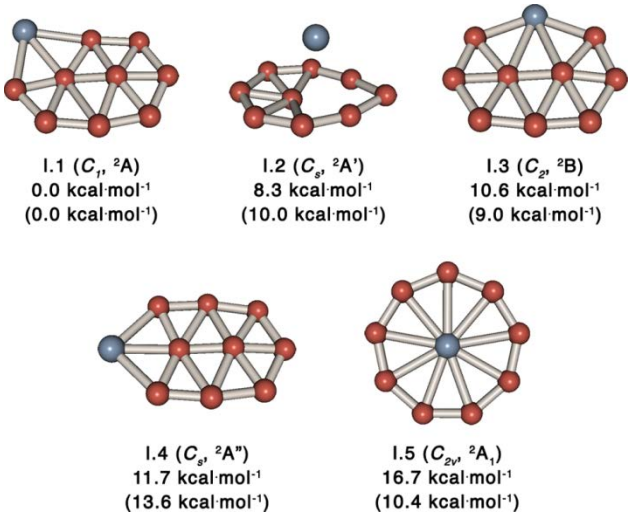

Figure 5-3. Isomers of the AlB_9^- cluster, their point group symmetries, spectroscopic states, and relative energies. Relative energies are given at the RCCSD(T)/6-311+G(2df)//B3LYP/6-311+G* and the B3LYP/6-311+G* (in brackets) levels of theory. All the relative energies are ZPE corrected.

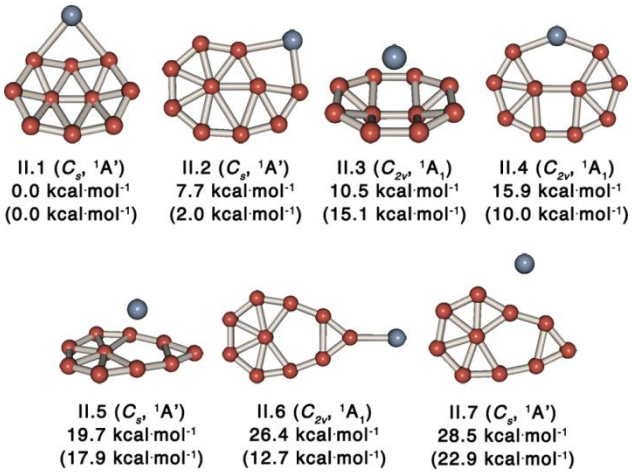

Figure 5-4. Isomers of the AlB_{10}^- cluster, their point group symmetries, spectroscopic states, and relative energies. Relative energies are given at the RCCSD(T)/6-311+G(2df)//B3LYP/6-311+G* and the B3LYP/6-311+G* (in brackets) levels of theory. All the relative energies are ZPE corrected.

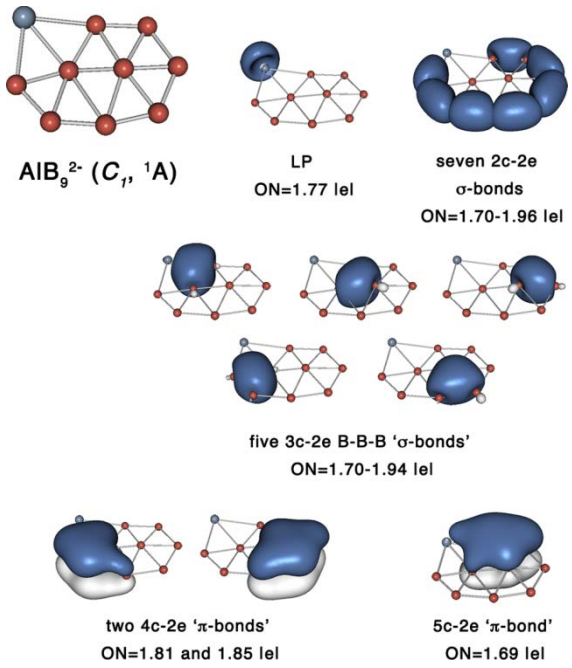

Figure 5-5. Chemical bonding elements revealed by AdNDP for the AlB_9^{2-} (C_1, ^1A) at the geometry

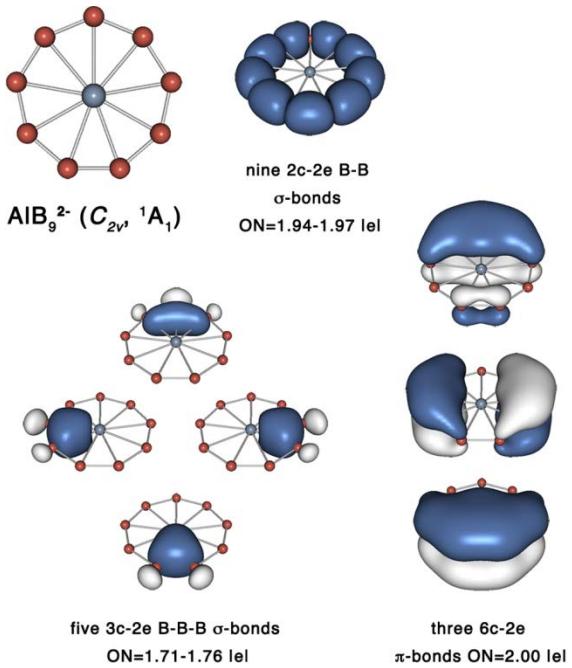

Figure 5-6. AdNDP analysis (B3LYP/6-311+G*) of the AlB_9^{2-} (C_{2v}, $^1A_1$) at the geometry optimized for the isomer I.5 of the AlB_9^- (C_{2v}, $^2A_1$) cluster.

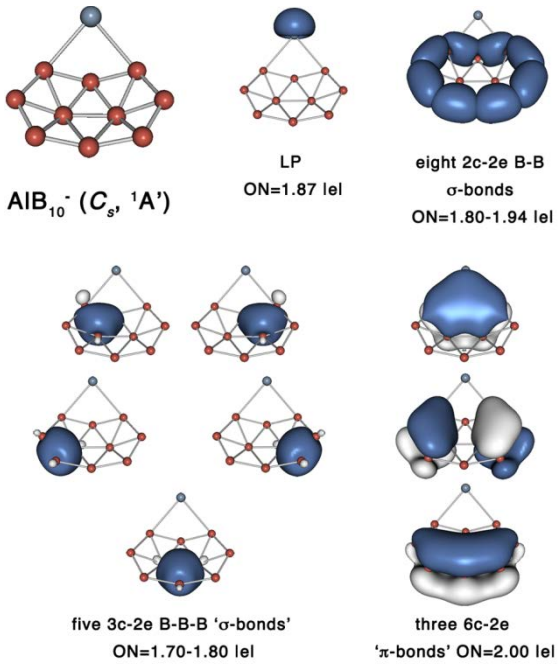

Figure 5-7. AdNDP analysis (B3LYP/6-311+G*) of the global minimum isomer II.1 (C_s, ^{1}A') of AlB_{10}^-.

CHAPTER 6

AROMATIC METAL-CENTERED MONOCYCLIC BORON RINGS: $Co©B_8^-$ AND $Ru©B_9^-$ *

Abstract

Perfect symmetry: Photoelectron spectroscopy and theoretical calculations show that the B_8 and B_9 rings are stabilized by the metal atoms in $Co©B_8^-$ and $Ru©B_9^-$, which possess D_{8h} and D_{9h} symmetry, respectively. The bonding between the metal atom and the boron ring is described by six delocalized σ electrons and six delocalized π electrons, which result in double aromaticity.

Bulk boron, which is characterized by 3D cage-like structural features, is a refractory material.[1,2] However, 3D cage structures were suggested to be unstable for small boron clusters, and planar or quasi-planar structures have been proposed instead.[3-5] Experimental studies combined with high-level calculations have shown that small boron cluster ions are planar up to at least B_{20}^-,[6-10] whereas B_n^+ ions have been found to be planar up to n=16.[11] The chemical bonding in the planar boron clusters has been found to be quite remarkable;[6-9] in addition to the strong and localized bonding in the circumferences, there are two types of delocalized bonding – the in-plane σ and the out-of-plane π bonding, each of which follows the $(4N+2)$ Hückel rule for aromaticity. In particular, systems with six σ and six π electrons (N=1) are doubly aromatic, and give rise

* Coauthored by Constantin Romanescu, Timur R. Galeev, Wei-Li Li, Alexander I. Boldyrev, and Lai-Sheng Wang. Reproduced with permission from *Angew. Chem. Int. Ed.*. **2011**, *50*, 9334-9337.

to highly symmetric planar clusters, such as B_8^{2-} and B_9^-, which each contain a central B atom and a B_7 and B_8 monocyclic ring, respectively.[6] In the D_{7h} B_8^{2-} and D_{8h} B_9^- molecular wheels, each B atom in the circumference contributes two electrons to the B–B peripheral covalent bonds and one electron to the delocalized bonds, whereas the central B atom contributes all its valence electrons to the delocalized bonds. These novel bonding situations suggest that other atoms with appropriate numbers of valence electrons and sizes may be able to replace the central boron atom to produce M©B_n-type clusters.[12]

Hexagonal, heptagonal, and octagonal C©B_n-type clusters have been proposed from theoretical calculations as examples of hexa-, hepta-, and octacoordinate planar carbons.[13-15] However, photoelectron spectroscopy (PES) studies showed that carbon occupies the peripheral position in such clusters rather than the center,[16,17] because C is more electronegative than B and thus prefers to participate in localized two-center-two-electron (2c-2e) σ bonding, which is possible only at the circumference of the wheel structure. Transition-metal atoms are better suited for the central position in the M©B_n clusters, as these metals favor participation in delocalized bonding at the center over localized bonding at the periphery. For an M©B_n cluster, the electronic requirement for the central atom is $x=12-n$ or $x=12-n-k$ for an M©B_n^{k-} anion, where x is the valence of the transition-metal atom M, in order to satisfy the peripheral B-B σ bonding and the σ and π Hückel aromaticity for $N=1$. Indeed, all 3d transition-metal atoms have been tested computationally for the M©B_n-type hypercoordinate complexes.[18-21] Two complexes, namely Co©B_8^- and Fe©B_9^-, in which the Co and Fe atoms are trivalent and divalent,

respectively, were found to be closed-shell global minima, in agreement with our electronic design principle.

We have focused our experimental efforts on transition-metal-doped boron clusters that involve Group 8 (Fe, Ru, Os) and 9 (Co, Rh, Ir) elements. The experiments were carried out using a PES apparatus equipped with a laser vaporization supersonic cluster source and a magnetic-bottle PES analyzer (see the Experimental Section). Spectra were obtained for a wide range of MB_n^- clusters. The spectra of CoB_8^- and RuB_9^- (Figure 6-1) were different, in that, they both displayed relatively high electron binding energies and simple spectral patterns (see Figure 6-2 for a comparison of the spectra of RuB_n^- for n=3–10).[22] The first adiabatic detachment energies (ADEs) and the vertical detachment energies (VDEs) of all the spectral features for the two doped boron clusters are given in Table 6-1 and are compared with theoretical calculations. Four detachment features (X, A–C) were observed for CoB_8^- (Figure 6-1a).[23] At 266 nm (Figure 6-1b), the X band was vibrationally resolved: two vibrational modes were observed, one with a frequency of (1200±50) cm^{-1} and another with a frequency of (520±50) cm^{-1}. The A band was weak at 193 nm (Figure 6-1a) and became even weaker at 266 nm (Figure 6-1b). Four well-resolved bands (X, A–C) were also observed in the spectrum of RuB_9^- (Figure 6-1c). At 266 nm (Figure 6-1d), the X band was observed to be fairly sharp without any resolved vibrational structures, thus suggesting that a very low frequency mode was involved and that there was little geometry change between the anion and the neutral ground state. The A band of RuB_9^- was vibrationally resolved with three vibrational modes (Figure 6-1d): (550±50), (1240±50), and (1560±50) cm^{-1}. The

simple spectral patterns and the resolved vibrational structures for such complicated systems suggest that CoB_8^- and RuB_9^- should have high symmetries.

To confirm the symmetries of CoB_8^- and RuB_9^-, we optimized their structures (see Experimental Section) and found that the D_{8h} Co©B_8^- ($^1A_{1g}$, …$3a_{1g}^2\,2e_{1u}^4$) and D_{9h} Ru©B_9^- ($^1A_1'$, …$2e_1'^4\,3a_1'^2$) are indeed minima on the potential energy surfaces (Figure 6-3). Our result for Co©$B_8^-$is consistent with previous calculations.[20] We computed the VDEs for these clusters at several levels of theory (Table 6-1) and found excellent agreement with the experimental data. Optimization of the neutral clusters led to a lower symmetry D_{2h} Co©B_8 and a C_{9v} Ru©B_9 (Figure 6-2). The actual structural distortions are relatively minor. The Ru atom is only approximately 0.1 Å out of plane in the neutral C_{9v} RuB_9. The highest occupied molecular orbital (HOMO) of the D_{8h} Co©B_8^- is degenerate ($2e_{1u}$). Detachment of an electron from the $2e_{1u}$ HOMO results in Jahn–Teller distortions that reduce the symmetry of Co©B_8 to D_{2h}. We calculated the vibrational frequencies of the D_{2h} Co©B_8 and found four totally symmetric modes: 442 (ν_1), 549 (ν_2), 754 (ν_3), and 1160 (ν_4) cm^{-1}. The frequencies of two of these modes (ν_2 and ν_4), which are responsible for the D_{8h} to D_{2h} distortion, are in excellent agreement with the observed vibrational frequencies of (520±50) and (1200±50) cm^{-1} in the X band of the photoelectron spectrum (Figure 6-1b). The calculated ADE of CoB_8^- is also in excellent agreement with the experimental value (Table 6-1).

The HOMO of the D_{9h} Ru©B_9^- is $3a_1'$, which is primarily of Ru $4d_z^2$ character (Figure 6-4). The out-of-plane distortion is consistent with the nature of this HOMO. This structural distortion suggests that the vibrational mode, which is active upon removing an

electron from the HOMO, should involve the Ru atom moving up and down. This mode has a calculated frequency of 36 cm^{-1}, which is in agreement with the unresolved low frequency vibration of the X band (Figure 6-1d). The HOMO-1 ($2\,e_1'$) of $Ru©B_9^-$ is degenerate and Jahn–Teller distortions are expected for detachment from this orbital, consistent with the observed vibrational features in the A band (Figure 6-1d). The calculated ADE of $Ru©B_9^-$ is also in good agreement with the experimental value (Table 6-1). Overall, the theoretical results and the experimental observations are in excellent agreement, thus confirming unequivocally that the D_{8h} $Co©B_8^-$ and D_{9h} $Ru©B_9^-$ structures are highly stable and should be the global minima on their respective potential energy surfaces.

The valence MOs for the D_{8h} $Co©B_8^-$ and D_{9h} $Ru©B_9^-$ are shown in Figure 6-4. The MOs responsible for the B-B bonding in the circumference, the delocalized π bonding (HOMO-2 ($1\,a_{2u}$) and HOMO-4 ($1\,e_{1g}$) for $Co©B_8^-$; HOMO-2 ($1\,a_2''$) and HOMO-4 ($1\,e_1''$) for $Ru©B_9^-$), and the delocalized σ bonding (HOMO ($2\,e_{1u}$) and HOMO-6 ($2\,a_{1g}$) for $Co©B_8^-$; HOMO-1 ($2\,e_1'$) and HOMO-5 ($2\,a_1'$) for $Ru©B_9^-$) can be readily recognized. Each complex contains six delocalized π and six delocalized σ electrons, thus resulting in double aromaticity and high electronic stability. Each complex also has three primarily d-based orbitals (d_z^2, d_{xy}, and $d_{x^2-y^2}$), which can also be readily recognized. The adaptive natural density partitioning (AdNDP) analyses[24] show the bonding situations in the two complexes more clearly (Figure 6-5). These results show the lone pairs of electrons in the d orbitals, the B-B peripheral bonds, and the double aromaticity in both clusters. The occupation numbers for the localized and delocalized

MOs are all close to 2. However, the two d-based MOs (d_{xy} and $d_{x^2-y^2}$) have occupation numbers significantly less than 2 (1.81|e| in CoB_8^- and 1.65|e| in RuB_9^-), thus suggesting that these MOs are involved in covalent interactions between the monocyclic ligands and the central metal atoms with the contribution of the 4d element (Ru) being higher than that of the 3d element (Co). Co is formally trivalent in $Co©B_8^-$ and Ru is formally divalent in $Ru©B_9^-$, consistent with our electronic design principle.

According to this design principle, the smaller the B_n ring, the higher the required valence of the central atom M. For example, for a B_6 ring, a hexavalent atom is required for $M©B_6$ or a pentavalent atom for an $M©B_6^-$ ion. The C-centered CB_6^{2-} and CB_7^-, which were studied computationally,[13] are consistent with our design principle, even though they are not the global minima.[16,17] Geometrical effects, that is, the size of the central atom has to be appropriate for optimal stability of the $M©B_n$ clusters, dictate that the B_6 or even the B_7 ring is too small to host a transition-metal atom in the center. Thus, the B_8 and B_9 rings are optimal for hosting a central transition-metal atom. The B_{10} ring is most likely too large to host a divalent (for $M©B_{10}$) or monovalent atom (for $M©B_{10}^-$). For example, the global minimum of AuB_{10}^- has been shown to be an Au atom that interacts with a B_{10} cluster on its periphery, whilst the D_{10h} $Au©B_{10}^-$, albeit a local minimum, is much higher in energy.[25]

The first transition-metal atom centered in a planar monocyclic ring appears to be $Fe©Sn_5^+$ and $Fe©Bi_5^+$, although these structures are not the global minima on their respective potential energy surfaces.[26] The $Co©B_8^-$ and $Ru©B_9^-$ clusters reported here are unprecedented in chemistry with coordination numbers of 8 and 9 in perfect planar

environments. The M©B_n^- systems are unique because of the ability of boron to form multicenter bonds and the ensuring multiple aromaticity. Because of the central position of the transition-metal atom in M©B_n^-, appropriate ligands may be conceived for coordination above and below the molecular plane, thus rendering chemical protection and allowing syntheses of this new class of novel boron-based metal complexes with unexpected chemical properties.

6-1. Experimental Section

6-1.1. Photoelectron spectroscopy

Mixed boron (enriched in ^{11}B) and transition metal (M) targets were ablated by a pulsed laser. Clusters formed from the laser-induced plasma were entrained into a helium carrier gas and underwent a supersonic expansion. Anions in the cold cluster beam were analyzed using a time-of-flight mass spectrometer. Clusters of interest were selected by a mass gate and decelerated before being intercepted by a laser beam. Two detachment photon energies were used: 193 nm (6.424 eV) from an ArF excimer laser and 266 nm (4.661 eV) from a Nd:YAG laser. Photoelectrons were analyzed by a magnetic-bottle-type analyzer and calibrated by the known spectrum of Bi^-. The electron binding energy spectra presented in Figure 6-1 were obtained by subtracting the kinetic energy spectra from the respective photon energies. The electron kinetic energy resolution of the apparatus was $\Delta E_k/E_k \approx 2.5$ %, that is, about 25 meV for 1 eV electrons.[27]

6-1.2. Theoretical calculations

Geometry optimizations and frequency analyses for $Co©B_8^-$ and $Co©B_8$ were performed using the PBE1PBE and B3LYP hybrid density functionals with the 6–311+G* basis set. VDE and ADE calculations were performed at three levels of theory: ROCCSD(T)/6–311+G(2df) and ROPBE1PBE/6–311+G(2df) (both at PBE1PBE/6–311+G* geometries) and ROB3LYP/6–311+G(2df)//B3LYP/6–311+G*. ROPBE1PBE/Ru/Stuttgart/B/aug-cc-pvTZ and ROB3LYP/Ru/Stuttgart/B/aug-cc-pvTZ were used for similar calculations on $Ru©B_9^-$ and $Ru©B_9$. VDE and ADE values were also calculated at ROCCSD(T)/Ru/Stuttgart/B/aug-cc-pvTZ (at PBE1PBE/Ru/Stuttgart/B/aug-cc-pvTZ geometries). Chemical bonding analyses (PBE1PBE/LANL2DZ) of both clusters were performed using the AdNDP method.[24] All calculations were carried out using Gaussian 03 and Gaussian 09.[28] Molekel 5.4.0.8 was used for MO visualization.[29]

References

[1] H. Hubert, B. Devouard, L. A. J. Garvie, M. O'Keeffe, P. R. Buseck, W. T. Petuskey, P. F. McMillan, *Nature* **1998**, *391*, 376.

[2] M. Fujimori, T. Nakata, T. Nakayama, E. Nishibori, K. Kimura, M. Takata, M. Sakata, *Phys. Rev. Lett.* **1999**, *82*, 4452.

[3] R. Kawai, J. H. Weare, *J. Chem. Phys.* **1991**, *95*, 1151.

[4] A. Ricca, C. W. Bauschlicher, *Chem. Phys.* **1996**, *208*, 233.

[5] I. Boustani, *Phys. Rev. B* **1997**, *55*, 16426.

[6] H. J. Zhai, A. N. Alexandrova, K. A. Birch, A. I. Boldyrev, L. S. Wang, *Angew. Chem.* 2003, **115**, 6186; *Angew. Chem. Int. Ed.* **2003**, *42*, 6004.

[7] H. J. Zhai, B. Kiran, Li, J., L. S. Wang, *Nat. Mater.* **2003**, *2*, 827.

[8] A. P. Sergeeva, D. Y. Zubarev, H. J. Zhai, A. I. Boldyrev, L. S. Wang, *J. Am. Chem. Soc.* **2008**, *130*, 7244.

[9] W. Huang, A. P. Sergeeva, H. J. Zhai, B. B. Averkiev, L. S. Wang, A. I. Boldyrev, *Nat. Chem.* **2010**, *2*, 202.

[10] B. Kiran, S. Bulusu, H. J. Zhai, S. Yoo, X. C. Zeng, L. S. Wang, *Proc. Natl. Acad. Sci. USA* **2005**, *102*, 961.

[11] E. Oger, N. R. M. Crawford, R. Kelting, P. Weis, M. M. Kappes, R. Ahlrichs, *Angew. Chem.* **2007**, *119*, 8656; *Angew. Chem. Int. Ed.* **2007**, *46*, 8503.

[12] The @ sign has already been used to indicate endohedral doping in 3D cage clusters, such as in He@C_{60} or Cu@Au_{16}. We propose the © sign to designate the central position of the doped atom in monocyclic structures in M©B_n-type planar clusters.

[13] K. Exner, P. von R. Schleyer, *Science* **2000**, *290*, 1937.

[14] Z. X. Wang, P. von R. Schleyer, *Science* **2001**, *292*, 2465.

[15] R. M. Minyaev, T. N. Gribanova, A. G. Starikov, V. I. Minkin, *Mendeleev Commun.* **2001**, *11*, 213.

[16] L. M. Wang, W. Huang, B. B. Averkiev, A. I. Boldyrev, L. S. Wang, *Angew. Chem.* 2007, **119**, 4634; *Angew. Chem. Int. Ed.* **2007**, *46*, 4550.

[17] B. B. Averkiev, D. Y. Zubarev, L. M. Wang, W. Huang, L. S. Wang, A. I. Boldyrev, *J. Am. Chem. Soc.* **2008**, *130*, 9248–9250.

[18] Q. Luo, *Sci. China Ser. B* **2008**, *51*, 607.

[19] Q. Y. Wu, Y. P. Tang, X. H. Zhang, *Sci. China Ser. B* **2009**, *52*, 288.

[20] K. Ito, Z. Pu, Q. S. Li, P. von R. Schleyer, *Inorg. Chem.* **2008**, *47*, 10906.

[21] Z. Pu, K. Ito, P. von R. Schleyer, Q. S. Li, *Inorg. Chem.* **2009**, *48*, 10679.

[22] Although D_{9h} FeB_9^- was suggested to be a closed-shell global minimum (Ref. [20]), its photoelectron spectrum displays broad features, thus indicating the existence of possible low-lying isomers.

[23] The weak signal near 2.6 eV was likely due to the presence of a triplet excited state of CoB_8^- in the cluster beam, which would be metastable and long-lived. The signals above 5.5 eV were too noisy to allow identification of definitive spectral transitions.

[24] D. Y. Zubarev, A. I. Boldyrev, *Phys. Chem. Chem. Phys.* **2008**, *10*, 5207.

[25] H. J. Zhai, C. Q. Miao, S. D. Li, L. S. Wang, *J. Phys. Chem. A* **2010**, *114*, 12155.

[26] M. Lein, J. Frunzke, G. Frenking, *Angew. Chem.* **2003**, *115*, 1341; *Angew. Chem. Int. Ed.* **2003**, *42*, 1303.

[27] L. S. Wang, H. S. Cheng, J. Fan, *J. Chem. Phys.* **1995**, *102*, 9480.

[28] M. J. Frisch, et al., GAUSSIAN 03, Rev. C.02, Gaussian, Inc., Wallingford, CT, **2004** and GAUSSIAN 09, Rev. B.01, Gaussian, Inc., Wallingford, CT, **2009**.

[29] U. Varetto, Molekel 5.4.0.8, Swiss National Supercomputing Centre, Manno, Switzerland, **2009**.

Table 6-1. Comparison between experimental and theoretical results. Observed vertical electron detachment energies (VDEs) for CoB_8^- and RuB_9^- compared with theoretical values calculated from the D_{8h} $Co©B_8^-$ ($^1A_{1g}$) and D_{9h} $Ru©B_9^-$ ($^1A_1'$)

Observed features	VDE (exp)[a]	Final State and Electronic Configuration	VDE (theoretical) PBE1PBE[b]	B3LYP[c]	ROCCSD(T)[d]
		$Co©B_8^-$ (D_{8h}, $^1A_{1g}$)			
X[e]	3.84 (1)	$^2E_{1u}$ … $1b_{2g}^2 1e_{1g}^4 2e_{2g}^4 1a_{2u}^2 3a_{1g}^2 2e_{1u}^3$	3.81	3.72	3.88
A	4.23 (2)	$^2A_{1g}$ … $1b_{2g}^2 1e_{1g}^4 2e_{2g}^4 1a_{2u}^2 3a_{1g}^1 2e_{1u}^4$	3.90	3.97	4.20
B	4.82 (3)	$^2E_{2g}$ … $1b_{2g}^2 1e_{1g}^4 2e_{2g}^3 1a_{2u}^2 3a_{1g}^2 2e_{1u}^4$	4.60	4.58	4.82
C	5.21 (4)	$^2E_{1g}$ … $1b_{2g}^2 1e_{1g}^3 2e_{2g}^4 1a_{2u}^2 3a_{1g}^2 2e_{1u}^4$	5.12	5.17	5.58
		$^2A_{2u}$ … $1b_{2g}^2 1e_{1g}^4 2e_{2g}^4 1a_{2u}^1 3a_{1g}^2 2e_{1u}^4$	5.27	5.15	
		$Ru©B_9^-$ (D_{9h}, $^1A_1'$)			
X[f]	3.85 (1)	$^2A_1'$ ...$2a_1'^2 1e_1''^4 2e_2'^4 1a_2''^2 2e_1'^4 3a_1'^1$	3.68	3.70	3.80
A[g]	4.15 (1)	$^2E_1'$ ... $2a_1'^2 1e_1''^4 2e_2'^4 1a_2''^2 2e_1'^3 3a_1'^2$	4.17	4.05	4.28
B	5.11 (3)	$^2E_2'$ ... $2a_1'^2 1e_1''^4 2e_2'^3 1a_2''^2 2e_1'^4 3a_1'^2$	5.22	5.12	5.30
C	5.29 (3)	$^2A_2$" ... $2a_1'^2 1e_1''^4 2e_2'^4 1a_2''^1 2e_1'^4 3a_1'^2$	5.30	5.16	5.45

[a]Numbers in parentheses represent the uncertainty in the last digit. [b]VDEs for $Co©B_8^-$ were calculated at ROPBE1PBE/6-311 + G(2df)//PBE1PBE/6-311+G*; VDEs for $Ru©B_9^-$ were calculated at ROPBE1PBE/Ru/Stuttgart/B/aug-cc-pvTZ.[c]VDEs for $Co©B_8^-$ were calculated at ROB3LYP/6-311+G(2df)//B3LYP/6-311+G*; VDEs for $Ru©B_9^-$ were calculated at ROB3LYP/Ru/Stuttgart/B/aug-cc-pvTZ. [d]VDEs for $Co©B_8^-$ were calculated at ROCCSD(T)/6-311+G(2df)//PBE1PBE/6-311+G*. VDEs for $Ru©B_9^-$ were calculated at ROCCSD(T)/Ru/Stuttgart/B/aug-cc-pvTZ. [e]Measured adiabatic detachment energy (ADE) is the same as the VDE. [f]Measured ADE = 3.83 ± 0.02 eV. Calculated ADE at ROCCSD(T)/Ru/Stuttgart/B/aug-cc-pvTZ//PBE1PBE/Ru /Stuttgart/B/aug-cc-pvTZ with ZPE correction = 3.75 eV. [g]Observed vibrational frequencies: 550 ± 50, 1240 ± 1240 ± 50, and 1560 ± 50 cm$^-$

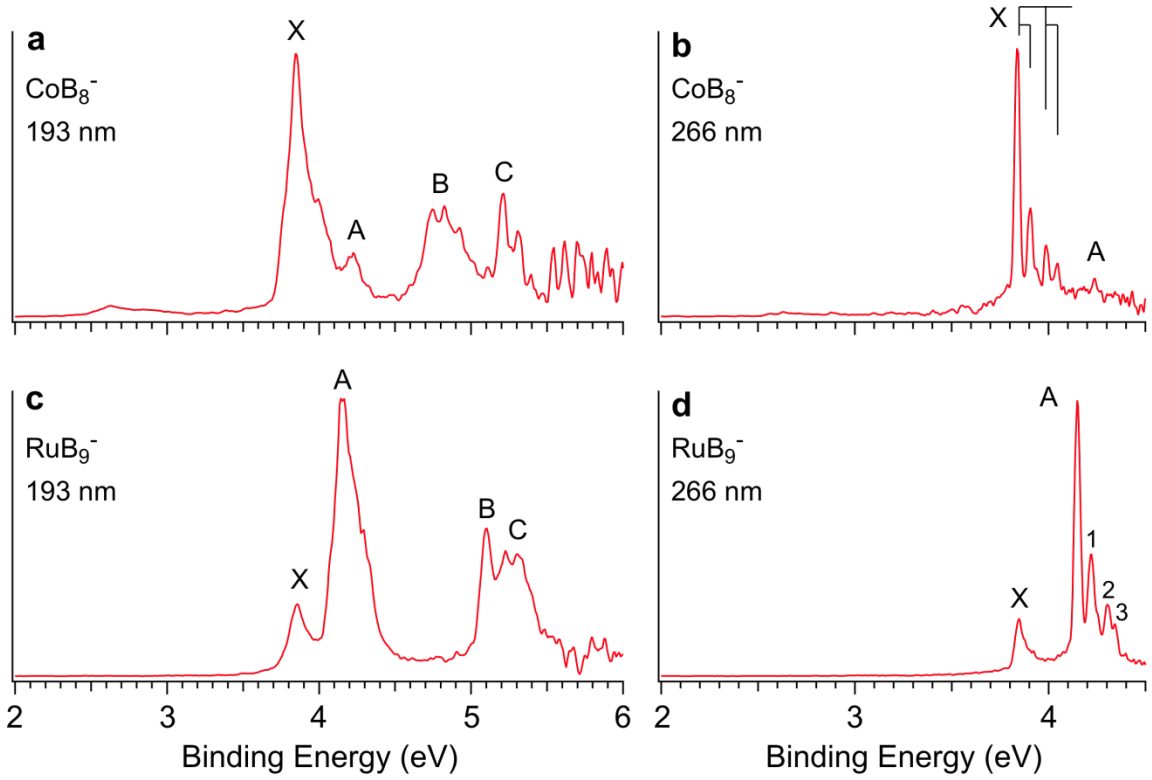

Figure 6-1. Photoelectron spectra of CoB_8^- at a) 193 nm (6.424 eV) and b) 266 nm (4.661 eV). Photoelectron spectra of RuB_9^- at c) 193 nm and d) 266 nm. The vertical lines in (b) and the numbers in (d) indicate vibrational structures.

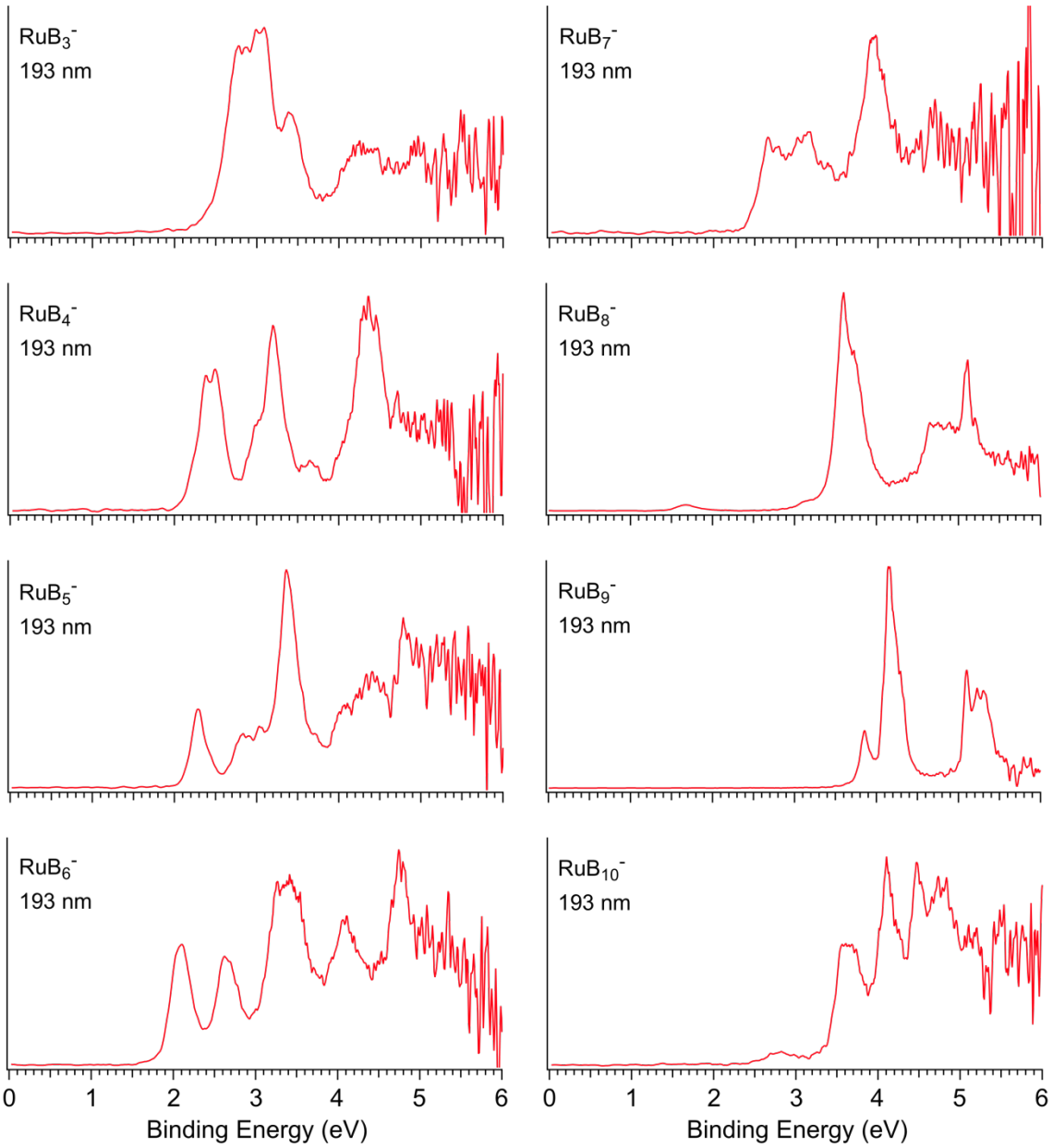

Figure 6-2. Photoelectron spectra of RuB_n^- at 193 nm (6.424 eV)

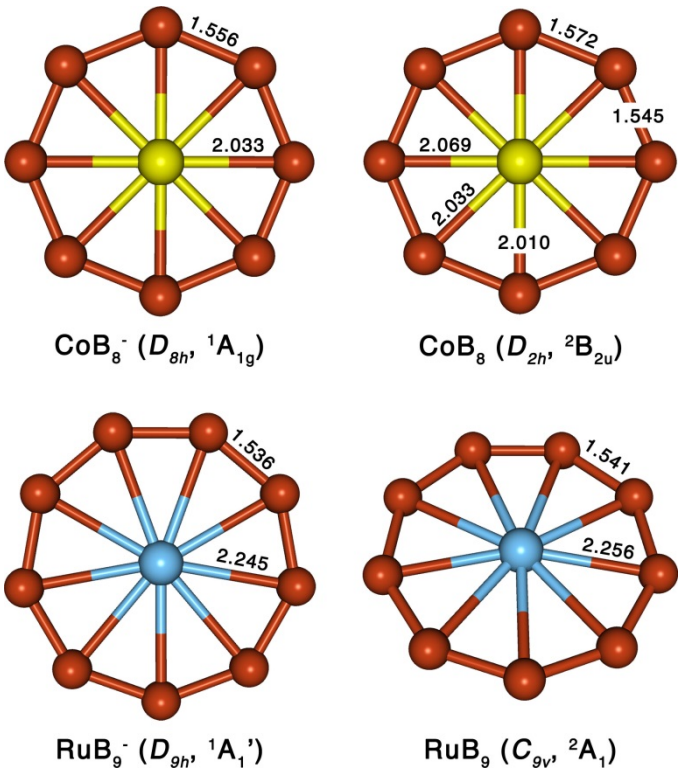

Figure 6-3. Optimized structures for Co©B_8^-, Co©B_8, Ru©B_9^-, and Ru©B_9. The structures presented are at the PBE1PBE/6-311+G* level for Co©B_8^- and Co©B_8 and PBE1PBE/Ru/Stuttgart/B/aug-cc-pvTZ level for Ru©B_9^- and Ru©B_9 (see Experimental Section). Symmetries and spectroscopic states are given in the parentheses. Bond lengths are given in Å.

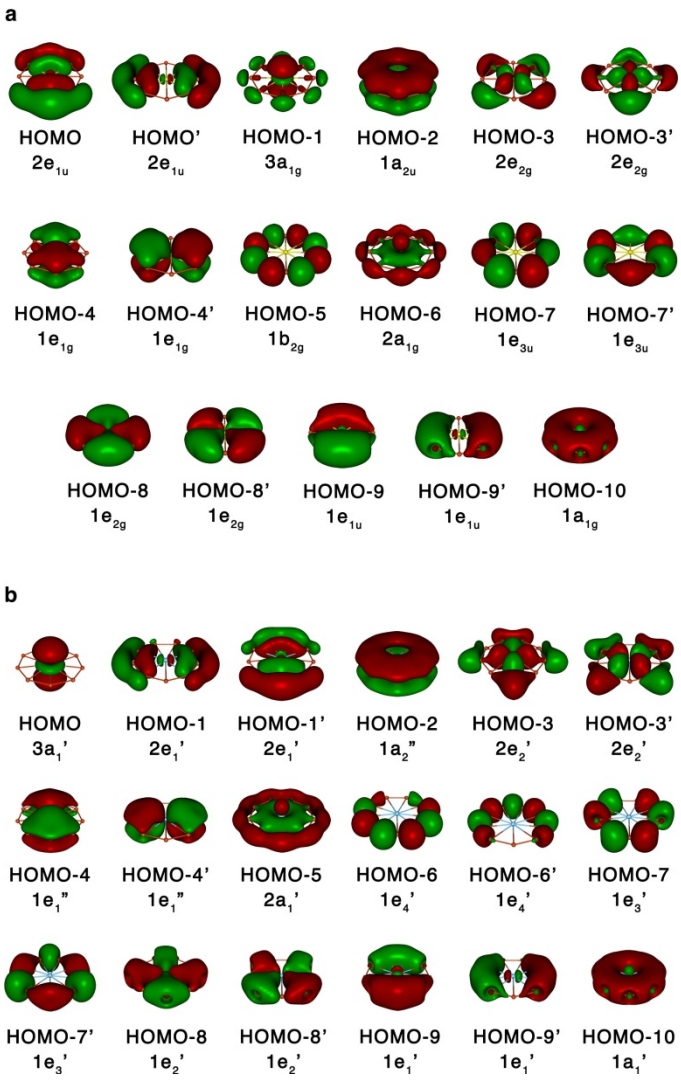

Figure 6-4. Molecular orbital pictures a) $Co©B_8^-$, b) $Ru©B_9^-$.

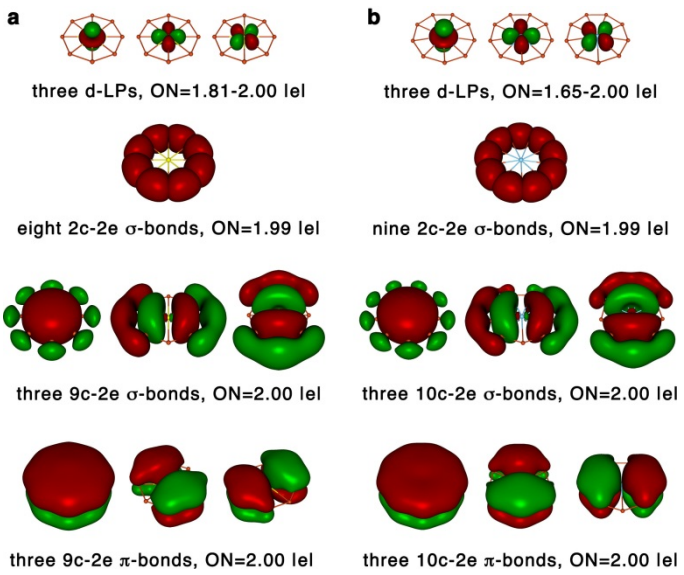

Figure 6-5. a) AdNDP analysis for $Co©B_8^-$. b) AdNDP analysis for $Ru©B_9^-$. The 2c-2e σ-bonds are superimposed on the circumference B-B framework. Note the double aromaticity derived from the three delocalized σ and π bonds in each cluster.

CHAPTER 7

TRANSITION-METAL-CENTERED NINE-MEMBERED BORON RINGS: M©B_9 AND M©B_9^- (M= Rh, Ir) *

Abstract

We report the observation of two transition-metal-centered nine-atom boron rings, Rh©$B_9^-$and Ir©B_9^-. These two doped-boron clusters are produced in a laser-vaporization supersonic molecular beam and characterized by photoelectron spectroscopy and ab initio calculations. Large HOMO–LUMO gaps are observed in the anion photoelectron spectra, suggesting that neutral Rh©B_9 and Ir©B_9 are highly stable, closed shell species. Theoretical calculations show that Rh©B_9 and Ir©B_9 are of D_{9h} symmetry. Chemical bonding analyses reveal that these complexes are doubly aromatic, each with six completely delocalized π and σ electrons, which describe the bonding between the central metal atom and the boron ring. This work establishes firmly the metal-doped B rings as a new class of novel aromatic molecular wheels.

Photoelectron spectroscopy (PES) studies in conjunction with ab initio calculations have shown that small anionic boron clusters (B_n^-) are planar or quasi-planar for an extended size range at least up to n = 20.[1-4] All planar boron clusters consist of a peripheral ring built from strong classical two-center-two-electron (2c-2e) σ-B–B bonds and one or more inner atoms, which are bound to the peripheral boron ring via

* Coauthored by Wei-Li Li, Constantin Romanescu, Timur R. Galeev, Zachary A. Piazza, Alexander I. Boldyrev, and Lai-Sheng Wang. Reprinted with permission from *J. Am. Chem. Soc*. **2012**, *134*, 165-168.

delocalized in-plane σ- and out-of-plane π-bonds. The delocalized bonding renders multiple aromaticity and enhances the stability of the planar clusters. Two clusters, B_8^{2-} and B_9^-, stand out as perfectly symmetric D_{7h}-B©B_7^{2-} and D_{8h}-B©B_8^- molecular wheel-type clusters.[5-7] In both systems, each peripheral boron atom contributes two valence electrons to the 2c-2e localized σ-bonds and one electron to participate in the delocalized σ- and π-bonding, while the central boron atom contributes all three valence electrons to delocalized bonding. In total, each cluster has six delocalized σ- and six delocalized π-electrons and therefore fulfills the Hückel rule ($4N$+2) for both σ- and π-aromaticity. A question arises: can we replace the central boron atom with a metal atom? If the metal atom can participate in the delocalized bonding, do these systems thereby form a new class of thermodynamically stable aromatic compounds?

In a recent study on isoelectronic substitution of a boron atom in B_8^- and B_9^- with aluminum, we have shown that Al avoids the central position in AlB_7^- or AlB_8^-.[8] Instead, both clusters have nonplanar umbrella-type structures, consisting of a positively charged Al ion bound to a B_7^{3-} or a B_8^{2-} counterion. Transition metals with unfilled d-orbitals may be more favorable to bond with the peripheral atoms in a planar geometry if they have the right atomic size to fit inside an eight- or nine-membered boron ring. Indeed, a number of theoretical calculations have proposed substitution of the central B atoms in the B_8 and B_9 molecular wheels by a transition metal atom.[9-13] In particular, the Fe-centered FeB_9^- cluster has been suggested to be doubly aromatic using both NICS and MO analyses.[9-10] This conclusion is corroborated by chemical bonding analyses using the Adaptive Natural Density Partitioning (AdNDP) method.[14]

Recently, we proposed an electronic design principle that can predict stable transition-metal-centered planar boron clusters, $M©B_n^{k-}$.[15] The design principle is based on the double aromaticity requirement and states that the total number of bonding electrons ($3n + x + k$) should be equal to the number of electrons in the peripheral bonds ($2n$) and the two sets of delocalized aromatic bonds (6 + 6) or $n + x + k = 12$, where x is the formal valence of the metal. Two metal-doped boron clusters have been observed recently, according to the design principle, D_{8h}-Co©B_8^- and D_{9h}-Ru©B_9^-, in which the Co atom has a valence of 3 and the Ru atom has a valence of 2.[15]

In this communication, we report the investigation of two neutral transition-metal-centered nine-atom boron rings, Rh©B_9 and Ir©B_9 and their anions. Photoelectron spectra of Rh©$B_9^-$and Ir©B_9^- revealed a large energy gap for both species, suggesting that the neutral clusters are highly stable electronic systems. Ab initio calculations show that the anions are of C_{2v} symmetry due to the Jahn–Teller effect, whereas neutral Rh©B_9 and Ir©B_9 are closed-shell, doubly aromatic, and possess highly symmetric D_{9h} structures. The central metal atom in M©B_9, which has a valence of 3 and possesses six localized d electrons, is involved significantly in bonding with the B_9 ring.

The experiment was carried out using a magnetic-bottle PES apparatus equipped with a laser vaporization cluster source, details of which have been published elsewhere.[16] In brief, the M©B_9^- (M = Rh, Ir) clusters were generated by laser vaporization of a disk target containing isotopically enriched boron (96% ^{11}B, ~10% wt.) and transition metal (Rh or Ir, ~15% wt.), balanced by Bi, which acted as a binder and at the same time provided the Bi^- atomic anion as a convenient calibrant for the PES

apparatus. The clusters were entrained by a gas mixture containing 5% Ar in He supplied by two pulsed valves and underwent a supersonic expansion to form a collimated and vibrationally cold cluster beam.[17] The anionic clusters were analyzed with a time-of-flight mass spectrometer. The clusters of interest were mass-selected and decelerated before being intercepted by the photodetachement laser beam operated at 193 nm (6.424 eV), 266 nm (4.661 eV), or 355 nm (3.496 eV). Photoelectrons were collected at nearly 100% efficiency by the magnetic bottle and analyzed in a 3.5 m long electron flight tube. The resolution of the apparatus $\Delta E/E$, was better than 2.5%, i.e. ~25 meV for 1 eV electrons.

The photoelectron spectra of RhB_9^- and IrB_9^- are found to be similar, as shown in Figure 7-1 at the three photodetachment laser energies. Lower photon energies provide better spectral resolution while the high photon energy at 193 nm reveals more detachment transitions. The PES bands are labeled with letters (X, A, B, ...) and the vertical detachment energies (VDEs) are given in Table 7-1. In each spectrum, the X band represents the transition from the anionic cluster ground state to the neutral ground state. The A, B, ... bands denote transitions to the excited states of the neutral.

The 355 nm spectrum (Figure 7-1b, inset) of RhB_9^- displays a nicely resolved short vibrational progression with an average spacing of 380 ± 50 cm^{-1}. The 0–0 transition defines the adiabatic detachment energy (ADE) or the electron affinity of neutral RhB_9 at 2.86 ± 0.03 eV. The short vibrational progression suggests that there is a very small geometry change between the anionic and neutral ground state. The 266 nm spectrum (Figure 7-1b) reveals four more features A, B, C, and D with VDEs of 4.07 ±

0.03 eV, 4.18 ± 0.03 eV, 4.33 ± 0.04 eV, and 4.39 ± 0.04 eV, respectively, following a large energy gap (1.21 eV) from band X. Both features A and B are very sharp, and feature B is vibrationally resolved with a spacing of 350 ± 50 cm^{-1}. Two relatively weak features E (VDE: 4.54 eV) and F (VDE: 4.80 eV) are observed in the 193 nm spectrum (Figure 7-1a), followed by nearly continuous spectral features starting at band G at a VDE of 5.13 ± 0.04 eV. No other definitive bands can be labeled in the high binding energy side due to the spectral congestion.

The 355 nm spectrum of IrB_9^- (Figure 7-1d, inset) exhibits a sharp peak with discernible vibrational structures. The 0–0 peak defines an ADE of 2.59 ± 0.03 eV, which is also the electron affinity of the neutral IrB_9 cluster. Following a large energy gap (1.59 eV), a sharp and intense band A with a VDE of 4.18 ± 0.03 eV is observed in the 266 nm spectrum (Figure 7-1d). Two more sharp features, B and C, are also observed in the 266 nm spectrum with VDEs of 4.27 ± 0.03 eV and 4.48 ± 0.03 eV, respectively. At 193 nm (Figure 7-1c), more transitions are observed. Features D and E are observed at 4.60 ± 0.04 eV and 4.65 ± 0.04 eV, respectively. The weak feature F at 4.79 eV is similar to the corresponding feature in the 193 nm spectrum of RhB_9^-. Again, following an energy gap, a strong band G is observed at 5.31 ± 0.04 eV, beyond which the signal-to-noise ratios are poor, but there appear to be continuous signals similar to the spectrum of RhB_9^-. There is a weak feature at 3.5 eV in the 193 nm spectrum of IrB_9^- in the band gap region. This feature is most likely due to autodetachment,[18,19] because of its photon energy dependence.

The large X–A gaps in the PES spectra of RhB_9^- and IrB_9^- suggest that their corresponding neutrals must be closed shell with large HOMO–LUMO gaps, and they should be electronically stable and chemically inert. The simplicity of the spectra and the sharpness of the various electronic bands indicate high-symmetry cluster species and minimum geometry changes during photodetachment transitions.

To aid the assignments of the PES spectra, we carried out ab initio calculations at different levels of theory. We first performed global minimum searches for the RhB_9^- and IrB_9^- clusters using the Coalescence Kick program[3] at the PBE0/LanL2DZ level of theory. Low-lying isomers revealed by Coalescence Kick (ΔE < 40 kcal mol^{-1} for RhB_9^- and ΔE < 55 kcal mol^{-1} for IrB_9^-) were reoptimized using the PBE0/M/Stuttgart'97/B/aug-cc-pVTZ (M = Rh or Ir) level of theory (Figures 7-2 and 7-3). To examine the possible multiconfigurational character of the global minimum C_{2v} species found by Coalescence Kick, we also optimized these geometries using the CASSCF method with the Ahlrichs pVDZ basis set for boron and the Stuttgart '97 basis set and ECP for Rh and Ir. Due to discrepancies in the order of ROHF molecular orbital symmetries of the two species, different active spaces were employed: CASSCF(7,8) for RhB_9^- and CASSCF(9,9) for IrB_9^-. We found that for both species the Hartree–Fock configuration is dominant ($C_{HF,RhB9^-}$ = 0.929, $C_{HF,IrB9^-}$ = 0.927), and thus single determinant methods should provide a sufficient description of the ground-state wave functions.

Our geometry optimizations showed that the perfectly symmetric D_{9h} structures are minima on the potential energy surfaces of the neutral species, while the presence of an unpaired electron in the anion's doubly degenerate HOMO (the LUMO for neutral

species) lowers the symmetry to C_{2v} due to the Jahn–Teller effect. The global minimum structures of the RhB_9^- and IrB_9^- clusters and the optimized perfectly symmetric Rh©B_9 and Ir©B_9 wheel-structures are shown in Figure 7-4a–d.

We then calculated the ab initio VDEs using four different methods to confirm that the C_{2v} structures are the global minima for RhB_9^- and IrB_9^-. PBE0/M/Stuttgart'97/B/aug-cc-pVTZ and B3LYP/M/Stuttgart'97/B/aug-cc-pVTZ (M = Rh, Ir) were used at their respective optimized geometries. VDEs were calculated also with the ROHF-UCCSD(T)[20,21]/M/Stuttgart'97/B/6-311+ G(2d) and EOM-CCSD(T)[22–26]/M/Stuttgart'97/B/6-311+G(2d)[27] methods at the PBE0/M/Stuttgart'97/B/aug-cc-pVTZ optimized geometries. On the basis of the literature and our previous work with transition-metal-doped boron clusters,[15,25] we believe that this basis set combination provides a reasonable balance between accuracy and computational efficiency for these approaches. EOM neutral excitation energies were used to offset the ΔCCSD(T) VDE for the lowest singlet state. The frozen core approximation was utilized in all CCSD(T) and EOM-CCSD(T) calculations. All DFT calculations were performed with the Gaussian 09 program.[28] CASSCF calculations were performed with the Gaussian 03 program.[29] All CCSD(T) calculations were performed with the tensor contraction engine module in NWChem version 6.0.[30]

Because of the open-shell nature of the Rh©B_9^- and Ir©B_9^- anions, the detachment transitions are quite complicated, in qualitative agreement with the congested spectral features at the higher binding energy range. The computed VDEs are compared with the experimental data in Table 7-1. For Rh©B_9^-, the first and second VDEs at

CCSD(T) level are 2.87 and 4.22 eV, in good agreement with features X and A observed in the experimental spectra at 2.86 and 4.07 eV, respectively. The next two calculated VDEs correspond to the transition to the $^3A_2$ and $^3B_1$ final states with electrons detached from HOMO–2 ($6b_2$) and HOMO–3 ($8a_1$). We were not able to calculate these detachment channels at CCSD(T), but the VDEs calculated at the UPBE1PBE and UB3LYP are in good agreement with the experimental data (features B and C). The next three detachment channels correspond to singlet final states resultant of detachment from the fully occupied HOMO–1, HOMO–2, and HOMO–3 orbitals. These detachments correspond to the observed features D, E, and F. We were not able to calculate these values at UPBE1PBE and UB3LYP levels, but the VDEs calculated using EOM-CCSD(T), 4.40, 4.55, and 4.60 eV, are in reasonable agreement with the experimental data. The next major detachment channel is from HOMO–4 ($2b_1$), resulting in the $^3A_1$ final state. Electron detachment from HOMO–4 gives a VDE of 5.04 and 4.94 eV at UPBE1PBE and UB3LYP, respectively, compared to 5.13 eV in the experimental spectrum. As seen from Table 7-1, the congested spectral features beyond the F band are consistent with the high density of detachment channels beyond HOMO–4. For IrB_9^-, the observed spectral features and assignments are very similar to those of RhB_9^-, as can be seen in Table 7-1. In some cases, the spectra of IrB_9^- are better resolved, for example, the C band. Overall, for both species, the computational results are in excellent agreement with the experimental data, lending considerable credence to the molecular wheel structures for $Rh©B_9^-$ and $Ir©B_9^-$.

The ground state of the two $M©B_9^-$ anions is $^2B_1$ with C_{2v} symmetry due to the Jahn–Teller effect. The neutral ground state of $M©B_9$ is $^1A_1$ with perfect D_{9h} symmetry. The observed vibrational mode in the ground state transition should correspond to the distortion from the D_{9h} symmetry to the C_{2v} symmetry. The observed frequency of 380 cm^{-1} for $Rh©B_9$ is in excellent agreement with the calculated frequency for this mode, 386 cm^{-1}.

The neutral $Rh©B_9$ and $Ir©B_9$ clusters are valence isoelectronic to $Ru©B_9^-$, and they exhibit similar bonding patterns and strength.[15] Valence canonical molecular orbitals of $Rh©B_9$ and $Ir©B_9$ are presented in (e) and (f) of Figure 7-4. Similar to $Ru©B_9^-$, we can understand the chemical bonding as follows. HOMO–2 ($1a_2''$) and HOMO–4 ($1e_1''$) of $Rh©B_9$ as HOMO–2 ($1a_2''$) and HOMO–5 ($1e_1''$) of $Ir©B_9$ are responsible for delocalized π-bonding (rendering π-aromaticity in the systems); HOMO ($2e_1'$) and HOMO–6 ($2a_1'$) of both clusters are responsible for delocalized σ-bonding (rendering their σ-aromaticity). HOMO–1 ($3a_1'$) and HOMO–3 ($2e_2'$) of both clusters are formed mainly by d electron lone-pairs of the central atoms and the remaining nine valence MOs are responsible for the B–B bonding in the circumference. Thus, both clusters are doubly aromatic, and the central metal has a formal valence of 3.

The current work has firmly established that transition-metal-centered monocyclic molecular wheels are a new class of highly stable and aromatic compounds. We have also confirmed our electronic design priciple, which can be used to construct or screen other transition-metal–boron systems. With the availability of the transition-metal centers,

which can accept ligands perpendicular to the molecular plane, this class of M©B_n complexes may be viable for chemical synthesis in the condensed phases.

References

(1) Alexandrova, A. N.; Boldyrev, A. I.; Zhai, H. J.; Wang, L. S. *Coord. Chem. Rev.* **2006**, *250*, 2811.

(2) Zhai, H. J.; Kiran, B.; Li, J.; Wang, L. S. *Nat. Mater.* **2003**, 2, *827.*

(3) (a) Sergeeva, A. P.; Zubarev, D. Y.; Zhai, H. J.; Boldyrev, A. I.; Wang, L. S. *J. Am. Chem. Soc.* **2008**, *130*, 7244. (b) Sergeeva, A. P.; Averkiev, B. B.; Zhai, H. J.; Boldyrev, A. I.; Wang, L. S. *J. Chem. Phys.* **2011**, *134*, 224304.

(4) (a) Huang, W.; Sergeeva, A. P.; Zhai, H. J.; Averkiev, B. B.; Wang, L. S.; Boldyrev, A. I. *Nature Chem.* **2010**, 2, *202*. (b) Kiran, B.; Bulusu, S.; Zhai, H. J.; Yoo,S.; Zeng, X. C.; Wang, L. S. *Proc. Natl. Acad. Sci. U.S.A.* **2005**, *102*, 961.

(5) Zhai, H. J.; Alexandrova, A. N.; Birch, K. A.; Boldyrev, A. I.; Wang, L. S. *Angew. Chem., Int. Ed.* **2003**, *42*, 6004.

(6) Alexandrova, A. N.; Zhai, H. J.; Wang, L. S.; Boldyrev, A. I. *Inorg. Chem.* **2004**, *43*, 3552.

(7) Fowler, P. W.; Gray, B. R. *Inorg. Chem.* **2007**, *46*, 2892.

(8) Galeev, T. R.; Romanescu, C.; Li, W. L.; Wang, L. S.; Boldyrev, A. I. *J. Chem. Phys.* **2011**, *135*, 104301.

(9) Luo, Q. O. *Sci. China B* **2008**, *51*, 607.

(10) Ito, K.; Pu, Z.; Li, Q. S.; Schleyer, P. v. R. *Inorg. Chem.* **2008**, *47*, 10906.

(11) Li, S. D.; Miao, C. Q.; Guo, J. C. *Sci. China B* **2009**, *52*, 900.

(12) Wu, Q. Y.; Tang, Y. P.; Zhang, X. H. *Sci. China B* **2009**, *52*, 288.

(13) Pu, Z. F.; Ito, K.; Schleyer, P. V.; Li, Q. S. *Inorg. Chem.* **2009**, *48*, 10679.

(14) Averkiev, B. B.; Wang, L. M.; Huang, W.; Wang, L. S.; Boldyrev, A. I. *Phys. Chem. Chem. Phys.* **2009**, *11*, 9840.

(15) Romanescu, C.; Galeev, T. R.; Li, W. L.; Boldyrev, A. I.; Wang, L. S. *Angew. Chem., Int. Ed.* **2011**, *50*, 9334.

(16) Wang, L. S.; Cheng, H. S.; Fan, J. W. *J. Chem. Phys.* **1995**, *102*, 9480.

(17) Huang, W.; Wang, L. S. *Phys. Rev. Lett.* **2009**, *102*, 153401.

(18) Wang, X. B.; Ding, C. F.; Wang, L. S. *J. Chem. Phys.* **1999**, *110*, 8217.

(19) Li, J.; Li, X.; Zhai, H. J.; Wang, L. S. *Science* **2003**, *299*, 864.

(20) Purvis, G. D.; Bartlett, R. J. *J. Chem. Phys.* **1982**, *76*, 1910.

(21) Raghavachari, K.; Trucks, G. W.; Pople, J. A.; Head-Gordon, M. *Chem. Phys. Lett.***1989**, *157*, 479.

(22) Rowe, D. J. *Rev. Mod. Phys.* **1968**, *40*, 153.

(23) Simons, J.; Smith, W. D. *J. Chem. Phys.* **1973**, *58*, 4899.

(24) Sekino, H.; Bartlett, R. J. *Int. J. Quantum Chem.* **1984**, 255.

(25) Stanton, J. F.; Bartlett, R. J. *J. Chem. Phys.* **1993**, *98*, 7029.

(26) Levchenko, S. V.; Krylov, A. I. *J. Chem. Phys.* **2004**, *120*, 175.

(27) Krishnan, R.; Binkley, J. S.; Seeger, R.; Pople, J. A. *J. Chem. Phys.* **1980**, *72*, 650.

(28) Frisch, M. J.; G. W. Trucks, H. B. Schlegel, G. E. Scuseria, M. A. Robb, J. R. Cheeseman, G. Scalmani, V. Barone, B. Mennucci, G. A. Petersson, H. Nakatsuji, M. Caricato, X. Li, H. P. Hratchian, A. F. Izmaylov, J. Bloino, G. Zheng, J. L. Sonnenberg,

M. Hada, M. Ehara, K. Toyota, R. Fukuda, J. Hasegawa, M. Ishida, T. Nakajima, Y. Honda, O. Kitao, H. Nakai, T. Vreven, J. A. Montgomery, Jr., J. E. Peralta, F. Ogliaro, M. Bearpark, J. J. Heyd, E. Brothers, K. N. Kudin, V. N. Staroverov, T. Keith, R. Kobayashi, J. Normand, K. Raghavachari, A. Rendell, J. C. Burant, S. S. Iyengar, J. Tomasi, M. Cossi, N. Rega, J. M. Millam, M. Klene, J. E. Knox, J. B. Cross, V. Bakken, C. Adamo, J. Jaramillo, R. Gomperts, R. E. Stratmann, O. Yazyev, A. J. Austin, R. Cammi, C. Pomelli, J. W. Ochterski, R. L. Martin, K. Morokuma, V. G. Zakrzewski, G. A. Voth, P. Salvador, J. J. Dannenberg, S. Dapprich, A. D. Daniels, O. Farkas, J. B. Foresman, J. V. Ortiz, J. Cioslowski, and D. J. Fox, *Gaussian 09*, Revision B.01; Gaussian, Inc., Wallingford, CT, 2010.

(29) Frisch, M. J.; G. W. Trucks, H. B. Schlegel, G. E. Scuseria, M. A. Robb, J. R. Cheeseman, J. A. Montgomery, Jr., T. Vreven, K. N. Kudin, J. C. Burant, J. M. Millam, S. S. Iyengar, J. Tomasi, V. Barone, B. Mennucci, M. Cossi, G. Scalmani, N. Rega, G. A. Petersson, H. Nakatsuji, M. Hada, M. Ehara, K. Toyota, R. Fukuda, J. Hasegawa, M. Ishida, T. Nakajima, Y. Honda, O. Kitao, H. Nakai, M. Klene, X. Li, J. E. Knox, H. P. Hratchian, J. B. Cross, V. Bakken, C. Adamo, J. Jaramillo, R. Gomperts, R. E. Stratmann, O. Yazyev, A. J. Austin, R. Cammi, C. Pomelli, J. W. Ochterski, P. Y. Ayala, K. Morokuma, G. A. Voth, P. Salvador, J. J. Dannenberg, V. G. Zakrzewski, S. Dapprich, A. D. Daniels, M. C. Strain, O. Farkas, D. K. Malick, A. D. Rabuck, K. Raghavachari, J. B. Foresman, J. V. Ortiz, Q. Cui, A. G. Baboul, S. Clifford, J. Cioslowski, B. B. Stefanov, G. Liu, A. Liashenko, P. Piskorz, I. Komaromi, R. L. Martin, D. J. Fox, T. Keith, M. A. Al-Laham, C. Y. Peng, A. Nanayakkara, M.

Challacombe, P. M. W. Gill, B. Johnson, W. Chen, M. W. Wong, C. Gonzalez, and J. A. Pople, *Gaussian 03*, Revision D.01; Gaussian, Inc., Wallingford, CT, 2004.

(30) Valiev, M.; Bylaska, E. J.; Govind, N.; Kowalski, K.; Straatsma, T. P.; Van Dam, H. J. J.; Wang, D.; Nieplocha, J.; Apra, E.; Windus, T. L.; de Jong, W. *Comput. Phys. Commun.***2010**, *181*, 1477.

Table 7-1. Comparison of the experimental VDEs with the calculated values of M©B_9^- (C_{2v}, $^2B_1$). All energies are in eV.

Feature	VDE (exp)[a]	Final State and Electronic Configuration	VDE (theoretical)		
			UPBE 1PBE[b]	UB3LYP[c]	CCSD(T)[d]
		Rh©B_9^-			
X	2.86(3)	$^1A_1\ldots1a_2^2\ 1b_1^2\ 5b_2^2\ 7a_1^2\ 2b_1^2\ 8a_1^2\ 6b_2^2\ 9a_1^2\ 3b_1^0$	2.88	2.78	2.87 (2.69)[e]
A	4.07(3)	$^3B_1\ldots1a_2^2\ 1b_1^2\ 5b_2^2\ 7a_1^2\ 2b_1^2\ 8a_1^2\ 6b_2^2\ 9a_1^1\ 3b_1^1$	4.06	3.97	4.22 (4.40)
B	4.18(3)	$^3A_2\ldots1a_2^2\ 1b_1^2\ 5b_2^2\ 7a_1^2\ 2b_1^2\ 8a_1^2\ 6b_2^1\ 9a_1^2\ 3b_1^1$	4.17	4.08	[f]
C	4.33(4)	$^3B_1\ldots1a_2^2\ 1b_1^2\ 5b_2^2\ 7a_1^2\ 2b_1^2\ 8a_1^1\ 6b_2^2\ 9a_1^2\ 3b_1^1$	4.16	4.16	[f]
D	4.39(4)	$^1B_1\ldots1a_2^2\ 1b_1^2\ 5b_2^2\ 7a_1^2\ 2b_1^2\ 8a_1^2\ 6b_2^2\ 9a_1^1\ 3b_1^1$	[f]	[f]	(4.40)
E	4.54(4)	$^1A_2\ldots1a_2^2\ 1b_1^2\ 5b_2^2\ 7a_1^2\ 2b_1^2\ 8a_1^2\ 6b_2^1\ 9a_1^2\ 3b_1^1$	[f]	[f]	(4.55)
F	4.80(4)	$^1B_1\ldots1a_2^2\ 1b_1^2\ 5b_2^2\ 7a_1^2\ 2b_1^2\ 8a_1^1\ 6b_2^2\ 9a_1^2\ 3b_1^1$	[f]	[f]	(4.60)
G	5.13(4)	$^3A_1\ldots1a_2^2\ 1b_1^2\ 5b_2^2\ 7a_1^2\ 2b_1^1\ 8a_1^2\ 6b_2^2\ 9a_1^2\ 3b_1^1$	5.04	4.94	(5.33)
	5.2 ~ >6	$^3B_1\ldots1a_2^2\ 1b_1^2\ 5b_2^2\ 7a_1^1\ 2b_1^2\ 8a_1^2\ 6b_2^2\ 9a_1^2\ 3b_1^1$	[f]	5.40	[f]
		$^3A_2\ldots1a_2^2\ 1b_1^2\ 5b_2^1\ 7a_1^2\ 2b_1^2\ 8a_1^2\ 6b_2^2\ 9a_1^2\ 3b_1^1$	5.51	5.43	[f]
		$^3A_1\ldots1a_2^2\ 1b_1^1\ 5b_2^2\ 7a_1^2\ 2b_1^2\ 8a_1^2\ 6b_2^2\ 9a_1^2\ 3b_1^1$	5.57	5.54	(5.66)
		$^3B_2\ldots1a_2^1\ 1b_1^2\ 5b_2^2\ 7a_1^2\ 2b_1^2\ 8a_1^2\ 6b_2^2\ 9a_1^2\ 3b_1^1$	6.12	[f]	(6.14)
		Ir©B_9^-			
X	2.59(3)	$^1A_1\ldots1a_2^2\ 1b_1^2\ 5b_2^2\ 7a_1^2\ 2b_1^2\ 8a_1^2\ 6b_2^2\ 9a_1^2\ 3b_1^0$	2.56	2.48	2.50 (2.29)[e]
A	4.18(3)	$^3B_1\ldots1a_2^2\ 1b_1^2\ 5b_2^2\ 7a_1^2\ 2b_1^2\ 8a_1^2\ 6b_2^2\ 9a_1^1\ 3b_1^1$	4.20	4.40	4.40 (4.56)
B	4.27(3)	$^3A_2\ldots1a_2^2\ 1b_1^2\ 5b_2^2\ 7a_1^2\ 2b_1^2\ 8a_1^2\ 6b_2^1\ 9a_1^2\ 3b_1^1$	4.31	4.21	[f]
C	4.48(3)	$^3B_1\ldots1a_2^2\ 1b_1^2\ 5b_2^2\ 7a_1^2\ 2b_1^2\ 8a_1^1\ 6b_2^2\ 9a_1^2\ 3b_1^1$	4.41	4.43	[f]
D	4.60(4)	$^1B_1\ldots1a_2^2\ 1b_1^2\ 5b_2^2\ 7a_1^2\ 2b_1^2\ 8a_1^2\ 6b_2^2\ 9a_1^1\ 3b_1^1$	[f]	[f]	(4.60)
E	4.65(4)	$^1A_2\ldots1a_2^2\ 1b_1^2\ 5b_2^2\ 7a_1^2\ 2b_1^2\ 8a_1^2\ 6b_2^1\ 9a_1^2\ 3b_1^1$	[f]	[f]	(4.63)
F	4.79(4)	$^1B_1\ldots1a_2^2\ 1b_1^2\ 5b_2^2\ 7a_1^2\ 2b_1^2\ 8a_1^1\ 6b_2^2\ 9a_1^2\ 3b_1^1$	[f]	[f]	(4.67)
G	5.31(4)	$^3A_1\ldots1a_2^2\ 1b_1^2\ 5b_2^2\ 7a_1^2\ 2b_1^1\ 8a_1^2\ 6b_2^2\ 9a_1^2\ 3b_1^1$	5.20	5.09	(5.46)
	5.5 ~ >6	$^3B_1\ldots1a_2^2\ 1b_1^2\ 5b_2^2\ 7a_1^1\ 2b_1^2\ 8a_1^2\ 6b_2^2\ 9a_1^2\ 3b_1^1$	[f]	[f]	[f]
		$^3A_2\ldots1a_2^2\ 1b_1^2\ 5b_2^1\ 7a_1^2\ 2b_1^2\ 8a_1^2\ 6b_2^2\ 9a_1^2\ 3b_1^1$	5.65	5.55	(5.61)
		$^3A_1\ldots1a_2^2\ 1b_1^1\ 5b_2^2\ 7a_1^2\ 2b_1^2\ 8a_1^2\ 6b_2^2\ 9a_1^2\ 3b_1^1$	5.91	5.85	(5.99)
		$^3B_2\ldots1a_2^1\ 1b_1^2\ 5b_2^2\ 7a_1^2\ 2b_1^2\ 8a_1^2\ 6b_2^2\ 9a_1^2\ 3b_1^1$	[f]	[f]	(6.32)

[a]Numbers in parentheses represent the uncertainty in the last digit. [b]VDEs were calculated at PBE1PBE/M/Stuttgart'97/B/aug-cc-pVTZ, M=Rh, Ir. [c]VDEs were calculated at B3LYP/M/Stuttgart'97/B/aug-cc-pVTZ, M=Rh, Ir. [d]VDEs were calculated at ROHF-UCCSD(T)/M/Stuttgart'97/B/6-311+G(2d)//PBE1PBE/M/Stuttgart'97/B/aug-cc-pVTZ, M=Rh, Ir. [e]VDEs in parenthesis were calculated at EOM-CCSD(T)/M/Stuttgart'97/B/6-311+G(2d)// PBE1PBE/M/Stuttgart'97/B/aug-cc-pVTZ, M=Rh, Ir. [f]VDE could not be calculated at this level of theory

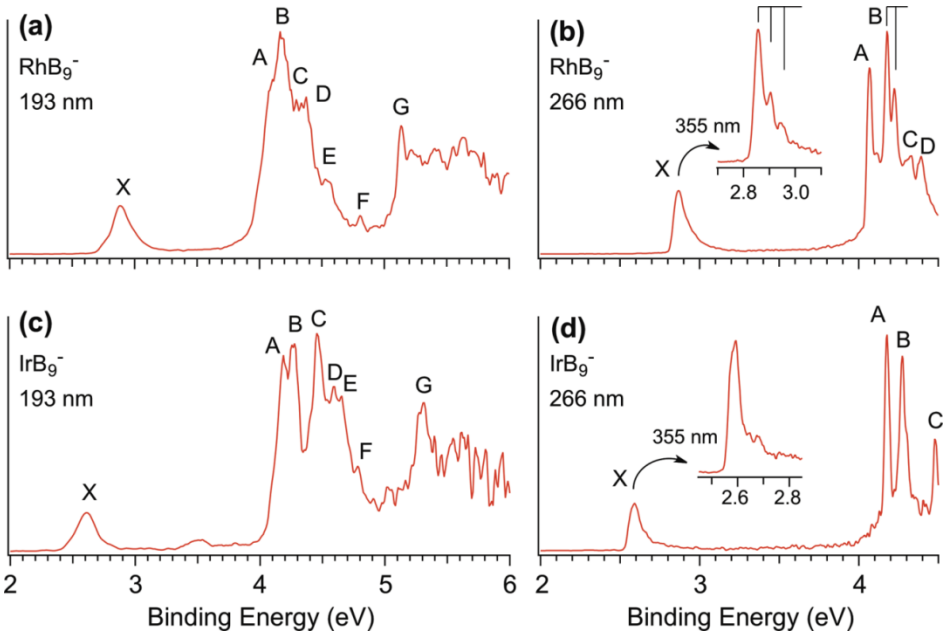

Figure 7-1. Photoelectron spectra of RhB_9^- and IrB_9^- at 355, 266, and 193 nm. The vertical lines in the 355 and 266 nm spectra of RhB_9^- indicate vibrational structures

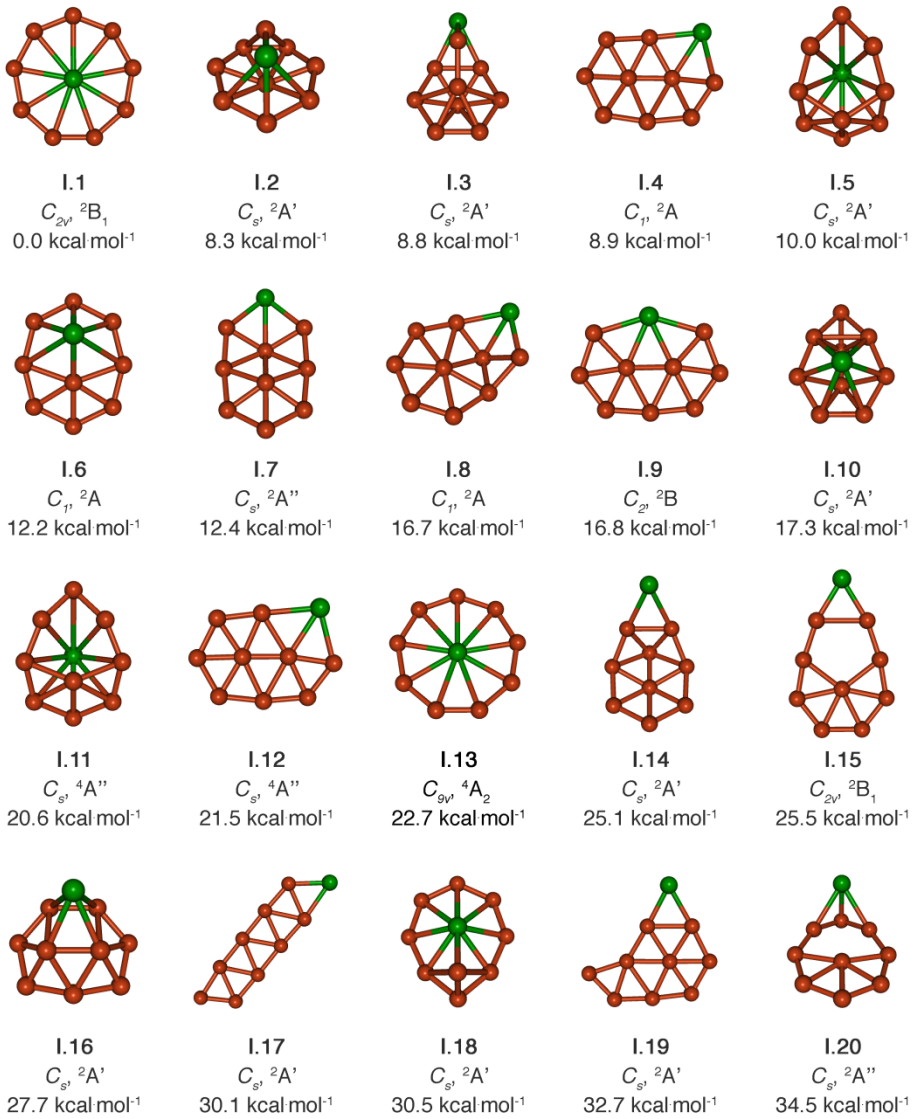

Figure 7-2. Optimized isomers of RhB_9^-, their point group symmetries, spectroscopic states and ZPE corrected relative energies (PBE0/Rh/Stuttgart'97/B/aug-cc-pVTZ).

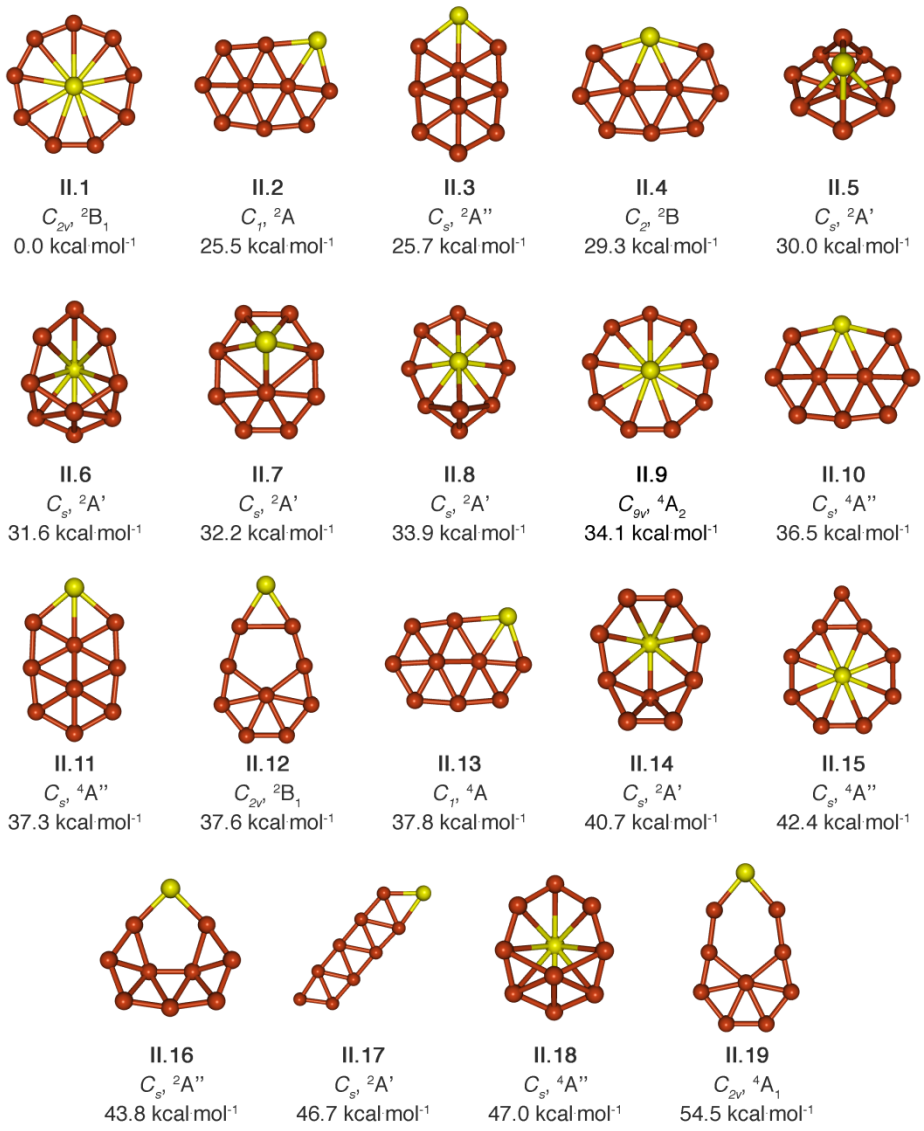

Figure 7-3. Optimized isomers of IrB_9^-, their point group symmetries, spectroscopic states and ZPE corrected relative energies (PBE0/Ir/Stuttgart'97/B/aug-cc-pVTZ).

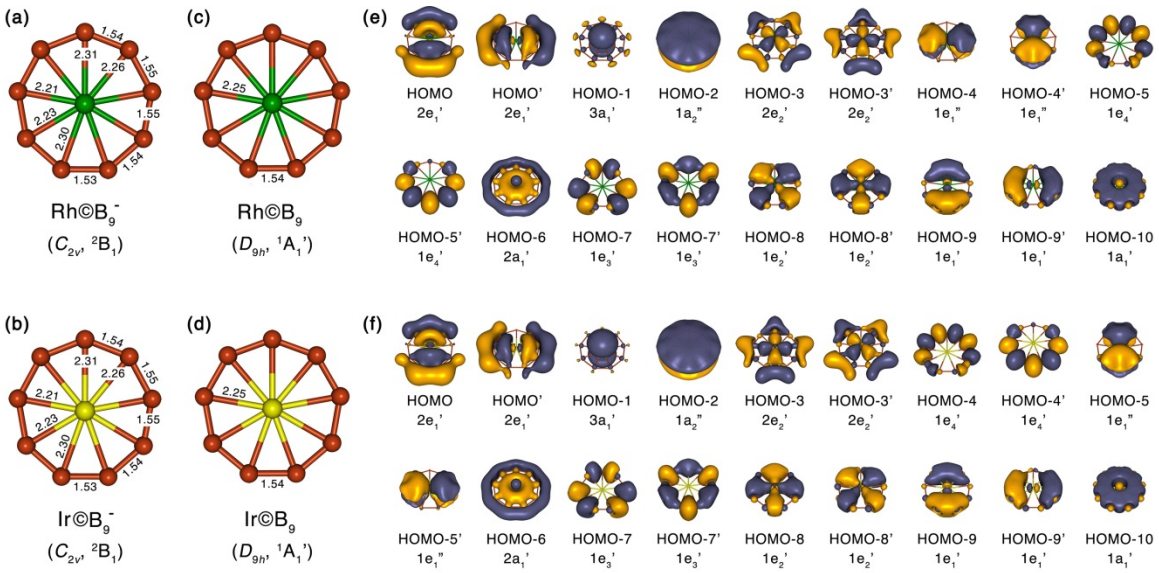

Figure 7-4. Optimized geometries of (a) Rh©B_9^-, (b) Ir©B_9^-, (c) Rh©B_9, (d) Ir©B_9 and valence canonical molecular orbitals of (e) Rh©B_9 and (f) Ir©B_9 at PBE0/M/Stuttgart'97/B/aug-cc-pVTZ (M = Rh, Ir) level. Bond lengths are given in Å.

CHAPTER 8

OBSERVATION OF THE HIGHEST COORDINATION NUMBER IN PLANAR SPECIES: DECACOORDINATED $Ta©B_{10}^-$ AND $Nb©B_{10}^-$ ANIONS [*]

Abstract

Molecular wheels: Decacoordinated molecular wheels, $Ta©B_{10}^-$ and $Nb©B_{10}^-$, showing the highest coordination number for the central atom in a planar environment at present, were produced in a laser-vaporization supersonic molecular beam and characterized by photoelectron spectroscopy and ab initio calculations. The highly symmetric $Ta©B_{10}^-$ and $Nb©B_{10}^-$ anions are doubly aromatic with six delocalized π electrons and ten delocalized σ electrons.

Coordination number is one of the most fundamental characteristics of molecular structures. Molecules with high coordination numbers often violate the octet and the 18 electron rules and push the boundary of our understanding of chemical bonding and structures. We have been searching for the highest possible coordination number in a planar species with equal distances between the central atom and all peripheral atoms. To successfully design planar chemical species with such high coordination one must take into account both mechanical and electronic factors. The mechanical factor requires the right size of the central atom to fit into the cavity of a monocyclic ring. The electronic factor requires the right number of valence electrons to achieve electronic stability of the

[*] Coauthored by Timur R. Galeev, Constantin Romanescu, Wei-Li Li, Lai-Sheng Wang, and Alexander I. Boldyrev. Reprinted with permission from *Angew. Chem. Int. Ed.* **2012**, *51*, 2101-2105.

high-symmetry structure. Boron is known to form highly symmetric planar structures owing to its ability to participate simultaneously in localized and delocalized bonding.[1-7] The planar boron clusters consist of a peripheral ring featuring strong two-center-two-electron (2c-2e) B–B σ bonds and one or more central atoms bonded to the outer ring through delocalized σ and π bonds. The starting point for the present work is that the bare eight-atom and nine-atom planar boron clusters were found to reach coordination number seven in the D_{7h} B_8 neutral or B_8^{2-} as a part of the LiB_8^- cluster[1,3] or eight in the D_{8h} B_9^- molecular wheel.[1]

The CB_6^{2-}, C_3B_4, and CB_7^- wheel-type structures with hexa- and heptacoordinated carbon atom were first considered computationally by Schleyer and co-workers.[8,9] The high symmetry hypercoordinated structures were found to be local minima because they "fulfill both the electronic and geometrical requirements for good bonding."[8,9] In particular, Schleyer and co-workers pointed out that the wheel structures are π aromatic with 6 π electrons. In joint photoelectron spectroscopy (PES) and theoretical studies it was shown that carbon occupies the peripheral position in such clusters rather than the center, because C is more electronegative than B and thus prefers to participate in localized 2c-2e σ bonding, which is possible only at the circumference of the wheel structures.[10,11] A series of planar wheel-type boron rings with a main group atom in the center and coordination numbers 6–10 have been probed theoretically.[12-14] So far the joint PES and ab initio studies of aluminum-doped boron clusters showed that the aluminum atom avoids the central position in the AlB_6^-, AlB_7^-, AlB_8^-, AlB_9^-, AlB_{10}^-, and AlB_{11}^-systems.[15-17]

Recently, a transition-metal-doped boron cluster, $Ru©B_9^-$, with the highest coordination number known to date was reported.[18] We developed a chemical bonding model, which allows the design of planar molecules with high coordination numbers.[18] According to the model, $2n$ electrons in the $M©B_n$ species form n 2c-2e peripheral B–B σ bonds. The remaining valence electrons form two types of delocalized bonding, in-plane σ and out-of-plane π bonding, and therefore, should satisfy the $(4N+2)$ Hückel rule separately for σ and π aromaticity to attain highly symmetric structures with high electronic stability. In pure wheel-type boron clusters each B atom in the circumference contributes two electrons to the B–B peripheral covalent bonds and one electron to the delocalized bonds, whereas the central B atom contributes all its valence electrons to the delocalized bonds. Thus, out of 26 valence electrons in B_8^{2-} or 28 in B_9^-, 14 or 16 valence electrons form peripheral covalent 2c-2e σ bonds, leaving six σ and six π electrons (N=1 for the $4N+2$ rule) for double (σ and π) aromaticity. However, pure planar boron clusters cannot go beyond coordination number eight because of the mechanical factor (the small size of the central boron atom). For example, the B_{10} cluster does not contain a nine-coordinated boron atom, because the boron atom is too small to fit in the central position of a B_9 ring.[2] Since the central atom participates only in delocalized bonding, atoms more electronegative than boron such as carbon avoid the central position.[10,11,19] Transition-metal atoms, on the other hand, are well-suited for the central position in $M©B_n$ species. To satisfy the peripheral B-B bonding and the σ and π Hückel aromaticity for N=1, the electronic requirement for the central atom in high-symmetry species, such as $M©B_n^{k-}$, is $x=12-n-k$, where x is the valence of the transition-metal

atom M. $Ru©B_9^-$ satisfies the formula and is the first example of an experimentally observed planar species with coordination number nine.[18]

The quest for higher coordination numbers was limited primarily to theoretical calculations.[12,20,21] The highest coordination number considered computationally was ten for a broad range of atoms: CB_{10}^{2+}, SiB_{10}^{2+}, GeB_{10}^{2+}, SnB_{10}^{2+}, PbB_{10}^{2+},[12] AuB_{10}^-, AgB_{10}^-, CdB_{10}, HgB_{10}, InB_{10}^+, TlB_{10}^+,[20] and ScB_{10}^{3-}, TiB_{10}^{2-}, VB_{10}^-, FeB_{10}^{2+}, NiB_{10}^{2+}, CuB_{10}^{3+}, CuB_{10}^-, ZnB_{10}.[21] Though some of these proposed species satisfy our electronic design principle, none was known to be the global minimum. Among these species, only AuB_{10}^- has been experimentally observed,[22] but its global minimum was shown to be an Au atom interacting with a B_{10}^- cluster on the outside: the wheel-type structure is a high-energy isomer, around 45 kcal mol^{-1} above the ground state.[22] The instability of the $Au©B_{10}^-$ wheel isomer is caused by the fact that only the 6s valence electron participates in the delocalized bonding in this species while the 5d orbitals of the central Au atom are completely filled and have little interaction with the peripheral B_{10} ring. Our recent finding of the nonacoordinated $Ru©B_9^-$ complex shows that the interactions of the 4d orbitals with the B_9 ring play an important role in stabilizing the wheel structure. Early 4d and 5d transition metals have larger atomic sizes and more diffused d orbitals, conducive to participation in bonding with the peripheral boron rings. Thus, our search for higher coordination metal-doped boron clusters has been focused on the early 4d or 5d transition metals.

Here we show that Nb and Ta fit into the B_{10} decagonal ring and the resulting singly charged wheel-type anions $Nb©B_{10}^-$ and $Ta©B_{10}^-$ are closed-shell and doubly

aromatic systems. Furthermore, all five valence electrons of Nb and Ta participate in the delocalized bonding, providing considerable stability to the wheel structures, which were found to be the lowest energy isomers by unbiased global minimum searches (alternative structures found for TaB_{10}^- and NbB_{10}^- are presented in Figures 8-1 and 8-2). The theoretical results are in excellent agreement with the experimental photoelectron data, confirming the first decacoordinated 2D chemical species.

The TaB_{10}^- and NbB_{10}^- clusters were produced in a laser-vaporization supersonic molecular beam cluster source and probed using photoelectron spectroscopy (see the Experimental Section). The photoelectron spectra of TaB_{10}^- and NbB_{10}^- at two different photon energies are shown in Figure 8-3. The spectrum of TaB_{10}^- at 193 nm (Figure 8-3a) shows a fairly simple spectral pattern with three strong peaks (X, A, B) between 3.9–4.7 eV and two weak bands (C, D) between 5.2–5.6 eV. At 266 nm (Figure 8-3b), an additional peak was resolved between the X and A band. This peak is due to a vibrational feature of the X band, yielding a vibrational spacing of (1050±50) cm^{-1}. The first adiabatic detachment energy (ADE) and the vertical detachment energy (VDE) for TaB_{10}^-, both defined by the 0–0 transition of the X band, are (4.04±0.03) eV, which also represents the electron affinity of neutral Ta©B_{10}. The spectra of NbB_{10}^- (Figure 8-3c and 8-3d) are very similar to those of TaB_{10}^- except for the weak low binding energy features labeled as X′, A′, B′, and C′. This observation suggests the presence of a higher energy isomer in the beam of NbB_{10}^-, whereas the main isomer of NbB_{10}^- should be similar to that of TaB_{10}^-. The X, A, B features in the NbB_{10}^- spectra are more congested and fine features are also resolved at 266 nm (Figure 8-3d), yielding a vibrational

frequency for the ground state of NbB_{10} as (600±50) cm^{-1}. The vibrationally resolved X band yields an accurate ADE for NbB_{10}^- as (4.10±0.03) eV, very close to that for TaB_{10}^-. The observed VDEs for all spectral features for TaB_{10}^- and NbB_{10}^- are given in Table 8-1, where they are compared with the computational data.

According to the highest level of theory we used, the wheel-type structures (D_{10h} M©B_{10}^-) are the global minima for both anions (Figure 8-4). The second lowest isomers of both species involve the metal atom interacting with the B_{10} cluster from above (C_{2v}). This C_{2v} isomer is close in energy to the global minimum for NbB_{10}^- and is likely to be present in the experiment.

To verify the wheel-type structures we computed VDEs for the two lowest isomers of each species (see the Experimental Section). Theoretical VDEs calculated for the M©B_{10}^- structures at two non-relativistic levels of theory predict two detachment channels in the 4.0–4.5 eV binding energy range (Table 8-1), though there are more peaks in the experimental spectra in this region. As shown in Figure 8-5, both the HOMO (e_{2g}) and HOMO-1 (e_{1u}) of the M©B_{10}^- clusters are doubly degenerate involving interactions between the d orbitals and the B_{10} ring. Thus, spin–orbit coupling is expected to yield two photoelectron bands from electron detachment from each orbital, thereby resulting in four detachment bands in this energy region. Hence, the three observed peaks could result from the overlap of the four expected spin–orbit split peaks. Indeed, spin–orbit calculations for Ta©B_{10}^- revealed a splitting of around 0.2 eV in these peaks (see Tables 8-2 and 8-3), in excellent agreement with the experiment. The calculated VDEs from HOMO-2 and HOMO-3 are also in excellent agreement with the observed bands C

and D. We also calculated the vibrational frequencies for the neutral $Ta©B_{10}$ species (see Table 8-4), the symmetry of which is reduced by the Jahn–Teller effect. The frequency for one of the totally symmetric mode [$\omega_4(a_g)$=1050 cm^{-1}] is in excellent agreement with the observed vibrational frequency for the X band. On the other hand, the predicted VDEs for the higher energy C_{2v} isomer of TaB_{10}^- totally disagree with the experimental spectra. Overall, the theoretical results for the D_{10h} $Ta©B_{10}^-$ structure are in excellent agreement with the experimental data, confirming unequivocally that the molecular wheel is the global minimum for TaB_{10}^-. The VDEs calculated for the D_{10h} structure of $Nb©B_{10}^-$ can explain the high energy features (Table 8-1, X, A–D), which are similar to those of the features in the $Ta©B_{10}^-$ spectra. The smaller spin–orbit effects expected in $Nb©B_{10}^-$ result in the more congested spectral features in the 4.0–5.4 eV energy range (Figure 8-3c and 8-3d). The additional features (X′, A′, B′, C′) observed for NbB_{10}^- are in excellent agreement with the calculated VDEs for the C_{2v} isomer. The lower intensities of these features suggest that the C_{2v} isomer is energetically less stable than the wheel-type structure, again confirming that the global minimum of NbB_{10}^- is also the D_{10h} molecular wheel.

According to the design principle that we proposed recently for stable $M©B_n^{k-}$-type molecular wheels,[18] the valence of the central metal atom should be one for a B_{10} ring. However, both Ta and Nb are known to have five valence electrons. To understand the bonding in the $M©B_{10}^-$ molecular wheels, we present results of the Adaptive Natural Density Partitioning (AdNDP) analysis (see the Experimental Section) for $Ta©B_{10}^-$ in

Figure 8-6. The advantage of the AdNDP analysis is the ability to recover simultaneously both localized and delocalized bonding in chemical species.

The AdNDP analysis revealed ten 2c-2e peripheral σ bonds, five delocalized σ bonds (satisfying the 4*N*+2 rule for aromaticity with *N*=2), and three delocalized π bonds (satisfying the 4*N*+2 rule for aromaticity with *N*=1). A similar bonding pattern was found for $Nb©B_{10}^-$. Thus, both clusters are doubly σ and π aromatic and satisfy the construction model. However, in contrast to the molecular wheels of B_8^{2-}, B_9^-, and $Ru©B_9^-$, there are 10 delocalized σ electrons for the current $M©B_{10}^-$ molecular wheels owing to the strong bonding between the 4d/5d orbitals of Nb/Ta with the peripheral B_{10} ring. Therefore, in these cases, the electronic design principle needs to be revised as $x=16-n-k$ to account for the 10 delocalized σ electrons. This result suggests that more delocalized bonding electrons are required, either in the σ or π framework, to build ever highly coordinated planar molecular wheels.

The two delocalized σ bonds involving the Ta 5d orbitals can be alternatively shown by the AdNDP analysis with low threshold values as d_{xy} and $d_{x^2-y^2}$ lone pairs on the Ta atom with low occupation number (ON) of 1.11 |e| (compared to the ideal value of 2.00 |e|) and therefore the estimated contribution of the Ta 5d atomic orbitals (AOs) to the delocalized bonding is 55 %. On the contrary, the molecular wheel structure of the above-mentioned $Au©B_{10}^-$ anion is not the global minimum because the Au 5d AOs remain atom-like and do not participate in delocalized bonding. The availability of d AOs in Nb and Ta for participation in the σ-delocalized bonding with the peripheral ring leads to substantial stabilization of the decagonal doubly aromatic structures of $Nb©B_{10}^-$ and

$Ta©B_{10}^-$ and makes them the global minimum structures. Thus, it is conceivable that other early 4d or 5d elements will be able to form not only decagonal $M©B_{10}^{k-}$-type species, but also species with even higher coordination numbers.

8-1. Experimental Section

8-1.1. Photoelectron Spectroscopy

The experiment was performed using a magnetic bottle photoelectron spectroscopy apparatus equipped with a laser vaporization cluster source that was described in detail previously.[23] Briefly, the transition metal (M)-doped boron clusters were produced by laser ablation (532 nm) of a disk target made of isotopically enriched ^{11}B (around 10 %), M (around 10–15 %), balanced by Bi or Ag which acted as target binders and also provided calibrants (Bi^- and Ag^-) for the photoelectron spectra. The clusters were entrained by a He carrier gas seeded with 5 % Ar and underwent a supersonic expansion to form a collimated and cold molecular beam. The composition and the cooling of the clusters were controlled by the time delay between the carrier gas pulse and the ablation laser. The negatively charged clusters were extracted and analyzed with a time-of-flight mass spectrometer. The species of interest were mass-selected and decelerated before being photodetached by pulsed laser beams at 193 nm (6.424 eV) or 266 nm (4.661 eV). Photoelectrons were collected at nearly 100 % efficiency by a magnetic bottle and analyzed in a 3.5 m long electron flight tube. The resolution of the apparatus, $\Delta E/E$, was better than 2.5 %, that is, 25 meV for 1 eV electron.

8-1.2. Theoretical Calculations

The search for the global minimum structures of the TaB_{10}^- and NbB_{10}^- species was performed using the Coalescence Kick program, written by Averkiev.[7] These calculations were performed at the PBE0/LANL2DZ[24-26] level of theory. The lowest energy isomers (ΔE<50 kcal mol^{-1}) were then reoptimized at PBE0/Ta, Nb/Stuttgart/ B/aug-cc-pVTZ[27-31] (see Figures 8-1 and 8-2) and single-point calculations for the four lowest isomers were performed using the RCCSD(T)/Ta, Nb/Stuttgart/B/aug-cc-pVTZ level of theory.

Theoretical VDEs were calculated at the PBE0/Ta, Nb/Stuttgart/B/aug-cc-pVTZ and ROCCSD(T)/Ta, Nb/Stuttgart/B/aug-cc-pVTZ//PBE0/Ta, Nb/Stuttgart/B/aug-cc-pVTZ levels of theory. To explain the around 0.2 eV experimental splitting in the first two peaks of the TaB_{10}^- photoelectron spectrum we performed zero-order relativistic approximation (ZORA) calculations[32,33] with PBE0/QZ4P and M06-2X/QZ4P[34,35] exchange correlation potentials using the ADF program.[36] Results presented in Tables 8-2 and 8-3 show spin–orbit splitting of around 0.2 eV for both peaks, in an excellent agreement with the experimental observation. Chemical bonding analyses (PBE0/LANL2DZ) of both clusters were performed using the AdNDP method and the AdNDP program written by Zubarev.[37] All non-relativistic calculations were done using Gaussian 09.[38] Molekel 5.4.0.8 was used for MO visualization.[39]

References

[1] H. J. Zhai, A. N. Alexandrova, K. A. Birch, A. I. Boldyrev, L. S. Wang, *Angew. Chem.* 2003, **115**, 6186–6190; *Angew. Chem. Int. Ed.* **2003**, *42*, 6004–6008.

[2] H. J. Zhai, B. Kiran, J. Li, L. S. Wang, *Nat. Mater.* **2003**, *2*, 827–833.

[3] A. N. Alexandrova, H. J. Zhai, L. S. Wang, A. I. Boldyrev, *Inorg. Chem.* **2004**, *43*, 3552–3554.

[4] A. N. Alexandrova, A. I. Boldyrev, H. J. Zhai, L. S. Wang, *Coord. Chem. Rev.* **2006**, *250*, 2811–2866.

[5] D. Yu. Zubarev, A. I. Boldyrev, *J. Comput. Chem.* **2007**, *28*, 251–268.

[6] W. Huang, A. P. Sergeeva, H. J. Zhai, B. B. Averkiev, L. S. Wang, A. I. Boldyrev, *Nat. Chem.* **2010**, *2*, 202–206.

[7] A. P. Sergeeva, B. B. Averkiev, H. J. Zhai, A. I. Boldyrev, L. S. Wang, *J. Chem. Phys.* **2011**, *134*, 224304.

[8] K. Exner, P. v. R. Schleyer, *Science* **2000**, *290*, 1937–1940.

[9] Z.-X. Wang, P. v. R. Schleyer, *Science* **2001**, *292*, 2465–2469.

[10] L. M. Wang, W. Huang, B. B. Averkiev, A. I. Boldyrev, L. S. Wang, *Angew. Chem.* **2007**, **119**, 4634–4637; *Angew. Chem. Int. Ed.* **2007**, *46*, 4550–4553.

[11] B. B. Averkiev, D. Y. Zubarev, L. M. Wang, W. Huang, L. S. Wang, A. I. Boldyrev, *J. Am. Chem. Soc.* **2008**, *130*, 9248–9250.

[12] R. Islas, T. Heine, K. Ito, P. v. R. Schleyer, G. Merino, *J. Am. Chem. Soc.* **2007**, *129*, 14767–14774.

[13] B. B. Averkiev, A. I. Boldyrev, *Russ. J. Gen. Chem.* **2008**, *78*, 769–773.

[14] J. C. Guo, W. Z. Yao, Z. Li, S. D. Li, *Sci. China Ser. B* **2009**, *52*, 566–570.

[15] C. Romanescu, A. P. Sergeeva, W. L. Li, A. I. Boldyrev, L. S. Wang, *J. Am. Chem. Soc.* **2011**, *133*, 8646–8653.

[16] T. R. Galeev, C. Romanescu, W. L. Li, L. S. Wang, A. I. Boldyrev, *J. Chem. Phys.* **2011**, *135*, 104301.

[17] W. L. Li, C. Romanescu, T. R. Galeev, L. S. Wang, A. I. Boldyrev, *J. Phys. Chem. A* **2011**, *115*, 10391–10397.

[18] C. Romanescu, T. R. Galeev, W. L. Li, A. I. Boldyrev, L. S. Wang, *Angew. Chem.* **2011**, *123*, 9506–9509; *Angew. Chem. Int. Ed.* 2011, *50*, 9334–9337.

[19] B. B. Averkiev, L. M. Wang, W. Huang, L. S. Wang, A. I. Boldyrev, *Phys. Chem. Chem. Phys.* **2009**, *11*, 9840–9849.

[20] C. Q. Miao, J. C. Guo, S. D. Li, *Sci. China Ser. B* **2009**, *52*, 900–904.

[21] Z. Pu, K. Ito, P. v. R. Schleyer, Q. S. Li, *Inorg. Chem.* **2009**, *48*, 10679–10686.

[22] H. J. Zhai, C. Q. Miao, S. D. Li, L. S. Wang, *J. Phys. Chem. A* **2010**, *114*, 12155–12161.

[23] L. S. Wang, H. S. Cheng, J. Fan, *J. Chem. Phys.* **1995**, *102*, 9480–9493.

[24] C. Adamo, V. Barone, *J. Chem. Phys.* **1999**, *110*, 6158.

[25] J. P. Perdew, K. Burke, M. Ernzerhof, *Phys. Rev. Lett.* **1996**, *77*, 3865–3868.

[26] P. J. Hay, W. R. Wadt, *J. Chem. Phys.* **1985**, *82*, 270.

[27] R. A. Kendall, T. H. Dunning, Jr., R. J. Harrison, *J. Chem. Phys.* **1992**, *96*, 6796.

[28] T. H. Dunning, Jr., *J. Chem. Phys.* **1989**, *90*, 1007.

[29] A. Bergner, M. Dolg, W. Kuechle, H. Stoll, H. Preuss, *Mol. Phys.* **1993**, *80*, 1431–1441.

[30] M. Kaupp, P. v. R. Schleyer, H. Stoll, H. Preuss, *J. Chem. Phys.* **1991**, *94*, 1360.

[31] M. Dolg, H. Stoll, H. Preuss, R. M. Pitzer, *J. Phys. Chem.* **1993**, *97*, 5852–5859.

[32] C. Chang, M. Pelissier, P. Durand, *Phys. Scr.* **1986**, *34*, 394.

[33] S. Faas, J. G. Snijders, J. H. van Lenthe, E. van Lenthe, E. J. Baerends, *Chem. Phys. Lett.* **1995**, **246**, 632–640.

[34] Y. Zhao, D. G. Truhlar, *Theor. Chem. Acc.* **2008**, *120*, 215–241.

[35] Y. Zhao, D. G. Truhlar, *Acc. Chem. Res.* **2008**, *41*, 157–167.

[36] ADF 2010, E.J. Baerends, T. Ziegler, J. Autschbach, D. Bashford, A. Bérces, F.M. Bickelhaupt, C. Bo, P.M. Boerrigter, L. Cavallo, D.P. Chong, L. Deng, R.M. Dickson, D.E. Ellis, M. van Faassen, L. Fan, T.H. Fischer, C. Fonseca Guerra, A. Ghysels, A. Giammona, S.J.A. van Gisbergen, A.W. Götz, J.A. Groeneveld, O.V. Gritsenko, M. Grüning, S. Gusarov, F.E. Harris, P. van den Hoek, C.R. Jacob, H. Jacobsen, L. Jensen, J.W. Kaminski, G. van Kessel, F. Kootstra, A. Kovalenko, M.V. Krykunov, E. van Lenthe, D.A. McCormack, A. Michalak, M. Mitoraj, J. Neugebauer, V.P. Nicu, L. Noodleman, V.P. Osinga, S. Patchkovskii, P.H.T. Philipsen, D. Post, C.C. Pye, W. Ravenek, J.I. Rodríguez, P. Ros, P.R.T. Schipper, G. Schreckenbach, J.S. Seldenthuis, M. Seth, J.G. Snijders, M. Solà, M. Swart, D. Swerhone, G. te Velde, P. Vernooijs, L. Versluis, L. Visscher, O. Visser, F. Wang, T.A. Wesolowski, E.M. van Wezenbeek, G. Wiesenekker, S.K. Wolff, T.K. Woo, A.L. Yakovlev, SCM, Theoretical Chemistry, Vrije Universiteit, Amsterdam, The Netherlands, http://www.scm.com

[37] D. Yu. Zubarev, A. I. Boldyrev, *Phys. Chem. Chem. Phys.* **2008**, *10*, 5207–5217.

[38] Gaussian 09, Revision B.0.1, M. J. Frisch, G. W. Trucks, H. B. Schlegel, G. E. Scuseria, M. A. Robb, J. R. Cheeseman, G. Scalmani, V. Barone, B. Mennucci, G.

A. Petersson, H. Nakatsuji, M. Caricato, X. Li, H. P. Hratchian, A. F. Izmaylov, J. Bloino, G. Zheng, J. L. Sonnenberg, M. Hada, M. Ehara, K. Toyota, R. Fukuda, J. Hasegawa, M. Ishida, T. Nakajima, Y. Honda, O. Kitao, H. Nakai, T. Vreven, J. A. Montgomery, Jr., J. E. Peralta, F. Ogliaro, M. Bearpark, J. J. Heyd, E. Brothers, K. N. Kudin, V. N. Staroverov, R. Kobayashi, J. Normand, K. Raghavachari, A. Rendell, J. C. Burant, S. S. Iyengar, J. Tomasi, M. Cossi, N. Rega, J. M. Millam, M. Klene, J. E. Knox, J. B. Cross, V. Bakken, C. Adamo, J. Jaramillo, R. Gomperts, R. E. Stratmann, O. Yazyev, A. J. Austin, R. Cammi, C. Pomelli, J. W. Ochterski, R. L. Martin, K. Morokuma, V. G. Zakrzewski, G. A. Voth, P. Salvador, J. J. Dannenberg, S. Dapprich, A. D. Daniels, Ö. Farkas, J. B. Foresman, J. V. Ortiz, J. Cioslowski, and D. J. Fox, Gaussian, Inc., Wallingford CT, **2009**.

[39] U. Varetto, Molekel 5.4.0.8, Swiss National Supercomputing Centre, Manno, Switzerland, **2009**.

Table 8-1: Observed vertical electron detachment energies (VDEs) of TaB_{10}^- and NbB_{10}^- compared with the theoretically calculated values for the two lowest isomers of TaB_{10}^- and NbB_{10}^-. All energies are in eV.

Observed Features	VDE (exp)[a]	Final State and Electronic Configuration	VDE (theoretical) ROPBE1PBE[b]	VDE (theoretical) ROCCSD(T)[c]
$Ta©B_{10}^-$ (D_{10h}, $^1A_{1g}$)				
X[d]	4.04(3)	$^2E_{2g}$ …$2a_{1g}^2\ 1b_{2u}^2\ 1a_{2u}^2\ 1e_{1g}^4\ 2e_{1u}^4\ 2e_{2g}^3$	4.13	4.16
A	4.29(3)	$^2E_{1u}$ …$2a_{1g}^2\ 1b_{2u}^2\ 1a_{2u}^2\ 1e_{1g}^4\ 2e_{1u}^3\ 2e_{2g}^4$	4.37	4.46
B[e]	4.55(5)			
C	5.36(5)	$^2E_{1g}$ …$2a_{1g}^2\ 1b_{2u}^2\ 1a_{2u}^2\ 1e_{1g}^3\ 2e_{1u}^4\ 2e_{2g}^4$	5.37	5.47
D	5.51(5)	$^2A_{2u}$ …$2a_{1g}^2\ 1b_{2u}^2\ 1a_{2u}^1\ 1e_{1g}^4\ 2e_{1u}^4\ 2e_{2g}^4$	5.49	5.61
TaB_{10}^- (C_{2v}, $^1A_1$)				
		$^2A_1$ … $5a_1^2\ 4b_2^2\ 4b_1^2\ 3a_2^2\ 6a_1^2\ 7a_1^1$	2.52	2.64
		$^2A_1$ … $5a_1^2\ 4b_2^2\ 4b_1^2\ 3a_2^2\ 6a_1^1\ 7a_1^2$	2.70	[f]
		$^2A_2$ … $5a_1^2\ 4b_2^2\ 4b_1^2\ 3a_2^1\ 6a_1^2\ 7a_1^2$	3.34	3.42
		$^2B_1$ … $5a_1^2\ 4b_2^2\ 4b_1^1\ 3a_2^2\ 6a_1^2\ 7a_1^2$	4.37	4.43
		$^2B_2$ … $5a_1^2\ 4b_2^1\ 4b_1^2\ 3a_2^2\ 6a_1^2\ 7a_1^2$	5.00	5.06
$Nb©B_{10}^-$ (D_{10h}, $^1A_{1g}$)				
X[g]	4.12(3)	$^2E_{2g}$ … $1b_{2u}^2\ 2a_{1g}^2\ 1a_{2u}^2\ 1e_{1g}^4\ 2e_{1u}^4\ 2e_{2g}^3$	4.16	4.21
A	4.26(3)	$^2E_{1u}$ … $1b_{2u}^2\ 2a_{1g}^2\ 1a_{2u}^2\ 1e_{1g}^4\ 2e_{1u}^3\ 2e_{2g}^4$	4.29	4.36
B[e]	4.34(5)			
C	5.28(5)	$^2E_{1g}$ … $1b_{2u}^2\ 2a_{1g}^2\ 1a_{2u}^2\ 1e_{1g}^3\ 2e_{1u}^4\ 2e_{2g}^4$	5.32	5.44
D	5.41(5)	$^2A_{2u}$ … $1b_{2u}^2\ 2a_{1g}^2\ 1a_{2u}^1\ 1e_{1g}^4\ 2e_{1u}^4\ 2e_{2g}^4$	5.42	5.50
NbB_{10}^- (C_{2v}, $^1A_1$)				
X’	2.65(4)	$^2A_1$ … $5a_1^2\ 4b_2^2\ 4b_1^2\ 3a_2^2\ 6a_1^2\ 7a_1^1$	2.48	2.57
A’	2.89(4)	$^2A_1$ … $5a_1^2\ 4b_2^2\ 4b_1^2\ 3a_2^2\ 6a_1^1\ 7a_1^2$	2.69	2.84
B’	3.4(1)	$^2A_2$ … $5a_1^2\ 4b_2^2\ 4b_1^2\ 3a_2^1\ 6a_1^2\ 7a_1^2$	3.23	3.30
		$^2B_1$ … $5a_1^2\ 4b_2^2\ 4b_1^1\ 3a_2^2\ 6a_1^2\ 7a_1^2$	4.33	4.37
C’	4.91(5)	$^2B_2$ … $5a_1^2\ 4b_2^1\ 4b_1^2\ 3a_2^2\ 6a_1^2\ 7a_1^2$	4.95	4.99

[a] Numbers in parentheses represent the uncertainty in the last digit. [b] VDEs were calculated at ROPBE0/Ta,Nb/Stuttgart/B/aug-cc-pVTZ. [c] VDEs were calculated at ROCCSD(T)/Ta,Nb/Stuttgart/B/aug-cc-pVTZ//PBE0/Ta,Nb/Stuttgart/B/aug-cc-pVTZ. [d] Measured ADE = 4.04(3) eV. Calculated ADE at ROCCSD(T)/Ta/Stuttgart/B/aug-cc-pVTZ//PBE0/Ta/Stuttgart/B/aug-cc-pVTZ with ZPE correction: 4.05 eV. [e] The peak is assigned to the transition to the second spin-orbit component of the $^2E_{1u}$ electronic state. [f] We were not able to calculate this VDE at this level of theory. [g] Measured ADE = 4.10(3) eV. Calculated ADE at ROCCSD(T)/Nb/Stuttgart/B/aug-cc-pVTZ//PBE0/Nb/Stuttgart/B/aug-cc-pVTZ with ZPE correction: 4.03 eV.

***Table 8-2**:* Orbital Energies of $Ta©B_{10}^-$ calculated with ZORA at M06-2X/QZ4P.

Relativistic scalar ZORA			Relativistic spin-orbit zora		
symmetry	occupancy	orbital energy, eV	symmetry	occupancy	orbital energy, eV
E'_2 (HOMO)	4.00	-3.66	$E_{3/2}$	2.00	-3.76
			$E_{5/2}$	2.00	-3.53
E'_1	4.00	-3.98	$E_{9/2}$	2.00	-4.10
			$E_{7/2}$	2.00	-3.90
E''_1	4.00	-4.76	$E_{1/2}$	2.00	-4.80
			$E_{3/2}$	2.00	-4.73
A''_2	2.00	-5.04	$E_{9/2}$	2.00	-5.05
A'_1	2.00	-6.03	$E_{1/2}$	2.00	-6.03
A'_1	2.00	-6.05	$E_{1/2}$	2.00	-6.05
E'_1	4.00	-6.97	$E_{9/2}$	2.00	-6.97
E'_2	4.00	-9.05	$E_{3/2}$	2.00	-9.06
			$E_{5/2}$	2.00	-9.05

Table 8-3: Orbital Energies of $Ta©B_{10}^-$ calculated with ZORA at PBE0/QZ4P.

Relativistic scalar ZORA			Relativistic spin-orbit ZORA		
symmetry	occupancy	orbital energy, eV	symmetry	occupancy	orbital energy, eV
E'_2 (HOMO)	4.00	-2.80	$E_{3/2}$	2.00	-2.88
			$E_{5/2}$	2.00	-2.70
E'_1	4.00	-3.05	$E_{9/2}$	2.00	-3.15
			$E_{7/2}$	2.00	-2.96
E''_1	4.00	-4.01	$E_{1/2}$	2.00	-4.04
			$E_{3/2}$	2.00	-3.97
A''_2	2.00	-4.13	$E_{9/2}$	2.00	-4.14
A'_1	2.00	-4.93	$E_{1/2}$	2.00	-4.93
A'_1	2.00	-4.96	$E_{1/2}$	2.00	-4.96
E'_1	4.00	-5.82	$E_{9/2}$	2.00	-5.82
			$E_{7/2}$	2.00	-5.82
E'_2	4.00	-7.79	$E_{3/2}$	2.00	-7.79
			$E_{5/2}$	2.00	-7.79

Table 8-4: Vibrational frequencies for the neutral TaB_{10} species (D_{2h}, ^2A_g) at PBE0/Ta/Stuttgart/B/aug-cc-pVTZ.

	ω (a_g), cm^{-1}		ω (b_{1g}), cm^{-1}		ω (b_{2g}), cm^{-1}		ω (b_{3g}), cm^{-1}		ω (a_u), cm^{-1}		ω (b_{1u}), cm^{-1}		ω (b_{2u}), cm^{-1}		ω (b_{3u}), cm^{-1}
1	290	**6**	273	**7**	281	**9**	103	**13**	116	**15**	114	**20**	167	**25**	51
2	486			**8**	482	**10**	350	**14**	436	**16**	449	**21**	328	**26**	105
3	624					**11**	1064			**17**	501	**22**	725	**27**	437
4	1051					**12**	1094			**18**	713	**23**	1204		
5	1588									**19**	1192	**24**	1656		

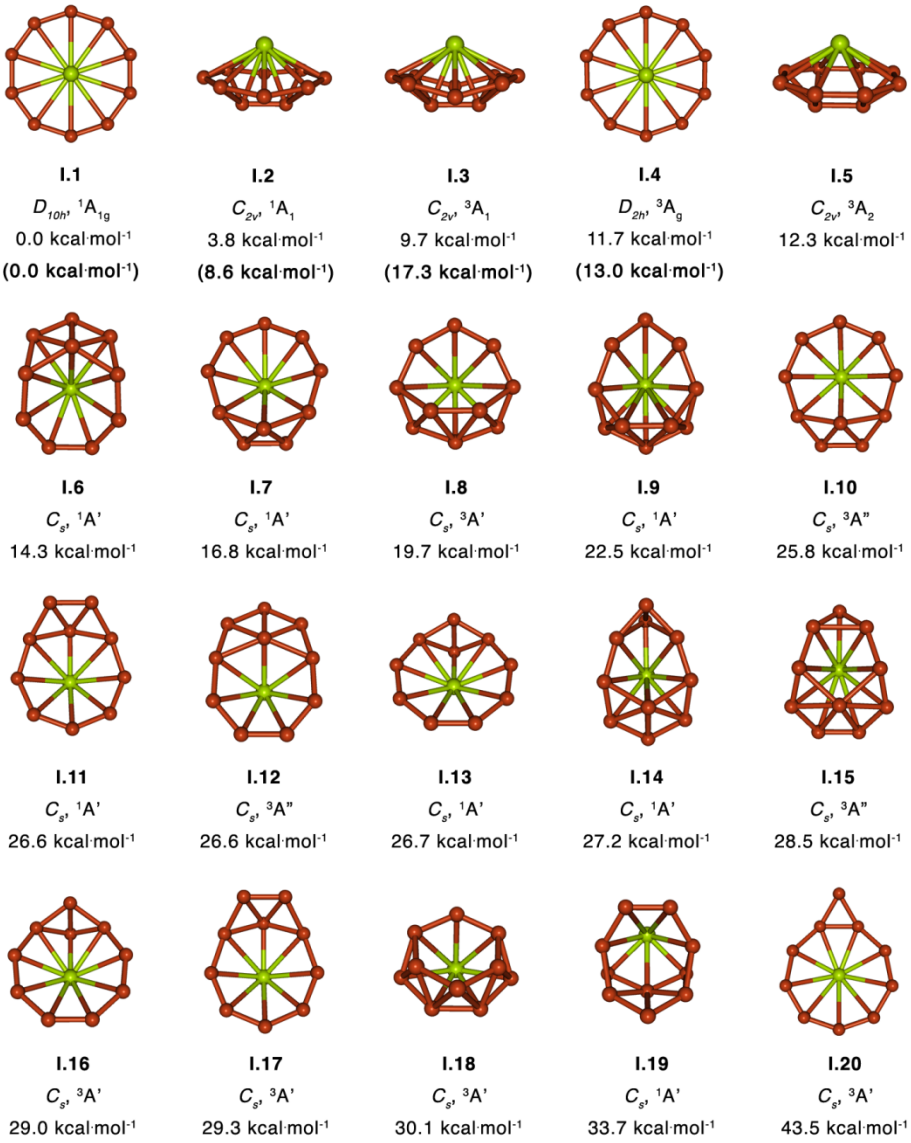

Figure 8-1. Optimized structures of the TaB_{10}^- cluster, their point group symmetries, spectroscopic states, and relative energies. ZPE corrected relative energies are given at PBE0/Ta/Stuttgart/B/aug-cc-pVTZ and RCCSD(T)/Ta/Stuttgart/B/aug-cc-pVTZ// PBE0/Ta/Stuttgart/B/aug-cc-pVTZ (in parentheses).

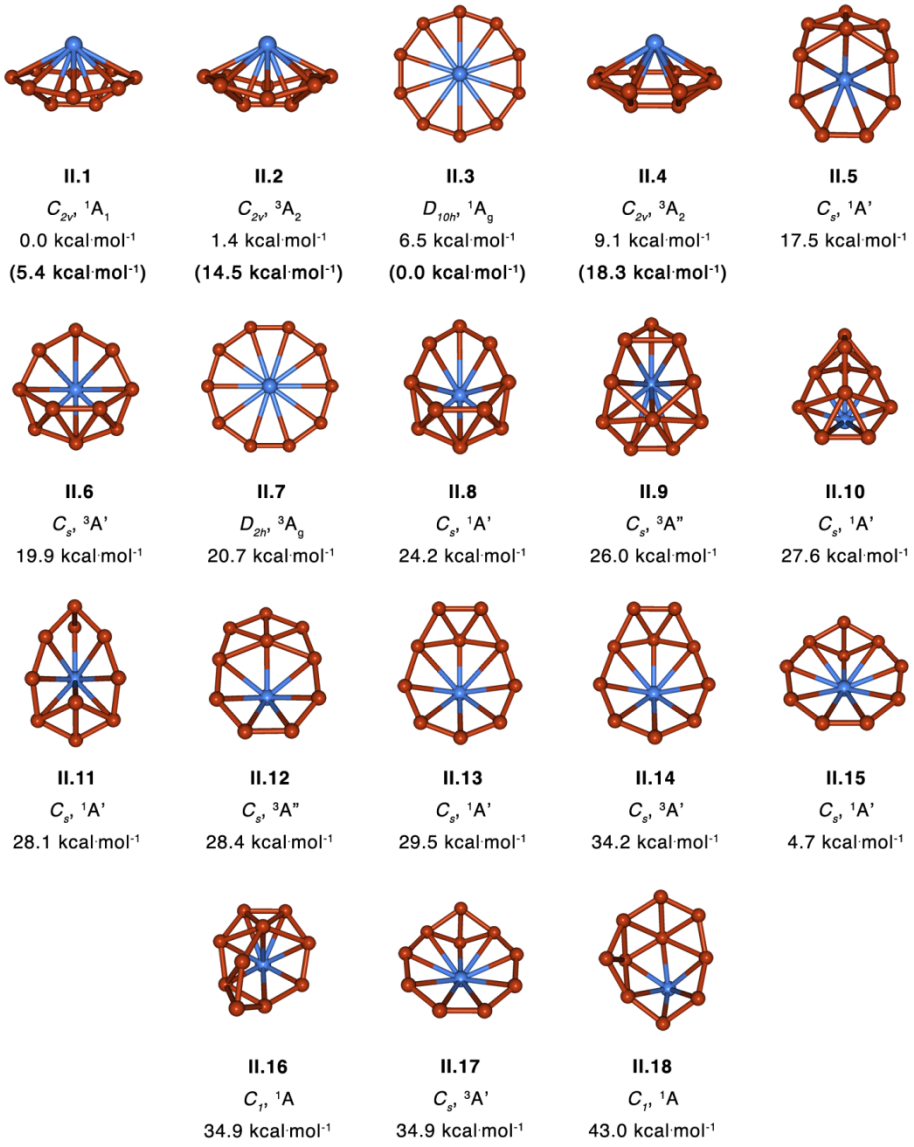

Figure 8-2. Optimized structures of the NbB_{10}^- cluster, their point group symmetries, spectroscopic states, and relative energies. ZPE corrected relative energies are given at PBE0/Nb/Stuttgart/B/aug-cc-pVTZ and RCCSD(T)/Nb/Stuttgart/B/aug-cc-pVTZ// PBE0/Nb/Stuttgart/B/aug-cc-pVTZ (in parentheses). Notice that II.3 is the global minimum isomer at the higher level of theory.

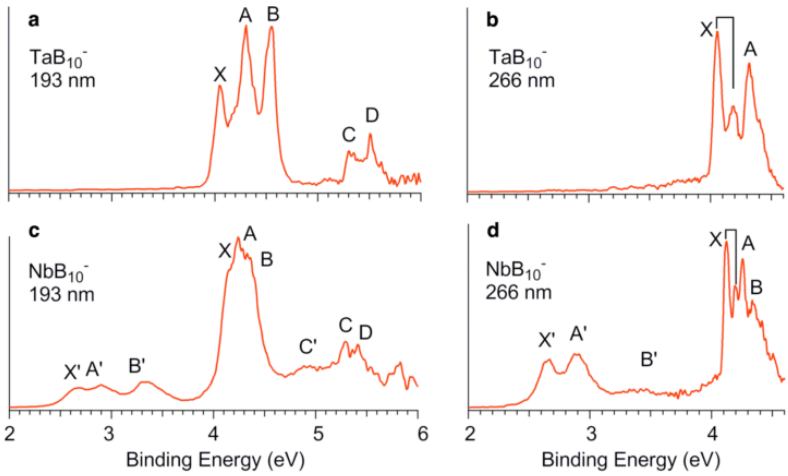

Figure 8-3. Photoelectron spectra of TaB_{10}^- at a) 193 nm and b) 266 nm. Photoelectron spectra of NbB_{10}^- at c) 193 nm and d) 266 nm. The vertical lines in (b) and (d) are vibrational structures.

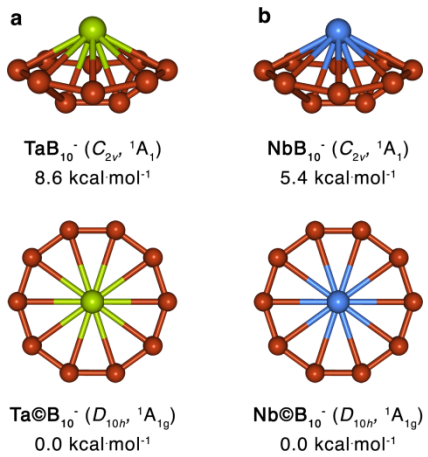

Figure 8-4. Structures of the two lowest energy isomers of a) TaB_{10}^- and b) NbB_{10}^-, and the their point group symmetries, spectroscopic states, and zero-point energy (ZPE) corrected relative energies (RCCSD(T)/Ta, Nb/Stuttgart/B/aug-cc-pVTZ//PBE0/Ta, Nb/Stuttgart/B/aug-cc-pVTZ).

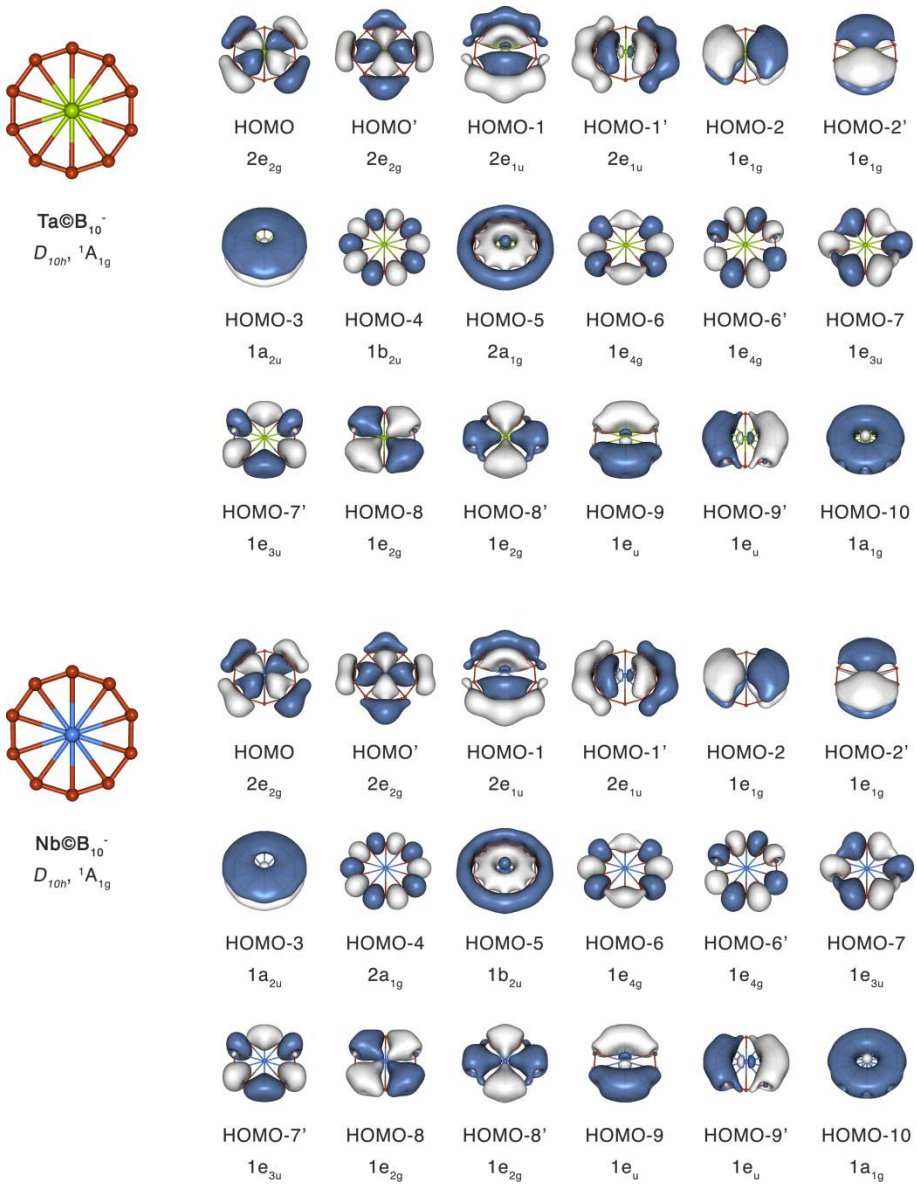

Figure 8-5. Valence canonical molecular orbitals of $Ta©B_{10}^-$ and $Nb©B_{10}^-$ (PBE0/Ta, Nb/Stuttgart/B/aug-cc-pVTZ).

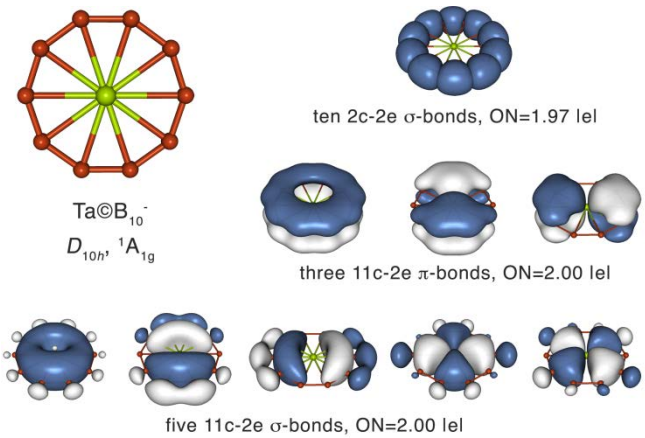

Figure 8-6. Chemical bonding pattern of $Ta©B_{10}^-$ shown by the AdNDP analysis. ON stands for occupation number.

CHAPTER 9

EXPERIMENTAL AND COMPUTATIONAL EVIDENCE OF OCTA- AND NONA-COORDINATED PLANAR IRON-DOPED BORON CLUSTERS: $Fe©B_8^-$ AND $Fe©B_9^-$ *

Abstract

We report the observation of two Fe-doped boron clusters with wheel-type structures, containing an octa-coordinate (C_{8v}-$Fe©B_8^-$) and a nona-coordinate (D_{9h}-$Fe©B_9^-$) Fe atom. The clusters were produced in a laser vaporization supersonic molecular beam and characterized by combined photoelectron spectroscopy and *ab initio* studies. Chemical bonding analyses revealed that in the ground state both clusters are doubly ($\sigma+\pi$) aromatic and that the iron atom interacts with the peripheral boron ring exclusively through delocalized bonds. These findings provide further support to the design principle for metal-doped boron clusters with highly symmetric molecular wheel-type structures.

9-1. Introduction

The study of atomic clusters, with structures and properties intermediate between the individual entities and the bulk condensed phase, has significantly enriched our understanding of chemical bonding and the rational design of molecules with tailored physical and chemical properties [1]. Bulk boron and boranes usually have three-

* Coauthored by Constantin Romanescu, Timur R. Galeev, Alina P. Sergeeva, Wei-Li Li, Lai-Sheng Wang, and Alexander I. Boldyrev. Reprinted from *Journal of Organometallic Chemistry*, Vol. 721-722, C. Romanescu, T. R. Galeev, A. P. Sergeeva, W. L. Li, L. S. Wang, A. I. Boldyrev, Experimental and computational evidence of octa- and nona-coordinated iron-doped boron clusters: $Fe©B_8^-$ and $Fe©B_9^-$. Pages 148-154, Copyright 2012, with permission from Elsevier.

dimensional (3D) structures [2]. However, joint photoelectron spectroscopy and computational studies over the last decade have demonstrated that negatively charged boron clusters (B_n^-) have planar or quasi-planar structures at least up to $n = 21$ [3-13]. Neutral boron clusters were shown to become 3D at B_{20} [9], which have been corroborated by recent computational studies [14,15]. Positively charged boron clusters have been shown to become 3D at B_{16}^+ [16], while negatively charged boron clusters are still planar at B_{21}^- [13]. All planar boron clusters confirmed experimentally consist of an outer ring featuring strong two-center-two-electron (2c-2e) B-B bonds and one or more inner atoms interacting with the peripheral ring via delocalized σ and π bonding.

Two planar anionic boron clusters stand out as perfectly symmetric molecular wheel systems with unprecedented multi-center electron delocalization: B_8^{2-} ($B©B_7^{2-}$) and B_9^- ($B©B_8^-$) [4,17]. Detailed bonding analyses of the two clusters demonstrated that both species have closed shell electronic configurations and are doubly aromatic with 6 σ and 6 π delocalized electrons. The doubly aromatic character and the multi-center electron delocalization were confirmed by ring current calculations [18] and Adaptive Natural Density Partitioning (AdNDP) [19,20] analyses. Pure all-boron clusters have been proposed as novel building blocks of solid materials [21], and recently a remarkable $Ti_7Rh_4Ir_2B_8$ compound containing planar B_6 ring has been synthesized [22,23]. Fehlner and co-workers [24,25] synthesized earlier the $(Cp^*ReH_2)B_5Cl_5$ and $(Cp^*)_2B_6H_4Cl_2$ triple-decker compounds, containing the first planar B_5Cl_5 and $B_6H_4Cl_2$ structural fragments, respectively.

Numerous theoretical reports have concerned carbon-doped boron clusters featuring a carbon atom with high coordination numbers [26-30]. However, joint experimental and theoretical studies have proved that carbon avoids hyper-coordination in B_xC_y clusters [20,31-33]. One question arises: is it possible to substitute the central boron atom in the B_8^{2-} and B_9^- molecular wheels with a metal atom and therefore create metal-centered monocyclic boron clusters? We have shown previously that simple valence isoelectronic substitution of the central boron atom by aluminum in B_8^- and B_9^- lowers the symmetry of the system and gives rise to "umbrella"-type structures in AlB_7^- (C_{7v}) and AlB_8^- (C_{8v}) [34]. In these clusters, Al is bound ionically to a doubly aromatic B_7^{3-} or B_8^{2-} moiety and does not participate in delocalized bonding. Formation of ionic bonds in Al-doped boron clusters was also observed for larger AlB_n^- ($n = 9-11$) clusters [35,36]. Doping boron rings with transition metals with partially filled d-orbitals hence becomes the natural choice for creating thermodynamically stable metal-centered aromatic compounds.

Recently, we proposed a design principle for such compounds that uses the formal valence of the transition metal (x), the number of peripheral boron atoms (n), and the cluster's charge (q) to predict doubly aromatic structures ($M^{(x)}©B_n^{q-}$) and tested it for anionic, $Co©B_8^-$, $Ru©B_9^-$ [37], $Ta©B_{10}^-$, $Nb©B_{10}^-$ [38], and neutral, $Rh©B_9$ and $Ir©B_9$ [39] clusters. The design principle, derived from the bonding model of the doubly aromatic $B©B_7^{2-}$ and $B©B_8^-$ clusters [4], requires that the bonding electrons in the system, $3n + x + q$, participate in n(2c-2e) B-B peripheral bonds and 2 sets of aromatic

delocalized bonds, each set fulfilling Hückel's rule for aromaticity ($4N + 2$ electrons). Geometric constraints are expected to set the minimum boron ring size (n) to 8 atoms or more, depending on the size of the dopant. When applied to Fe, the design principle predicts the following closed-shell doubly aromatic species: FeB_8^{2-}, FeB_9^-, and FeB_{10}^0. In all these clusters, the Fe atom has a formal valence of 2. Open-shell doubly aromatic systems may, also, exist for FeB_8^- and FeB_9^0, where the formal valence of Fe is 3.

Prior to this study there were no experimental reports on any Fe-doped boron clusters and there are only a few computational reports on wheel-type clusters. The most relevant works [40,41] investigated the electronic structures and geometries of a number of metal-centered boron clusters using global minimum search and DFT calculations. These studies showed that in the ground state FeB_9^- is aromatic and has a D_{9h} symmetry and that the D_{8h}-Fe©B_8^{2-} wheel structure is also the global minimum on the FeB_8^{2-} potential energy surface. There have been also several other studies about the geometry optimizations and energy calculations using DFT methods for neutral and charged Fe-doped boron clusters [42-44].

In the current work, we report experimental and computational evidence demonstrating that Fe©B_8^- and Fe©B_9^- are doubly aromatic metal-centered borometallic compounds.

9-2. Experimental and computational methods

9-2.1. Photoelectron spectroscopy

The experiment was performed using a magnetic-bottle PES apparatus equipped with a laser vaporization cluster source that was described in detail previously [45,46]. Briefly, the iron-doped boron clusters were produced by means of laser ablation of a disk target made of isotopically enriched ^{10}B (96%), which contained ~10% ^{10}B and ~2.5% Fe by mass, balanced by Bi, which acted as a target binder and also provided the Bi^- calibrant for the photoelectron spectra. The clusters were entrained by a He carrier gas containing 5% Ar and underwent a supersonic expansion to form a collimated cluster beam. The composition and the cooling of the clusters were controlled by the time delay between the carrier gas pulse and the ablation laser [47,48]. The negatively charged clusters were extracted and analyzed with a time-of-flight mass spectrometer. The species of interest were mass-selected and decelerated before being photodetached by a pulsed laser beam at 193 nm (6.424 eV) or 266 nm (4.661 eV). Photoelectrons were collected at nearly 100% efficiency by a magnetic bottle and analyzed in a 3.5 m long electron flight tube. The electron kinetic energy resolution of the apparatus, $\Delta E/E$, was better than 2.5%, *i.e.* 25 meV for 1 eV electrons.

9-2.2. Computational methods

Since $Fe©B_9^-$ was already established as the global minimum of FeB_9^- in a previous theoretical report [40], we ran an extensive global minimum search only for FeB_8^-. The search was conducted using the Coalescence Kick method [49] and the

UPBE0 [50,51]/LANL2DZ [52] level of theory. Low-lying isomers, within 50 kcal/mol with respect to the lowest energy isomer, were reoptimized using the aug-cc-pVTZ [53-55] basis set and the BP86 density functional [56,57], which was shown to perform slightly better than hybrid functionals for molecules containing first row transition metals [58]. Frequency calculations were performed at UBP86/aug-cc-pVTZ to ensure that all the found structures are true minima on the potential energy surface (see Fig 9-1). ROCCSD(T) [59-61]/6-311 + G(2df) [62-65]//UBP86/aug-cc-pVTZ single-point energies were calculated for low-lying isomers within 30 kcal/mol of the global minimum at the BP86 level (Fig. 9-1). Theoretical VDEs for FeB_8^- and FeB_9^- were calculated for the global minimum structures at the following levels of theory: U(RO)BP86/aug-cc-pVTZ, ROPBE0/aug-cc-pVTZ and ROCCSD(T)/aug-cc-pVTZ; all at the anion geometries optimized at the UBP86/aug-cc-pVTZ level of theory. The calculations were performed using Gaussian 09 [66] and Molekel 5.4.0.8 [67] was used for visualization.

9-3. Experimental results

The photoelectron spectra of FeB_8^- and FeB_9^- are shown in Figs. 9-2 and 9-3, respectively, each at two photodetachment photon energies: 266 nm and 193 nm. The detachment features are labeled with letters and the measured vertical detachment energies (VDE) are given in Table 9-1, where they are compared with theoretical calculations at various levels of theory (*vide infra*). Commonly, the peak marked as X represents the transition between the ground electronic states of the anion and the neutral

species, while the higher binding energy peaks (A, B···) denote transitions to excited electronic states of the neutral cluster.

9-3.1. FeB_8^-

The 266 nm spectrum of FeB_8^- (Fig. 9-2a) displays a broad and weak low binding energy band (X'), an intense vibrationally resolved band (X), and a weak band A. As will be shown below, the first band (X') represents probably a transition from a higher energy isomer. The strong feature in the 266 nm spectrum (X) corresponds to the transition from the ground state of FeB_8^- to that of its neutral with a VDE value of 3.75 eV and a partially resolved vibrational progression. Two vibrational modes are tentatively assigned with average spacings of 510 ± 50 cm^{-1} and 1300 ± 100 cm^{-1}, respectively. Since this band does not have a sharp rise, it is likely that there may be unresolved low frequency vibrational excitations associated with each resolved peak. The adiabatic detachment energy (ADE) of band X is evaluated to be 3.65 eV. The third weak feature, A, with a VDE of 4.15 eV, was not well resolved at 266 nm, but it is better defined in the 193 nm spectrum (Fig. 9-2b). At the high binding energy side, we observed three additional bands B-D with VDEs of 4.60, 5.21, and 5.60 eV, respectively. All the spectral features of FeB_8^- are broad, suggesting that there are significant geometry changes between FeB_8^- and its neutral states.

9-3.2. FeB_9^-

The 266 nm photoelectron spectrum of FeB_9^- (Fig. 9-3a) displays two detachment bands: X and A. The first band, X, is weak with a vertical detachment energy (VDE)

value of 3.42 eV and does not show any resolved vibrational structure. The ADE is 3.38 (3) eV. The second band, A, is intense and has a VDE value of 4.22 eV. The A band has a sharp rise and shows a short vibrational progression with an average spacing of 440 ± 40 cm^{-1}. We assign the most intense peak of the A band to the 0–0 vibrational transition, as the measured ADE and VDE values are equal. At 193 nm (Fig. 9-3b), two more features are identified, B and C, with VDE values of 5.03 and 5.23 eV. No discernable spectral features were observed beyond 6 eV. All detachment transitions were relatively sharp, suggesting that there are only minor geometry changes between the anion and the neutral states.

9-4. Theoretical results

The global minimum structures of FeB_8^- and FeB_9^- are presented in Fig 9-4. FeB_9^- has a perfectly symmetric planar D_{9h} structure whereas the FeB_8^- species is a slightly distorted wheel-type structure of C_{8v} symmetry. The extent of distortion could be evaluated by noting that the largest B–Fe–B angle in the C_{8v} structure is 160.0°. The valence canonical molecular orbitals of the anionic species are presented in Fig. 9-5. The global minimum of FeB_8^- has one unpaired electron in the singly occupied molecular orbital (HOMO, $4a_1$) giving rise to the lowest doublet $^2A_1$ state of the C_{8v} structure (Fig. 9-5a) while all the molecular orbitals of FeB_9^- are doubly occupied rendering the closed-shell $^1A_1$' state of the species (Fig. 9-5b). The diagrams of highest occupied and lowest unoccupied orbitals of both FeB_8^- and FeB_9^-, as well as the orbital energies at ROBP86/aug-cc-pVTZ are given in Fig. 9-5c.

9-4.1. FeB_8^-

We performed an unbiased global minimum search for FeB_8^- using the Coalescence Kick method [49]. All of the structures found in this search within 50 kcal/mol at PBE0/LANL2DZ were further reoptimized at UBP86/aug-cc-pVTZ following the energy gradient to the closest minima (Fig. 9-1). The C_{8v} structure of FeB_8^- (Fig 9-4a) was found to be the lowest energy isomer with all the other structures lying higher than 20 kcal/mol with respect to the global minimum at UBP86/aug-cc-pVTZ. The subsequent single point calculations at ROCCSD(T)/6-311 + G(2df)//UBP86/aug-cc-pVTZ for all the low-lying isomers of FeB_8^-, identified within 30 kcal/mol at UBP86/aug-cc-pVTZ, confirmed that the C_{8v}-FeB_8^-structure is the true global minimum on the potential energy surface of FeB_8^- (Fig. 9-1). It should be pointed out that we encountered a very high value of Norm(A) = 2.05 (Norm(A) gives a measure of the correlation correction to the wavefunction; the coefficient of the HF configuration is 1) in our calculation of the ROCCSD(T) energy for the second lowest isomer of FeB_8^- (slightly distorted octa-coordinate wheel-type structure in a quartet state, isomer I.2, Fig. 9-1). Therefore, the relative energy of 27.1 kcal/mol at the ROCCSD(T) level for the second lowest isomer of FeB_8^- is highly questionable. It suggests that multi-configurational calculations are needed for this high spin isomer, which are beyond the scope of the current work.

We calculated the VDEs for the global minimum at UBP86, ROPBE0 and ROCCSD(T) levels (see Table 9-1) and for the second lowest isomer of FeB_8^- at UBP86

(see Table 9-2) and found a good agreement between the experimental features X, A, B, C, D and transitions in the C_{8v} structure of FeB_8^-, whereas the first VDE of the second lowest isomer of FeB_8^- agrees well with the broad X' band in the lower binding energy region.

9-4.2. FeB_9^-

The lowest planar wheel-type structure featuring a nona-coordinate iron (Fig. 9-4b) was identified in the work by Ito et al. in stochastic searches of both singlet and triplet potential energy surfaces of FeB_9^- [40]. All other structures were found to lie higher in energy [40]. Therefore, in the current study we did not perform a global minimum search for FeB_9^-. Instead we reoptimized the D_{9h} global minimum structure of FeB_9^- at UBP86/aug-cc-pVTZ, further calculated its VDEs at the U(RO)BP86, ROPBE0, and ROCCSD(T) levels, and compared the VDEs with the experimental data to confirm the calculated structure. All the calculated VDE values were found to be in good agreement with the experimental values.

9-5. Comparison of experimental and theoretical results

9-5.1. FeB_8^-

The unbiased search for the lowest structure of FeB_8^- revealed that the global minimum structure is an octa-coordinate wheel with the central Fe atom slightly shifted out of the boron ring plane (~0.2 Å) in the C_{8v}-Fe©B_8^- structure.

The ground state detachment transition is from the removal of an electron from the doubly degenerate $3e_1$orbital, corresponding to the X band at 3.75 eV. This transition results in a final triplet $^3E_1$ state and the calculated VDE was found to be in good agreement with the experimental value: 3.62 eV at UBP86, 3.71 eV at ROPBE0, and 3.84 eV at ROCCSD(T). As a result of the electron removal from a doubly degenerate orbital, the geometry of the neutral FeB_8 cluster undergoes a small Jahn-Teller distortion leading to a lowerC_{2v} symmetry (see Fig. 9-6). The geometry change was, also, reflected by the observation of the two vibrational modes of FeB_8 that are responsible for the C_{8v} to C_{2v} distortion. The experimental values, 510 (50) cm^{-1} and 1300 (100) cm^{-1}, are indeed in good agreement with the UBP86 values: 516 cm^{-1} and 1286 cm^{-1}, respectively. The A band comes from the removal of an electron from the $2e_2$ orbital, resulting in the triplet $^3E_2$ excited state of the neutral species. The B band corresponds to electron detachment from the $4a_1$ orbital. All of the other transitions are explained as electron detachments from the $3a_1$, $2a_1$, and $2e_1$ orbitals with final triplet states. All of the VDE values calculated for the photodetachment transitions are in good agreement with the experimentally measured values (Table 9-1) with the exception of the transition marked as X' in Fig. 9-3.

This transition could be assigned to photodetachment from a higher energy isomer I.2 (Fig. 9-1 and Table 9-2). The presence of a similar low binding energy peak was previously observed for the $Co©B_8^-$ cluster [37] and explained as contribution from a higher spin (triplet) isomer. Isomer I.2 was the only low-energy isomer for which we could not accurately evaluate the relative energy at the ROCCSD(T) level due to a high

NORM value (2.05) in our calculation. Therefore, we think it could actually be closer in energy to the global minimum than the predicted value of 27.1 kcal/mol. This isomer has an octa-coordinate distorted wheel-type structure in the lowest quartet $^4A_1$ state. The detachment from a singly occupied HOMO ($5b_1$) occurs at a VDE of 2.59 eV at UBP86, which is in good agreement with the X' band. We have also calculated VDEs of the lowest transitions for isomer I.3 and isomer I.4 to be 2.67 eV and 2.53 eV, respectively. We could not exclude contributions of these isomers to the X' band, though we believe that they should be minor because these isomers are quite high in energy. The highly multi-configurational character of the electronic states of the open shell FeB_8^- makes *ab initio* calculations at higher levels of theory extremely challenging. The good agreement between the theoretical VDEs and the experimental data lends support for the slightly distorted C_{8v} molecular wheel structure as the global minimum for FeB_8^-. Thus, we found the global minimum of $Fe©B_8^-$ to possess an octa-coordinate iron atom in which Fe is slightly shifted out of the molecular plane formed by the outer boron ring (Fig. 9-4a).

The optimized geometries of the dianionic, anionic, and neutral $FeB_8^{2-/1-/0}$ cluster at BP86/aug-cc-pVTZ are compared in Fig. 9-6. It can be clearly seen that the peripheral B–B distance becomes somewhat shorter (1.572 Å for $Fe©B_8^{2-}$; 1.563 Å for $Fe©B_8^-$; 1.548 Å for $Fe©B_8$) while the central iron atom gets more and more out of plane as we gradually remove two electrons from the octa-coordinate $Fe©B_8^{2-}$ species introduced by Pu et al. [41].

The canonical molecular orbitals (CMO) of the open-shell global minimum of $Fe©B_8^-$ are presented in Fig. 9-5a. We expect that the 33 valence electrons of $Fe©B_8^-$

could form the following bonds and lone pairs: 1) three π delocalized bonds making this cluster π aromatic; 2) three σ delocalized bonds making this cluster σ aromatic; 3) two lone pairs of d-type participating in a minor covalent bonding with the peripheral boron ring; 4) a singly occupied 1c-2e bond of d_z^2-type localized on the central atom; 5) eight 2c-2e peripheral B-B σ bonds. The double aromaticity of the FeB_8^- global minimum explains its stability and presence in the photoelectron spectrum.

9-5.2. FeB_9^-

The previously reported global minima stochastic searches revealed that the wheel-type structure is the lowest energy isomer of FeB_9^- [40]. The first low-lying isomer (C_s) was shown to be 14.9 kcal/mol higher in energy at the BP86/TZVPP level of theory [40] and, therefore, we expect that only the wheel structure should contribute to the photoelectron signal in the photodetachment spectra.

The AdNDP analysis reported previously [20] showed that the system is doubly aromatic (σ+π) and that Fe acts as valence 2 element. The six 3d electrons of Fe are localized as lone pairs (d_z^2, $d_{x^2-y^2}$, d_{xy}), however, there is some bonding interaction between the peripheral boron ring and the $d_{x^2-y^2}$ and d_{xy} electrons (occupation number, ON = 1.80|e|). Even though this system is valence isoelectronic to $Ru©B_9^-$ we note that there are differences between their MO patterns [37]. In the case of $Ru©B_9^-$ the HOMO (3a') is essentially the $4d_z^2$ atomic orbital of Ru and does not contribute to bonding (ON = 2.00|e|). Removal of a single electron from the $4d_z^2$ HOMO does not lead to a large geometry change and causes only a slight out-of-plane displacement of the Ru

atom. Its HOMO-1 ($2e_1'$) consists of a set of doubly degenerate σ bonding orbitals and Jahn-Teller geometric distortions are expected for the electron detachment.

The experimental spectra show that the lowest binding energy transition in $Fe©B_9^-$ is relatively sharp and has no vibrationally resolved features, suggesting that this transition should involve the removal of one electron from a non-bonding orbital. This observation was confirmed by our DFT energy calculations: the first detachment channel corresponds to the removal of an electron from the $3a_1'$ HOMO similar to the HOMO of $Ru©B_9^-$ (Fig. 9-4) to result in the $^2A_1'$ ground state for the neutral species (Table 9-1). Furthermore, the geometry optimization of the neutral cluster starting from the wheel structure indicates that the D_{9h}-$Fe©B_9$ is at least a minimum on the potential energy surface of FeB_9. The minimal change in the geometry of the $Fe©B_9^-$ upon one electron photodetachment is consistent with our previous observations on the $Ru©B_9^-$ cluster [37]. In the latter case, the Ru atom was found to be slightly too large to fit inside a neutral B_9 ring and was pushed outside the ring and formed a highly symmetric C_{9v} symmetry structure. The theoretical first VDE, computed at BP86 (3.58 eV) or at PBE0 (3.40 eV), is in good agreement with the experimental feature X at 3.42 eV (Table 9-1). The next four photodetachment transitions occur from HOMO-1, HOMO-2, HOMO-3, and HOMO-4. The calculated VDEs for these transitions also show good agreement with the experimental data, confirming that the Fe-centered wheel structure is the global minimum of FeB_9^- [20,40].

The stability of FeB_9^- was previously attributed to its doubly aromatic character [40]. We present the canonical molecular orbitals of $Fe©B_9^-$ (Fig. 9-5b), which are also

reported in Ref. [40]. The MOs show that this species is indeed 1) π aromatic with six delocalized π electrons (HOMO-3, HOMO-3', and HOMO-4) satisfying the $4N + 2$ rule for π-aromaticity; 2) σ aromatic with six delocalized σ electrons (HOMO-1, HOMO-1', and HOMO-5) satisfying the $4N + 2$ rule for σ aromaticity. The HOMO is a completely non-bonding lone pair of $3d_z^2$-type centered on the Fe atom, whereas HOMO-2 and HOMO-2' can be viewed as mainly composed of Fe 3d-type lone pairs with some minor contributions to electron density from the peripheral boron atoms. The remaining nine valence canonical molecular orbitals (HOMO-6, HOMO-6', HOMO-7, HOMO-7', HOMO-8, HOMO-8', HOMO-9, HOMO-9', and HOMO-10) are responsible for the bonding of the peripheral boron atoms with each other. Therefore, the stability of the $Fe©B_9^-$ structure was thoroughly substantiated [20,40], in agreement with our design principle.

While a ten-membered boron ring with a deca-coordinated Fe atom may exist as FeB_{10}, we believe that a 3d transition metal is too small to stabilize B_{10} ring, as we demonstrated for VB_{10}^- [68].

9-6. Conclusions

Joint photoelectron spectroscopy and *ab initio* studies of two Fe-doped boron clusters, FeB_8^- and FeB_9^-, have established that both clusters are doubly aromatic possessing octa- and nona-coordinate iron atom, respectively, conforming with our design principle for transition-metal-centered $M©B_n$ type molecular wheels. These novel

planar metal-boron species constitute a new class of borometallic compounds and may be viable for condensed phase syntheses.

References

[1] T.P. Fehlner, J.-F. Halet, J.-Y. Saillard, Molecular Clusters: a Bridge to Solid-State Chemistry, Cambridge University Press, Cambridge, UK, 2007.

[2] F.A. Cotton, G. Wilkinson, C.A. Murillo, M. Bochmann, Advanced Inorg. Chem. sixth ed. Wiley-Interscience, New York, 1999.

[3] H.J. Zhai, L.S. Wang, A.N. Alexandrova, A.I. Boldyrev, J. Chem. Phys., 117 (2002), 7917.

[4] H.J. Zhai, A.N. Alexandrova, K.A. Birch, A.I. Boldyrev, L.S. Wang, Angew. Chem. Int. Ed., 42 (2003), 6004.

[5] H.J. Zhai, B. Kiran, J. Li, L.S. Wang, Nat. Mater., 2 (2003), 827.

[6] H.J. Zhai, L.S. Wang, A.N. Alexandrova, A.I. Boldyrev, V.G. Zakrzewski, J. Phys. Chem. A, 107 (2003), 9319.

[7] A.N. Alexandrova, A.I. Boldyrev, H.J. Zhai, L.S. Wang, E. Steiner, P.W. Fowler, J. Phys. Chem. A, 107 (2003), 1359.

[8] A.N. Alexandrova, A.I. Boldyrev, H.J. Zhai, L.S. Wang, J. Phys. Chem. A, 108 (2004), 3509.

[9] B. Kiran, S. Bulusu, H.J. Zhai, S. Yoo, X.C. Zeng, L.S. Wang, Proc. Natl. Acad. Sci. U. S. A., 102 (2005), 961.

[10] A.P. Sergeeva, D.Y. Zubarev, H.J. Zhai, A.I. Boldyrev, L.S. Wang, J. Am. Chem. Soc., 130 (2008), 7244.

[11] W. Huang, A.P. Sergeeva, H.J. Zhai, B.B. Averkiev, L.S. Wang, A.I. Boldyrev, Nat. Chem., 2 (2010), 202.

[12] A.P. Sergeeva, B.B. Averkiev, H.J. Zhai, A.I. Boldyrev, L.S. Wang, J. Chem. Phys., 134 (2011), 224304.

[13] Z.A. Piazza, W.L. Li, C. Romanescu, A.P. Sergeeva, L.S. Wang, A.I. Boldyrev, J. Chem. Phys., 136 (2012), 104310.

[14] T.B. Tai, N.M. Tam, M.T. Nguyen, Chem. Phys. Lett., 530 (2012), 71.

[15] F. Li, P. Jin, D.e. Jiang, L. Wang, S.B. Zhang, J. Zhao, Z. Chen, J. Chem. Phys., 136 (2012), 074302.

[16] E. Oger, N.R.M. Crawford, R. Kelting, P. Weis, M.M. Kappes, R. Ahlrichs, Angew. Chem. Int. Ed., 46 (2007), 8503.

[17] A.N. Alexandrova, H.J. Zhai, L.S. Wang, A.I. Boldyrev, Inorg. Chem., 43 (2004), 3552.

[18] P.W. Fowler, B.R. Gray, Inorg. Chem., 46 (2007), 2892.

[19] D.Y. Zubarev, A.I. Boldyrev, Phys. Chem. Chem. Phys., 10 (2008), 5207.

[20] B.B. Averkiev, L.M. Wang, W. Huang, L.S. Wang, A.I. Boldyrev, Phys. Chem. Chem. Phys., 11 (2009), 9840.

[21] A.N. Alexandrova, A.I. Boldyrev, H.J. Zhai, L.S. Wang, Coord. Chem. Rev., 250 (2006), 2811.

[22] B.P.T. Fokwa, M. Hermus, Angew. Chem. Int. Ed., 51 (2012), 1702.

[23] V.L. Deringer, C. Goerens, M. Esters, R. Dronskowski, B.P.T. Fokwa, Inorg. Chem., 51 (2012), 5677.

[24] S. Ghosh, A.M. Beatty, T.P. Fehlner, J. Am. Chem. Soc., 123 (2001), 9188.

[25] B. Le Guennic, H. Jiao, S. Kahlal, J.Y. Saillard, J.F. Halet, S. Ghosh, M. Shang, A.M. Beatty, A.L. Rheingold, T.P. Fehlner, J. Am. Chem. Soc., 126 (2004), 3203.

[26] K. Exner, P.v.R. Schleyer, Science, 290 (2000), 1937.

[27] Z.X. Wang, P.v.R. Schleyer, Science, 292 (2001), 2465.

[28] S. Erhardt, G. Frenking, Z.F. Chen, P.v.R. Schleyer, Angew. Chem. Int. Ed., 44 (2005), 1078.

[29] R. Islas, T. Heine, K. Ito, P.v.R. Schleyer, G. Merino, J. Am. Chem. Soc. 129 (2007) 14767.

[30] K. Ito, Z.F. Chen, C. Corminboeuf, C.S. Wannere, X.H. Zhang, Q.S. Li, P.v.R. Schleyer J. Am. Chem. Soc., 129 (2007), 1510.

[31] L.M. Wang, W. Huang, B.B. Averkiev, A.I. Boldyrev, L.S. Wang, Angew. Chem. Int. Ed., 46 (2007), 4550.

[32] B.B. Averkiev, D.Y. Zubarev, L.M. Wang, W. Huang, L.S. Wang, A.I. Boldyrev, J. Am. Chem. Soc., 130 (2008), 9248.

[33] T.R. Galeev, A.S. Ivanov, C. Romanescu, W.L. Li, K.V. Bozhenko, L.S. Wang, A.I. Boldyrev, Phys. Chem. Chem. Phys., 13 (2011), 8805.

[34] T.R. Galeev, C. Romanescu, W.L. Li, L.S. Wang, A.I. Boldyrev, J. Chem. Phys., 135 (2011), 104301.

[35] W.L. Li, C. Romanescu, T.R. Galeev, L.S. Wang, A.I. Boldyrev, J. Phys. Chem. A, 115 (2011), 10391.

[36] C. Romanescu, A.P. Sergeeva, W.L. Li, A.I. Boldyrev, L.S. Wang, J. Am. Chem. Soc., 133 (2011), 8646.

[37] C. Romanescu, T.R. Galeev, W.L. Li, A.I. Boldyrev, L.S. Wang, Angew. Chem. Int. Ed., 50 (2011), 9334.

[38] T.R. Galeev, C. Romanescu, W.L. Li, L.S. Wang, A.I. Boldyrev, Angew. Chem. Int. Ed., 51 (2012), 2101.

[39] W.L. Li, C. Romanescu, T.R. Galeev, Z.A. Piazza, A.I. Boldyrev, L.S. Wang, J. Am. Chem. Soc., 134 (2012), 165.

[40] K. Ito, Z. Pu, Q.S. Li, P.v.R. Schleyer, Inorg. Chem., 47 (2008), 10906.

[41] Z.F. Pu, K. Ito, P.v.R. Schleyer, Q.S. Li, Inorg. Chem., 48 (2009), 10679.

[42] Q.O. Luo, Sci. China Ser. B – Chem., 51 (2008), 607.

[43] Q.Y. Wu, Y.P. Tang, X.H. Zhang, Sci. China Ser. B – Chem., 52 (2009), 288.

[44] Z. Yang, S.J. Xiong, J. Chem. Phys., 128 (2008), 184310.

[45] L.S. Wang, H.S. Cheng, J.W. Fan, J. Chem. Phys., 102 (1995), 9480.

[46] L.S. Wang, H. Wu, in: M.A. Duncan (Ed.), Advances in Metal and Semiconductor Clusters, JAI Press, Greenwich, CT, 1998, pp. 299–343.

[47] J. Akola, M. Manninen, H. Hakkinen, U. Landman, X. Li, L.S. Wang, Phys. Rev. B, 60 (1999), 11297.

[48] L.S. Wang, X. Li, in: P. Jena, S.N. Khanna, B.K. Rao (Eds.), Proc. Int. Symp. on Clusters and Nanostructure Interfaces, World Scientific, River Edge, New Jersey, 2000, pp. 293–300.

[49] B.B. Averkiev, Ph.D. thesis, Utah State University, Logan, UT, USA, 2009.

[50] C. Adamo, V. Barone, J. Chem. Phys., 110 (1999), 6158.

[51] J.P. Perdew, K. Burke, M. Ernzerhof, Phys. Rev. Lett., 77 (1996), 3865.

[52] P.J. Hay, W.R. Wadt, J. Chem. Phys., 82 (1985), 299.

[53] T.H. Dunning, J. Chem. Phys., 90 (1989), 1007.

[54] R.A. Kendall, T.H. Dunning, R.J. Harrison, J. Chem. Phys., 96 (1992), 6796.

[55] N.B. Balabanov, K.A. Peterson, J. Chem. Phys., 123 (2005), 064107.

[56] A.D. Becke, Phys. Rev. A, 38 (1988), 3098.

[57] J.P. Perdew, Phys. Rev. B, 33 (1986), 8822.

[58] K.P. Jensen, B.O. Roos, U. Ryde, J. Chem. Phys., 126 (2007), 014103.

[59] J. Cizek, Adv. Chem. Phys., 14 (1969), 35.

[60] G.D. Purvis, R.J. Bartlett, J. Chem. Phys., 76 (1982), 1910.

[61] K. Raghavachari, G.W. Trucks, J.A. Pople, M. Head-Gordon, Chem. Phys. Lett., 157 (1989), 479.

[62] M.S. Gordon, J.S. Binkley, J.A. Pople, W.J. Pietro, W.J. Hehre, J. Am. Chem. Soc., 104 (1982), 2797.

[63] A.D. McLean, G.S. Chandler, J. Chem. Phys., 72 (1980), 5639.

[64] W.J. Pietro, M.M. Francl, W.J. Hehre, D.J. Defrees, J.A. Pople, J.S. Binkley, J. Am. Chem. Soc., 104 (1982), 5039.

[65] T. Clark, J. Chandrasekhar, G.W. Spitznagel, P.v.R. Schleyer, J. Comput. Chem., 4 (1983), 294.

[66] M.J. Frisch, G.W. Trucks, H.B. Schlegel, G.E. Scuseria, M.A. Robb, J.R. Cheeseman, G. Scalmani, V. Barone, B. Mennucci, G.A. Petersson, H. Nakatsuji,

M. Caricato, X. Li, H.P. Hratchian, A.F. Izmaylov, G.Z.J. Bloino, J.L. Sonnenberg, M. Hada, M. Ehara, K. Toyota, R. Fukuda, J. Hasegawa, M. Ishida, T. Nakajima, Y. Honda, O. Kitao, H. Nakai, T. Vreven, J.A. Montgomery, J.E. Peralta Jr., F. Ogliaro, M. Bearpark, J.J. Heyd, E. Brothers, K.N. Kudin, V.N. Staroverov, R. Kobayashi, J. Normand, K. Raghavachari, A. Rendell, J.C. Burant, S.S. Iyengar, M.C.J. Tomasi, N. Rega, J.M. Millam, M. Klene, J.E. Knox, J.B. Cross, V. Bakken, C. Adamo, J. Jaramillo, R. Gomperts, R.E. Stratmann, O. Yazyev, A.J. Austin, R. Cammi, C. Pomelli, J.W. Ochterski, R.L. Martin, K. Morokuma, V.G. Zakrzewski, G.A. Voth, P. Salvador, J.J. Dannenberg, S. Dapprich, A.D. Daniels, Ö Farkas, J.B. Foresman, J.V. Ortiz, J. Cioslowski, D.J. Fox, GAUSSIAN 09, Rev. C.02, Gaussian Inc., Wallingford, CT, 2009.

[67] U. Varetto, Molekel 5.4.0.8, Swiss National Supercomputing Centre, Manno (Switzerland), 2009.

[68] W.L. Li, C. Romanescu, Z.A. Piazza, L.S. Wang, Phys. Chem. Chem. Phys., 14, 13663-13669.

Table 9-1. Theoretically calculated VDEs for the $FeCB_8^-$ (C_{8v}, $^2A_1$) and $FeCB_9^-$ (D_{9h}, $^1A_1$') clusters. All energies are in eV.

Feature	VDE (exp)[a]	Final State and Electronic Configuration	VDE (theoretical)		
			UBP86[b]	ROPBE0[c]	ROCCSD(T)[d]
FeB_8^- (C_{8v}, $^2A_1$)					
X	3.75(3)	$^3E_1$ … $2e_1^4\,2a_1^2\,3a_1^2\,2e_2^4\,3e_1^3\,4a_1^1$	3.62 (0.80)	3.71	3.84 (1.41)
A	4.15(4)	$^3E_2$ … $2e_1^4\,2a_1^2\,3a_1^2\,2e_2^3\,3e_1^4\,4a_1^1$	4.17 (2.04)	3.81	4.06 (1.34)
B	4.60(5)	$^1A_1$ … $2e_1^4\,2a_1^2\,3a_1^2\,2e_2^4\,3e_1^4\,4a_1^0$	4.58 (0.00)	4.79	5.06 (1.68)[f]
C	5.21(5)	$^3A_1$ … $2e_1^4\,2a_1^2\,3a_1^1\,2e_2^4\,3e_1^4\,4a_1^1$	5.17 (2.03)	5.16	5.30 (1.33)
		$^3E_1$ … $2e_1^3\,2a_1^2\,3a_1^2\,2e_2^4\,3e_1^4\,4a_1^1$	5.35 (2.07)	[e]	5.24 (1.36)
D	5.6(1)	$^3A_1$ … $2e_1^4\,2a_1^1\,3a_1^2\,2e_2^4\,3e_1^4\,4a_1^1$	5.60 (2.08)	5.78	5.66 (1.37)
$FeCB_9^-$ (D_{9h}, $^1A_1$')					
X	3.42(3)	$^2A_1$' … $1a_2$"$^2\,1e_1$'$^4\,2e_2$'$^4\,2e_1$'$^4\,3a_1$'^{1}	3.58[g]	3.40	[h]
A	4.22(3)	$^2E_1$' … $1a_2$"$^2\,1e_1$'$^4\,2e_2$'$^4\,2e_1$'$^3\,3a_1$'^{2}	4.05 (0.77)	4.19	[h]
		$^2E_2$' … $1a_2$"$^2\,1e_1$'$^4\,2e_2$'$^3\,2e_1$'$^4\,3a_1$'^{2}	4.42[g]	4.10	[h]
B	5.03(4)	$^2E_1$" … $1a_2$"$^2\,1e_1$'$^3\,2e_2$'$^4\,2e_1$'$^4\,3a_1$'^{2}	5.08 (0.80)	4.69	[h]
C	5.23(4)	$^2A_2$" … $1a_2$"$^1\,1e_1$'$^4\,2e_2$'$^4\,2e_1$'$^4\,3a_1$'^{2}	5.26[g]	5.26	[h]

[a] Numbers in parentheses represent the uncertainty in the last digit.
[b] VDEs were calculated at UBP86/aug-cc-pVTZ. The values of $<S^2>$ are given in parentheses following the computed VDE values.
[c] VDEs were calculated at ROPBE0/aug-cc-pVTZ//UBP86/aug-cc-pVTZ.
[d] VDEs were calculated at ROCCSD(T)/6-311+G(2df)//UBP86/aug-cc-pVTZ. The NORM values are given in parentheses following the computed VDE values.
[e] We couldn't achieve convergence for this particular state.
[f] The validity of this VDE value is questionable due to the high NORM value.
[g] In these cases high spin contamination of the final neutral states was encountered (with $<S^2>$ higher than 0.8). Therefore the VDEs were calculated at ROBP86/aug-cc-pVTZ.
[h] The calculations of the neutral states of FeB_9 resulted in very high NORM values ranging from 1.54 to 2.67. Due to inaccuracy of the computed values, we are not presenting those in the table.

Table 9-2. Theoretically calculated VDEs for the second lowest isomer of FeB_8^- (C_{2v}, $^4A_1$), whose first VDE is believed to be responsible for feature X' in the experimental PES. All energies are in eV.

Feature	VDE (exp)[a]	Final State and Electronic Configuration	VDE (theoretical)
			UBP86[b]
X'	~2.7	$^3B_1$ … $4a_1^2\,3b_1^2\,3a_2^2\,5a_1^2\,4b_2^2\,6a_1^1 4b_1^1\,5b_1^0$	2.59 (2.04)
		$^5B_2$ … $4a_1^2\,3b_1^2\,3a_2^2\,5a_1^2\,4b_2^1\,6a_1^1 4b_1^1\,5b_1^1$	3.55 (6.04)
		$^5A_1$ … $4a_1^2\,3b_1^2\,3a_2^2\,5a_1^1\,4b_2^2\,6a_1^1 4b_1^1\,5b_1^1$	3.95 (6.08)
		$^3A_1$ … $4a_1^2\,3b_1^2\,3a_2^2\,5a_1^2\,4b_2^2\,6a_1^0 4b_1^1\,5b_1^1$	4.36 (2.76)
		$^3B_1$ … $4a_1^2\,3b_1^2\,3a_2^2\,5a_1^2\,4b_2^2\,6a_1^1 4b_1^0\,5b_1^1$	4.38 (2.07)
		$^5B_1$ … $4a_1^2\,3b_1^1\,3a_2^2\,5a_1^2\,4b_2^2\,6a_1^1 4b_1^1\,5b_1^1$	4.89 (6.08)
		$^5A_1$ … $4a_1^1\,3b_1^2\,3a_2^2\,5a_1^2\,4b_2^2\,6a_1^1 4b_1^1\,5b_1^1$	5.04 (6.03)

[a] Numbers in parentheses represent the uncertainty in the last digit.
[b] VDEs were calculated at UBP86/aug-cc-pVTZ. The values of $<S^2>$ are given in parentheses following the computed VDE values.

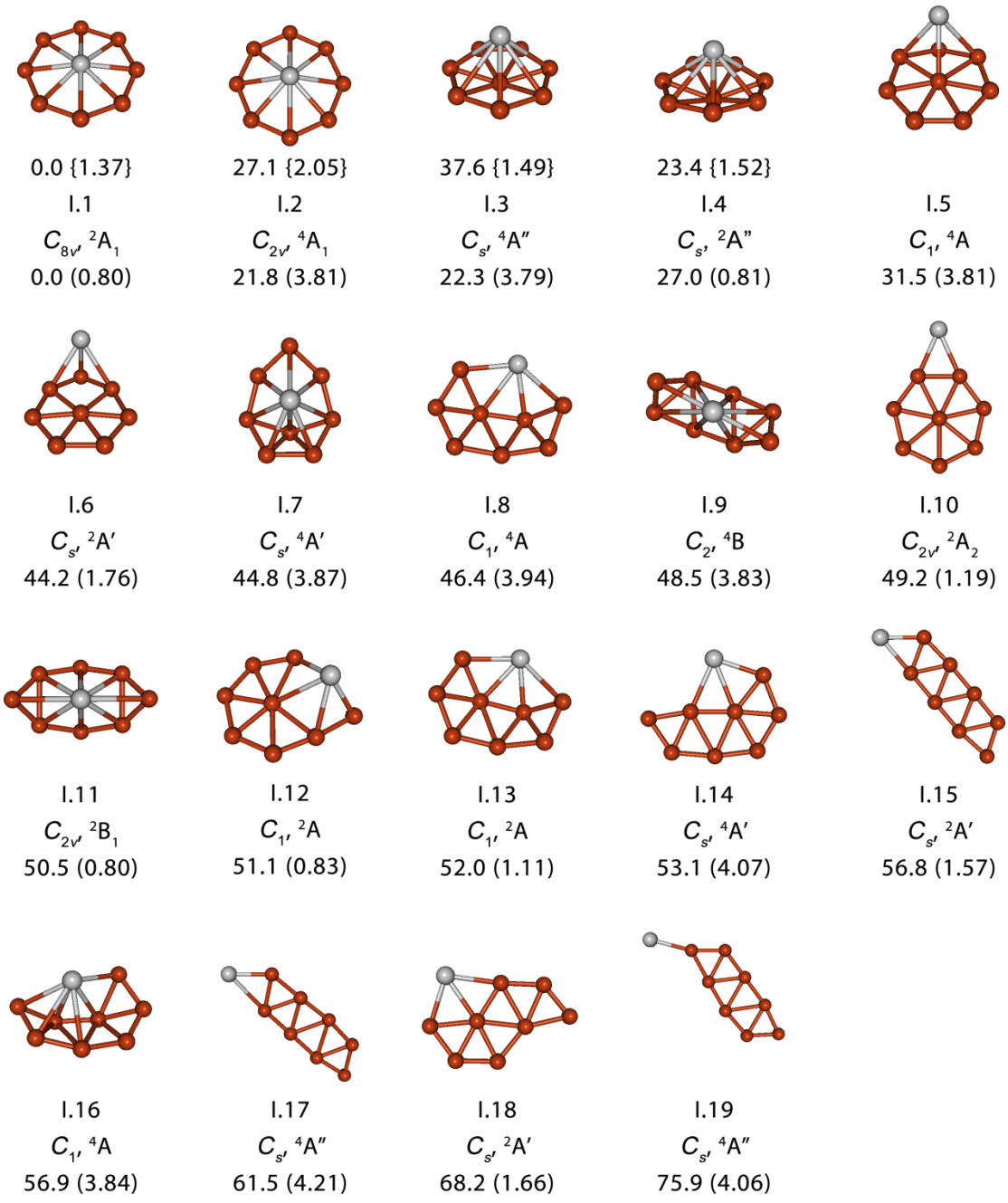

Fig. 9-1. Isomers of FeB_8^-, their point group symmetries and spectroscopic states. Relative energies are given in kcal/mol at UBP86/aug-cc-pVTZ followed by the $<S^2>$ value given in parentheses. The lowest isomers (within 30 kcal/mol at the uBP86 level) were recalculated at ROCCSD(T)/6-311+G(2df)//UBP86/aug-cc-pVTZ. The relative energies at ROCCSD(T)/6-311+G(2df)//UBP86/aug-cc-pVTZ are also given in kcal/mol followed by the NORM value in curly brackets (the relative energy of Isomer I.2 is highly questionable).

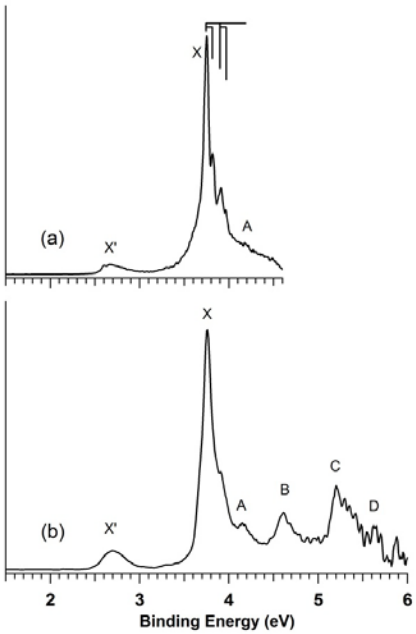

Fig.9-2. Photoelectron spectra of FeB_8^- at (a) 266 nm and (b) 193 nm photodetachment wavelengths. The vertical lines indicate resolved vibrational structures.

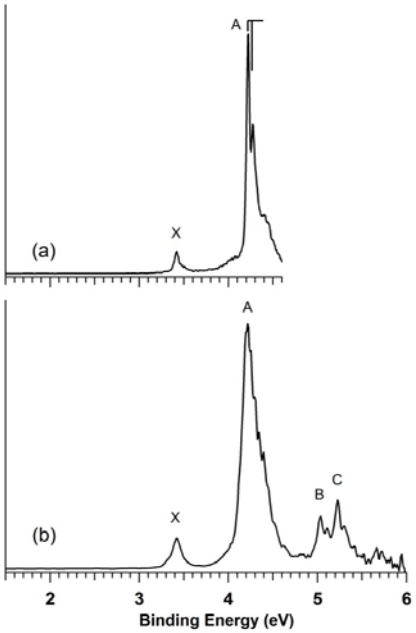

Fig.9-3. Photoelectron spectra of $Fe©B_9^-$ at (a) 266 nm and (b) 193 nm photodetachment wavelengths. The vertical lines represent resolved vibrational structures.

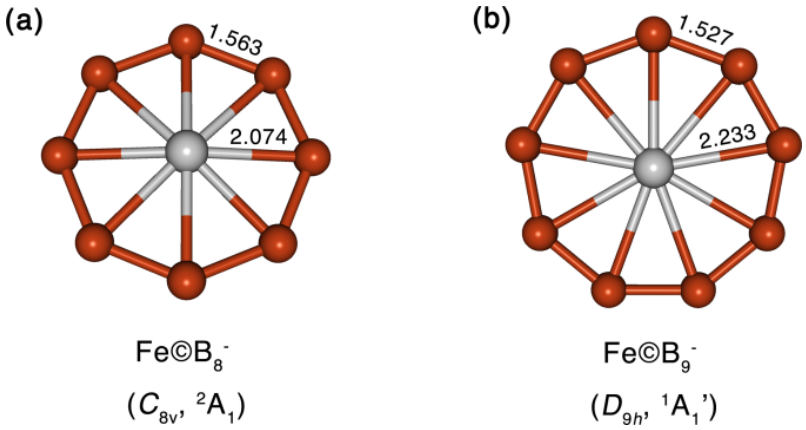

Fig. 9-4. Global minima of (a) $Fe©B_8^-$ and (b) $Fe©B_9^-$. Geometries are optimized at the BP86/aug-cc-pVTZ level. Bond lengths are given in Å.

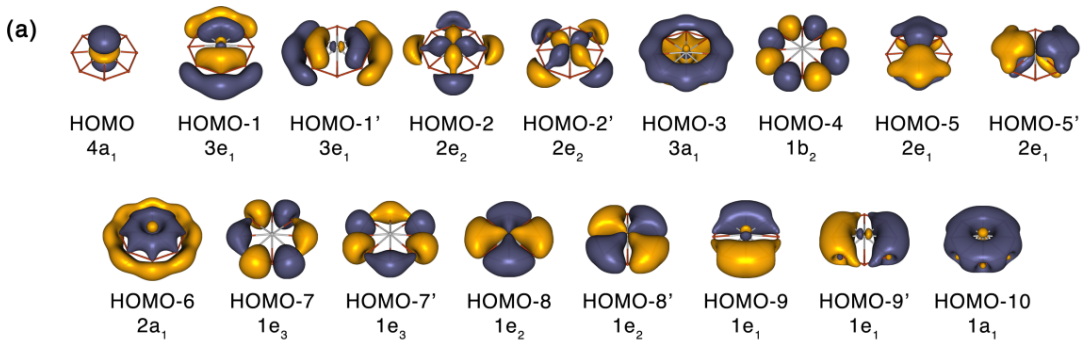

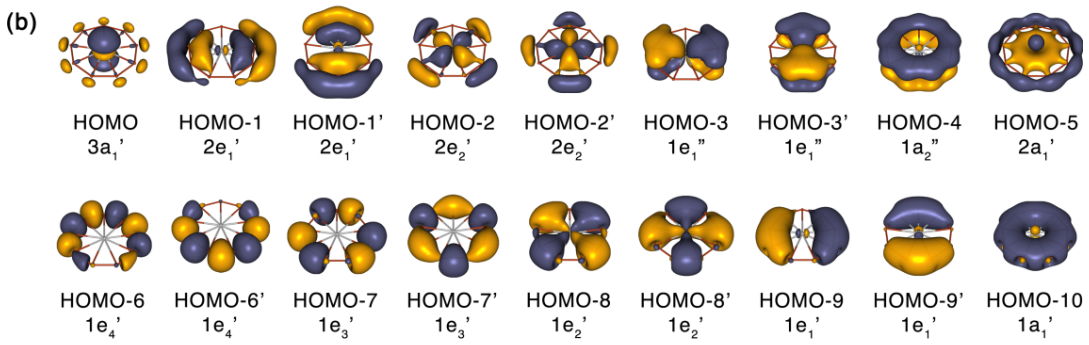

(c)

E, a.u.	FeB_8^- (C_{8v}, $^2A_1$)	E, a.u.	FeB_9^- (D_{9h}, $^1A_1'$)
+0.054640	LUMO+1, $2e_2$	+0.023860	LUMO+1, $1e_2"$
-0.002060	LUMO, $4e_1$	-0.015975	LUMO, $2e_1"$
-0.041620	HOMO, $4a_1$	-0.051670	HOMO, $3a_1'$
-0.051440	HOMO-1, $3e_1$	-0.070460	HOMO-1, $2e_1'$
-0.075700	HOMO-2, $2e_2$	-0.082400	HOMO-2, $2e_2'$
-0.108120	HOMO-3, $3a_1$	-0.107185	HOMO-3, $1e_1"$
-0.155600	HOMO-4, $1b_2$	-0.112510	HOMO-4, $1a_2"$
-0.119160	HOMO-5, $2e_1$	-0.128810	HOMO-5, $2a_1'$
-0.126120	HOMO-6, $2a_1$	-0.136670	HOMO-6, $1e_4'$
-0.161260	HOMO-7, $1e_3$	-0.197020	HOMO-7, $1e_3'$
-0.273000	HOMO-8, $1e_2$	-0.290210	HOMO-8, $1e_2'$
-0.340200	HOMO-9, $1e_1$	-0.352050	HOMO-9, $1e_1'$
-0.404140	HOMO-10, $1a_1$	-0.401560	HOMO-10, $1a_1'$

Fig. 9-5. The valence canonical molecular orbitals of $Fe©B_8^-$ (a) and $Fe©B_9^-$ (b) and their orbital energies (c) at the ROBP86/aug-cc-pVTZ level.

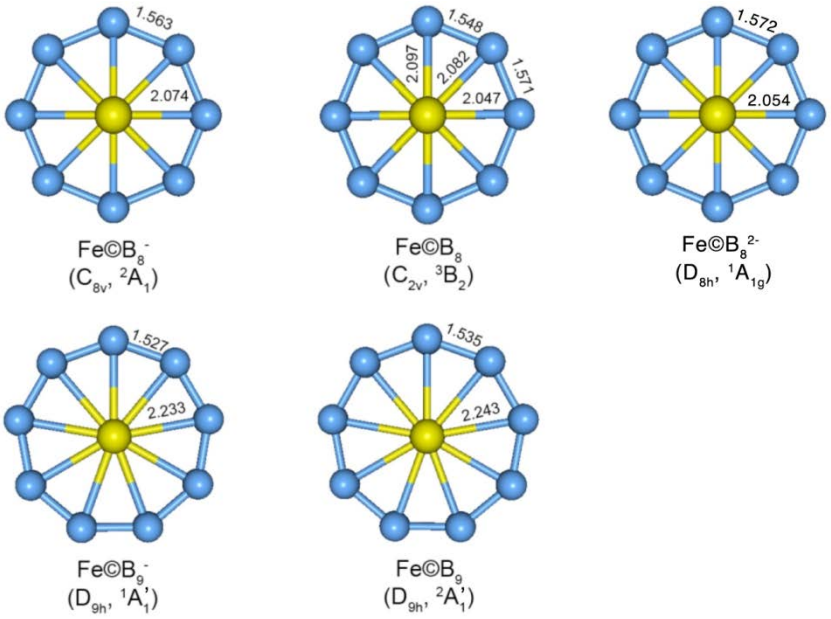

Fig. 9-6. Optimized geometries of the global minima of $Fe©B_8^-$ and $Fe©B_9^-$ and the corresponding neutral species produced upon detachment of an electron: $Fe©B_8$ and $Fe©B_9$ at the BP86/aug-cc-pVTZ level, as well as the optimized geometry of the $Fe©B_8^{2-}$ species for comparison. Bond lengths are given in Å.

CHAPTER 10

GEOMETRIC AND ELECTRONIC FACTORS IN THE RATIONAL DESIGN OF TRANSITION-METAL-CENTERED BORON MOLECULAR WHEELS [*]

Abstract

The effects of the electronic and geometric factors on the global minimum structures of MB_9^- (M = V, Nb, Ta) are investigated using photoelectron spectroscopy and *ab initio* calculations. Photoelectron spectra are obtained for MB_9^- at two photon energies, and similar spectral features are observed for all three species. The structures for all clusters are established by global minima searches and confirmed by comparison of calculated and experimental vertical electron detachment energies. The VB_9^- cluster is shown to have a planar C_{2v} $V©B_9^-$ structure, whereas both NbB_9^- and TaB_9^- are shown to have C_s $M©B_9^-$ type structures with the central metal atom slightly out of plane. Theoretical calculations suggest that the V atom fits perfectly inside the B_9 ring forming a planar D_{9h} $V©B_9^{2-}$ structure, while the lower symmetry of $V©B_9^-$ is due to the Jahn-Teller effect. The Nb and Ta atoms are too large to fit in the B_9 ring, and they are squeezed out of the plane slightly even in the $M©B_9^{2-}$ dianions. Thus, even though all three $M©B_9^{2-}$ dianions fulfill the electronic design principle for the doubly aromatic molecular wheels, the geometric effect lowers the symmetry of the Nb and Ta clusters.

[*] Coauthored by Constantin Romanescu, Timur R. Galeev, Wei-Li Li, Alexander I. Boldyrev, and Lai-Sheng Wang. Reprinted with permission from *J. Chem. Phys*. **2013**, *138*, 134315. Copyright 2013, AIP Publishing LLC

10-1. Introduction

Atomic clusters not only exhibit size and shape dependent properties, but also provide a rich source to discover novel structures and chemical bonding, which allow rational design of molecules and nanostructures with tailored physical and chemical properties. A major goal of our research in the past decade has been the elucidation of the structure and chemical bonding of negatively charged boron clusters, B_n^-, using photoelectron spectroscopy (PES) and *ab initio* studies.[1–10] The prevalence of planar or quasi-planar (2D) structures for an extended range of cluster sizes ($n \leq 23$ for anions,[10] $n < 20$ for neutrals,[4] and $n < 16$ for cations[11]) can be traced to the electron deficient character of the boron atom and its propensity for delocalized multi-center chemical bonds.[12] As a result, all planar boron clusters consist of a peripheral ring formed of 2c-2e (two-center two-electron) σ bonds and one or more inner atoms bonded to the outer ring by delocalized σ and π bonds, giving rise to aromatic or antiaromatic boron clusters and all-boron hydrocarbon analogues.[2,6,7] More recent computational studies reaffirmed the planarity and the aromaticity of the small boron clusters.[13–17] More interestingly, planar B_6 rings have been observed to be major structural features in recently synthesized transition metal boride compounds,[18,19] suggesting that planar boron clusters can indeed become potential ligands or material building blocks, as proposed previously.[5]

Two of the boron cluster anions, B_9^- and B_8^{2-}, have highly symmetric (D_{nh}) wheel-type structures.[1,3] Chemical bonding analyses using the Adaptive Natural Density Partitioning (AdNDP) algorithm[20] revealed that both clusters are doubly aromatic with 6 π and 6 σ electrons, thus, fulfilling the Hückel rule for σ and π aromaticity ($4N_\pi + 2$ and

$4N_\sigma + 2$ electrons, $N_\pi, N_\sigma \geq 0$). Based on the bonding model developed for B_8^{2-} (or $B©B_7^{2-}$) and B_9^- (or $B©B_8^-$),[21] we advanced an electronic design principle for transition metal centered monocyclic boron clusters.[22,23] In essence, the design principle can be reduced to a simple electron counting rule, where the total number of valence electrons in $M©B_n^{q-}$ needs to satisfy the relationship

$$3n + q + x = 2n + 12 \quad \text{or} \qquad n + q + x = 12, \tag{1}$$

where x is the formal valence of the transition metal, q is the charge, and n is the size of the boron ring. The sum on the right-hand side of the first form of Eq. (1) represents the number of electrons required for n peripheral B–B bonds ($2n$ electrons) and two (σ and π) aromatic systems (2×6 electrons). The design principle was successfully applied to two boron ring sizes, n = 8, 9: $Co©B_8^-$ (x = 3) and $Ru©B_9^-$ (x = 2),[22] $Rh©B_9$ (x = 3) and $Ir©B_9$ (x = 3),[24] and $Fe©B_9^-$ (x = 2).[25] Two of these clusters, $Co©B_8^-$ and $Fe©B_9^-$, were previously calculated as the global minima on their potential energy surfaces.[26,27] Several other main-group element and transition-metal-centered boron rings were investigated theoretically before, but none was shown to be the global minimum.[28–35]

According to the design principle, a valence-I transition metal (x = 1) is required to stabilize a 10-membered boron ring. However, previous studies showed that the valence-I Au atom binds covalently to the periphery of a planar B_{10} motif in AuB_{10}^- and that $Au©B_{10}^-$ is only a high energy isomer.[36] The existence of $M©B_{10}^-$ wheel-type clusters was discovered in $Ta©B_{10}^-$ and $Nb©B_{10}^-$.[37] The bonding situation for these doubly (σ and π) aromatic clusters is slightly different from that encountered previously, as they both have 10 σ-delocalized electrons (N_σ = 2 in the $4N_\sigma + 2$ Hückel rule), even

though they have the same six π delocalized electrons. Hence, all valence electrons of the metals participate in delocalized bonding, with no lone pairs.[37] A modified electronic requirement for this type of molecular wheels is

$$3n + q + x = 2n + 16 \quad \text{or} \qquad n + q + x = 16 \qquad (2).$$

However, we have found that the fulfillment of the electronic requirement is not sufficient for achieving a perfectly planar molecular wheel: the geometric or steric constraints need also to be considered. In our previous work with 8- and 9-membered boron rings, we found that valence isoelectronic substitution of the central atom by larger atoms leads to clusters where the metal atoms lie above the ring (C_{nv} symmetry).[22,24] More significant structural changes were observed upon valence isoelectronic substitution by smaller atoms in the B_{10} ring systems $M©B_{10}^-$. Two isomers were found to compete for the global minimum of the MB_{10}^- (M = V, Nb, Ta) series: the $M©B_{10}^-$ and a "boat"-like isomer.[37,38] The energy difference between the isomers decreased with the decrease of atomic size and, as a consequence, $V©B_{10}^-$ became an extremely high energy isomer relative to the "boat"-like global minimum isomer, even though it fulfills the modified electronic design principle given by Eq. (2).[23,38]

In order to better understand the relationship between the electronic and the geometric constraints on the stability of metal-centered wheel-type boron clusters, here we investigate a new group of clusters, MB_9^-, MB_9, and MB_9^{2-} (M = V, Nb, Ta). Photoelectron spectra of the MB_9^- species are obtained and theoretical calculations are carried out for species of all three charge states. Global minimum searches were performed for the MB_9^- species. The structures of the neutral and doubly charged clusters

were obtained by following imaginary mode(s) revealed in the respective D_{9h} geometry optimizations and frequency calculations. We find that the MB_9^{2-} species are all closed shell and fulfill the electronic design principle, but only $V©B_9^{2-}$ possesses the perfect D_{9h} molecular wheel structure, whereas $Nb©B_9^{2-}$ and $Ta©B_9^{2-}$ both have C_{9v} structures because of the slightly larger atomic sizes of Nb and Ta. All the neutral $M©B_9$ clusters are found to be in a triplet state with C_{9v} symmetry, whereas all the $M©B_9^-$species have lower symmetries due to the Jahn-Teller effect. These clusters provide the opportunity for understanding the electronic and geometric requirements for designing metal-centered aromatic boron wheel clusters and the relationship between spectroscopy, bonding, and structures of the new class of borometallic complexes.

10-2. Experimental and Computational Methods

10-2.1. Photoelectron Spectroscopy

The experiment was performed using a magnetic-bottle PES apparatus equipped with a laser vaporization cluster source, as described in detail previously.[39,40] Briefly, the metal-doped boron clusters were produced by laser vaporization of a disk target made of isotopically enriched ^{11}B and V or Nb or Ta. The clusters were entrained by a He carrier gas seeded with 5% Ar and underwent a supersonic expansion to form a collimated molecular beam. The composition and cooling of the clusters were controlled by the time delay between the carrier gas pulse and the ablation laser pulse.[41,42] Negatively charged clusters were extracted and analyzed with a time-of-flight mass spectrometer. The species of interest were mass-selected and decelerated before being photodetached by a pulsed laser beam at 193 nm (6.424 eV) from an ArF excimer laser or 266 nm (4.661 eV) from a

Nd:YAG laser. Photoelectrons were collected at nearly 100% efficiency by a magnetic bottle and analyzed in a 3.5 m long electron flight tube. The spectra were calibrated with the known spectra of Bi^-. The kinetic energy resolution of the apparatus, ΔEk/Ek, was better than 2.5%, i.e., ~25 meV for 1 eV electrons.

10-2.2. Computational Methods

The search for the global minimum structures of VB_9^-, NbB_9^-, and TaB_9^- was performed using the Coalescence Kick (CK) method.[8] The initial CK search was performed using the PBE0 hybrid density functional[43–45] and the LANL2DZ basis set.[46] Low energy isomers ($\Delta E < 50$ kcal mol^{-1}) found at the PBE0/LANL2DZ level were reoptimized with subsequent frequency calculations at the PBE0/M/Stuttgart[47]/B/aug-cc-pVTZ[48,49] level for NbB_9^- and TaB_9^- and the ROPBE0/V/Stuttgart/B/aug-cc-pVTZ level for VB_9^-. Figures 10-1 – 10-3[50] display all the optimized structures. Single-point energy calculations for all the MB_9^- species were performed using the restricted open-shell coupled cluster method ROCCSD(T),[51–54] at the ROCCSD(T)/M/Stuttgart/B/aug-cc-pVTZ level. Vertical detachment energies (VDEs) were calculated for the global minimum structures at ROPBE0/M/Stuttgart/B/aug-cc-pVTZ, ROCCSD(T)/M/Stuttgart/B/aug-cc-pVTZ, and EOM-CCSD[55–58]/M/Stuttgart/B/6-311+G(*d*) levels for comparison with the experimental data. The calculations were performed using GAUSSIAN 09.[59] Molekel 5.4.0.8 was used for visualization.[60]

10-3. Experimental Results

The photoelectron spectra of VB_9^-, NbB_9^-, and TaB_9^- are presented in Figs. 10-4 – 10-6, respectively, at two photodetachment energies. The 266 nm spectra give better

spectral resolutions for the low binding energy features. All observed PES features are labeled with letters and the measured VDEs are given in Tables 10-1 – 10-3, where they are compared with theoretical calculations at various levels of theory. The peak labeled as X represents the transition between the ground electronic state of the anion and the neutral species, while the higher binding energy features (A, B…) denote transitions to excited electronic states of the neutral species.

10-3.1. VB_9^-

The 266 nm photoelectron spectrum of VB_9^- (Fig. 10-4a) displays intense and congested features around 4 eV and a weak feature at lower binding energies (labeled as X′). The congested main spectral region consists of at least five relatively sharp bands, labeled as X, A, B, C, and D. The C and D bands are very closely spaced. The adiabatic detachment energy (ADE) of the ground state detachment transition is 3.64 eV, obtained by drawing a straight line along the leading edge of band X and taking the intersection with the binding energy axis plus the spectral resolution. The ADE also represents the electron affinity of neutral VB_9. The vertical detachment energy of band X measured from the peak maximum is 3.70 eV.

The 193 nm spectrum (Fig. 10-4b) seems to exhibit continuous and relatively weak signals throughout the higher binding energy region. Only one prominent band F with a VDE of 5.03 eV can be identified in this range, whereas congested features appear to be present around 4.5 eV (E). The signal-to-noise ratios are too poor beyond the F band to allow identifications of definitive spectral bands. The X′ feature at the low binding energy range is probably due to a low-lying isomer. The weak signals throughout

the low binding energy range (<3.5 eV) are probably all due to the same weakly populated low-lying isomer.

10-3.2. NbB_9^-

The photoelectron spectra of NbB_9^- (Fig. 10-5) are somewhat similar to those of VB_9^-. In the 266 nm spectrum, a weak feature (X′) at the low binding energy side, probably due to a low-lying isomer, is followed by a series of intense and congested features at higher binding energies around 4 eV. An intense and relatively sharp band X defines the transition from the ground state of NbB_9^- to that of neutral NbB_9. The ADE of band X, measured from its leading edge, is 3.58 eV, which represents the electron affinity of NbB_9. The VDE of band X is measured to be 3.64 eV. Beyond band X, the spectral features become more congested and slightly weaker in intensity. Four bands (A, B, C, and D) are assigned. In the 193 nm spectrum (Fig. 10-5b), only one additional broad band is observed at 4.88 eV (E), which is somewhat similar to band F of VB_9^-.

10-3.3. TaB_9^-

The spectra of TaB_9^- (Fig. 10-6) are almost identical to those of NbB_9^-, except the spectral features are slightly better separated and resolved. In addition, the weak low binding energies features, attributed to a low-lying isomer, are almost negligible in the spectra of TaB_9^-. The 266 nm spectrum of TaB_9^- displays three intense bands (X, A, and B) and a weaker, broader band C. The ADE of band X, measured to be 3.57 eV, defines the electron affinity of neutral TaB_9, which is identical to that of NbB_9 within our uncertainty. The 193 nm spectrum (Fig. 10-6b) reveals two more bands, a relatively weak

band D, and a broad band E, both of which are similar to those observed in the 193 nm spectrum of NbB_9^-.

10-4. Theoretical Results

Our global minimum search and geometry optimization show that the wheel-like structures are the global minima for all the MB_9^-clusters considered here, as presented in Fig. 10-7. The boron rings in all clusters are slightly distorted from a perfect circle, because of the Jahn-Teller effect. VB_9^- has a planar C_{2v} structure, while NbB_9^- and TaB_9^- both have non-planar C_s structures with the Nb and Ta atoms located approximately 0.7 Å out of the averaged boron plane. Extensive sets of alternative low-lying isomers are shown in Figs. 10-1 – 10-3 for MB_9^- (M = V, Nb, and Ta), respectively, at the PBE0 level. Energies from single-point CCSD(T) calculations are given for selected low-lying isomers, assuring that the $M©B_9^-$ molecular wheel structures are the global minimum in each case.

Geometry optimization of the neutral $M©B_9$ (M = V, Nb, Ta) clusters in the D_{9h} symmetry leads to an imaginary frequency corresponding to out-of-plane distortions of the central metal atom in each case. Following the imaginary mode, C_{9v} structures were obtained (Fig. 10-8, upper row) for all three clusters with an open-shell triplet ground electronic state. Consequently, we considered the closed-shell doubly charged $M©B_9^{2-}$ clusters (Fig. 10-8, lower row). The $V©B_9^{2-}$ cluster was found to be a perfect D_{9h} planar cluster, whereas NbB_9^{2-} and TaB_9^{2-} were found to have C_{9v} symmetry with the central metal atom slightly out-of-plane.

Because of the open-shell nature of the anion and neutral ground states, both singlet and triplet final states can be accessed during photodetachment, consistent with the complicated photoelectron spectra observed experimentally. In particular, the open-shell anions and neutrals make it challenging to compute the detachment channels. Thus, we calculated the VDEs for the global minimum structures of $M©B_9^-$ using three different methods: PBE0, CCSD(T), and EOM-CCSD. The theoretical results are compared with the experimental data in Tables 10-1 – 10-3. We found that the three methods give consistent results and together they allow almost quantitative interpretation of the experimental data.

10-5. Discussion and Interpretation of the Photoelectron Spectra

10-5.1. The X' feature and possible presence of low-lying isomers

According to the relative energies calculated at the CCSD(T) level of theory, the global minima of these clusters are significantly more stable compared to the nearest low-lying isomers (see Figs. 10-1 – 10-3). Despite the relatively high energies of the "boat"-like isomers found at the CCSD(T) level, we find that their calculated VDEs are in agreement with the experimental values for the peaks labeled as X′ in the spectra of VB_9^- and NbB_9^-, suggesting that the boat-like isomers were weakly populated in the cluster beams. These observations are similar to the case of NbB_{10}^-, which has a perfect D_{10h} global minimum with a boat-like low-lying isomer being 5.4 kcal/mol higher in energy. Despite the relatively high energy of the boat-like isomer, it was substantially populated in the cluster beam, giving rise to low binding energy features in the photoelectron spectra of NbB_{10}^-.[37] The fact that the boat-like isomers were present in all

of the current cases suggests that the stability of the boat-like isomers relative to the global minima was probably underestimated. Nevertheless, the trend is consistent with the experimental observation: the energy of the boat-like isomer relative to the molecular wheel global minimum increases from VB_9^- to TaB_9^-, and experimentally, the relative intensities of the weak low binding energy features due to the boat-like isomer decrease in the same direction (Figs. 10-4 – 10-7).

We focus our discussion on the global minimum molecular-wheel structures (Fig. 10-7), which are responsible for the main spectral features observed experimentally. The photoelectron spectral data are compared with the calculated VDEs in Tables 10-1 – 10-3, where the final states and MO configurations for the final states are also given.

10-5.2. The MOs and bonding in the closed-shell M©B_9^{2-} (M = V, Nb, Ta) dianions

Given the similarity of the electronic and the geometrical structures of these clusters, we will discuss in more detail the assignments of the photoelectron spectra of VB_9^-. The geometry of VB_9^- can be best understood by considering one electron removal from the closed-shell V©B_9^{2-} cluster. The valence MOs of the D_{9h} V©B_9^{2-} cluster are plotted in Fig. 10-9 and they can be understood as follows: the degenerate HOMO ($2e_2'$) and HOMO-1 ($2e_1'$), plus HOMO-4 ($2a_1'$), are delocalized σ bonding orbitals between the central V atom and the B_9 ring; the degenerate HOMO-2 ($1e_1''$) and HOMO-3 ($1a_2''$) are delocalized π bonding orbitals between the V atom and the B_9 ring; and remaining nine valence orbitals are responsible for the nine 2c-2e peripheral B–B bonds. Thus, V©B_9^{2-} is doubly aromatic, with 10 σ ($N_\sigma = 2$) and 6 π ($N_\pi = 1$) electrons and the formal valence

of V in $V©B_9^{2-}$ is 5. Thus, $V©B_9^{2-}$ obeys the modified electronic design principle devised for $Nb©B_{10}^-$ and $Ta©B_{10}^-$, Eq. (2), where $x = 5$, $n = 9$, and $q = 2$.

For the closed-shell $Nb©B_9^{2-}$ and $Ta©B_9^{2-}$ clusters, we found that the size of the central metal atom is too big to fit inside a B_9 ring and these clusters have quasi-planar structures and a C_{9v} symmetry (Fig. 10-8, bottom), even though they obey the modified electronic design principle [Eq. (2)] and display bonding features almost identical to the non-distorted D_{9h} structure. The MOs of $Nb©B_9^{2-}$ and $Ta©B_9^{2-}$ (not shown) are similar to those of $V©B_9^{2-}$.

10-5.3. Interpretation of the photoelectron spectra of $M©B_9^-$ (M = V, Nb, Ta)

Removal of one electron from the degenerate $2e_2'$ HOMO of the D_{9h} $V©B_9^{2-}$ results in the low symmetry C_{2v} $V©B_9^-$, owing to the Jahn-Teller effect. The MOs of the C_{2v} $V©B_9^-$ are shown in Fig. 10-10 and they bear close resemblance to those of $V©B_9^{2-}$, except that its $6b_2$ HOMO is now singly occupied to give the $^2B_2$ ground electronic state (Fig.10-7). The other component of the degenerate $2e_2'$ orbital becomes the $7a_1$ (HOMO-3) orbital in $V©B_9^-$ (Fig. 10-10). Similarly, removal of an electron from the doubly degenerate HOMO orbitals of $Nb©B_9^{2-}$ and $Ta©B_9^{2-}$ results in slightly distorted pyramidal structures with C_s symmetry for $Nb©B_9^-$ and $Ta©B_9^-$ (Fig. 10-7), due to the Jahn-Teller effect. The MOs of $Nb©B_9^-$ and $Ta©B_9^-$ are given in Figs.10-11 and 10-12, respectively, and their similarities to those of $V©B_9^-$ (Fig. 10-7) are evident. In the case of $Nb©B_9^-$, the degenerate HOMOs in the closed-shell dianion transform into $10a'$ (HOMO) and $6a''$ (HOMO-3) (Fig. 10-11), whereas in $Ta©B_9^-$ they transform into

$10a'$ (HOMO) and $7a''$ (HOMO-1) (Fig.10-12). These MOs together with the calculated VDEs in Tables 10-1 – 10-3 are used to interpret the photoelectron spectra.

The calculated neutral states all have C_{9v} symmetry and triplet spin state ($^3A_2$, Fig. 10-8), with their doubly degenerate σ HOMOs half-occupied. The lack of a HOMO-LUMO gap in the photoelectron spectra (Figs. 10-4 – 10-6) is consistent with the triplet configuration of the neutral clusters for all three cases. Therefore, the first detachment channel from $M©B_9^-$ should be from electron removal from the fully occupied σ delocalized orbital that corresponds to one of the $2e_2'$ orbitals in $V©B_9^{2-}$ (Fig.10-9), i.e., the $7a_1$ orbital in $V©B_9^-$, the $6a''$ orbital in $Nb©B_9^-$, and the $7a''$ orbital in $Ta©B_9^-$. The calculated first VDE in each case is in very good agreement with the experimental data, except for the case of $Nb©B_9^-$, where the calculated VDE from the $9a'$ orbital is the same as the first VDE (Tables 10-1 – 10-3). In reality, the top four molecular orbitals in all $M©B_9^-$ anions (Figs. 10-10 – 10-12) lie very close in energy and they give rise to seven detachment channels in a narrow energy range, accounting for the congested spectral features from about 3.6 eV to 4.8 eV in the photoelectron spectra (Figs. 10-4 – 10-6 and Tables 10-1 – 10-3). Overall, the calculated spectral features are in good agreement with the observed features in these congested spectral regions, as shown in Tables 10-1 – 10-3 Remarkably, the feature around 5 eV (band F in Fig. 10-4(b) and band E in Figs. 10-5(b) and 10-6(b)) is very similar in all three cases. As shown in Tables 10-1 – 10-3, this feature is from detachment from the same orbitals in all three cases, i.e., the $2b_1$ and $1a_2$ orbitals in $V©B_9^-$ (Fig. 10-10) and $8a'$ and $5a''$ for $Nb©B_9^-$ (Fig. 10-11) and $Ta©B_9^-$ (Fig. 10-12), which correspond to the degenerate delocalized π orbitals ($1e_1''$ in

Fig. 10-9). The splitting of these MOs in the M©B_9^- anions seems to be very small, giving rise to the same calculated VDEs, consistent with the experimental band around 5 eV in each case. The excellent agreement and consistency between theory and experiment for this feature in all three anions provide an anchoring point for the validity of the spectral assignment. Overall, the agreement between the calculated VDEs and the experimental data, as shown in Tables 10-1 – 10-3, is almost quantitative, confirming unequivocally the obtained global minima for all three clusters.

10-5.4. Electronic vs. geometrical factors in determining the structures of M©B_9, M©B_9^-, and M©B_9^{2-} (M = V, Nb, Ta)

The M©B_9^{2-} dianions are all closed-shell species and obey the electronic design principle, as discussed above in Sec. 10-5.2. However, only V©B_9^{2-} is a perfect planar molecular wheel according to our calculations, whereas both Nb©B_9^{2-} and Ta©B_9^{2-}have C_{9v} symmetry (Fig. 10-8). These species provide another example of the interplay between electronic and geometrical factors in determining the structures of the M©B_n^{q-} type molecular wheels. The covalent radii of V, Nb, and Ta are 1.53, 1.64, and 1.79 Å, respectively.[61] Clearly, the V atom fits perfectly inside a B_9 ring in V©B_9^{2-}, but the B_9 ring is too small to accommodate Ta and Nb, so that they are squeezed out of the ring center slightly to give the C_9v Nb©B_9^{2-} and Ta©B_9^{2-}, as well as in the singly charged or neutral species of these clusters. These are in contrast to the MB_{10}^- systems (M = V, Nb, Ta), which all obey the modified electronic design principle [Eq. (2)] for planar doubly aromatic M©B_{10}^- molecular wheels. However, the B_{10} ring has only the right size to fit Ta and Nb comfortably to give rise to the perfectly planar Nb©B_{10}^- and

$Ta©B_{10}^-$ molecular wheels,[37] whereas the V atom is too small to form stable wheel-type $V©B_{10}^-$ and the global minimum of VB_{10}^- has a boat-like 3D structure.[38] Thus, we show again that both electronic and geometric factors are important to form perfectly planar $M©B_n^{q-}$ type molecular wheels. TheC_{2v} distortion in $V©B_9^-$ is due to the Jahn-Teller effect, as discussed above in Sec. 10-5.3. The C_{9v} distortion in the triplet $V©B_9$ is due to a pseudo Jahn-Teller effect.[62]

10-6. Conclusions

We have investigated a new group of clusters, MB_9^-, MB_9, and MB_9^{2-} (M = V, Nb, Ta) and demonstrated that, for the design of $M©B_n^{q-}$ type molecular wheel borometallic compounds, both electronic and geometric factors should be taken into account. Photoelectron spectroscopy of MB_9^- (M = V, Nb, Ta) was combined with theoretical calculations to show that the global minimum of VB_9^- has a planar C_{2v} $V©B_9^-$ structure, whereas NbB_9^- and TaB_9^- possess $M©B_9^-$ pyramidal type structures with C_s symmetry. Theoretical calculations show that the VB_9^{2-} anion has a perfect planar D_{9h} $V©B_9^{2-}$ molecular wheel structure, whereas NbB_9^{2-} and TaB_9^{2-} have C_{9v} $M©B_9^{2-}$ type structures. All the MB_9^{2-} dianions obey the electronic design principle [Eq.(2)] for $M©B_n^{q-}$ type doubly aromatic molecular wheels. But only the V atom can fit perfectly inside the B_9 ring, whereas because of the larger sizes of Nb and Ta, they get squeezed out of the B_9 ring slightly. The lower symmetries of the $M©B_9^-$ monoanions are all due to the Jahn-Teller effect. All the MB_9 neutrals (M = V, Nb, Ta) are found to have triplet C_{9v} structures. The C_{9v} symmetry of the triplet $V©B_9$ neutral is due to a pseudo Jahn-Teller effect. The current study provides another example of the importance of the

interplay between electronic and geometric factors in designing M©B_n^{q-} type molecular wheel type systems.

References

[1] H. J. Zhai, A. N. Alexandrova, K. A. Birch, A. I. Boldyrev, and L. S. Wang, *Angew. Chem., Int. Ed.* **42**, 6004 (2003).

[2] H. J. Zhai, B. Kiran, J. Li, and L. S. Wang, *Nature Mater.* **2**, 827 (2003).

[3] A. N. Alexandrova, H. J. Zhai, L. S. Wang, and A. I. Boldyrev, *Inorg. Chem.* **43**, 3552 (2004).

[4] B. Kiran, S. Bulusu, H. J. Zhai, S. Yoo, X. C. Zeng, and L. S. Wang, *Proc. Natl. Acad. Sci. U.S.A.* **102**, 961 (2005).

[5] A. N. Alexandrova, A. I. Boldyrev, H. J. Zhai, and L. S. Wang, *Coord. Chem. Rev.* **250**, 2811 (2006).

[6] A. P. Sergeeva, D. Y. Zubarev, H. J. Zhai, A. I. Boldyrev, and L. S. Wang, *J. Am. Chem. Soc.* **130**, 7244 (2008).

[7] W. Huang, A. P. Sergeeva, H. J. Zhai, B. B. Averkiev, L. S. Wang, and A. I. Boldyrev, *Nat. Chem.* **2**, 202 (2010).

[8] A. P. Sergeeva, B. B. Averkiev, H. J. Zhai, A. I. Boldyrev, and L. S. Wang, *J. Chem. Phys.***134**, 224304 (2011).

[9] Z. A. Piazza, W. L. Li, C. Romanescu, A. P. Sergeeva, L. S. Wang, and A. I. Boldyrev, *J. Chem. Phys.* **136**, 104310 (2012).

[10] A. P. Sergeeva, Z. A. Piazza, C. Romanescu, W. L. Li, A. I. Boldyrev, and L. S. Wang, *J. Am. Chem. Soc.* **134**, 18065 (2012).

[11] E. Oger, N. R. M. Crawford, R. Kelting, P. Weis, M. M. Kappes, and R. Ahlrichs, *Angew. Chem., Int. Ed.* **46**, 8503 (2007).

[12] W. N. Lipscomb, *Acc. Chem. Res.* **6**, 257 (1973).

[13] B. Kiran, G. G. Kumar, M. T. Nguyen, A. K. Kandalam, and P. Jena, *Inorg. Chem.* **48**, 9965 (2009).

[14] T. B. Tai, D. J. Grant, M. T. Nguyen, and D. A. Dixon, *J. Phys. Chem. A* **114**, 994 (2009).

[15] T. B. Tai, N. M. Tam, and M. T. Nguyen, *Chem. Phys. Lett.* **530**, 71 (2012).

[16] T. B. Tai, A. Ceulemans, and M. T. Nguyen, *Chem.-Eur. J.* **18**, 4510 (2012).

[17] F. Li, P. Jin, D. E. Jiang, L. Wang, S. B. Zhang, J. Zhao, and Z. F. Chen, *J. Chem. Phys.* **136**, 074302 (2012).

[18] B. P. T. Fokwa and M. Hermus, *Angew. Chem., Int. Ed.* **51**, 1702 (2012).

[19] Q. Zheng, M. Kohout, R. Gumeniuk, N. Abramchuk, H. Borrmann, Y. Prots, U. Burkhardt, W. Schnelle, L. Akselrud, H. Gu, A. Leithe-Jasper, and Y. Grin, *Inorg. Chem.* **51**, 7472 (2012).

[20] D. Y. Zubarev and A. I. Boldyrev, *Phys. Chem. Chem. Phys.* **10**, 5207 (2008).

[21] The symbol © is used to denote wheel-type structures with a central atom, according to Ref. 22.

[22] C. Romanescu, T. R. Galeev, W.-L. Li, A. I. Boldyrev, and L.-S. Wang, *Angew. Chem., Int. Ed.* **50**, 9334 (2011).

[23] C. Romanescu, T. R. Galeev, W.-L. Li, A. I. Boldyrev, and L.-S. Wang, *Acc. Chem. Res.* **46**(2), 350–358 (2012).

[24] W. L. Li, C. Romanescu, T. R. Galeev, Z. A. Piazza, A. I. Boldyrev, and L. S. Wang, *J. Am. Chem. Soc.* **134**, 165 (2012).

[25] C. Romanescu, T. R. Galeev, A. P. Sergeeva, W. L. Li, L. S. Wang, and A. I. Boldyrev, *J. Organomet. Chem.* **721–722**, 148 (2012).

[26] K. Ito, Z. Pu, Q. S. Li, and P. V. R. Schleyer, *Inorg. Chem.* **47**, 10906 (2008).

[27] Z. F. Pu, K. Ito, P. V. Schleyer, and Q. S. Li, *Inorg. Chem.* **48**, 10679 (2009).

[28] K. Exner and P. V. Schleyer, *Science* **290**, 1937 (2000).

[29] Z. X. Wang and P. V. Schleyer, *Science* **292**, 2465 (2001).

[30] R. Islas, T. Heine, K. Ito, P. V. R. Schleyer, and G. Merino, *J. Am. Chem. Soc.* **129**, 14767 (2007).

[31] Q. Luo, *Sci. China, Ser. B: Chem.* **51**, 607 (2008).

[32] Q. Y. Wu, Y. P. Tang, and X. H. Zhang, *Sci. China, Ser. B: Chem.* **52**, 288 (2009).

[33] B. B. Averkiev and A. I. Boldyrev, *Russ. J. Gen. Chem.* **78**, 769 (2008).

[34] C. Q. Miao, J. C. Guo, and S. D. Li, *Sci. China, Ser. B: Chem.* **52**, 900 (2009).

[35] J. C. Guo, W. Z. Yao, Z. Li, and S. D. Li, *Sci. China, Ser. B: Chem.* **52**, 566 (2009).

[36] H. J. Zhai, C. Q. Miao, S. D. Li, and L. S. Wang, *J. Phys. Chem. A* **114**, 12155 (2010).

[37] T. R. Galeev, C. Romanescu, W. L. Li, L. S. Wang, and A. I. Boldyrev, *Angew. Chem., Int. Ed.* **51**, 2101 (2012).

[38] W. L. Li, C. Romanescu, Z. A. Piazza, and L. S. Wang, *Phys. Chem. Chem. Phys.* **14**, 13663 (2012).

[39] L. S. Wang, H. S. Cheng, and J. W. Fan, *J. Chem. Phys.* **102**, 9480 (1995).

[40] L. S. Wang and H. Wu, in *Advances in Metal and Semiconductor Clusters*, edited by M. A. Duncan (JAI Press, Greenwich, CT, 1998), Vol. 4, pp. 299–343.

[41] J. Akola, M. Manninen, H. Häkkinen, U. Landman, X. Li, and L.-S. Wang, *Phys. Rev. B* **60**, R11297 (1999).

[42] W. Huang and L. S. Wang, *Phys. Rev. Lett.* **102**, 153401 (2009).

[43] J. P. Perdew, K. Burke, and Y. Wang, *Phys. Rev. B* **54**, 16533 (1996).

[44] J. P. Perdew, K. Burke, and M. Ernzerhof, *Phys. Rev. Lett.* **78**, 1396 (1997).

[45] C. Adamo and V. Barone, *J. Chem. Phys.* **110**, 6158 (1999).

[46] P. J. Hay and W. R. Wadt, *J. Chem. Phys.* **82**, 299 (1985).

[47] K. L. Schuchardt, B. T. Didier, T. Elsethagen, L. S. Sun, V. Gurumoorthi, J. Chase, J. Li, and T. L. Windus, *J. Chem. Inf. Model.* **47**, 1045 (2007).

[48] T. H. Dunning, *J. Chem. Phys.* **90**, 1007 (1989).

[49] R. A. Kendall, T. H. Dunning, and R. J. Harrison, *J. Chem. Phys.* **96**, 6796 (1992).

[50] See supplementary material at http://dx.doi.org/10.1063/1.4798935 for all the optimized low-lying isomers of VB_9^-, NbB_9^-, and TaB_9^-.

[51] J. Cizek, *Adv. Chem. Phys.* **14**, 35 (1969).

[52] G. D. Purvis and R. J. Bartlett, *J. Chem. Phys.* **76**, 1910 (1982).

[53] K. Raghavachari, G. W. Trucks, J. A. Pople, and M. Head-Gordon, *Chem. Phys. Lett.* **157**, 479 (1989).

[54] P. J. Knowles, C. Hampel, and H. J. Werner, *J. Chem. Phys.* **99**, 5219 (1993).

[55] H. Koch and P. Jorgensen, *J. Chem. Phys.* **93**, 3333 (1990).

[56] J. F. Stanton and R. J. Bartlett, *J. Chem. Phys.* **98**, 7029 (1993).

[57] H. Koch, R. Kobayashi, A. S. de Meras, and P. Jorgensen, *J. Chem. Phys.* **100**, 4393 (1994).

[58] M. Kallay and J. Gauss, *J. Chem. Phys.* **121**, 9257 (2004).

[59] M. J. Frisch, G. W. Trucks, H. B. Schlegel *et al.*, GAUSSIAN 09, Revision B.01, Gaussian, Inc., Wallingford, CT, 2009.

[60] M. U. Varetto, Molekel 5.4.0.8 (Swiss National Supercomputing Centre, Manno, Switzerland, 2009).

[61] B. Cordero, V. Gómez, A. E. Platero-Prats, M. Revés, J. Echeverría, E. Cremades, F. Barragánand, and S. Alvarez, *Dalton Trans.* **2008**, 2832.

[62] See I. B. Bersuker, *Chem. Rev.* **101**, 1067 (2001); I. B. Bersuker, *Chem. Rev.* **113**, 1351 (2013). "The pseudo-Jahn–Teller effect is the only source of instability and distortions of high-symmetry configurations of polyatomic systems in nondegenerate states, and it contributes essentially to the instability of degenerate states."

Table 10-1. Observed vertical electron detachment energies (VDEs) of VB_9^- compared with the calculated values for the lowest energy isomer in each case. All energies are in eV.

Observed bands	VDE (exp)[a]	Final State and Electronic Configuration	VDE (theoretical)		
			PBE0[b]	CCSD(T)[c]	EOM-CCSD[d,e]
		VB_9^- (C_{2v}, $^2B_2$)			
X	3.70 (3)	$^3B_2$ … $1b_1^2 1a_2^2 2b_1^2 7a_1^1 5b_2^2 8a_1^2 6b_2^1$	3.72	3.79	
A	3.79 (3)	$^3B_2$ … $1b_1^2 1a_2^2 2b_1^2 7a_1^2 5b_2^2 8a_1^1 6b_2^1$	3.87	3.98	
B	3.93 (3)	$^3A_1$ … $1b_1^2 1a_2^2 2b_1^2 7a_1^2 5b_2^1 8a_1^2 6b_2^1$	3.86	3.98	
C	4.03 (3)	$^1A_1$ … $1b_1^2 1a_2^2 2b_1^2 7a_1^2 5b_2^2 8a_1^2 6b_2^0$	4.17	4.09	4.04
D	4.10 (3)	$^1B_2$ … $1b_1^2 1a_2^2 2b_1^2 7a_1^2 5b_2^2 8a_1^1 6b_2^1$			4.14
E	~4.6	$^1B_2$ … $1b_1^2 1a_2^2 2b_1^2 7a_1^1 5b_2^2 8a_1^2 6b_2^1$			4.57
		$^1A_1$ … $1b_1^2 1a_2^2 2b_1^2 7a_1^2 5b_2^1 8a_1^2 6b_2^1$			4.57
F	4.94 (4)	$^3A_2$ … $1b_1^2 1a_2^2 2b_1^1 7a_1^2 5b_2^2 8a_1^2 6b_2^1$	4.92	5.14	
		$^3B_1$ … $1b_1^2 1a_2^1 2b_1^2 7a_1^2 5b_2^2 8a_1^2 6b_2^1$	4.92		
		$^1A_2$ … $1b_1^2 1a_2^2 2b_1^1 7a_1^2 5b_2^2 8a_1^2 6b_2^1$			5.22
		$^1B_1$ … $1b_1^2 1a_2^1 2b_1^2 7a_1^2 5b_2^2 8a_1^2 6b_2^1$			5.22
		$^1A_2$ … $1b_1^1 1a_2^2 2b_1^2 7a_1^2 5b^2 8a^2 6b_2^1$			5.45

[a] Numbers in parentheses represent the uncertainty in the last digit.

[b] VDEs were calculated at ROPBE0/V/Stuttgart/B/aug-cc-pVTZ//(RO)PBE0/V /Stuttgart/ B/aug-cc-pVTZ.

[c] VDEs were calculated at ROCCSD(T)/V/Stuttgart/B/aug-cc-pVTZ//(RO)PBE0/V/ Stuttgart/B/aug-cc-pVTZ.

[d] VDEs were calculated at EOM-CCSD/V/Stuttgart/B/6-311+G(*d*)//(RO)PBE0/V/Stuttgart/B/aug-cc-pVTZ.

[e] EOM-CCSD values for triplet states of VB_9^- are not presented because of high spin contamination observed in the calculations.

Table 10-2. Observed vertical electron detachment energies (VDEs) of NbB_9^- compared with the calculated values for the lowest energy isomer in each case. All energies are in eV.

Observed bands	VDE (exp)[a]	Final State and Electronic Configuration	VDE (theoretical)		
			PBE0[b]	CCSD(T)[c]	EOM-CCSD[d]
		NbB_9^- (C_s, ^{2}A')			
X	3.64 (3)	^{3}A" … $7a'^2 5a"^2 8a'^2 6a"^2 9a'^2 7a"^1 10a'^1$	3.65	3.73	3.67
		^{3}A' … $7a'^2 5a"^2 8a'^2 6a"^2 9a'^1 7a"^2 10a'^1$	3.64	3.78	3.67
A	3.84 (3)	^{3}A" … $7a'^2 5a"^2 8a'^2 6a"^1 9a'^2 7a"^2 10a'^1$	3.77	3.78	3.74
B	3.93 (3)	^{1}A' ... $7a'^2 5a"^2 8a'^2 6a"^2 9a'^2 7a"^2 10a'^0$	4.06	3.97	3.98
C	4.12 (4)	^{1}A' ... $7a'^2 5a"^2 8a'^2 6a"^1 9a'^2 7a"^2 10a'^1$			4.08
D	~4.4	^{1}A" ... $7a'^2 5a"^2 8a'^2 6a"^2 9a'^2 7a"^1 10a'^1$			4.38
		^{1}A' ... $7a'^2 5a"^2 8a'^2 6a"^2 9a'^1 7a"^2 10a'^1$			4.38
E	4.88 (5)	^{3}A' … $7a'^2 5a"^2 8a'^1 6a"^2 9a'^2 7a"^2 10a'^1$	4.94	5.06	5.01
		^{3}A" … $7a'^2 5a"^1 8a'^2 6a"^2 9a'^2 7a"^2 10a'^1$	4.94		5.01
		^{3}A' … $7a'^1 5a"^2 8a'^2 6a"^2 9a'^2 7a"^2 10a'^1$			5.26
		^{1}A" ... $7a'^2 5a"^1 8a'^2 6a"^2 9a'^2 7a"^2 10a'^1$			5.32
		^{1}A' ... $7a'^2 5a"^2 8a'^1 6a"^2 9a'^2 7a"^2 10a'^1$			5.32
		^{1}A' ... $7a'^1 5a"^2 8a'^2 6a"^2 9a'^2 7a"^2 10a'^1$			5.40

[a] Numbers in parentheses represent the uncertainty in the last digit.

[b] VDEs were calculated at ROPBE0/ Nb /Stuttgart/B/aug-cc-pVTZ//(RO)PBE0/Nb/Stuttgart/ B/aug-cc-pVTZ.

[c] VDEs were calculated at ROCCSD(T)/Nb/Stuttgart/B/aug-cc-pVTZ//(RO)PBE0/Nb/ Stuttgart/B/aug-cc-pVTZ.

[d] VDEs were calculated at EOM-CCSD/Nb/Stuttgart/B/6-311+G(*d*)//(RO)PBE0/Nb/Stuttgart/B/aug-cc-pVTZ.

Table 10-3. Observed vertical electron detachment energies (VDEs) of TaB_9^- compared with the calculated values for the lowest energy isomer in each case. All energies are in eV.

Observed bands	VDE (exp)[a]	Final State and Electronic Configuration	VDE (theoretical)		
			PBE0[b]	CCSD(T)[c]	EOM-CCSD[d]
		TaB_9^- (C_s, $^2A'$)			
X	3.64 (3)	$^3A''$ … $7a'^2 5a''^2 8a'^2 6a''^2 9a'^2 7a''^1 10a'^1$	3.72	3.71	3.70
A	3.89 (4)	$^3A'$ … $7a'^2 5a''^2 8a'^2 6a''^2 9a'^1 7a''^2 10a'^1$	3.70	3.85	3.75
		$^3A''$ … $7a'^2 5a''^2 8a'^2 6a''^1 9a'^2 7a''^2 10a'^1$	3.70	3.85	3.75
B	4.03 (3)	$^1A'$ ... $7a'^2 5a''^2 8a'^2 6a''^2 9a'^2 7a''^2 10a'^0$	4.04	3.89	3.90
C	4.36 (5)	$^1A''$ ... $7a'^2 5a''^2 8a'^2 6a''^2 9a'^2 7a''^1 10a'^1$			4.01
D	4.68 (5)	$^1A'$ ... $7a'^2 5a''^2 8a'^2 6a''^2 9a'^1 7a''^2 10a'^1$			4.54
		$^1A''$ ... $7a'^2 5a''^2 8a'^2 6a''^1 9a'^2 7a''^2 10a'^1$			4.54
E	5.07 (5)	$^3A'$ … $7a'^2 5a''^2 8a'^1 6a''^2 9a'^2 7a''^2 10a'^1$	[e]	5.08	5.06
		$^3A''$ … $7a'^2 5a''^1 8a'^2 6a''^2 9a'^2 7a''^2 10a'^1$	[e]	5.08	5.06
		$^1A'$ … $7a'^2 5a''^2 8a'^1 6a''^2 9a'^2 7a''^2 10a'^1$			5.32
		$^1A''$ ... $7a'^2 5a''^1 8a'^2 6a''^2 9a'^2 7a''^2 10a'^1$			5.32
		$^3A'$ … $7a'^1 5a''^2 8a'^2 6a''^2 9a'^2 7a''^2 10a'^1$	5.26	5.38	5.50
		$^1A'$ ... $7a'^1 5a''^2 8a'^2 6a''^2 9a'^2 7a''^2 10a'^1$			5.61

[a] Numbers in parentheses represent the uncertainty in the last digit.

[b] VDEs were calculated at ROPBE0/Ta/Stuttgart/B/aug-cc-pVTZ//(RO)PBE0/Ta/Stuttgart/ B/aug-cc-pVTZ.

[c] VDEs were calculated at ROCCSD(T)/Ta/Stuttgart/B/aug-cc-pVTZ//(RO)PBE0/Ta/ Stuttgart/B/aug-cc-pVTZ.

[d] VDEs were calculated at EOM-CCSD/Ta/Stuttgart/B/6-311+G(*d*)//(RO)PBE0/Ta/ Stuttgart/B/aug-cc-pVTZ.

[e] VDEs could not be calculated at this level of theory.

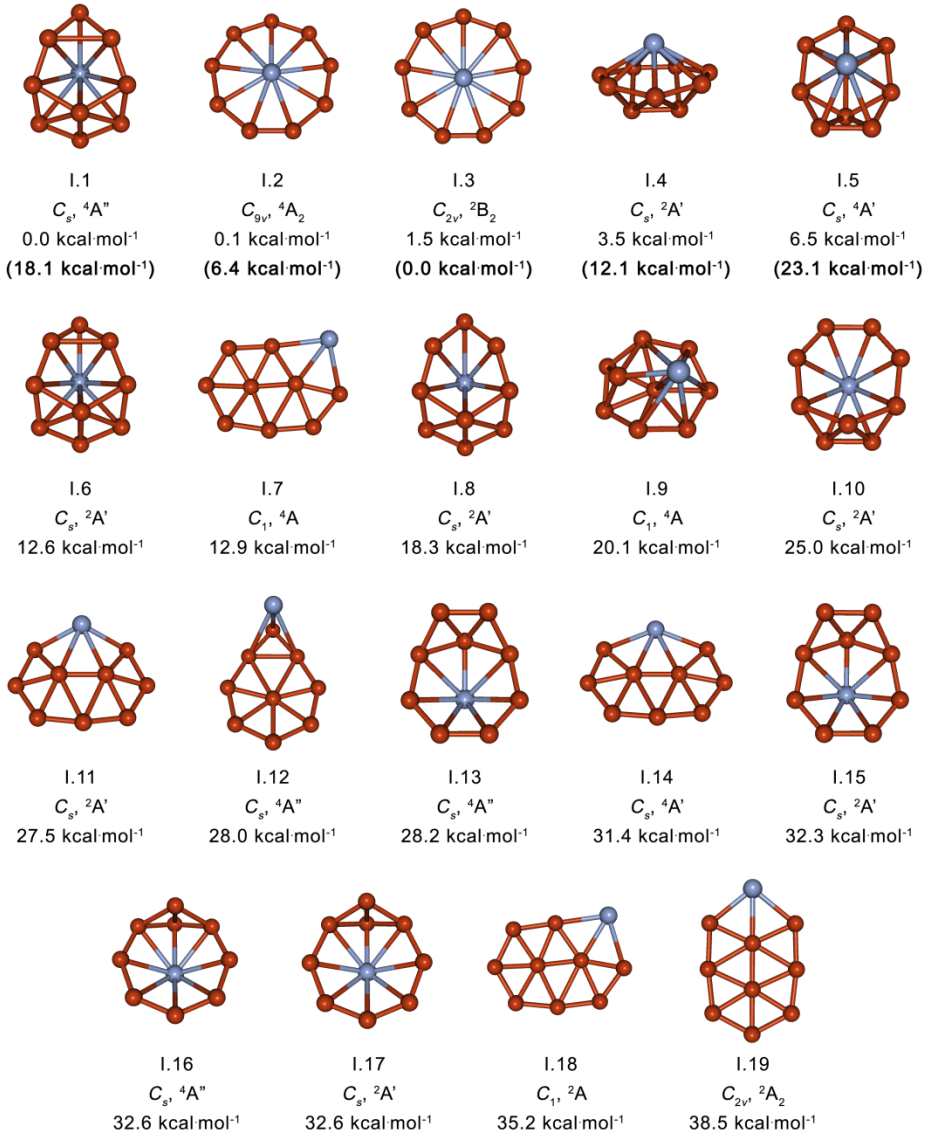

FIG. 10-1. Alternative isomers of VB_9^- (ROPBE0/V/Stuttgart/B/aug-cc-pVTZ). The ROCCSD(T)/V/ Stuttgart/B/aug-cc-pVTZ//ROPBE0/V/Stuttgart/B/aug-cc-pVTZ relative energies calculated for the lowest isomers are given in parentheses. I.4 is the "boat" structure.

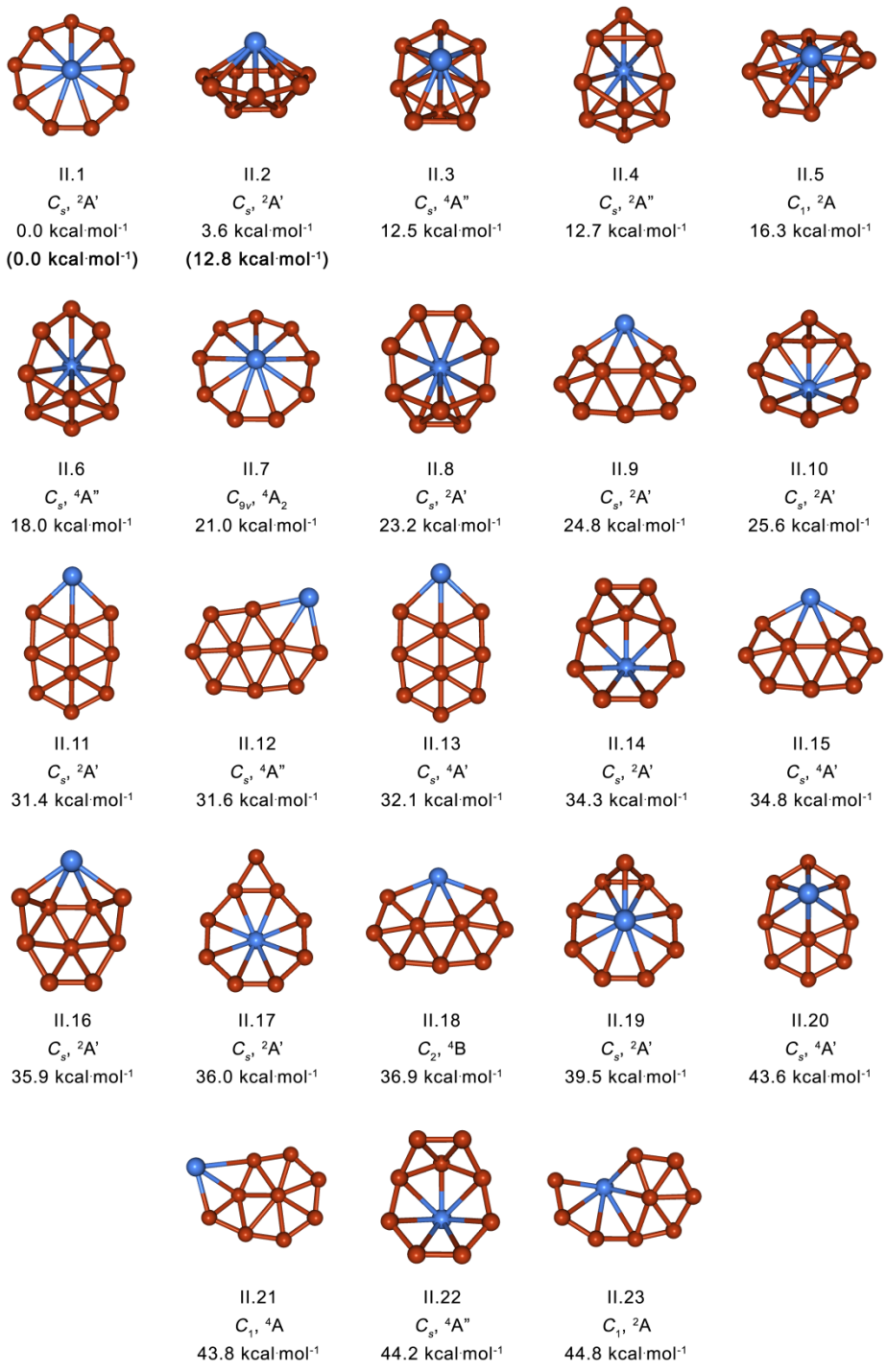

FIG. 10-2. Alternative isomers of NbB_9^- (PBE0/Nb/Stuttgart/B/aug-cc-pVTZ). The ROCCSD(T)/Nb/Stuttgart/B/aug-cc-pVTZ//PBE0/Nb/Stuttgart/B/aug-cc-pVTZ relative energies calculated for the lowest isomers are given in parentheses. II.2 is the "boat" structure.

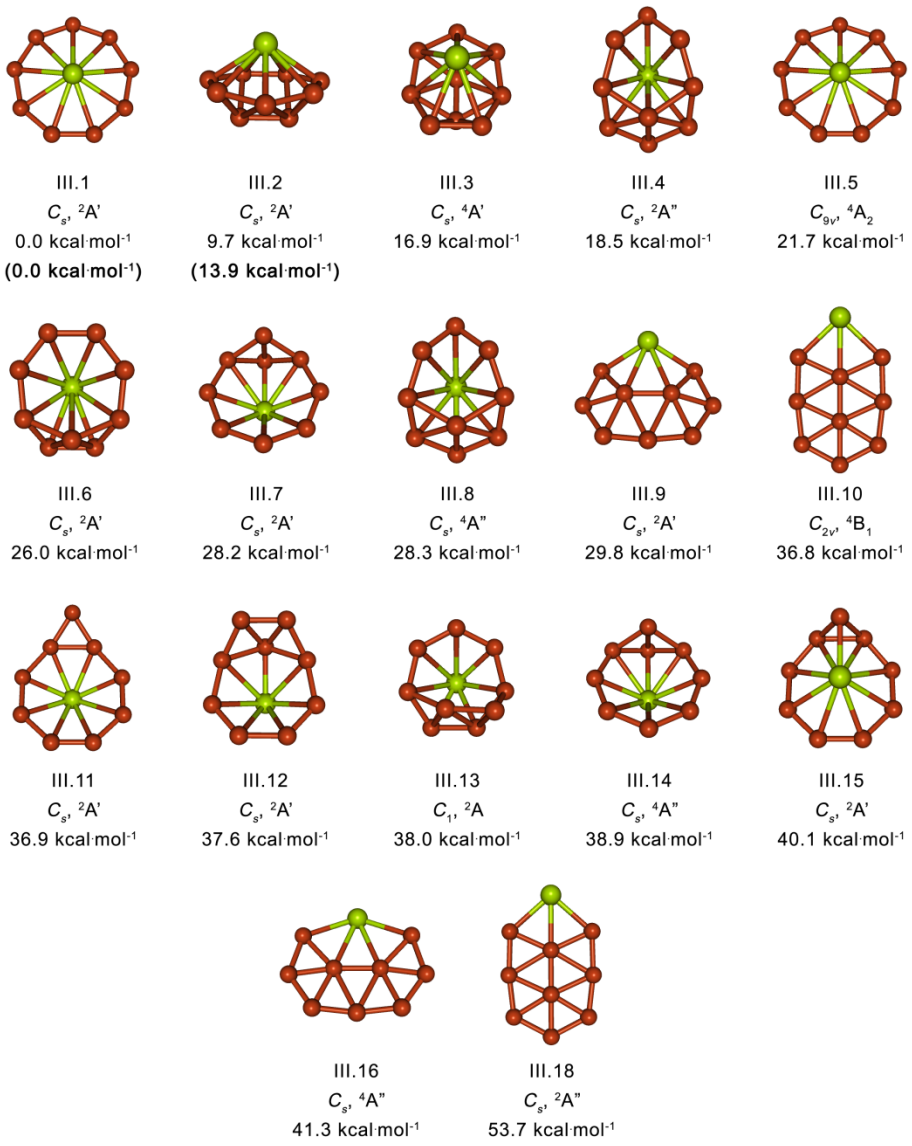

FIG 10-3. Alternative isomers of TaB_9^- (PBE0/Ta/Stuttgart/B/aug-cc-pVTZ). The ROCCSD(T)/Ta/Stuttgart/B/aug-cc-pVTZ//PBE0/Ta/Stuttgart/B/aug-cc-pVTZ relative energies calculated for the lowest isomers are given in parentheses. III.2 is the boat structure.

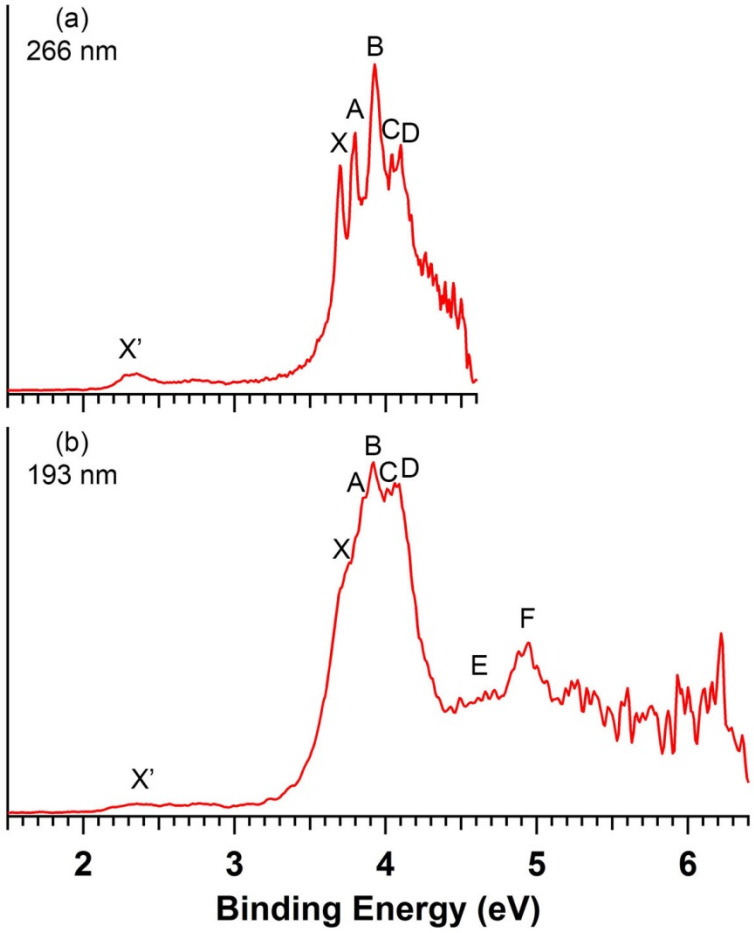

FIG. 10-4. Photoelectron spectra of VB_9^- at (a) 266 nm (4.661 eV) and (b) 193 nm (6.424 eV).

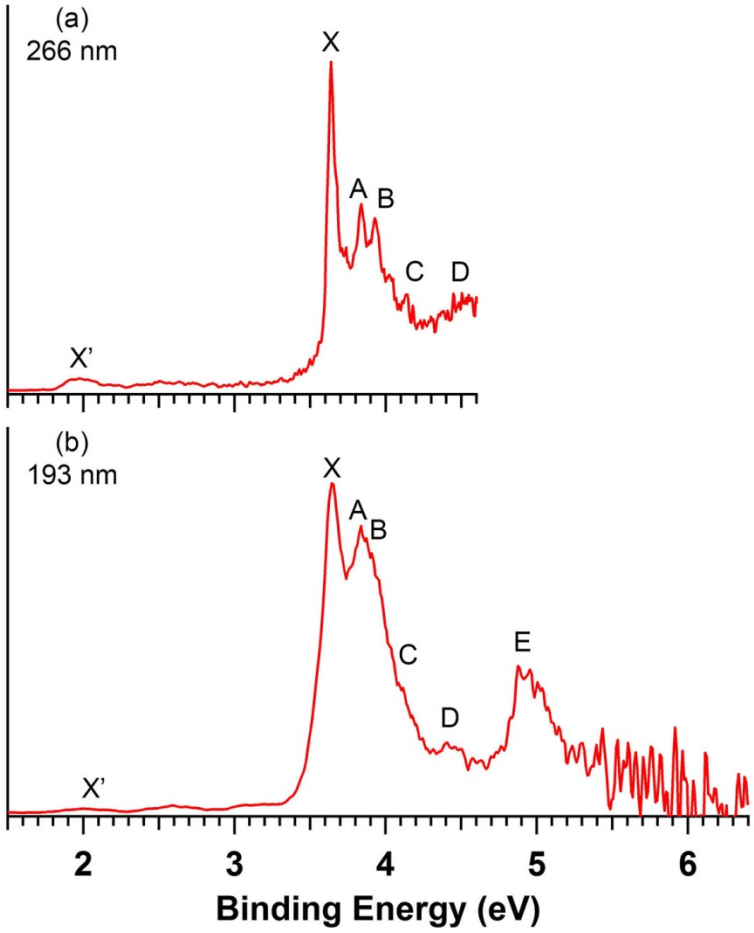

FIG. 10-5. Photoelectron spectra of NbB_9^- at (a) 266 nm and (b) 193 nm.

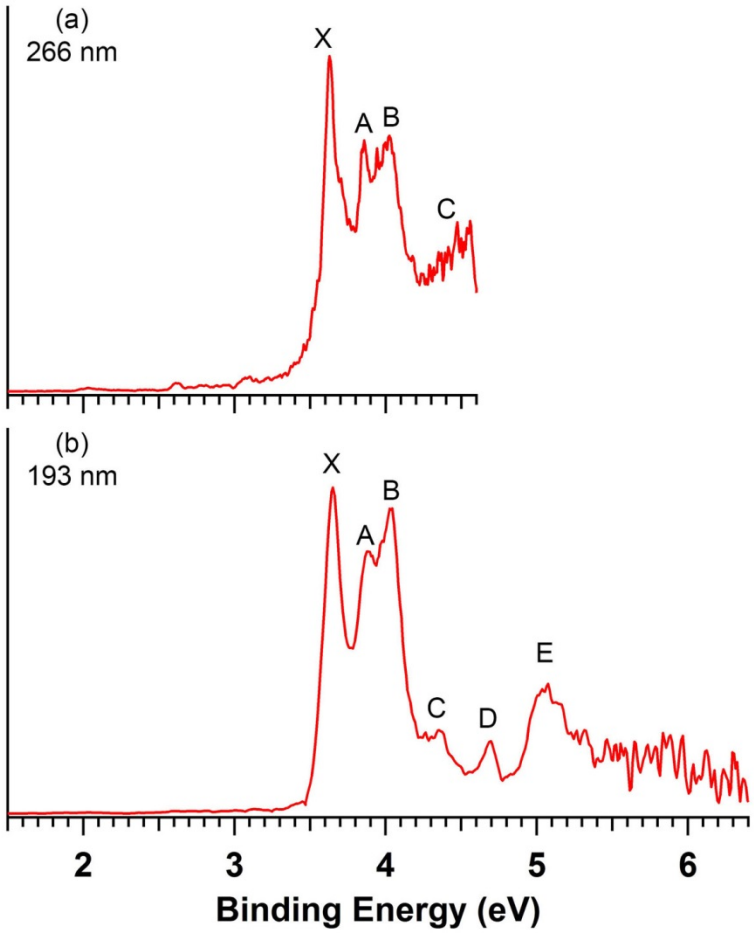

FIG. 10-6. Photoelectron spectra of TaB_9^- at (a) 266 nm and (b) 193 nm.

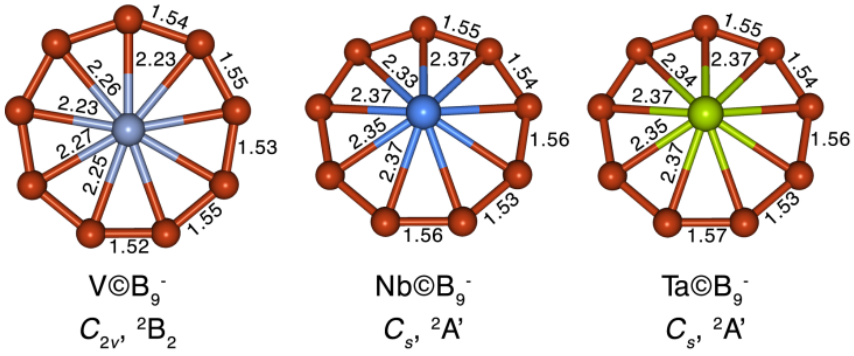

FIG. 10-7. Global minimum structures of VB_9^-, NbB_9^-, and TaB_9^-. Bond lengths are given in Å at the (RO)PBE0/V,Nb,Ta/Stuttgart/B/aug-cc-pVTZ level.

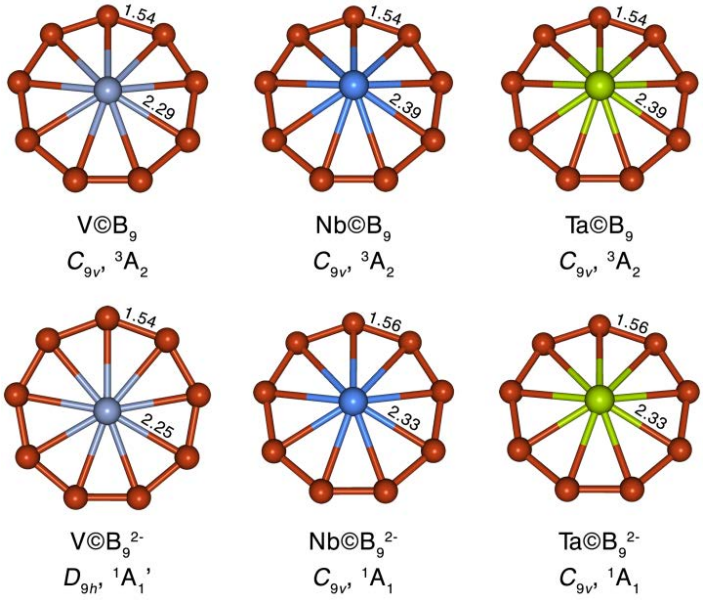

FIG. 10-8. Optimized structures of neutral VB_9, NbB_9, and TaB_9 and the doubly charged VB_9^{2-}, NbB_9^{2-}, and TaB_9^{2-} clusters. Bond lengths are given in Å at the PBE0/V,Nb,Ta/Stuttgart/B/ aug-cc-pVTZ level.

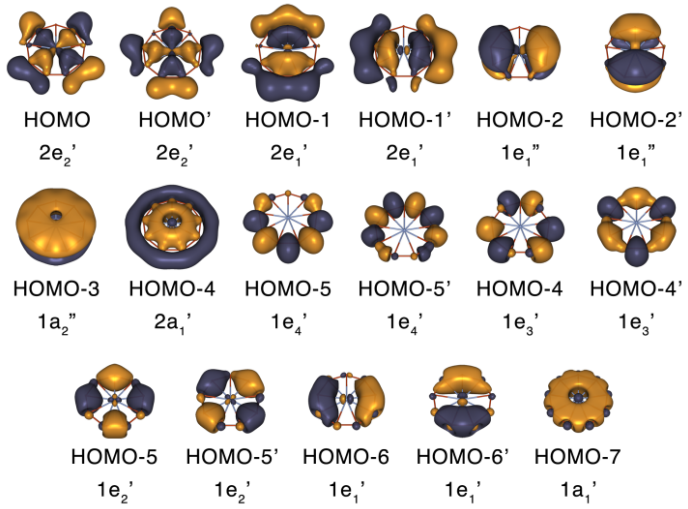

FIG. 10-9. Molecular orbital plots of $V©B_9^{2-}$ (D_{9h}, $^2A_1'$) at the PBE0/V/Stuttgart/ B/aug-cc-pVTZ level.

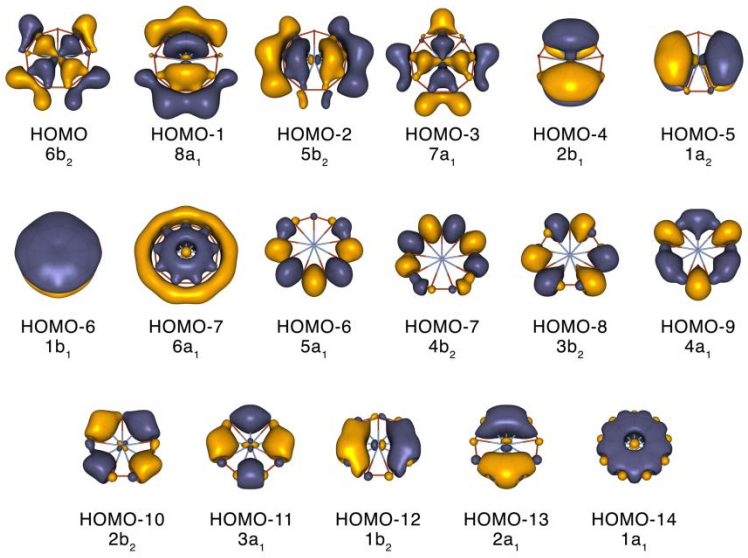

FIG. 10-10. Valence canonical molecular orbital plots of $V©B_9^-$ (ROPBE0/V/Stuttgart/ B/aug-cc-pVTZ).

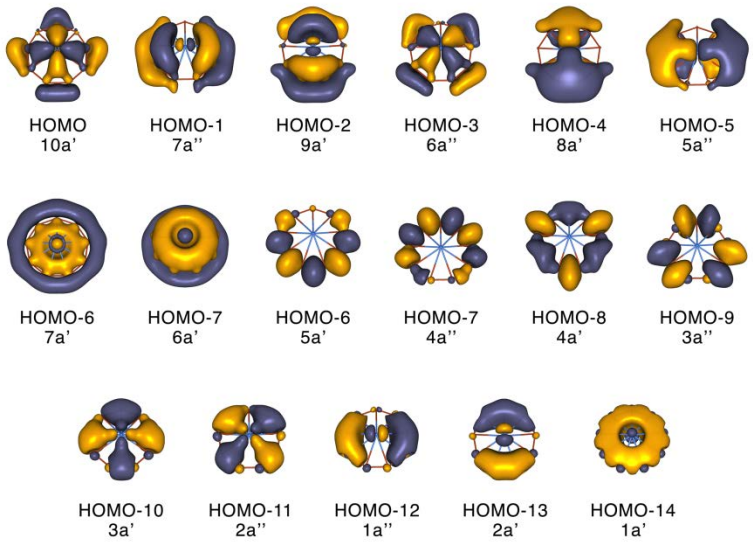

FIG. 10-11. Valence canonical molecular orbital plots of $Nb©B_9^-$ (ROPBE0/ Nb/Stuttgart/B/aug-cc-pVTZ).

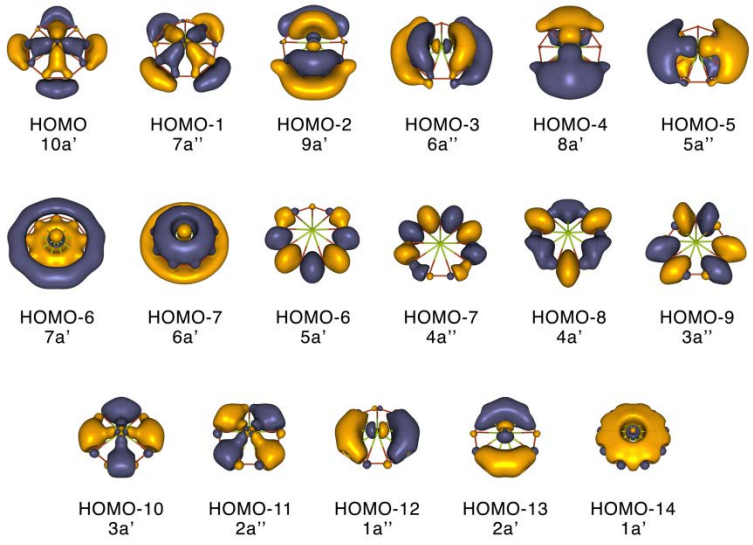

FIG. 10-12. Valence canonical molecular orbital plots of $Ta©B_9$ (ROPBE0/ Ta/Stuttgart/B/aug-cc-pVTZ).

CHAPTER 11

TRANSITION-METAL-CENTERED MONOCYCLIC BORON WHEEL CLUSTERS (M©B_n): A NEW CLASS OF AROMATIC BOROMETALLIC COMPOUNDS [*]

Abstract

Atomic clusters have intermediate properties between that of individual atoms and bulk solids, which provide fertile ground for the discovery of new molecules and novel chemical bonding. In addition, the study of small clusters can help researchers design better nanosystems with specific physical and chemical properties. From recent experimental and computational studies, we know that small boron clusters possess planar structures stabilized by electron delocalization both in the σ and π frameworks. An interesting boron cluster is B_9^-, which has a D_{8h} molecular wheel structure with a single boron atom in the center of a B_8 ring. This ring in the D_{8h}-B_9^- cluster is connected by eight classical two-center, two-electron bonds. In contrast, the cluster's central boron atom is bonded to the peripheral ring through three delocalized σ and three delocalized π bonds. This bonding structure gives the molecular wheel double aromaticity and high electronic stability. The unprecedented structure and bonding pattern in B_9^- and other planar boron clusters have inspired the designs of similar molecular wheel-type structures. But these mimics instead substitute a heteroatom for the central boron.

Through recent experiments in cluster beams, chemists have demonstrated that transition metals can be doped into the center of the planar boron clusters. These new

[*] Coauthored by Constantin Romanescu, Timur R. Galeev, Wei-Li Li, Alexander I. Boldyrev, and Lai-Sheng Wang. Reprinted with permission from *Acc. Chem. Res*. **2013**, *46*, 350-358. Copyright 2013 American Chemical Society.

metal-centered monocyclic boron rings have variable ring sizes, $M©B_n$ and $M©B_n^-$ with n = 8–10. Using size-selected anion photoelectron spectroscopy and *ab initio* calculations, researchers have characterized these novel borometallic molecules. Chemists have proposed a design principle based on σ and π double aromaticity for electronically stable borometallic cluster compounds, featuring a highly coordinated transition metal atom centered inside monocyclic boron rings. The central metal atom is coordinatively unsaturated in the direction perpendicular to the molecular plane. Thus, chemists may design appropriate ligands to synthesize the molecular wheels in the bulk. In this Account, we discuss these recent experimental and theoretical advances of this new class of aromatic borometallic compounds, which contain a highly coordinated central transition metal atom inside a monocyclic boron ring. Through these examples, we show that atomic clusters can facilitate the discovery of new structures, new chemical bonding, and possibly new nanostructures with specific, advantageous properties.

11-1. Introduction

The study of atomic clusters, with structures and properties intermediate between individual atoms and bulk solids, has a profound impact on our understanding of chemical bonding and the rational design of nanosystems with tailored physical and chemical properties.[1] Joint experimental and computational investigations over the past decade have demonstrated that negatively charged boron clusters (B_n^-) possess planar (2D) structures at least up to n = 23.[2-11] The propensity for planar structures in pure boron clusters, which can be traced to the electron-deficient character of the boron atoms, is in stark contrast with the three-dimensional (3D) structural motifs found in bulk boron and

many solid boron derivatives. Even though the 2D–3D structural transition has been found to occur at $n = 16$ for cationic boron clusters[12] and $n = 20$ for neutral boron clusters,[6,13] this transition has not been found for anionic clusters. All planar boron clusters confirmed experimentally thus far consist of an outer ring, featuring strong two-center, two-electron (2c–2e) B–B bonds, and one or more inner atoms interacting with the peripheral ring via delocalized σ and π bonding.[3,6-11] To emphasize the role electron delocalization plays in the stability of planar boron clusters, we note that the inner boron atoms in the anionic clusters ($n \leq 20$) are bonded to the outer ring almost exclusively by multicenter, two-electron bonds (nc–2e). One prototypical example is the circular B_{19}^- cluster ($B©B_5©B_{13}$),[14] which consists of two different delocalized π systems,[9] in addition to σ delocalized bonding. These delocalized bondings characterize the interactions between the central B atom and the middle B_5 ring and between the B_5 ring and the outer B_{13} ring. Interestingly, the inner $B©B_5$ moiety has been found to rotate almost freely inside the B_{13} outer ring, akin to an aromatic Wankel motor.[15] Similar fluxional behavior has also been found for the inner B_3 ring in the planar B_{13}^+ cluster, entirely owing to delocalized bonding between the B_3 unit and the outer B_{10} ring.[16]

The planar boron clusters that provided the inspiration for metal doping are the eight- and nine-atom boron clusters.[2,4] These two clusters stand out as perfectly symmetric molecular wheels: B_8^{2-} (D_{7h}) and B_9^- (D_{8h}), each with six σ and six π electrons conforming to the $(4N + 2)$ Hückel rule for aromaticity.[2,4] Chemical bonding analyses using the adaptive natural density partitioning (AdNDP) method[17] confirmed that both clusters are doubly aromatic with unprecedented multicenter electron delocalization. It

should be pointed out that the concept of double (σ and π) aromaticity was introduced for organic molecules previously.[18] However, attempts to substitute the central B atom with C to form carbon-centered wheel structures[19-21] were not successful and yielded only higher energy structures, because C avoids hypercoordination in B_xC_y clusters and prefers to participate in localized 2c–2e σ bonding on the periphery in the B–C mixed clusters.[22-24]

One interesting question was whether it would be possible to substitute the central B atom with a metal atom to create clusters with a central metal atom coordinated by a monocyclic boron ring ($M©B_n$).[14] It was shown that simple valence isoelectronic substitution by Al was not possible, only resulting in "umbrella"-type structures in AlB_7^- (C_{7v}) and AlB_8^- (C_{8v}),[25] in which Al interacts with a concave B_7 or B_8 unit primarily through ionic bonding and does not participate in delocalized bonding within the 2D boron frameworks. Similar ionic interactions have also been observed in larger AlB_n^- (n = 9–11) clusters.[26] Gold was also considered in a prior experiment, but it was found to form a covalent bond with a corner boron atom on the periphery of a planar B_{10} in AuB_{10}^-, whereas the D_{10h}-$Au©B_{10}^-$ is a high-energy local minimum.[27]

Recently, we have successfully produced a series of transition-metal-centered boron rings in a supersonic cluster beam by laser vaporization of mixed boron–metal targets: $Co©B_8^-$ and $Ru©B_9^-$,[28] $Rh©B_9^-$ and $Ir©B_9^-$,[29] and $Nb©B_{10}^-$ and $Ta©B_{10}^-$.[30] All these clusters have been shown to be the global minima on their respective potential energy curves. A design principle has been proposed for electronically stable $M©B_n^{k-}$-

type compounds. These recent advances are discussed in this Account, and some future perspectives are outlined.

11-2. Experimental and Computational Methods

11-2.1. Cluster Generation and Photoelectron Spectroscopy

The experiment was done using a magnetic-bottle photoelectron spectroscopy (PES) apparatus equipped with a laser vaporization cluster source that was described in detail before.[31] Briefly, the metal-doped boron clusters were produced by laser vaporization of a disk target made of isotopically enriched ^{10}B or ^{11}B powder and the respective transition metals, balanced by Bi or Ag. The latter acted as target binders and also provided atomic anions, Bi^- or Ag^-, as calibrants for the photoelectron spectra. Depending on the mass and the isotope distributions of the metal dopant, different isotopically enriched boron was used to avoid mass overlaps between the metal-doped and pure boron clusters that were usually formed in larger amounts. The clusters were entrained in a He carrier gas seeded with 5% Ar and underwent a supersonic expansion to form a collimated cluster beam. Negatively charged clusters were extracted and analyzed with a time-of-flight mass spectrometer. An example of a mass spectrum for the $Nb_mB_n^-$ clusters produced by laser vaporization of a B/Nb target is shown in Figure 11-1. The clusters of interest were mass-selected and decelerated before photodetachment by a laser beam at 193 nm (6.424 eV), 266 nm (4.661 eV), or 355 nm (3.496 eV). Photoelectrons were collected at nearly 100% efficiency by a magnetic bottle and analyzed in a 3.5 m long electron flight tube. The electron binding energy spectra were obtained by subtracting the electron kinetic energy spectra from the detachment photon energies. The

resolution of the apparatus (ΔKE/KE) was better than 2.5%, that is, ~25 meV for 1 eV electrons.

11-2.2. Theoretical Calculations

Detailed information on the theoretical methods used for a given cluster is provided in the literature.[28-30] Briefly, the first step in understanding the photoelectron spectra and the structures of the doped boron clusters was the search for the global minimum using the coalescence-kick method[10] with density functional theory (DFT) calculations and small basis sets. The low-energy structures identified were further optimized using larger basis sets. Vibrational frequency analyses were run to ensure that all the isomers were true minima on the respective potential energy surfaces. Finally, single point energies for the lowest isomers were calculated at CCSD(T), the "gold standard" of computational chemistry. Vertical detachment energies (VDEs) for the global minimum were calculated at DFT and CCSD(T) and were used to compare with the experimental data. When vibrational structures were resolved, the comparison of the experimental and theoretical vibrational frequencies provided further support to the identified global minimum. Chemical bonding was analyzed using molecular orbitals (MOs) and the AdNDP method,[17] which was particularly valuable for planar systems. The calculations were usually done using Gaussian 09,[32] except for those of $Ta©B_{10}^-$, which were done using the ADF program.[33] The MO visualization for the AdNDP analyses was done using Molekel 5.4.0.8.[34]

11-3. The Design Principle for Metal-Centered Boron Wheel Clusters ($M©B_n^{k-}$)

Despite numerous theoretical reports on molecular wheel-type clusters,[19-21] only the pure boron clusters, B_8^{2-} and B_9^-, with hepta- and octa-coordinated boron atoms were proven to be the global minima on their respective potential energy surfaces.[2-4] The chemical bonding of these two clusters involves classical 2c–2e bonds for the peripheral boron rings (seven for B_8^{2-} and eight for B_9^-) and six delocalized σ electrons and six delocalized π electrons. Thus, the bonding in these molecular wheels can be viewed as a monocyclic boron ring interacting with a central B atom entirely through delocalized bonds. Because the number of σ or π electrons each satisfies the $4N + 2$ Hückel rule for aromaticity, these molecular wheels are considered to be doubly aromatic. Thus, each peripheral B atom contributes two valence electrons to the 2c–2e bonds of the outer ring and one electron to the delocalized bonding between the outer ring and the central atom, whereas the central B atom contributes all three of its valence electrons to the delocalized bonding. Replacing the central B in B_8^{2-} by C would result in an isoelectronic D_{7h}-CB_7^-, which was found to be a local minimum.[22] In fact, all group-14 elements were found to give stable minima for D_{7h}-MB_7^-clusters.[21] However, C has been confirmed experimentally to avoid the central position, and the global minimum of CB_7^- has C_{2v} symmetry, in which the C atom is on the periphery.[22] The reason that C prefers the peripheral position is because C can form strong 2c–2e bonds, which is only possible on the periphery, whereas in the central position only delocalized multicenter bonding is possible. A D_{9h}-AlB_9^+ has been found to be a local minimum,[35] but we have shown that Al also does not favor the central planar position in AlB_9^-.[26a]

Once the main-group elements came out of favor as potential substituents for the central B atom to create molecular wheels, the focus of theoretical studies shifted to transition-metal-doped boron systems.[36-40] Two previous reports showed that D_{8h}-CoB_8^-, D_{9h}-FeB_9^-, and D_{8h}-FeB_8^{2-} were global minima, while a number of other transition metal doped boron rings (MB_n) with $n = 7–10$ were found to be only local minima.[36-38] Nucleus-independent chemical shift[41] calculations showed that all these clusters were highly aromatic. The introduction of the AdNDP method greatly simplified the bonding analysis and revealed that all planar wheel-type boron clusters featured double σ and π aromaticity.[40]

Based on the double aromaticity requirement, $(4N_\sigma + 2)$ delocalized σ electrons and $(4N_\pi + 2)$ delocalized π electrons to fulfill the Hückel aromaticity rule, a general electronic design principle has been proposed that involves the formal valence of the transition metal (x), the number of peripheral boron atoms (n), and the cluster's charge (k). To form electronically stable and doubly aromatic wheel-type clusters ($M^{(x)}©B_n^{k-}$), the design principle requires that the total number of bonding electrons present in the system, $3n + x + k$, participate in n 2c–2e B–B peripheral σ bonds and two sets of aromatic delocalized bonds (12 e for 6 σ and 6 π electrons), that is, $3n + x + k = 2n + 12$. In other words, for an electronically stable $M^{(x)}©B_n^{k-}$ cluster with double aromaticity, $n + x + k = 12$. For singly charged $M^{(x)}©B_n^-$ clusters ($k = 1$), $n + x = 11$. As shown below, in addition to the electron counting to satisfy double aromaticity, the ability of the central atom to form delocalized bonds and the favorable interactions between M and the B_n ring are also essential for the formation of the wheel structures.

However, geometric or steric considerations should probably limit the ring size to be at least seven atoms. For pure boron clusters, it was found that the B_7 cluster has a hexa-pyramidal structure,[5] which suggests that even the boron atom is too large to fit inside a B_6 ring. The smallest molecular wheel structure found experimentally is the D_{7h}-B_8^{2-} cluster, [4] while B_8^- has a slightly distorted planar structure with a D_{2h} symmetry due to the Jahn–Teller effect.[2] When applied to a hypothetical D_{7h}-M©B_7^- cluster, the design principle requires a valence IV element. The formal satisfaction of the electron counting rules may not be sufficient to make the wheel structure the global minimum. For example, even though Au has the right valence to make an electronically stable Au©B_{10}^- wheel, we have shown that the wheel structure is not the global minimum for AuB_{10}^-,[27] because the Au 5d-AOs do not participate in bonding with the boron B_{10} ring.

11-4. Case Studies of M©B_n^- Molecular Wheels: From Theoretical Analyses to Experimental Discoveries

Clusters with high symmetry often have lower densities of energy levels as a result of degeneracy. Furthermore, chemical and thermodynamic stabilities are related to the electron affinity for open-shell neutral species or the energy gap between the highest occupied molecular orbital (HOMO) and the lowest unoccupied molecular orbital (LUMO) for closed-shell neutral species. Therefore, there are a number of signatures that can be readily recognized in PES spectra for highly stable and symmetric clusters. In the initial experimental effort, we screened a large number of transition-metal-doped boron clusters using PES to find clues about structural and electronic stabilities. To exemplify the approach, we show the PES data in Figure 11-2 for a set of ruthenium-doped boron

clusters, RuB_n^- (n = 3–10). It can be clearly seen that RuB_9^-gives a relatively simple PES spectrum with a few narrow spectral features and an unusually high electron binding energies, providing hints for a highly stable and symmetric system. Similar screening experiments have been performed for many transition-metal-doped boron clusters, and a series of clusters have been discovered to form stable molecular wheel-type structures.[28-30]

11-4.1. M©B_8^- Molecular Wheels

When applied to a D_{8h}-M©B_8^- cluster, the design principle requires that the transition metal atom should contribute three valence electrons to delocalized bonding. Given the small size of the B_8 ring, the best candidate for such a cluster should be a 3d metal. Indeed, D_{8h}-CoB_8^- and -FeB_8^{2-}were calculated to be global minima.[36,38] CoB_8^- was the first D_{8h}-M©B_8^- molecular wheel characterized experimentally.[28] Figure 11-3 shows the PES spectra of CoB_8^- at two detachment photon energies. The global minimum D_{8h}-Co©B_8^- structure is shown in Figure 11-4a, which is similar to that reported in an earlier theoretical study.[36] To confirm that the D_{8h} structure is indeed the global minimum of CoB_8^-, we compared the computed VDEs with the experimental data and analyzed the vibrational structures resolved in the 266 nm spectrum. The calculated VDEs using both DFT and CCSD(T) methods showed good agreement with the experimental data.[28] To better understand the PES transitions and the structural changes that occur upon detachment of an electron from Co©B_8^-, it is instructive to analyze the MOs of Co©B_8^- (Figure 11-3b). The HOMO of Co©B_8^- ($2e_{1u}$) is a degenerate σ orbital. Removal of one electron from the HOMO lifts the degeneracy, and the ensuing Jahn–Teller effect causes

an in-plane distortion, reducing the symmetry of the neutral cluster to D_{2h} ($^2B_{2u}$) (Figure 11-4b). This geometry change is reflected in the resolved vibrational structures in the 266 nm spectrum (Figure 11-3), corresponding to two symmetric in-plane vibrational modes of the D_{2h}-Co©B_8 ground state. Good agreement was found between the calculated and the observed vibrational frequencies, lending further credence to the structural analyses.[28]

Further chemical bonding analyses using AdNDP clearly revealed 3d lone pairs, localized 2c–2e B–B bonds, and delocalized 9c–2e σ and π bonds in Co©B_8^-, as shown in Figure 11-5 Co ($3d^74s^2$) has 9 valence electrons, resulting in a total of 34 valence electrons for CoB_8^-. It is in its +3 oxidation state in this case, and the AdNDP analyses revealed clearly three 3d lone-pairs (d_z^2, d_{xy}, $d_{x^2-y^2}$). The remaining 28 electrons form eight 2c–2e peripheral B–B bonds, three completely delocalized 9c–2e π-bonds, and three completely delocalized 9c–2e σ-bonds. The latter bonding features give rise to double aromaticity for Co©B_8^-, very similar to that in B_9^-.[2]

In addition to Co©B_8^-, we have also examined the isoelectronic RhB_8^- and IrB_8^- clusters (Figure 11-6). Our preliminary analysis showed that these atoms are too large to fit inside a B_8-ring comfortably. As a consequence of the geometrical constraint, the metal atom is squeezed out of the plane slightly (~0.5 Å), distorting the RhB_8^- and IrB_8^- clusters to C_{8v} symmetry. Hence, D_{8h}-M©B_8^- type systems are probably the smallest borometallic molecular wheels.

11-4.2. M©B_9^- Molecular Wheels

For M©B_9^- systems, our design principle requires the central atom to be in its +2 oxidation state. The Fe-group elements are ideal to form closed-shell M©B_9^- clusters.

Indeed, $Fe©B_9^-$ was computed to be a stable minimum.[36-38,40] Our experimental PES spectra for $Fe©B_9^-$ display broader features, indicating the possible presence of other low-lying isomers.[42] As shown in Figure 11-2, RuB_9^- is the most promising example for a perfect D_{9h}-$M©B_9^-$ cluster. The photoelectron spectra of RuB_9^- at 193 and 266 nm are displayed in Figure 11-6. The relatively simple PES pattern and unusually high electron binding energies suggested that RuB_9^- must be highly stable electronically and possess high symmetry. Our global optimization found indeed that the ground state of RuB_9^- possesses D_{9h} symmetry (Figure 11-7a). The MOs of the D_{9h}-$Ru©B_9^-$ are shown in Figure 11-7b and can be used to understand the PES data.[28]

The HOMO of $Ru©B_9^-$ is the nonbonding $4d_z^2$ orbital of Ru. Removal of one electron from this orbital, corresponding to the X band in the PES spectra (Figure 11-6), should not affect the peripheral B_9 ring. However, a very slight out-of-plane distortion of the Ru atom was observed from our geometrical optimization of the doublet ground state of the neutral, resulting in a C_{9v}-$Ru©B_9$ (Figure 11-7a).[28] The unresolved vibrational structure in the X band is consistent with the structural distortion: the vibrational frequency for the out-of-plane mode by Ru is computed to be only 36 cm^{-1}, which was too low to be resolved in our experiment. The HOMO – 1 of $Ru©B_9^-$ is a doubly degenerate σ orbital, similar to the HOMO of $Co©B_8^-$ (Figure 11-4b). Detachment of an electron from this orbital corresponds to band A in the PES spectra (Figure 11-6). Indeed, we observed vibrational structures for this detachment band due to the expected Jahn–Teller effect, similar to the X band of $Co©B_8^-$ (Figure 11-2). The calculated VDEs for the first four detachment channels of $Ru©B_9^-$ are all in good agreement with the observed

PES bands. The agreement between the theoretical and experimental results confirmed unequivocally that the global minimum of RuB_9^- is the D_{9h} molecular wheel.[28]

The AdNDP analysis shown in Figure 11-8 reveals that $Ru©B_9^-$ is doubly aromatic with three σ and three π 10c–2e delocalized bonds consistent with the electronic requirement of our design principle, in addition to the nine 2c–2e B–B bonds for the B_9 ring and three 4d lone pairs.

11-4.3. Neutral M©B_9 Molecular Wheels

Our electronic design principle says $n + x = 12$ for doubly aromatic *neutral* clusters ($k = 0$). However, experimentally we can only study negatively charged species using PES of size-selected anions. For stable and closed-shell neutral M©B_n species, a large HOMO–LUMO gap is expected, which can be probed directly in the PES spectra of the corresponding anions. Based on the high stability of $Ru©B_9^-$ discussed above, we expected that the isoelectronic neutral Rh©B_9 should be a good candidate as a stable neutral M©B_9 species. Indeed, we found that both Rh©B_9 and Ir©B_9 are highly stable and symmetric D_{9h} doubly aromatic species, as revealed in the PES spectra of their anions in Figure 11-9. The HOMO–LUMO gap defined by the X and A bands was measured to be 1.21 and 1.59 eV for Rh©B_9 and Ir©B_9, respectively.

Vibrational structures were resolved in the X band in each species (Figure 11-9b,d), suggesting that slight structural changes take place between the ground state of the anion and that of the neutral. Our structural optimizations showed that the global minima of $Rh©B_9^-$ and $Ir©B_9^-$ have C_{2v} symmetry due to the Jahn–Teller effects,

whereas neutral Rh©B_9 and Ir©B_9 are perfect closed-shell molecular wheels with D_{9h} symmetry.[29]

11-4.4. M©B_{10}^- Molecular Wheels

The application of our design principle to a B_{10}-ring suggests that a transition metal with a valence of one is required to form stable M©B_{10}^- wheel structures ($x + n = 11$ for $k = 1$). However, previous experimental and computational results showed that the most promising candidate, Au©B_{10}^-, is more than 50 kcal/mol higher in energy relative to the global minimum structure, in which the Au atom is covalently bonded to a planar B_{10}^- cluster,[27] akin to a hydrogen atom.[43] The question was whether it would be possible to form metal-doped molecular wheels with B_{10} or larger boron rings.

Our extensive experimental screening of transition-metal-doped MB_n^- clusters led to a set of relatively simple PES spectra for TaB_{10}^-, as shown in Figure 11-10a.[30] The main PES features of the isoelectronic NbB_{10}^- cluster (Figure 11-10b) were observed to be similar to those of TaB_{10}^-, with additional low binding energy features (X′, A′, B′) probably due to a low-lying isomer. These observations prompted us to closely investigate the geometric structures and the bonding of these clusters. Global minimum searches for TaB_{10}^- revealed that its most stable structure possesses an unprecedented D_{10h} symmetry with a 3D "boat"-like isomer almost 9 kcal/mol higher in energy (Figure 11-11). The NbB_{10}^- cluster displays a similar set of structures, but its boat-like isomer is closer in energy to the global minimum D_{10h}-Nb@B_{10}^- structure. Most importantly, the calculated VDEs of the D_{10h} global minimum are in good agreement with the observed PES features, whereas for NbB_{10}^- the calculated VDEs for the boat-like isomer were in

good agreement with the low binding energy features. Clearly, under our experimental conditions, the boat isomer was weakly populated in the cluster beam of NbB_{10}^- because its energy was not too high relative to the global minimum molecular wheel.

We found that the relative stability of the D_{10h}-M©B_{10}^- wheel structure decreases going up the periodic table from M = Ta to V, as a result of the geometrical effects. For the valence isoelectronic VB_{10}^- cluster, we found that the wheel-type structure is only a high-lying isomer on the potential energy surface and is not present in the PES spectra.[44]

The chemical bonding analyses of the M©B_{10}^- molecular wheels are interesting. The MOs of Ta©B_{10}^-(Figure 11-12a) indicate that there are six electrons in three completely delocalized π orbitals (HOMO-2, HOMO-2′, and HOMO-3) similar to the π electron system of the other metal-doped boron clusters. However, there are no localized 5d orbitals on the Ta center, that is, Ta is in its +5 oxidation state in Ta©B_{10}^-. The AdNDP analysis gives a more complete picture of the bonding situation in Ta©B_{10}^-, as shown in Figure 11-12b. There are 10 localized 2c–2e bonds responsible for the B_{10} ring and three totally delocalized π bonds. Interestingly, we observed *five* completely delocalized σ bonds with 10 electrons, in contrast to the usual three delocalized σ bonds observed in aromatic molecular-wheel-type planar boron or doped-boron clusters up to now. The 10 delocalized σ electrons also fulfill the $4N_\sigma + 2$ Hückel rule for aromaticity.[45] Thus, Ta©B_{10}^- is doubly aromatic but with a total of 16 delocalized electrons. Therefore, the electronic design principle should be $x + 3n + k = 2n + 16$ or $x + n + k = 16$. For Ta©B_{10}^-, $x = 5$, $n = 10$, and $k = 1$. In other words, the 5d orbitals of Ta participate in the delocalized bonding with the peripheral B_{10}-ring. This bonding is critical for stabilizing

the M©B_{10}^- molecular wheels. Since Au has a filled 5d shell that cannot effectively participate in bonding with the B_{10}-ring, the corresponding Au©B_{10}^- molecular wheel is not stable.[27] In fact, even though the bonding in Nb©B_{10}^- is similar to that in Ta©B_{10}^-, Nb©B_{10}^- is less stable because the degree of the 4d bonding with the B_{10}-ring is weaker. The 3d-B_{10} bonding is even weaker, making V©B_{10}^- much less stable.[44]

11-5. Conclusions and Perspective

We have discussed recent experimental and theoretical discoveries of a new class of aromatic borometallic compounds, containing a highly coordinated central transition metal atom inside a monocyclic boron ring. Electronic design principles have been advanced that allow both rationalization of the stability of the D_{nh}-M©B_n^{k-} type molecular wheels and the prediction of new stable clusters. Research so far has focused on n = 8–10, which are the most promising size range. As concluded in a recent Perspective article by Heine and Merino,[46] "Are Ta©B_{10}^- and Nb©B_{10}^- the planar systems with the highest coordination number? We don't know." Indeed, we have not considered experimentally all the metal elements in the periodic table. The augmented design principle[45] for 6 delocalized π and 10 delocalized σ electrons predicts electronically stable M©B_{11}^- systems for valence IV metals. A more important and pertinent question is: can these molecular wheels be synthesized in bulk quantities and crystallized? Interestingly, planar monocyclic B_6 rings have been discovered recently as key structural building blocks in a multimetallic compound, $Ti_7Rh_4Ir_2B_8$.[47] A relevant question would be: what about transition metal doped boron rings in the bulk? On the other hand, because of the central position of the transition-metal atom in the M©B_n^{k-}

molecular wheels, appropriate ligands may be conceived for coordination above and below the molecular plane, rendering chemical protection and allowing syntheses of this new class of novel borometallic complexes. The examples discussed in this Account demonstrate that atomic clusters remain a fertile field to discover new structures, new chemical bonding, and maybe new nanostructures with tailored properties.

References

1 Fehlner, T. P.; Halet, J. F.; Saillard, J. Y. *Molecular Clusters: A Bridge to Solid-State Chemistry*; Cambridge University Press: Cambridge, U.K., 2007.

2 Zhai, H. J.; Alexandrova, A. N.; Birch, K. A.; Boldyrev, A. I.; Wang, L. S. Hepta- and octacoordinate boron in molecular wheels of eight- and nine-atom boron clusters: Observation and confirmation. *Angew. Chem., Int. Ed.* **2003**, *42*, 6004–6008.

3 Zhai, H. J.; Kiran, B.; Li, J.; Wang, L. S. Hydrocarbon analogues of boron clusters - planarity aromaticity and antiaromaticity. *Nat. Mater.* **2003**, *2*, 827–833.

4 Alexandrova, A. N.; Zhai, H. J.; Wang, L. S.; Boldyrev, A. I. Molecular wheel B_8^{2-} as a new inorganic ligand. Photoelectron spectroscopy and ab initio characterization of LiB_8^-. *Inorg. Chem.* **2004**, *43*, 3552– 3554.

5 Alexandrova, A. N.; Boldyrev, A. I.; Zhai, H. J.; Wang, L. S. Electronic structure, isomerism, and chemical bonding in B_7^- and B_7. *J. Phys. Chem. A* **2004**, *108*, 3509–3517.

6 Kiran, B.; Bulusu, S.; Zhai, H. J.; Yoo, S.; Zeng, X. C.; Wang, L. S. Planar-to-tubular structural transition in boron clusters: B_{20} as the embryo of single-walled boron nanotubes. *Proc. Natl. Acad. Sci. U.S.A.* **2005**, *102*, 961– 964.

7 Alexandrova, A. N.; Boldyrev, A. I.; Zhai, H. J.; Wang, L. S. All-boron aromatic clusters as potential new inorganic ligands and building blocks in chemistry. *Coord. Chem. Rev.* **2006**, *250*, 2811– 2866.

8 Sergeeva, A. P.; Zubarev, D. Y.; Zhai, H. J.; Boldyrev, A. I.; Wang, L. S. Photoelectron spectroscopic and theoretical study of B_{16}^- and B_{16}^{2-}: An all-boron naphthalene. *J. Am. Chem. Soc.* **2008**, *130*, 7244– 7246.

9 Huang, W.; Sergeeva, A. P.; Zhai, H. J.; Averkiev, B. B.; Wang, L. S.; Boldyrev, A. I. A concentric planar doubly π-aromatic B_{19}^- cluster. *Nat. Chem.* **2010**, *2*, 202– 206.

10 Sergeeva, A. P.; Averkiev, B. B.; Zhai, H. J.; Boldyrev, A. I.; Wang, L. S. All-boron analogues of aromatic hydrocarbons: B_{17}^- and B_{18}^-. *J. Chem. Phys.* **2011**, 134224304.

11 (a) Piazza, Z. A.; Li, W. L.; Romanescu, C.; Sergeeva, A. P.; Wang, L. S.; Boldyrev, A. I. A photoelectron spectroscopy and ab initio study of B_{21}^-: Negatively charged boron clusters continue to be planar at 21. *J. Chem. Phys.* **2012**, 136104310. (b) Sergeeva, A. P.; Piazza, Z. A.; Romanescu, C.; Li, W. L.; Boldyrev, A. I.; Wang, L. S. $B_{22}^-$and B_{23}^-: All-boron analogues of anthracene and phenanthrene. *J. Am. Chem. Soc.* **2012**, *134*, 18065– 18073.

12 Oger, E.; Crawford, N. R. M.; Kelting, R.; Weis, P.; Kappes, M. M.; Ahlrichs, R. Boron cluster cations: Transition from planar to cylindrical structures. *Angew. Chem., Int. Ed.* **2007**, *46*, 8503– 8506.

13 Tai, T. B.; Tam, N. M.; Nguyen, M. T. Structure of boron clusters revisited, B_n with n = 14–20. *Chem. Phys. Lett.* **2012**, *530*, 71– 76.

14 The © symbol is used to denote planar atom-centered wheel type structures. It was first suggested in ref 28.

15 Jimenez-Halla, J. O. C.; Islas, R.; Heine, T.; Merino, G. B_{19}^-: An aromatic Wankel motor. *Angew. Chem., Int. Ed.* **2010**, *49*, 5668– 5671.

16 Martinez-Guajardo, G.; Sergeeva, A. P.; Boldyrev, A. I.; Heine, T.; Ugalde, J. M.; Merino,G. Unraveling phenomenon of internal rotation in B_{13}^+ through chemical bonding analysis. *Chem. Commun.* **2011**, *47*, 6242– 6244.

17 Zubarev, D. Y.; Boldyrev, A. I. Developing paradigms of chemical bonding: Adaptive natural density partitioning. *Phys. Chem. Chem. Phys.* **2008**, *10*, 5207-5217.

18 (a) Chandrasekhar, J.; Jemmis, E. D.; Schleyer, P. v. R. Double aromaticity-aromaticity in orthogonal planes-3,5-dehydrophenyl cation. *Tetrahedron Lett.* **1979**, *39*, 3707–3710. (b) McEwen, A. B.; Schleyer, P. v. R. In-plane aromaticity and trishomoaromaticity: A computational evaluation. *J. Org. Chem.* **1986**, *51*, 4357– 4368. (c) Schleyer, P. v. R.; Jiao, H.; Glukhovtsev, M. N.; Chandrasekhar, J.; Kraka, E. Double aromaticity in the 3,5-dehydrophenyl cation and in cyclo[6]carbon. *J. Am. Chem. Soc.* **1994**, *116*, 10129– 10134.

19 (a) Exner, K.; Schleyer, P. v. R. Planar hexacoordinate carbon: A viable possibility. *Science* **2000**, *290*, 1937– 1940. (b) Wang, Z. X.; Schleyer, P. v. R. Construction principles of "hyparenes": Families of molecules with planar pentacoordinate carbons. *Science* **2001**, *292*, 2465– 2469.

20 Erhardt, S.; Frenking, G.; Chen, Z. F.; Schleyer, P. v. R. Aromatic boron wheels with more than one carbon atom in the center: C_2B_8, $C_3B_9^{3+}$, and $C_5B_{11}^{+}$. *Angew. Chem., Int. Ed.* **2005**,*44*, 1078– 1082.

21 Islas, R.; Heine, T.; Ito, K.; Schleyer, P. v. R.; Merino, G. Boron rings enclosing planar hypercoordinate group 14 elements. *J. Am. Chem. Soc.* **2007**, *129*, 14767– 14774.

22 Wang, L. M.; Huang, W.; Averkiev, B. B.; Boldyrev, A. I.; Wang, L. S. CB_7^{-}: Experimental and theoretical evidence against hypercoordinate planar carbon. *Angew. Chem., Int. Ed.* **2007**,*46*, 4550– 4553.

23 Averkiev, B. B.; Zubarev, D. Y.; Wang, L. M.; Huang, W.; Wang, L. S.; Boldyrev, A. I. Carbon avoids hypercoordination in CB_6^{-}, CB_6^{2-}, and $C_2B_5^{-}$ planar carbon-boron clusters. *J. Am. Chem. Soc.* **2008**, *130*, 9248– 9250.

24 Galeev, T. R.; Ivanov, A. S.; Romanescu, C.; Li, W. L.; Bozhenko, K. V.; Wang, L. S.; Boldyrev, A. I. Molecular wheel to monocyclic ring transition in boron-carbon mixed clusters $C_2B_6^{-}$ and $C_3B_5^{-}$. *Phys. Chem. Chem. Phys.* **2011**, *13*, 8805– 8810.

25 Galeev, T. R.; Romanescu, C.; Li, W. L.; Wang, L. S.; Boldyrev, A. I. Valence isoelectronic substitution in the B_8^{-} and B_9^{-} molecular wheels by an Al dopant

atom: Umbrella-like structures of AlB_7^- and AlB_8^-. *J. Chem. Phys.* **2011**, 135104301.

26 (a) Li, W. L.; Romanescu, C.; Galeev, T. R.; Wang, L. S.; Boldyrev, A. I. Aluminum avoids the central position in AlB_9^- and AlB_{10}^-: Photoelectron spectroscopy and ab initio study. *J. Phys. Chem. A* **2011**, *115*, 10391– 10397. (b) Romanescu, C.; Sergeeva, A. P.; Li, W. L.; Boldyrev, A. I.; Wang, L. S. Planarization of B_7^- and B_{12}^-clusters by isoelectronic substitution: AlB_6^- and AlB_{11}^-. *J. Am. Chem. Soc.* **2011**, *133*, 8646–8653.

27 Zhai, H. J.; Miao, C. Q.; Li, S. D.; Wang, L. S. On the analogy of B–BO and B–Au chemical bonding in $B_{11}O^-$ and $B_{10}Au^-$ clusters. *J. Phys. Chem. A* **2010**, *114*, 12155– 12161.

28 Romanescu, C.; Galeev, T. R.; Li, W. L.; Boldyrev, A. I.; Wang, L. S. Aromatic metal-centered monocyclic boron rings: $Co©B_8^-$ and $Ru©B_9^-$. *Angew. Chem., Int. Ed.* **2011**, *50*, 9334-9337.

29 Li, W. L.; Romanescu, C.; Galeev, T. R.; Piazza, Z. A.; Boldyrev, A. I.; Wang, L. S. Transition-metal-centered nine-membered boron rings: $M©B_9$ and $M©B_9^-$ (M = Rh, Ir) . *J. Am. Chem. Soc.* **2012**, *134*, 165-168.

30 Galeev, T. R.; Romanescu, C.; Li, W. L.; Wang, L. S.; Boldyrev, A. I. Observation of the highest coordination number in planar species: Decacoordinated $Ta©B_{10}^-$ and $Nb©B_{10}^-$ anions. *Angew. Chem., Int. Ed.* **2012**, *51*, 2101-2105.

31 Wang, L. S.; Cheng, H. S.; Fan, J. W. Photoelectron spectroscopy of size-selected transition-metal clusters: Fe_n^-, n = 3–24. *J. Chem. Phys.* **1995**, 102, 9480– 9493

32 Frisch, M. J. Gaussian 09, Rev. B.01. Gaussian Inc.: Wallingford, CT, **2009**.

33 ADF 2010. SCM, Theoretical Chemistry, Vrije Universiteit: Amsterdam, the Netherlands, **2010**.

34 Varetto, U. Molekel 5.4.0.8. Swiss National Supercomputing Centre: Manno (Switzerland), **2009**.

35 Averkiev, B. B.; Boldyrev, A. I. Theoretical design of planar molecules with a nona- and decacoordinate central atom. *Russ. J. Gen. Chem.* **2008**, *78*, 769– 773.

36 Ito, K.; Pu, Z.; Li, Q. S.; Schleyer, P. v. R.Cyclic boron clusters enclosing planar hypercoordinate cobalt, iron, and nickel. *Inorg. Chem.* **2008**, *47*, 10906– 10910.

37 Luo, Q. O. Boron rings containing planar octa- and enneacoordinate cobalt, iron and nickel metal elements. *Sci. China, Ser. B: Chem.* **2008**, *51*, 607– 613.

38 Pu, Z. F.; Ito, K.; Schleyer, P. v. R.; Li, Q. S. Planar hepta-, octa-, nona-, and decacoordinate first row d-block metals enclosed by boron rings. *Inorg. Chem.* **2009**, *48*,10679– 10686.

39 Miao, C. Q.; Guo, J. C.; Li, S. D. $M@B_9$ and $M@B_{10}$ molecular wheels containing planar nona- and deca-coordinate heavy group 11, 12, and 13 metals (M = Ag, Au, Cd, Hg, In, Tl) . *Sci. China, Ser. B: Chem.* **2009**, *52*, 900– 904.

40 Averkiev, B. B.; Wang, L. M.; Huang, W.; Wang, L. S.; Boldyrev, A. I. Experimental and theoretical investigations of CB_8^-: Towards rational design of

hypercoordinated planar chemical species. *Phys. Chem. Chem. Phys.* **2009**, *11*, 9840– 9849.

41 (a) Schleyer, P. v. R.; Maerker, C.; Dransfeld, A.; Jiao, H.; Hommes, N. J. R. v. E. Nucleus-independent chemical shifts: A simple and efficient aromaticity probe. *J. Am. Chem. Soc.* **1996**, *118*, 6317– 6318. (b) Chen, Z.; Wannere, C. S.; Corminboeuf, C.; Puchta, R.; Schleyer, P. v. R. Nucleus-independent chemical shifts (NICS) as an aromaticity criterion. *Chem. Rev.* **2005**, *105*, 3842– 3888. And its refinement: (c) Fallah-Bagher-Shaidaei, H.; Wannere, C. S.; Corminboeuf, C.; Puchta, R.; Schleyer, P. v. R. Which NICS aromaticity index for planar π rings is best? *Org. Lett.* **2006**, *8*, 863– 866.

42 Romanescu, C.; Galeev, T. R.; Li, W. L.; Boldyrev, A. I.; Wang, L. S. Experimental and computational evidence of octa- and nona-coordinated planar iron-doped boron clusters: $Fe©B_8^-$ and $Fe©B_9^-$. *J. Organomet. Chem.* **2012**, *721–722*, 148– 154.

43 Wang, L. S. Covalent gold. *Phys. Chem. Chem. Phys.* **2010**, *12*, 8694– 8705.

44 Li, W. L.; Romanescu, C.; Piazza, Z. A.; Wang, L. S. Geometric requirements for transition-metal-centered boron wheel clusters: The case of VB_{10}^-. *Phys. Chem. Chem. Phys.* **2012**, *14*,13663– 13669.

45 The electronic design principle can be expressed generally as $x + n + k = (4N_\sigma+2) + (4N_\pi + 2)$ for double σ- and π-aromaticity. However, we expect that N_σ should be equal to or larger than N_π for truly stable molecular wheels because σ bonding is usually more favorable than π bonding due to better in-plane orbital overlap.

46 Heine, T.; Merino, G. What is the maximum coordination number in a planar structure? *Angew. Chem., Int. Ed.* **2012**, *51*, 4275– 4276.

47 Fokwa, B. P. T.; Hermus, M. All-boron planar B_6 ring in the solid-state phase $Ti_7Rh_4Ir_2B_8$. *Angew. Chem., Int. Ed.* **2012**, *51*, 1702– 1705.

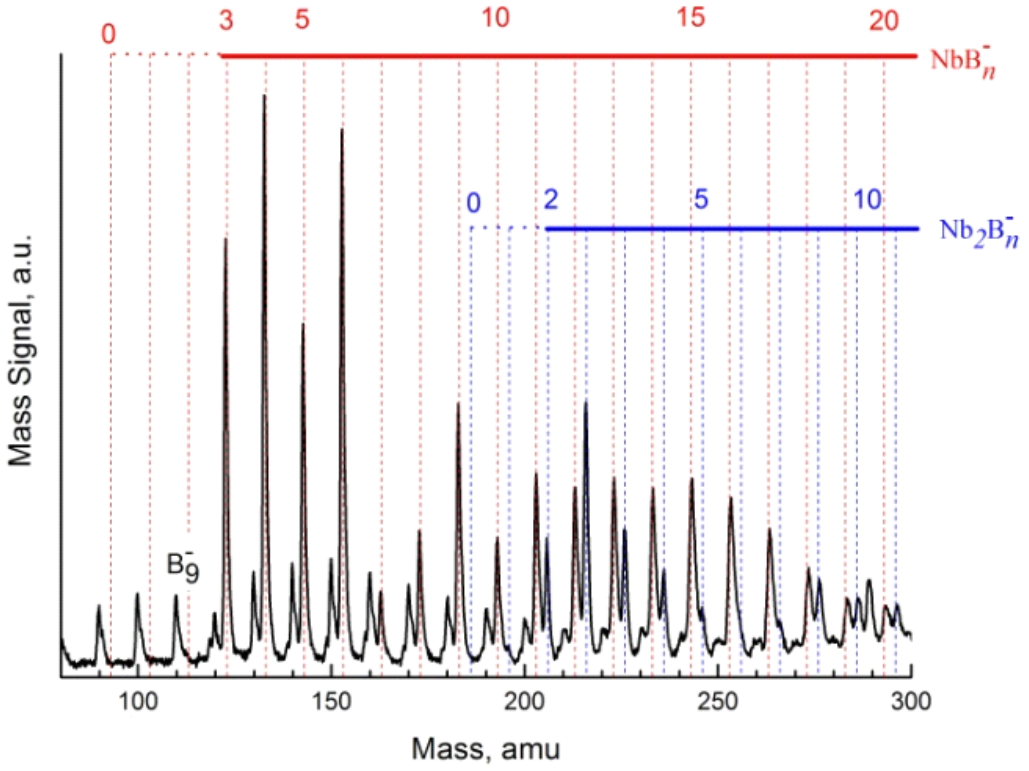

FIGURE 11-1. Mass spectrum from the laser vaporization of a mixed ^{10}B/Nb target. The vertical dashed lines represent the assignment of the NbB_n^- (tall lines, red) and $Nb_2B_n^-$ clusters (short lines, blue). The remaining peaks are due to the B_n^- clusters. Under the conditions that this spectrum was taken, the NbB_n^- series starts from n = 3, and the $Nb_2B_n^-$ series starts from n = 2.

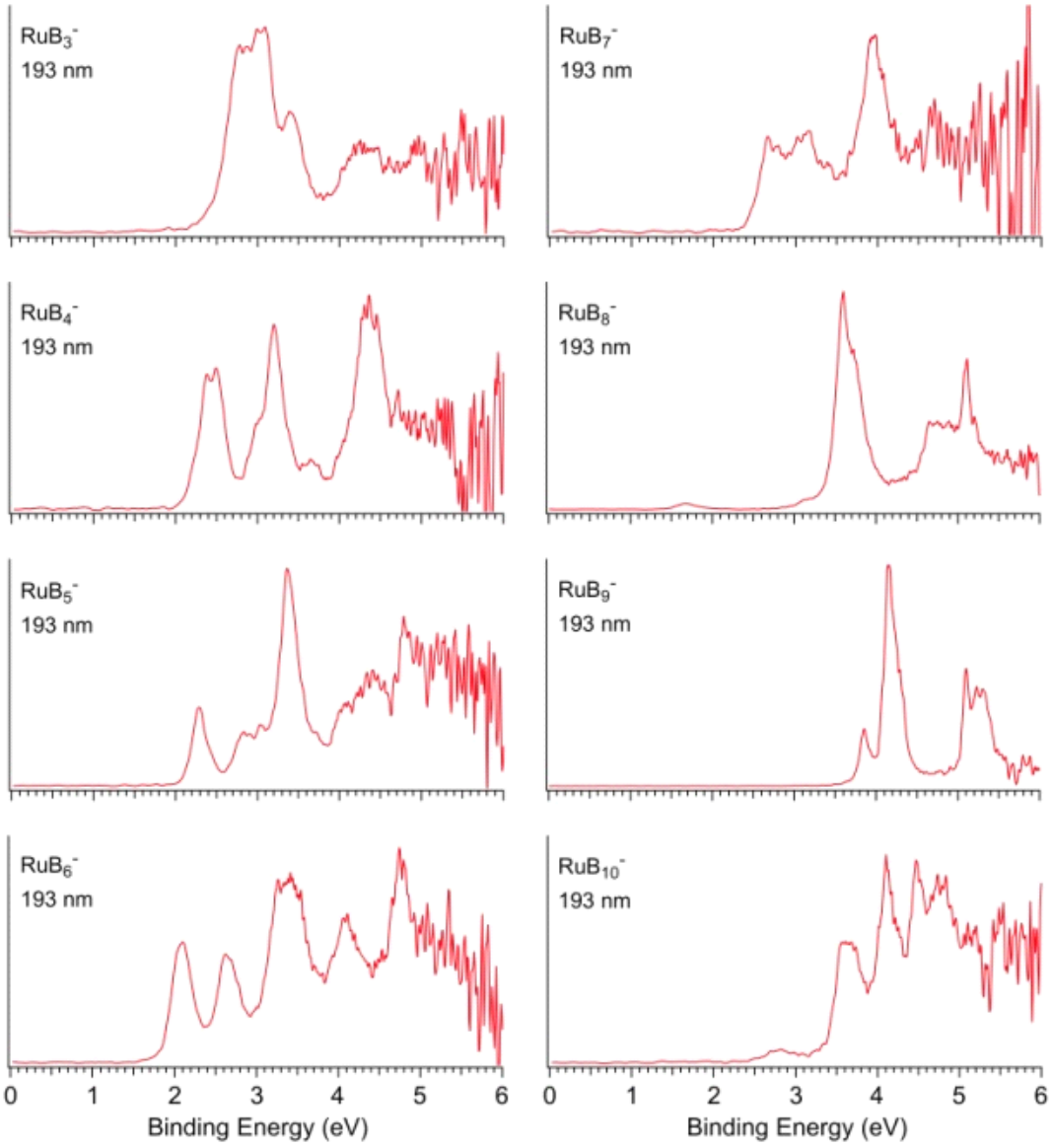

FIGURE 11-2. Photoelectron spectra of RuB_n^- (n = 3–10) at 193 nm (6.424 eV).

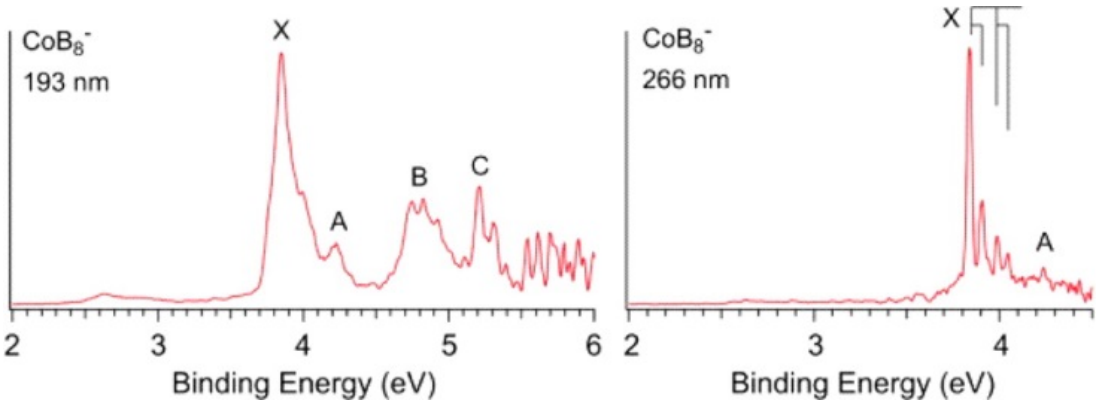

FIGURE 11-3. Photoelectron spectra of $Co©B_8^-$ at 193 nm (left) and 266 nm (right).(28) The vertical lines in the 266 nm spectrum indicate vibrational structures. Reproduced from ref 28. Copyright 2011 Wiley.

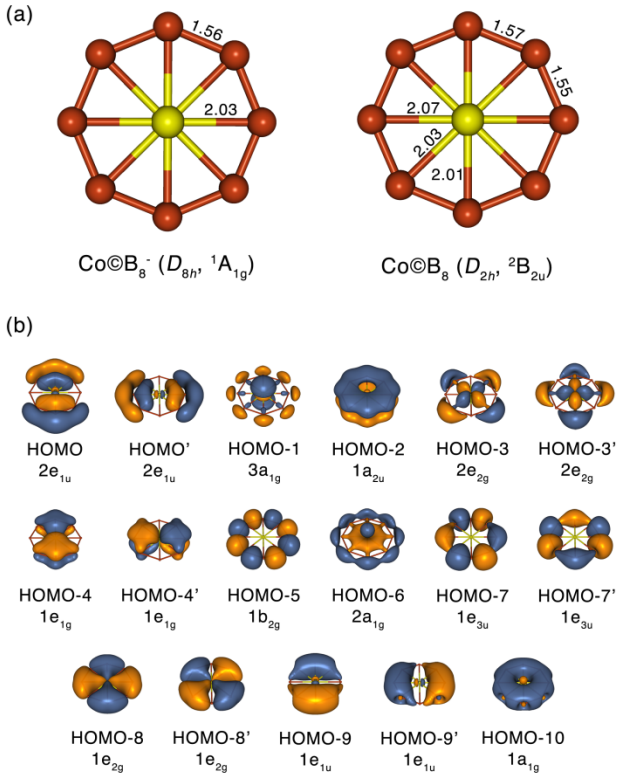

FIGURE 11-4. (A) Optimized structures for $Co©B_8^-$ and $Co©B_8$ along with their point group symmetries and spectroscopic states (bond lengths are given in Å). (B) Molecular orbitals and symmetries of $Co©B_8^-$.

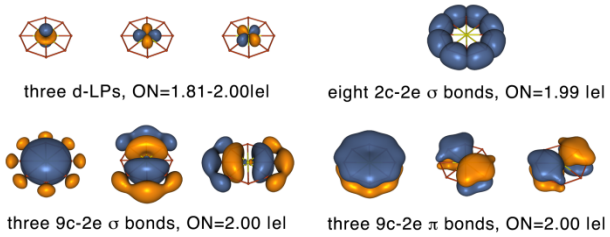

FIGURE 11-5. AdNDP analysis for $Co©B_8^-$

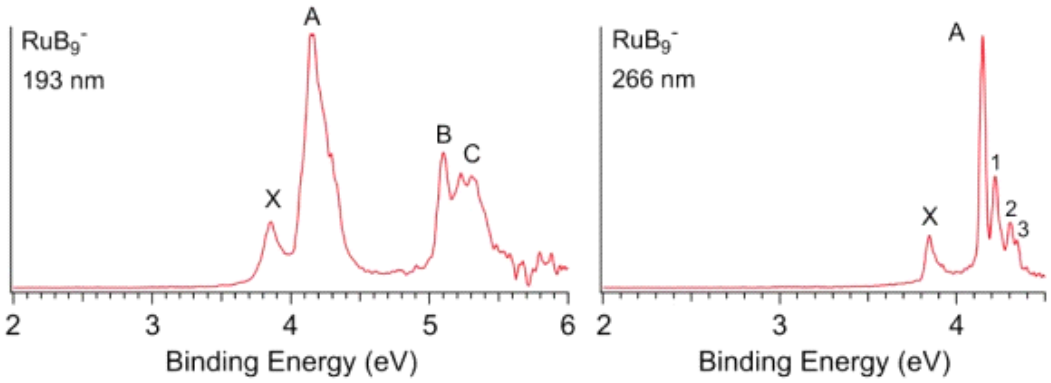

FIGURE 11-6. Photoelectron spectra of RuB_9^- at 193 nm (left) and 266 nm (right). The numbers in the 266 nm spectrum indicate vibrational structures. Reproduced from ref 28. Copyright 2011 Wiley.

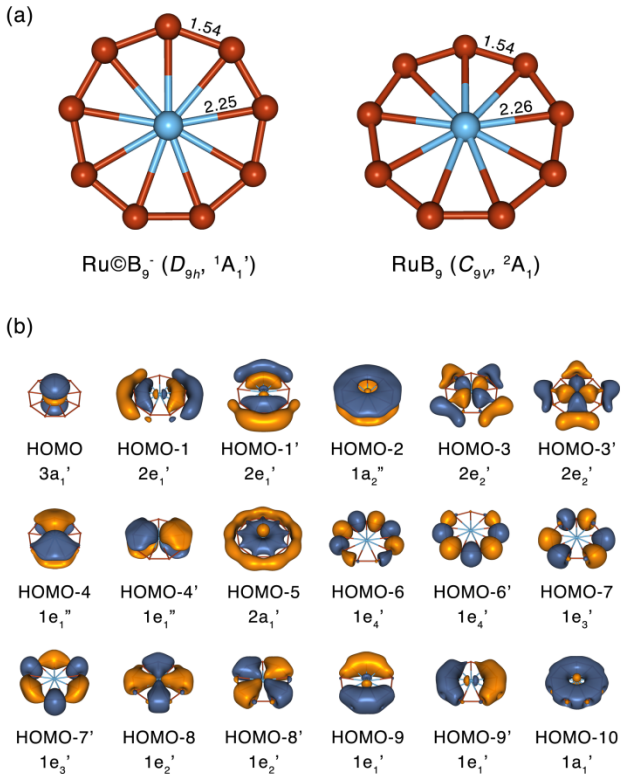

FIGURE 11-7. Optimized structures for $Ru©B_9^-$ and $Ru©B_9$ along with their point group symmetries and spectroscopic states (bond lengths are given in Å). (28) (B) Molecular orbitals and symmetries of $Ru©B_9^-$

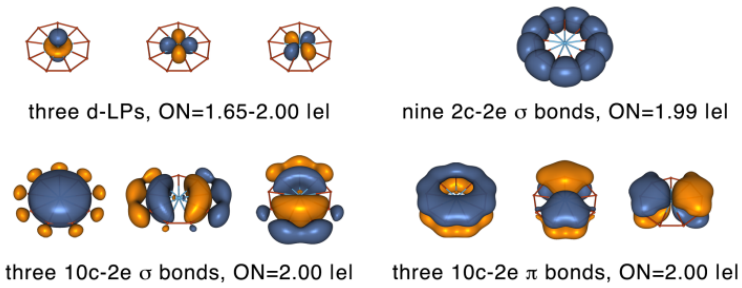

FIGURE 11-8. AdNDP analysis for $Ru©B_9^-$.

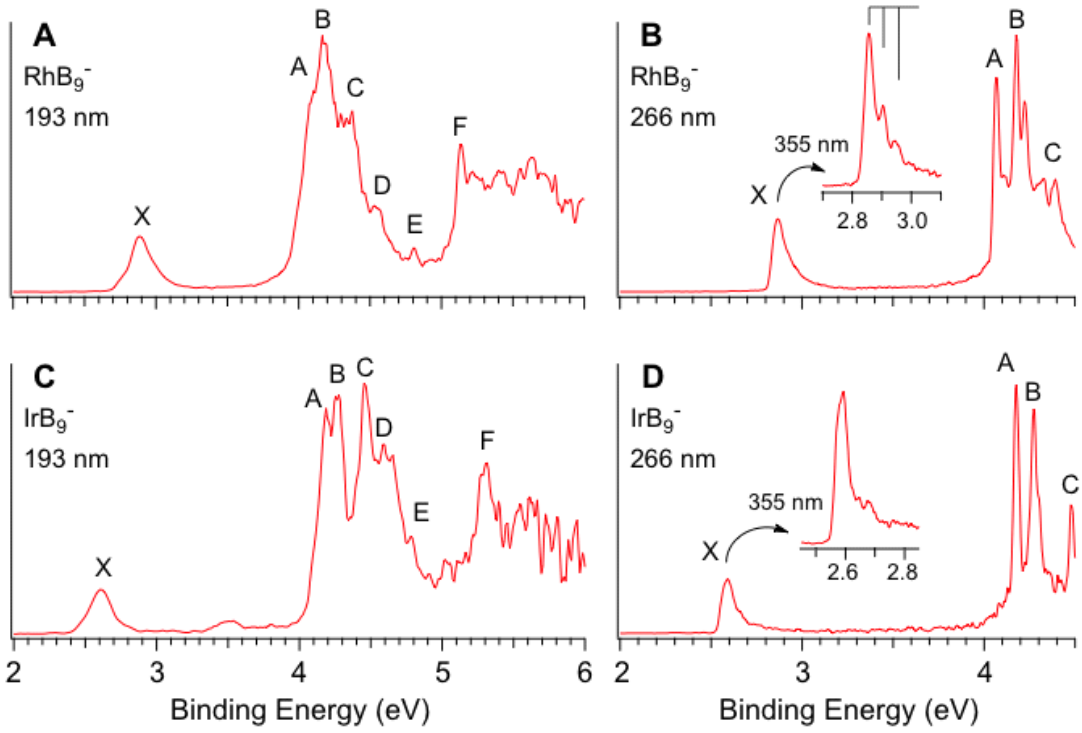

FIGURE 11-9. Photoelectron spectra of RhB_9^- and IrB_9^- at 355, 266, and 192 nm. The vertical lines in the 355 spectrum of RhB_9^- indicate vibrational structures. Reproduced from ref 29. Copyright 2012 American Chemical Society.

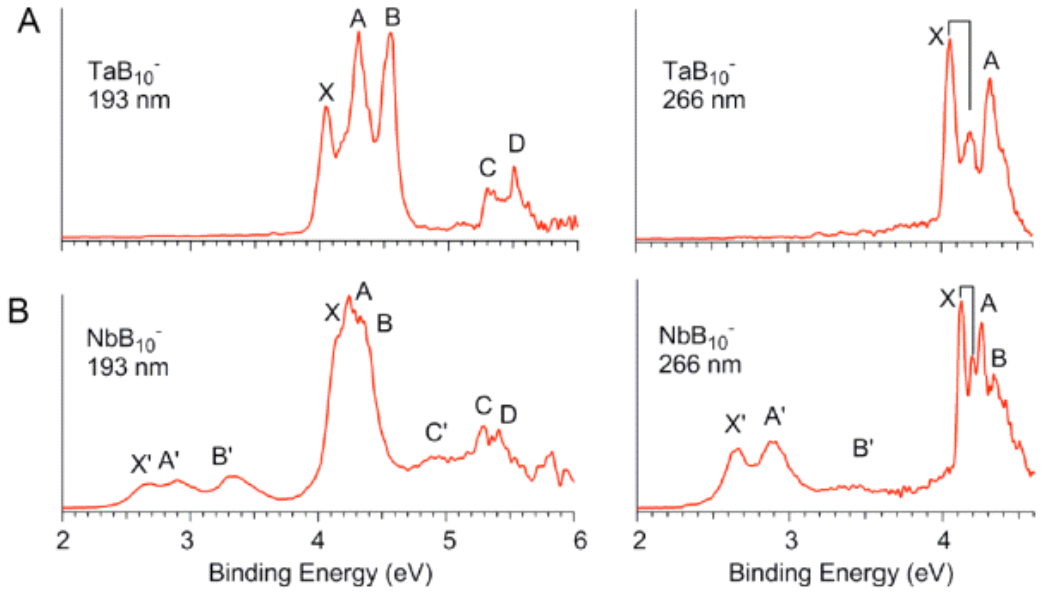

FIGURE 11-10. Photoelectron spectra of (A) TaB_{10}^- and (B) NbB_{10}^- at 193 and 266 nm. The vertical lines in the 266 nm spectra indicate vibrational structures. Reproduced from ref 30. Copyright 2012 Wiley.

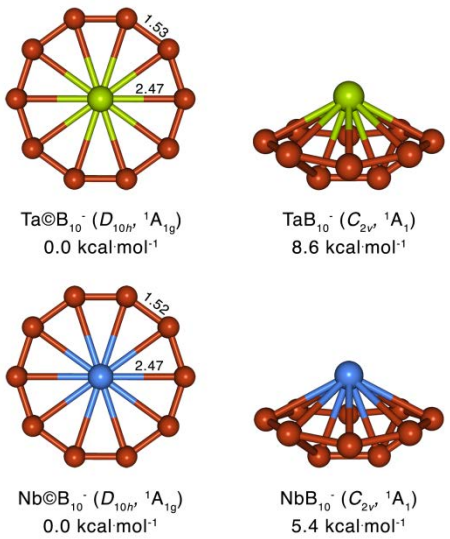

FIGURE 11-11. Optimized structures of the two lowest energy isomers of TaB_{10}^- and NbB_{10}^-, their point group symmetries, spectroscopic states, and relative energies (bond lengths are given in Å). Reproduced from ref 30. Copyright 2012 Wiley

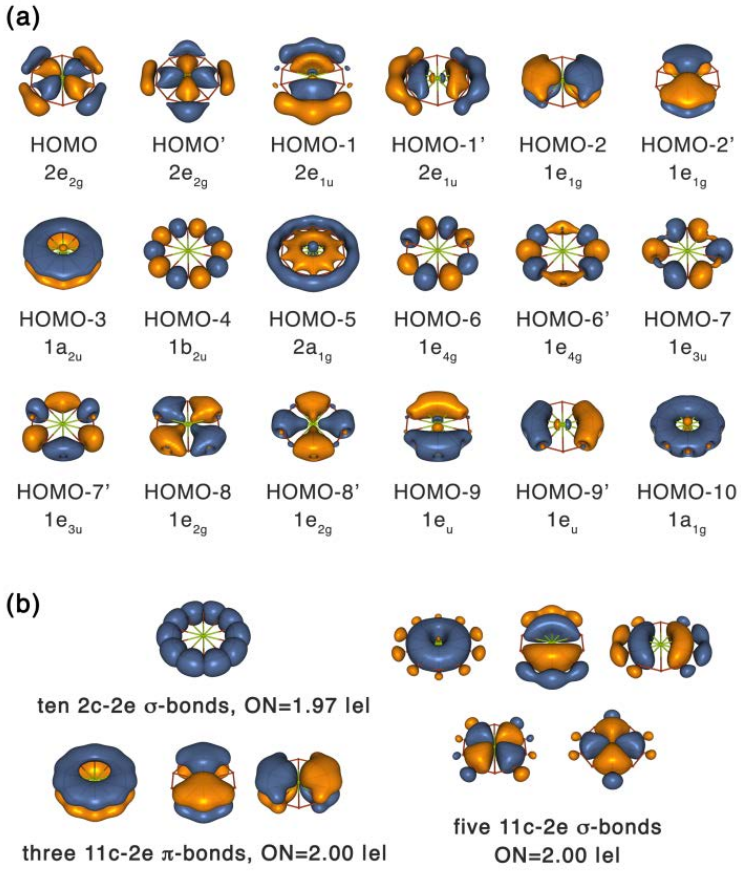

FIGURE 11-12. (a) Molecular orbitals and symmetries of $Ta©B_{10}^-$. (b) AdNDP analysis for $Ta©B_{10}^-$.

CHAPTER 12

PLANARITY TAKES OVER IN THE $C_xH_xP_{6-x}$ (x = 0–6) SERIES AT x = 4 *

Abstract

In this work we examine a structural transition from non-planar three-dimensional structures to planar benzene-like structures in the $C_xH_xP_{6-x}$ (x = 0–6) series. The global minima of P_6, CHP_5, and $C_2H_2P_4$ species are benzvalene-like structures. The benzvalene and benzene-like structures of $C_3H_3P_3$ are close in energy with the former being slightly more stable at our best level of theory. The transition occurs at x = 4 ($C_4H_4P_2$), where the benzene-like structures become significantly more stable than the benzvalene-like structures. We show that the pseudo Jahn–Teller effect, which is responsible for the deformation of planar P_6, CHP_5, and $C_2H_2P_4$ structures, is completely suppressed at x = 3 (benzene-like structures of $C_3H_3P_3$). We present $NICS_{zz}$ values of all the benzene-like isomers in the series.

12-1. Introduction

Hexaphosphabenzene is a valence isoelectronic analogue of benzene and similar to the latter is anticipated to have a planar structure due to resonance stabilization. Indeed, in 1985 Scherer *et al.*[1] obtained a triple-decker sandwich complex $\{(\eta^5\text{-}Me_5C_5)Mo\}_2(\mu,\eta^6\text{-}P_6)$, containing a planar P_6 ring with equal P–P bond lengths. However, theoretical calculations revealed that there are at least 7 non-planar P_6 isomers (Fig. 12-1) lower in energy than the planar benzene-like D_{6h} structure **I.11**.[2–11] According

* Coauthored by Timur R. Galeev and Alexander I. Boldyrev. Reproduced from *Phys. Chem. Chem. Phys*. **2011**, *13*, 20549-20556 with permission from the PCCP Owner Societies

to the most accurate calculations by Hiberty and Volatron,[11] the global minimum structure of P_6 is the benzvalene-like structure **I.1** with the prismane-like isomer **I.2** being the second lowest and the other isomers lying significantly higher in energy. Moreover, the D_{6h} structure **I.11** is not even a local minimum, but a second-order saddle point. Geometry optimization along the imaginary modes leads to the distorted structure **I.10** (D_2,^{1}A).

218 structures with the C_6H_6 stoichiometry were proposed in the literature.[12–16] A systematic computational study of the C_6H_6 species revealed 215 minimum energy structures (isomers) assuming the tetravalency for carbon, with 84 structures being within 100 kcal mol^{-1} in energy relative to the benzene global minimum structure.[16] On the other hand, all these alternative isomers of C_6H_6 were found to be significantly higher in energy than the planar D_{6h} benzene structure.[16]

A structural transition from the non-planar three-dimensional structures to the planar benzene-like structures is expected to take place in the $C_xH_xP_{6-x}$ (x = 0–6) series upon substitution of the P atoms by the CH groups. In this article we present our computational results for the series and show that benzene-like structures become the lowest energy isomers at x = 4 ($C_4H_4P_2$). The above-mentioned deformation of the D_{6h} structure of P_6 was traced in the series. We show that the pseudo Jahn–Teller (PJT) effect, which is responsible for this deformation, is completely suppressed at x = 3 (benzene-like structures of $C_3H_3P_3$).

A 2D–3D transition was observed in the series of mixed boron–aluminium cluster ions, $B_{6-n}Al_n^{2-}$ (n = 0–6), and their lithium salts.[17] It was shown that the transition occurs

late in the series, at BAl_5^{2-}, and that covalent bonding has an extraordinary effect that governs the cluster shape more than does the delocalized bonding.

12-2. Theoretical methods

Computational search for the global minima of the P_6, and CHP_5 species was performed using the Coalescence Kick (CK) program written by B. B. Averkiev.[18] The CK method subjects large populations of randomly generated structures to a coalescence procedure in which all atoms are pushed gradually to the molecular center of mass to avoid the generation of fragmented structures and are then optimized to the nearest local minima. The CK calculations were performed using the B3LYP[19–21] hybrid method with the 6-31G**[22] split-valence basis set. Low-lying isomers were reoptimized with follow-up frequency calculations at the B3LYP level of theory using the 6-311++G** basis set.[23–25] The benzvalene, prismane, Dewar benzene, and benzene-like structures were found to be among the lowest isomers of both species. We optimized all possible structures derived from these isomers and the benzene-like structure by the substitution of the P atoms with the CH groups leading to the $C_2H_2P_4$, $C_3H_3P_3$, $C_4H_4P_2$, C_5H_5P, and C_6H_6 stoichiometries. Single point energy calculations were performed using the restricted coupled cluster RCCSD(T) method[26–28] with the cc-pvDZ and cc-pvTZ basis sets[29–33] at the B3LYP/6-311++G** optimized geometries. Core electrons were frozen in treating the electron correlation at the RCCSD(T) levels of theory. All calculations were performed with the Gaussian 03 program.[34] RCCSD(T)/cc-pvXZ (X = D, T) energies were extrapolated to complete basis set (CBS) using the Truhlar formula.[35,36] Chemical bonding analysis was performed using Natural Bond Orbital Analysis[37,38] and Adaptive

Natural Density Partitioning (AdNDP) method[39,40] at B3LYP/6-311+G. Aromaticity in planar benzene-like species was assessed using the Nuclear Independent Chemical Shift ($NICS_{zz}$) index.[41,42] Molecular structure visualization was performed with the MOLDEN 3.4[43] and Molekel 5.4.0.8[44] programs.

12-3. Results and discussion

We examined two transitions in the $C_xH_xP_{6-x}$ (x = 0–6) series. First, we traced where the pseudo Jahn–Teller effect, responsible for the distortion found in the D_{6h} P_6 structure, is completely suppressed, and thebenzene-like isomers become local minima. Then, we wanted to find at what x the benzene-like isomers become lower in energy than the benzvalene-like structures of the same stoichiometry.

12-3.1. P_6 isomers

All low-lying isomers of P_6 ($\Delta E < 50$ kcal mol^{-1}, B3LYP/6-31G*) revealed by the CK search were reoptimized at B3LYP/6-311+G* and these geometries were used for single point energy calculations at RCCSD(T)/cc-pvDZ, RCCSD(T)/cc-pvTZ, RCCSD(T)/CBS (see Fig. 12-2). Seven structures studied by Hiberty and Volatron[11] and their relative energies at our highest level of theory (RCCSD(T)/CBS//B3LYP/6-311+G*) are presented in Fig. 12-1. We used the names of the analogous benzene valence isomers for the corresponding structures of P_6 and other species of the studied series: benzvalene (**I.1**), prismane (**I.2**), chair (**I.3**), Dewar benzene (**I.4**), bicyclopropenyl (**I.8**), benzene (**I.11**) and distorted benzene (**I.10**).

Our results for P_6 are very similar to those by Hiberty and Volatron.[11] The most stable isomer for P_6 is the benzvalene structure **I.1**, with the prismane structure **I.2** being

the second lowest isomer (3.0 kcal mol^{-1}above the global minimum). The D_{6h} benzene-like planar structure **I.11** is not a minimum, but is a second-order saddle point. Geometry optimization along the imaginary frequency modes leads to the isomer **I.10**. The structure **I.11** is 34.9 kcal mol^{-1} higher in energy than the global minimum structure **I.1**.

Jahn–Teller vibronic effects were shown by Bersuker[45–47] to be the only source of instability of high-symmetry configurations of polyatomic systems. The distortion of the structure **I.11** into the structure **I.10** along the e_{2u} doubly degenerate frequency mode occurs due to the pseudo Jahn–Teller effect (PJT), resulting from vibronic coupling of HOMO − 1 (e_{2g}) and LUMO (e_{2u}). Indeed, the direct product of their symmetries contains the symmetry of the imaginary mode:

$$e_{2g} \otimes e_{2u} = a_{1u} \oplus a_{2u} \oplus e_{2u} \qquad (1)$$

Thus, the symmetry rule[48] for the PJT effect is satisfied as is the second condition:[48] the symmetry of the imaginary mode (e_{2u}) of the D_{6h} structure corresponds to the totally symmetric (*a*) mode in the distorted D_2 isomer. The HOMO − 1 and LUMO gap is 8.29 eV (HF/cc-pvTZ//B3LYP/6-311+G*). Notice that the two MOs are of σ-type (HOMO − 1 (e_{2g})) and π-type (LUMO (e_{2u})), thus, their vibronic coupling is responsible for the out-of-plane distortion. The other two closest in energy OMO–UMO pairs [HOMO − 2 (e_{1u}) – LUMO + 2 (b_{2g}) and HOMO (e_{1g}) − LUMO + 3 (e_{1u})], satisfying the symmetry rule, have significantly higher energy gaps (12.45 and 13.23 eV, respectively). Apparently, the 8.29 eV OMO–UMO gap is small enough for the PJT effect to take place. The distorted structure **I.10** is only 2.7 kcal mol^{-1} lower in energy than the structure **I.11**.

The planarization of the P_6 ring in the above-mentioned $\{(\eta^5\text{-}Me_5C_5)Mo\}_2(\mu,\eta^6\text{-}P_6)$[1] triple-decker sandwich complex is due to the suppression of the PJT effect. Two mechanisms for the suppression of the PJT were proposed in the literature: (1) through the gap increase between the interacting OMO–UMO pair in the external electrostatic field of cations[49] and (2) through occupying the interacting UMO with an electron pair upon complexation.[50] However, additional studies are required to understand which mechanism takes place in this particular case.

We would like to stress that the benzene-like P_6 structure is aromatic, but aromaticity itself is not sufficient to stabilize the planar geometry and the PJT effect leads to the distortion.

We performed the AdNDP analysis for the seven representative low-lying P_6 structures (Fig. 12-3).

The AdNDP analysis of structures **I.1**, **I.2**, **I.4**, and **I.8** (Fig. 12-3a, b, d, and e, respectively) revealed classical Lewis model bonding elements: a lone pair on each phosphorus atom; a two-center–two-electron (2c–2e) σ-bond in every pair of adjacent P atoms; and an additional 2c–2e π-bond between adjacent 2-coordinated P atoms. Occupation numbers (ON) of all these elements are above 1.92 |e|. Thus, all these isomers can be well represented by classical Lewis structures.

The chemical bonding in the chair structure **I.3** is unusual. Hiberty and Volatron,[11] based on fragment orbital analysis, concluded that two linkages between the two P_3 fragments are of one-electron hemibond type. They proposed two ways of describing bonding in the structure **I.3**: with formula A or using resonance scheme B:

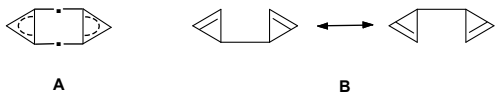

We performed NBO analysis, which was developed by Weinhold to describe resonance structures, and we obtained one of the resonance structures shown above in accordance with the Hiberty–Volatron scheme B. We then performed the AdNDP analysis (Fig. 12-3c), which revealed a lone pair on each P atom and six 2c–2e P–P σ-bonds. Then, one 3c–2e π-bond in every P_3 triangle was revealed with the user-directed form of the AdNDP analysis as well as a 4c–2e bond, responsible for bonding between the two P_3 triangles. The described bonding pattern is consistent with the Hiberty–Volatron scheme A. Thus, the bonding in this isomer cannot be represented by a single Lewis structure and requires a resonance of two Lewis structures, or it can be described by a single formula with the delocalized bonding elements (3c–2e and 4c–2e bonds) (Fig. 12-3c).

The AdNDP analysis revealed localized (2c–2e σ-bonds and lone pairs) and delocalized (6c-2e π-bonds) bonding elements in the benzene-like structure **I.11** (Fig. 12-3g) similar to the previously reported AdNDP bonding pattern of the C_6H_6 benzene molecule.[51] The distortion towards **I.10** due to the PJT effect does not significantly disturb the bonding picture (Fig. 12-3f).

12-3.2. CHP_5 isomers

The CK search of the CHP_5 species revealed that the potential energy surface has more low-lying structures than that of P_6 with the benzvalene structure **II.1** still being the lowest one. The lowest energy ($\Delta E < 30$ kcal mol^{-1}, B3LYP/6-31G**) structures found

by the CK search were reoptimized at the B3LYP/6-311++G** level of theory, and higher levels were then used for single point energy calculations (see Fig. 12-4 for CCSD(T)/CBS, CCSD(T)/cc-pvTZ, CCSD(T)/cc-pvDZ, and B3LYP/6-311++G** relative energies). The benzvalene structures **II.1**, **II.2**, and **II.4** and the prismane structure **II.3** are the lowest isomers (Fig. 12-4).

Four representative isomers of P_6 and CHP_5 are shown in Fig. 12-5a and b, respectively. The benzene-like structure **II.16** is 28.2 kcal mol^{-1} higher in energy. It is a local minimum at the B3LYP/6-31G** and B3LYP/6-311++G** levels of theory, but two imaginary frequency modes [$\omega_1(b_1) = 64.5i$ cm^{-1} and $\omega_2(a_2) = 36.5i$ cm^{-1})] were revealed when we reoptimized **II.16** with follow-up frequency calculation at the RCCSD(T)/6-311++G** level of theory. Again, the PJT effect is responsible for the two imaginary frequency modes (b_1 and a_2) in the planar C_{2v} structure. Optimization of CHP_5 along the b_1 imaginary vibrational mode would lead to the C_s structure and optimization along the a_2 symmetry mode would lead to the C_2 structure. Two OMO–UMO pairs giving the b_1 symmetry as a direct product of their symmetries (eqn (2) and (3)) are HOMO − 2 (a_1) − LUMO + 1 (b_1) and HOMO − 3 (b_2) − LUMO (a_2) with the energy gaps of 8.89 and 8.87 eV (HF/cc-pvTZ//B3LYP/6-311++G**), respectively.

$$a_1 \otimes b_1 = b_1 \tag{2}$$

$$b_2 \otimes a_2 = b_1 \tag{3}$$

The direct products of the symmetries of HOMO − 2 (a_1) and LUMO (a_2) as well as HOMO − 3 (b_2) and LUMO + 1 (b_1) (energy gaps are 8.68 and 9.09 eV, respectively) are a_2:

$$a_1 \otimes a_2 = a_2 \quad (4)$$

$$b_2 \otimes b_1 = a_2 \quad (5)$$

The symmetries of the two vibrational modes in the C_{2v} structure (b_1 and a_2) correspond to the totally symmetric modes in the distorted structures (a' in C_s and a in C_2). Thus, both PJT conditions are met. Substitution of one P atom with the CH group in P_6 leads to higher OMO–UMO gaps in CHP_5, but the increased gaps are not large enough to prevent orbital coupling and suppress the PJT effect. The lowest benzvalene **II.1**, the prismane **II.3** and the lowest Dewar benzene (**II.6**) structures are still appreciably more stable than the benzene-like isomer. The chair structure **II.14** is now comparable to the structure **II.16** (Fig. 12-4).

12-3.3. $C_2H_2P_4$ isomers

Further in the series we investigated only the derivatives (permutational isomers) of the four representative structures: benzvalene, prismane, Dewar benzene and benzene. There are seven benzvalene, three prismane, six Dewar benzene, and three isomers of benzene-like structures of the $C_2H_2P_4$ species (Fig. 12-6). The lowest isomers of each type are presented in Fig. 12-5c.

The lowest energy isomer is the benzvalene isomer **III.1** (Fig 12-5c). The benzene-like isomer **III.5** is still significantly higher in energy than **III.1** (23.5 kcal mol^{-1}), but is now lower in energy than the lowest Dewar benzene (**III.8**) and prismane (**III.9**) structures. We also calculated the chair structure **III.20** (Fig. 12-6), which is significantly higher in energy than the global minimum structure **III.1**. Its bis-substituted derivative was isolated by Canac *et al*.[52]

The benzene-like structure **III.5** is a local minimum at the B3LYP/6-31G** and B3LYP/6-311++G** levels of theory, but is a first-order saddle point at RCCSD(T)/6-311++G** [$\omega_1(a_2)$ = 89.1i cm^{-1} and$\omega_2(b_1)$ = 72.7 cm^{-1})]. The a_2 imaginary frequency mode in the C_{2v} structure is again a consequence of the PJT effect, but the b_1 mode is now real. Optimization of $C_2H_2P_4$ along the a_2 imaginary vibrational mode would lead to the C_2 structure. The direct product of HOMO − 2 (b_2) and LUMO (b_1) yields a_2, which is the symmetry of the imaginary mode:

$$b_2 \otimes b_1 = a_2 \qquad (6)$$

The HOMO − 2 and LUMO gap is 9.17 eV (HF/cc-pvTZ//B3LYP/6-311++G**). The b_1 vibrational mode, which was imaginary in CHP_5, is real in $C_2H_2P_4$. The closest in energy OMO–UMO pairs, giving b_1 as a direct product of symmetries, HOMO − 2 (b_2) − LUMO + 1 (a_2) and HOMO − 3 (a_1) − LUMO (b_1) have the energy gaps of 9.50 and 9.46 eV, respectively. Apparently, this small increase in the OMO–UMO gap is enough to suppress the PJT effect along the b_1 mode.

12-3.4. $C_3H_3P_3$ isomers

The permutational isomers of benzvalene, prismane, Dewar benzene, and benzene-like structures with the $C_3H_3P_3$ stoichiometry were investigated (Fig. 12-7). The lowest isomers of each type are presented in Fig 12-5d. The most stable isomer is still the benzvalene-type structure **IV.1**. However, the benzene-like isomer **IV.2**is now a close-lying (3.6 kcal mol^{-1}) second lowest isomer. The lowest Dewar benzene **IV.10** andprismane **IV.13** isomers are 25.3 and 32.3 kcal mol^{-1} higher in energy, respectively. 1,2,3-Triphosphabenzene **IV.2** is the most stable benzene-like structure, whereas, 1,2,4-

triphosphabenzene **IV.4** and 1,3,5-triphosphabenzene **IV.5** are 9.3 and 12.9 kcal mol^{-1} higher in energy (Fig. 12-7).

Hofmann *et al.*[53] performed a computational study of all possible (26) isomers, which can be obtained by replacing three P atoms by the CH groups in benzene, prismane, Dewar benzene, benzvalene and bicylopropenyl isomers of C_6H_6 at the MP4SDTQ/6-3+G*//MP2(full)/6-31G*+0.89 ZPE(HF/6-31G*) level of theory. According to their calculations, 1,2,3-triphosphabenzene is the global minimum with the most stable benzvalene structure **IV.1** being 4.7 kcal mol^{-1} higher in energy, which is different from our results. However, taking into account that the energy difference between 1,2,3-triphosphabenzene **IV.2** and benzvalene **IV.1** is only 0.8 kcal mol^{-1} at RCCSD(T)/cc-pvTZ//B3LYP/6-311++G**+ZPE (B3LYP/6-311++G**) and 3.6 kcal mol^{-1}at CCSD(T)/CBS//B3LYP//6-311++G**+ZPE(B3LYP/6-311++G**) we feel that these two isomers are too close in energy to make a definitive prediction which of them is a true global minimum.

According to our calculations, benzvalene structure **IV.1** is the lowest energy $C_3H_3P_3$ isomer and the 1,2,3-triphosphabenzene **IV.2** is the lowest benzene-like isomer, but the experimentally characterized compound[54–59] of $C_3H_3P_3$ stoichiometry is 1,3,5-triphosphabenzene **IV.5**. The crystal structure of the 1,3,5-triphosphinine has been published,[54] showing that the molecule is planar and all bond lengths are equal. We reoptimized 1,2,3-triphosphabenzene at CCSD(T)/6-311++G** and in agreement with B3LYP/6-311++G** found that it is a local minimum structure with two smallest frequencies [$\omega_1(b_1)$ = 121.7 cm^{-1} and$\omega_2(a_2)$ = 121.8 cm^{-1}) being real. The gap (HF/cc-

pVTZ//B3LYP/6-311++G**) between the closest OMO–UMO pair [HOMO − 2(b_2) − LUMO + 1 (a_2)] leading to b_1 symmetry is now 10.25 eV and the OMO–UMO pair [HOMO − 2 (b_2) − LUMO (b_1)] leading to a_2 symmetry is 10.01 eV. A substantial increase in the gap between the OMO–UMO pairs is responsible for quenching the PJT effect. The experimental observation of planarity of 1,3,5-triphosphinine also shows that the PJT is completely suppressed at $x = 3$.

12-3.5. $C_4H_4P_2$ isomers

Again, we studied the permutational isomers of benzvalene, prismane, Dewar benzene, and benzene-like structures (Fig. 12-8). The lowest isomers of each kind are presented in Fig. 12-5e. According to our results, the 2D to 3D transition occurs between $C_3H_3P_3$ and $C_4H_4P_2$: all three benzene-like isomers are lower in energy than any other isomer studied. The lowest benzvalene **V.4**, Dewar benzene **V.7**, and prismane **V.17** structures are 17.8, 33.5, and 55.5 kcal mol^{-1} higher in energy, respectively. Apparently, planarity took over in the $C_xH_xP_{6-x}$ ($x = 0$–6) series at $x = 4$. The lowest isomer is 1,2-diphosphinine. In spite of that, derivatives of two other planar isomers 1,4-diphosphinine[60] and the 1,3-diphosphinine[61] have been reported in the literature.

Colombet *et al.*[62] performed a study (MP2/6-31G**//MP2/6-31G**) of all possible (24) isomers of $C_4H_4P_2$, which can be obtained by replacing four P atoms by CH groups in benzene, prismane, Dewarbenzene, benzvalene and bicyclopropenyl-like isomers of C_6H_6. They also calculated three diphosphinine isomers at the CCSD(T)/6-31G**//MP2/6-31G** level of theory. According to their calculations, the 1,2-diphosphinine is the most stable structure with 1,3-diphosphinine and 1,4-diphosphinine

being 5.6 (5.4) and 7.4 (7.7) kcal mol^{-1} higher in energy at CCSD(T) (MP2). The lowest non-planar benzvalene isomer **V.4**was found to be 23.1 kcal mol^{-1} (MP2) higher in energy. Our values of the relative energies are somewhat different from those obtained by Colombet *et al.*,[62] but the qualitative conclusion that the planar structures are significantly more stable is in agreement.

12-3.6. C_5H_5P isomers

The structures and relative energies of three benzvalene, one prismane, two Dewar benzene, and one benzene-like isomers are presented in Fig. 12-9. The lowest isomers of each kind are also shown in Fig. 12-5f. The benzene-like structure **VI.1** is significantly more stable than the other isomers. The lowest benzvalene **VI.2**, Dewar benzene **VI.4** structures, and prismane isomer **VI.7** are 40.7, 49.6, and 80.6 kcal mol^{-1} higher in energy, respectively.

Phosphinine **VI.1** is a well characterized compound.[63] The synthesis of the first phosphinine derivative was reported by Markl[64] in 1966 and the unsubstituted phosphinine itself was synthesized by Ashe[65] in 1971. The structure of the phosphinine **VI.1** was experimentally determined by a joint electron diffraction–microwave study.[66] The structure is planar with small bond length alterations (0.03 Å). Numerous quantum chemical calculations[67–76] also predicted the planar structure for phosphinine, but with even smaller alterations (less than 0.01 Å).

12-3.7. C_6H_6 isomers

The aforementioned systematic computational study[16] of the C_6H_6 isomers revealed 215 minimum energy structures, with 84 structures being within 100 kcal mol^{-1}

in energy relative to the benzene global minimum structure. Benzene is the most stable structure. The benzvalene and Dewar benzene isomers are 72.3 and 74.8 kcal mol^{-1} higher in energy, respectively.[16] The prismane structure was predicted to be 114.9 kcal mol^{-1}higher in energy. Our highest-level relative energy values (Fig. 12-5g) of these isomers are in a good (within 2.5 kcal mol^{-1}) agreement with the most comprehensive data in the literature.

12-3.8. Probing of aromaticity in benzene-like structures with the NICS and $NICS_{zz}$ indices

In order to probe aromaticity in all planar ring-type structures of the $C_xH_xP_{6-x}$ (x = 0–6) series we used both the NICS (Table 12-1) and $NICS_{zz}$ (Table 12-2) indices, two of the most popular methods for evaluating aromaticity in planar species. For the NICS and $NICS_{zz}$ calculations we used only planar benzene-type structures, even though some of them are actually saddle points.

According to our calculations, the NICS indices (B3LYP/ 6-311++G**) of all the benzene-like structures in the $C_xH_xP_{6-x}$ (x = 0–6) series (Table 12-1) have their highest (negative) values at 0.8-1.1 Å. The maximum NICS value (-11.5 ppm, Z = 1.0 Å) for P_6 is almost the same as the highest index (-10.6 ppm, Z = 0.8 Å) of benzene. The maximum NICS values of all other benzene-like structures in the $C_xH_xP_{6-x}$ (x = 1-5) series are all very high and vary from -8.4 (**III.13**) to -10.3 (**VI.1**) ppm. Thus, according to the NICS indices, all benzene-like structures are almost as aromatic as hexaphosphabenzene and benzene. Schleyer *et al.*[77] calculated NICS(π) = -14.7 (-15.9) ppm, NICS(σ) = +1.2 (+3.0) ppm and NICS(tot) = -15.8 (-15.2) ppm (NICS calculated at 0.5 Å with values at Z = 0 Å

in parentheses) for planar P_6, which are comparable to those of benzene (NICS(π) = -16.8 (-20.7) ppm, NICS(σ) = +8.8 (+13.8) ppm and NICS(tot) = -10.7 (-8.9) ppm) at the same level of theory. Hofmann *et al.*[53] calculated NICS at the center of the benzene-like structures using the GIAO-SCF/6-31+G* method at the MP2(full)/6-31G* optimized geometries. They got the following values: -8.4 ppm (**VI.1**), -7.9 ppm (**V.1**), -7.1 ppm (**V.2**), -7.3 ppm (**V.3**), -7.3 ppm (**IV.2**), -6.4 ppm (**IV.4**), and -5.8 ppm (**IV.5**). Our NICS values calculated for the same species in the same positions are somewhat different from the reported numbers, but the overall picture is consistent with the other studies.[53,57]

The calculated maximum values of the $NICS_{zz}$ indices (Table 12-2) are significantly higher than the NICS indices and vary from -22.1 (**III.13**) ppm to -29.7 ppm (**I.11**). However these results lead to a similar conclusion on aromaticity in these planar structures: all benzene-like structures are almost as aromatic as hexaphosphabenzene and benzene. Thus, the relative stabilities of the benzene-like structures do not depend on aromaticity. Additional studies are required to make a reliable assessment of the aromaticity of benzene-like structures in the series.

12-4. Conclusions

We presented a systematic study of the $C_xH_xP_{6-x}$ (x = 0–6) series. We performed unbiased CK global minimum and low-lying isomers search for the P_6 and CHP_5 species at the B3LYP/6-31G** level of theory. The lowest isomers were recalculated at the CCSD(T)/CBS//B3LYP/6-311++G** level of theory. We confirmed that the benzvalene type structures are the most stable isomers of both species. We focused on all possible benzene, benzvalene, Dewar benzene, and prismane-like structures of the $C_xH_xP_{6-x}$

(x = 2–6) species. We found that the lowest benzvalene and benzene-like structures of $C_3H_3P_3$ are very close in energy, with the benzvalene structure being slightly more stable at our highest level of theory. The transition from 3D structure to 2D structure occurs at x = 4 ($C_4H_4P_2$), where benzene-like isomers become significantly more stable than the benzvalene-like structures. Hexaphosphabenzene has two imaginary frequencies due to the pseudo Jahn–Teller effect. Pentaphosphabenzene and the lowest tetraphosphabenzene were found to be planar at the B3LYP/6-311++G** level of theory but they are second- and first-order saddle points at the CCSD(T)/6-311++G** level of theory. We found that the OMO–UMO gap between MOs involved in the PJT effect is increasing with substitution of the P atoms with the CH groups, which gradually leads to complete suppression of the PJT effect in triphosphabenzene. We show that isolobal substitution of an atom or a group by a more electronegative atom or group is a new mechanism for the suppression of the PJT effect.

From the calculated $NICS_{zz}$ values for the $C_xH_xP_{6-x}$ ring-type isomers it is clear that other factors, such as stronger 2c–2e C–C σ-bonds compared to weaker 2c–2e C–P and P–P σ-bonds, should be taken into account along with aromaticity when assessing stability.

It can be seen from the survey of potential surfaces of $C_2H_2P_4$, $C_3H_3P_3$, and $C_4H_4P_2$ that in general the structures with more adjacent carbon atoms are more stable. In part, this is due to the stronger overlap between 2p–2p AOs compared to the 2p–3p AOs and 3p–3p AOs overlaps.

One of the most striking results of the studies of the $C_xH_xP_{6-x}$ (x = 0–6) series is that, to best of our knowledge, the lowest energy structures found in previous and the present works are not the ones that have been observed in experimental studies (excluding benzene and phosphabenzene). Hexaphosphabenzene was found to be a part of the triple-decker sandwich complex $\{(\eta^5\text{-}Me_5C_5)Mo\}_2(\mu,\eta^6\text{-}P_6)$.[1] Yet, the most stable benzvalene-like structure has not been experimentally characterized. A derivative of the $C_2H_2P_4$ chair structure was synthesized,[52] but the corresponding isomer is 16.8 kcal mol^{-1} higher than the global minimum. 1,3,5-Triphosphabenzene is another example.[54–58] It is 16.5 kcal mol^{-1} higher than the global minimum and is also higher in energy than 1,2,3-triphosphabenzene, the most stable planar structure. 1,2-Diphosphabenzene is the global minimum of $C_4H_4P_2$, yet a successful synthesis of a derivative of 1,4-diphosphabenzene[60] was reported. 1,2-Diphosphabenzene has not yet been synthesized. This lack of correspondence between the lowest energy isomers and experimentally synthesized compounds is an interesting and bizarre phenomenon in chemistry.

Notes and references

1 O. J. Scherer, H. Sitzmann and G. Wolmershauser, *Angew. Chem., Int. Ed. Engl.*, 1985, **24**, 351.

2 S. Nagase and K. Ito, *Chem. Phys. Lett.*, 1986, **126**, 43.

3 M. T. Nguyen and A. F. Hegarty, *J. Chem. Soc., Chem. Commun.*, 1986, 383.

4 R. O. Jones and D. J. Hohl, *J. Chem. Phys.*, 1990, **92**, 6710.

5 R. O. Jones and G. Seiferd, *J. Chem. Phys.*, 1992, **96**, 7564.

6 D. S. Warren and B. M. Gimarc, *J. Am. Chem. Soc.*, 1992, **114**, 5378.

7 B. M. Gimarc and M. Zhao, *Coord. Chem. Rev.*, 1997, **158**, 385.

8 M. Haser, U. Schneider and R. Alhrichs, *J. Am. Chem. Soc.*, 1992, **114**, 9551.

9 P. Ballone and R. O. Jones, *J. Chem. Phys.*, 1994, **100**, 4941.

10 M. Haser and R. O. Jones, *J. Chem. Phys.*, 1995, **102**, 3703.

11 P. C. Hiberty and F. Volatron, *Heteroat. Chem.*, 2007, **18**, 129.

12 H. Bock, *Angew. Chem., Int. Ed. Engl.*, 1989, **28**, 1627.

13 J. H. Potgieter, *J. Chem. Educ.*, 1991, **68**, 280.

14 I. Gutman and J. H. Potgieter, *J. Chem. Educ.*, 1994, **71**, 222.

15 G. Nagendrappa, *Resonance*, 2001, **6**, 74.

16 T. C. Dinadayalane, U. D. Priyakumar and G. N. Sastry, *J. Phys. Chem. A*, 2004, **108**, 11433.

17 M. T. Huynh and A. N. Alexandrova, *J. Phys. Chem. Lett.*, 2011, **2**, 2046.

18 A. P. Sergeeva, B. B. Averkiev, H.-J. Zhai, A. I. Boldyrev and L. S. Wang, *J. Chem. Phys.*, 2011, **134**, 224304.

19 A. D. Becke, *J. Chem. Phys.*, 1993, **98**, 5648.

20 S. H. Vosko, L. Wilk and M. Nusair, *Can. J. Phys.*, 1980, **58**, 1200.

21 C. Lee, W. Yang and R. G. Parr, *Phys. Rev. B: Solid State*, 1988, **37**, 785.

22 V. A. Rassolov, M. A. Ratner, J. A. Pople, P. C. Redfern and L. A. Curtiss, *J. Comput. Chem.*, 2001, **22**, 976.

23 M. S. Gordon, J. S. Binkley, J. A. Pople, W. J. Pietro and W. J. Hehre, *J. Am. Chem. Soc.*, 1982, **104**, 2797.

24 W. J. Pietro, M. M. Francl, W. J. Hehre, D. J. Defrees, J. A. Pople and J. S. Binkley, *J. Am. Chem. Soc.*, 1982, **104**, 5039.

25 T. Clark, J. Chandrasekhar, G. W. Spitznagel and P. v. R. Schleyer, *J. Comput. Chem.*, 1983, **4**, 294.

26 J. Cizek, *Adv. Chem. Phys.*, 1969, **14**, 35.

27 G. D. Purvis and R. J. Bartlett, *J. Chem. Phys.*, 1982, **76**, 1910.

28 K. Raghavachari, G. W. Trucks, J. A. Pople and M. Head-Gordon, *Chem. Phys. Lett.*, 1989, **157**, 479.

29 D. E. Woon and T. H. Dunning Jr., *J. Chem. Phys.*, 1993, **98**, 1358.

30 R. A. Kendall, T. H. Dunning Jr. and R. J. Harrison, *J. Chem. Phys.*, 1992, **96**, 6796.

31 T. H. Dunning Jr., *J. Chem. Phys.*, 1989, **90**, 1007.

32 K. A. Peterson, D. E. Woon and T. H. Dunning Jr., *J. Chem. Phys.*, 1994, **100**, 7410.

33 A. Wilson, T. van Mourik and T. H. Dunning Jr., *J. Mol. Struct. (THEOCHEM)*, 1997, **388**, 339.

34 *GAUSSIAN 03 (Revision D.01)*, M. J. Frisch, G. W. Trucks, H. B. Schlegel, G. E. Scuseria, M. A. Robb, J. R. Cheeseman, J. A. Montgomery, Jr., T. Vreven, K. N. Kudin, J. C. Burant, J. M. Millam, S. S. Iyengar, J. Tomasi, V. Barone, B. Mennucci, M. Cossi, G. Scalmani, N. Rega, G. A. Petersson, H. Nakatsuji, M. Hada, M. Ehara, K. Toyota, R. Fukuda, J. Hasegawa, M. Ishida, T. Nakajima, Y. Honda, O. Kitao, H. Nakai, M. Klene, X. Li, J. E. Knox, H. P. Hratchian, J. B.

Cross, V. Bakken, C. Adamo, J. Jaramillo, R. Gomperts, R. E. Stratmann, O. Yazyev, A. J. Austin, R. Cammi, C. Pomelli, J. W. Ochterski, P. Y. Ayala, K. Morokuma, G. A. Voth, P. Salvador, J. J. Dannenberg, V. G. Zakrzewski, S. Dapprich, A. D. Daniels, M. C. Strain, O. Farkas, D. K. Malick, A. D. Rabuck, K. Raghavachari, J. B. Foresman, J. V. Ortiz, Q. Cui, A. G. Baboul, S. Clifford, J. Cioslowski, B. B. Stefanov, G. Liu, A. Liashenko, P. Piskorz, I. Komaromi, R. L. Martin, D. J. Fox, T. Keith, M. A. Al-Laham, C. Y. Peng, A. Nanayakkara, M. Challacombe, P. M. W. Gill, B. Johnson, W. Chen, M. W. Wong, C. Gonzalez, J. A. Pople, Gaussian, Inc., Wallingford, CT, 2004.

35 D. G. Truhlar, *Chem. Phys. Lett.*, 1998, **294**, 45.

36 P. L. Fast, M. L. Sanchez and D. G. Truhlar, *J. Chem. Phys.*, 1999, **111**, 2921.

37 J. P. Foster and F. Weinhold, *J. Am. Chem. Soc.*, 1980, **102**, 7211.

38 A. E. Reed, L. A. Curtiss and F. Weinhold, *Chem. Rev.*, 1988, **88**, 899.

39 D. Yu. Zubarev and A. I. Boldyrev, *Phys. Chem. Chem. Phys.*, 2008, **10**, 5207.

40 D. Yu. Zubarev, N. Robertson, D. Domin, J. McClean, J. H. Wang, W. A. Lester, R. Whitesides, X. Q. You and M. Frenklach, *J. Phys. Chem. C*, 2010, **114**, 5429.

41 P. v. R. Schleyer, C. Maerker, A. Dransfeld, H. Jiao and N. v. E. Hommes, *J. Am. Chem. Soc.*, 1996, **118**, 6317.

42 C. Corminboeuf, T. Heine, G. Seifert, P. v. R. Schleyer and J. Weber, *Phys. Chem. Chem. Phys.*, 2004, **6**, 273.

43 G. Schaftenaar, *MOLDEN3.4*, CAOS/CAMM Center, The Netherlands, 1998.

44 U. Varetto, *Molekel 5.4.0.8*, Swiss National Supercomputing Centre, Manno, Switzerland, 2009.

45 I. B. Bersuker, *Chem. Rev.*, 2001, **101**, 1067.

46 I. B. Bersuker, *The Jahn–Teller Effect*, Cambridge University Press, New York, 2006.

47 *The Jahn–Teller Effect and Beyond: Selected Works of Isaac Bersuker with Commentaries*, ed. J. E. Boggs and V. Z. Polinger, The Academy of Sciences of Moldova, Chişinău, Moldova, 2008.

48 R. G. Pearson, *Proc. Natl. Acad. Sci. U. S. A.*, 1975, **72**, 2104.

49 A. P. Sergeeva and A. I. Boldyrev, *Organometallics*, 2010, **29**, 3951.

50 K. Pokhodnya, C. Olson, X. Dai, D. L. Schilz, P. Boudjouk, A. P. Sergeeva and A. I. Boldyrev, *J. Chem. Phys.*, 2011, **134**, 014105.

51 D. Yu. Zubarev and A. I. Boldyrev, *J. Org. Chem.*, 2008, **73**, 9251.

52 Y. Canac, D. Bourissou, A. Baceiredo, H. Gornitzka, W. W. Schoeller and G. Bertrand, *Science*, 1998, **279**, 2080.

53 M. Hofmann, P. v. R. Schleyer and M. Regitz, *Eur. J. Org. Chem.*, 1999, 3291.

54 R. Gleiter, H. Lange, P. Binger, J. Stannek, C. Kruger, J. Bruckmann, U. Zenneck and S. Kummer, *Eur. J. Inorg. Chem.*, 1998, 1619.

55 F. Tabellion, A. Nachbauer, S. Leininger, C. Peters, M. Regitz and F. Preuss, *Angew. Chem., Int. Ed.*, 1998, **37**, 1233.

56 P. Binger, S. Leininger, J. Stannek, B. Gabor, R. Mynott, J. Bruckmann and C. Kruger, *Angew. Chem., Int. Ed. Engl.*, 1995, **34**, 2227.

57 P. Binger, S. Stutzmann, J. Stanneck, B. Gabor and R. Mynott, *Eur. J. Inorg. Chem.*, 1999, 83.

58 S. B. Clendenning, J. C. Green and J. F. Nixon, *J. Chem. Soc., Dalton Trans.*, 2000, 1507.

59 S. M. Bachrach and P. Magdalinos, *THEOCHEM*, 1996, **368**, 1.

60 Y. Kobayashi, J. Kumadaki, A. Ohsawa and W. Hamana, *Tetrahedron Lett.*, 1976, **17**, 3715.

61 D. Bohm, F. Knoch, S. Kummer, U. Schmidt and U. Zenneck, *Angew. Chem., Int. Ed. Engl.*, 1995, **34**, 198.

62 L. Colombet, F. Volatron, P. Maitre and P. C. Hiberty, *J. Am. Chem. Soc.*, 1999, **121**, 4215.

63 L. Nyulaszi, *Chem. Rev.*, 2001, **101**, 1229.

64 G. Markl, *Angew. Chem., Int. Ed. Engl.*, 1966, **5**, 846.

65 A. J. Ashe III, *J. Am. Chem. Soc.*, 1971, **93**, 3293.

66 T. C. Wong and S. Bartell, *J. Chem. Phys.*, 1974, **61**, 2840.

67 T. Veszpremi, L. Nyulaszi, J. Reffy and J. Heinicke, *J. Phys. Chem.*, 1992, **96**, 623.

68 L. Nyulaszi, T. Veszpremi, J. Reffy, B. Burkhardt and M. Regitz, *J. Am. Chem. Soc.*, 1992, **114**, 9080.

69 K. K. Baldridge and M. S. Gordon, *J. Am. Chem. Soc.*, 1988, **110**, 4204.

70 C. W. Bock, M. Tratchman and P. George, *Struct. Chem.*, 1990, **1**, 345.

71 V. Jonas and G. Frenking, *Chem. Phys. Lett.*, 1993, **210**, 211.

72 L. Nyulaszi and Gy. Keglevich, *Heteroat. Chem.*, 1994, **5**, 131.

73 D. B. Chesnut, *J. Comput. Chem.*, 1995, **16**, 1227.

74 L. Nyulaszi, D. Szieberth and T. Veszpremi, *J. Org. Chem.*, 1995, **60**, 1647.

75 L. Nyulaszi and T. Veszpremi, *J. Phys. Chem.*, 1996, **100**, 6456.

76 G. Frison, A. Sevin, N. Avarvari, F. Mathey and P. LeFloch, *J. Org. Chem.*, 1999, **64**, 5524.

77 P. v. R. Schleyer, H. Jiao, N. J. R. van Eikema Hommes, V. G. Malkin and O. L. Malkina, *J. Am. Chem. Soc.*, 1997, **119**, 12669.

Table 12-1 NICS values (ppm) calculated at B3LYP/6-311++G**

Distance (Å)	P_6	CHP_5	$C_2H_2P_4$			$C_3H_3P_3$			$C_4H_4P_2$			C_5H_5P	C_6H_6
	I.11	**II.16**	**III.5**	**III.10**	**III.13**	**IV.2**	**IV.4**	**IV.5**	**V.1**	**V.2**	**V.3**	**VI.1**	**VII.1**
0.0	-9.7	-6.3	-5.7	-5.7	-5.0	-6.6	-5.9	-5.1	-6.7	-6.0	-6.0	-7.8	-8.0
0.1	-9.8	-6.4	-5.8	-5.8	-5.1	-6.7	-6.0	-5.2	-6.8	-6.1	-6.1	-7.9	-8.2
0.2	-9.9	-6.6	-6.0	-6.0	-5.3	-6.9	-6.3	-5.5	-7.1	-6.4	-6.4	-8.1	-8.5
0.3	-10.1	-6.9	-6.4	-6.3	-5.7	-7.2	-6.7	-5.9	-7.4	-6.9	-6.8	-8.5	-8.9
0.4	-10.4	-7.3	-6.8	-6.8	-6.1	-7.6	-7.1	-6.5	-7.9	-7.4	-7.3	-9.0	-9.4
0.5	-10.6	-7.7	-7.2	-7.2	-6.6	-8.1	-7.6	-7.0	-8.3	-7.9	-7.9	-9.5	-9.9
0.6	-10.9	-8.1	-7.7	-7.7	-7.1	-8.5	-8.1	-7.6	-8.7	-8.4	-8.4	-9.9	-10.2
0.7	-11.1	-8.5	-8.1	-8.1	-7.6	-8.8	-8.5	-8.0	-9.0	-8.8	-8.8	-10.1	-10.5
0.8	-11.3	-8.9	-8.4	-8.4	-7.9	-9.1	-8.8	-8.4	-9.3	-9.1	-9.0	-10.3	-10.6
0.9	-11.5	-9.1	-8.7	-8.7	-8.2	-9.3	-9.0	-8.6	-9.4	-9.2	-9.2	-10.3	-10.5
1.0	-11.5	-9.3	-8.8	-8.8	-8.4	-9.3	-9.1	-8.7	-9.4	-9.2	-9.2	-10.1	-10.2
1.1	-11.5	-9.4	-8.9	-8.8	-8.4	-9.3	-9.0	-8.7	-9.2	-9.1	-9.1	-9.8	-9.8
1.2	-11.3	-9.3	-8.8	-8.8	-8.4	-9.1	-8.9	-8.6	-9.0	-8.9	-8.8	-9.4	-9.3
1.3	-11.2	-9.2	-8.7	-8.6	-8.3	-8.9	-8.6	-8.3	-8.7	-8.5	-8.5	-8.9	-8.8
1.4	-10.9	-9.0	-8.5	-8.4	-8.1	-8.5	-8.3	-8.1	-8.3	-8.1	-8.1	-8.4	-8.2
1.5	-10.6	-8.8	-8.2	-8.1	-7.8	-8.2	-7.9	-7.7	-7.9	-7.7	-7.7	-7.9	-7.6
1.6	-10.2	-8.5	-7.9	-7.7	-7.5	-7.8	-7.5	-7.3	-7.4	-7.3	-7.2	-7.3	-7.0
1.7	-9.8	-8.1	-7.5	-7.4	-7.2	-7.4	-7.1	-6.9	-7.0	-6.8	-6.7	-6.8	-6.4
1.8	-9.4	-7.8	-7.1	-7.0	-6.8	-6.9	-6.7	-6.5	-6.5	-6.3	-6.3	-6.2	-5.8
1.9	-9.0	-7.4	-6.7	-6.6	-6.5	-6.5	-6.3	-6.1	-6.1	-5.9	-5.8	-5.7	-5.3
2.0	-8.5	-7.0	-6.4	-6.2	-6.1	-6.1	-5.8	-5.7	-5.6	-5.4	-5.4	-5.3	-4.8

Table 12-2 $NICS_{zz}$ values (ppm) calculated at B3LYP/6-311++G**

Distance (Å)	P_6	CHP_5	$C_2H_2P_4$			$C_3H_3P_3$			$C_4H_4P_2$			C_5H_5P	C_6H_6
	I.11	**II.16**	**III.5**	**III.10**	**III.13**	**IV.2**	**IV.4**	**IV.5**	**V.I**	**V.2**	**V.3**	**VI.1**	**VII.1**
0.0	-23.7	-12.1	-9.0	-9.1	-9.0	-9.2	-9.2	-8.9	-10.4	-10.4	-10.2	-12.5	-14.5
0.1	-23.8	-12.3	-9.3	-9.4	-9.2	-9.5	-9.5	-9.2	-10.7	-10.7	-10.5	-12.9	-14.9
0.2	-24.2	-12.9	-10.0	-10.1	-10.0	-10.4	-10.3	-10.1	-11.7	-11.7	-11.5	-14.1	-16.3
0.3	-24.8	-13.9	-11.2	-11.3	-11.1	-11.8	-11.7	-11.5	-13.2	-13.3	-13.1	-15.8	-18.2
0.4	-25.5	-15.1	-12.7	-12.8	-12.5	-13.5	-13.4	-13.2	-15.1	-15.2	-14.9	-17.9	-20.6
0.5	-26.3	-16.6	-14.4	-14.4	-14.2	-15.3	-15.3	-15.0	-17.1	-17.2	-17.0	-20.1	-23.0
0.6	-27.2	-18.0	-16.0	-16.2	-15.8	-17.2	-17.2	-16.9	-19.1	19.2	-19.0	-22.3	-25.2
0.7	-28.0	-19.4	-17.7	-17.8	-17.5	-19.0	-19.0	-18.7	-21.0	-21.0	-20.9	-24.1	-27.0
0.8	-28.7	-20.7	-19.2	-19.3	-18.9	-20.6	-20.5	-20.2	-22.5	-22.6	-22.4	-25.5	-28.3
0.9	-29.3	-21.8	-20.5	-20.5	-20.1	-21.9	-21.7	-21.5	-23.6	-23.7	-23.5	-26.5	-29.1
1.0	-29.6	-22.7	-21.4	-21.5	-21.1	-22.8	-22.6	-22.3	-24.4	-24.4	-24.2	-27.0	-29.2
1.1	-29.8	-23.3	-22.1	-22.1	-21.7	-23.4	-23.1	-22.9	-24.7	-24.7	-24.6	-27.0	-28.9
1.2	-29.7	-23.6	-22.5	-22.4	-22.1	-23.6	-23.3	-23.0	-24.7	-24.7	-24.5	-26.6	-28.2
1.3	-29.5	-23.7	-22.6	-22.5	-22.1	-23.5	-23.2	-22.9	-24.4	-24.3	-24.2	-26.0	-27.2
1.4	-29.0	-23.6	-22.4	-22.3	-22.0	-23.2	-22.8	-22.6	-23.8	-23.7	-23.6	-25.0	-26.0
1.5	-28.4	-23.2	-22.0	-21.9	-21.6	-22.6	-22.2	-22.0	-23.0	-22.9	-22.8	-23.9	-24.6
1.6	-27.7	-22.7	-21.5	-21.3	-21.0	-21.9	-21.5	-21.3	-22.1	-21.9	-21.8	-22.7	-23.2
1.7	-26.8	-22.0	-20.9	-20.7	-20.4	-21.0	-20.6	-20.4	-21.1	-20.9	-20.8	-21.5	-21.7
1.8	-25.9	-21.3	-20.0	-19.8	-19.6	-20.1	-16.7	-19.4	-20.0	-19.8	-19.7	-20.2	-20.2
1.9	-24.9	-20.5	-19.2	-19.0	-18.8	-19.1	-18.7	-18.5	-18.9	-18.7	-18.6	-18.9	-18.8
2.0	-23.8	-19.6	-18.3	-18.1	-17.9	-18.1	-17.7	-17.5	-17.8	-17.6	-17.4	-17.6	-17.4

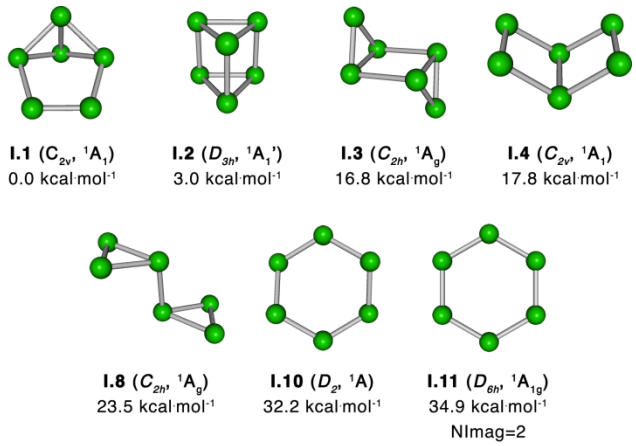

Fig 12-1. Representative optimized structures of P_6, their point group symmetries, spectroscopic states and ZPE corrected (B3LYP/6-311+G*) relative energies (RCCSD(T)/CBS//B3LYP/6-311+G*). The structures are labeled in accordance with Fig. 12-2.

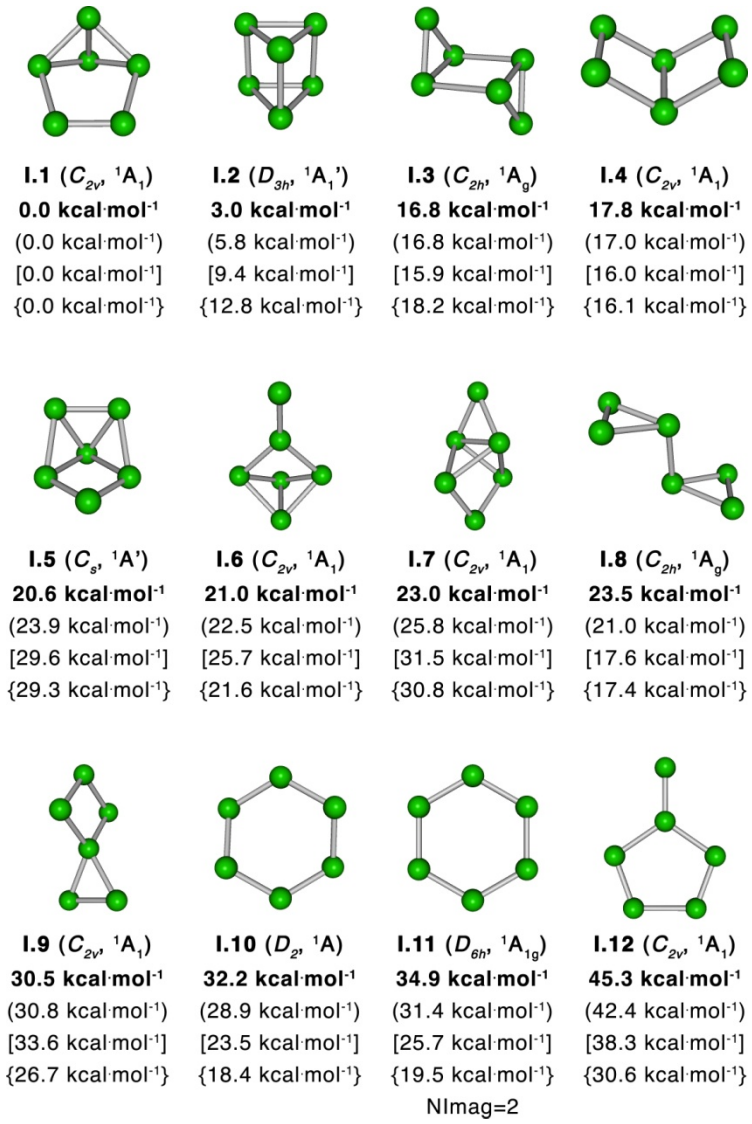

Fig 12-2. Lowest-lying structures of P_6, their point group symmetries, spectroscopic states and ZPE corrected relative energies. The energies are given at: CCSD(T)/CBS (bold), CCSD(T)/cc-pVTZ (in brackets), CCSD(T)/cc-pVDZ (square brackets), and B3LYP/6-311+G* (curly brackets), all at B3LYP/6-311+G* optimized geometries.

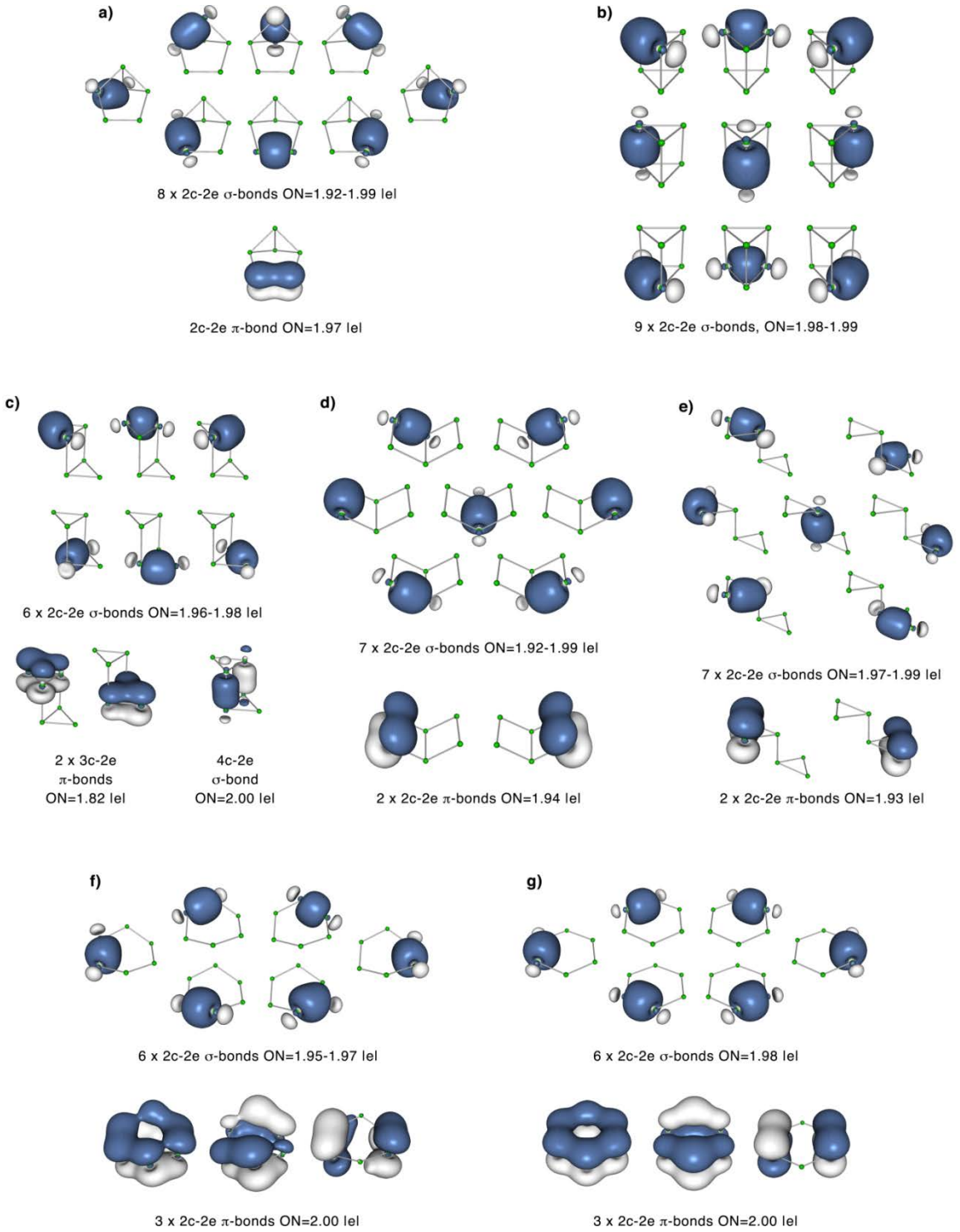

Fig 12-3. AdNDP revealed chemical bonding patterns of the (a) **I.1**, (b) **I.2**, (c) **I.3**, (d) **I.4**, (e) **1.8**, (f) **I.10**, and (g) **I.11** structures.

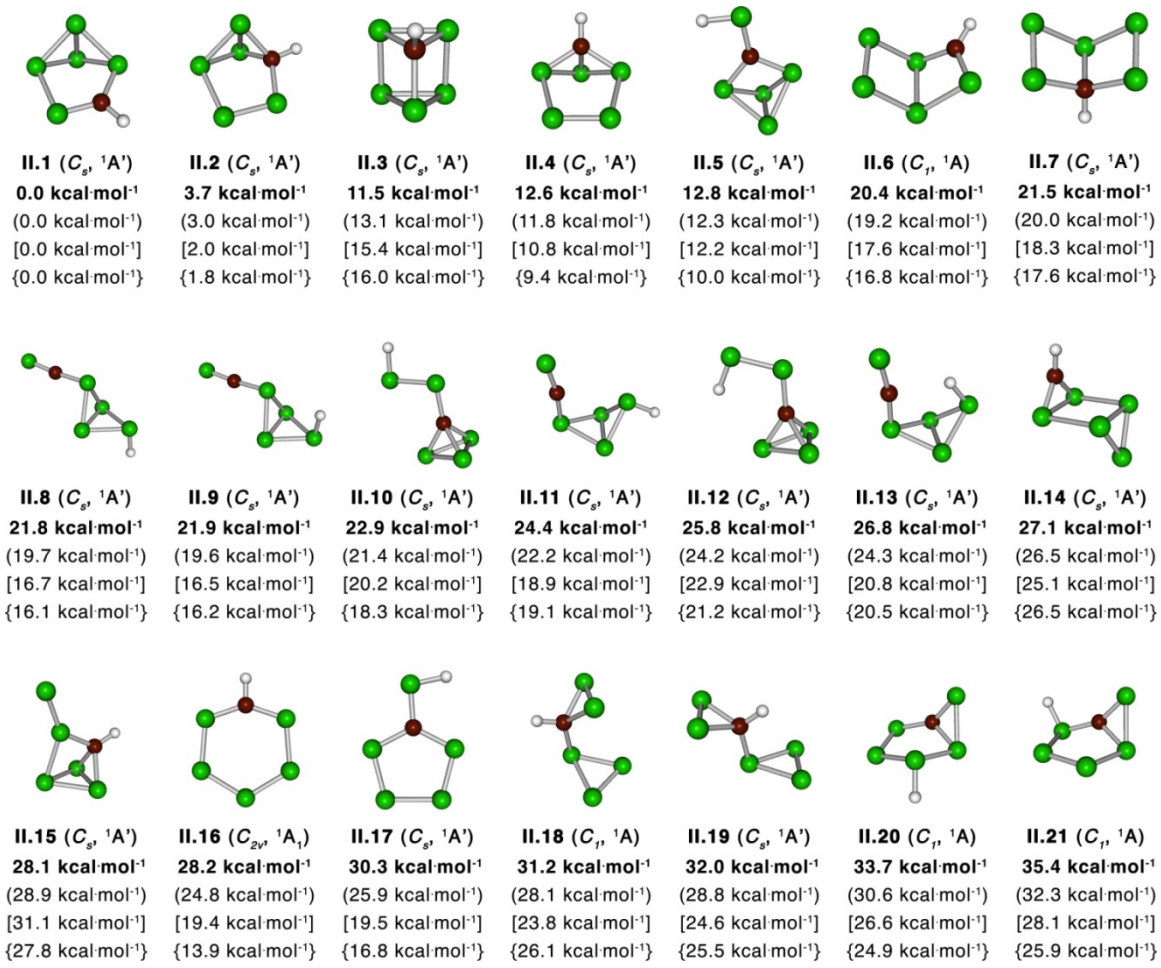

Fig 12-4. Lowest-lying structures of CHP_5, their point group symmetries, spectroscopic states and ZPE corrected relative energies. The energies are given at: CCSD(T)/CBS (bold), CCSD(T)/cc-pVTZ (in brackets), CCSD(T)/cc-pVDZ (square brackets), and B3LYP/6-311++G** (curly brackets), all at B3LYP/6-311++G** optimized geometries.

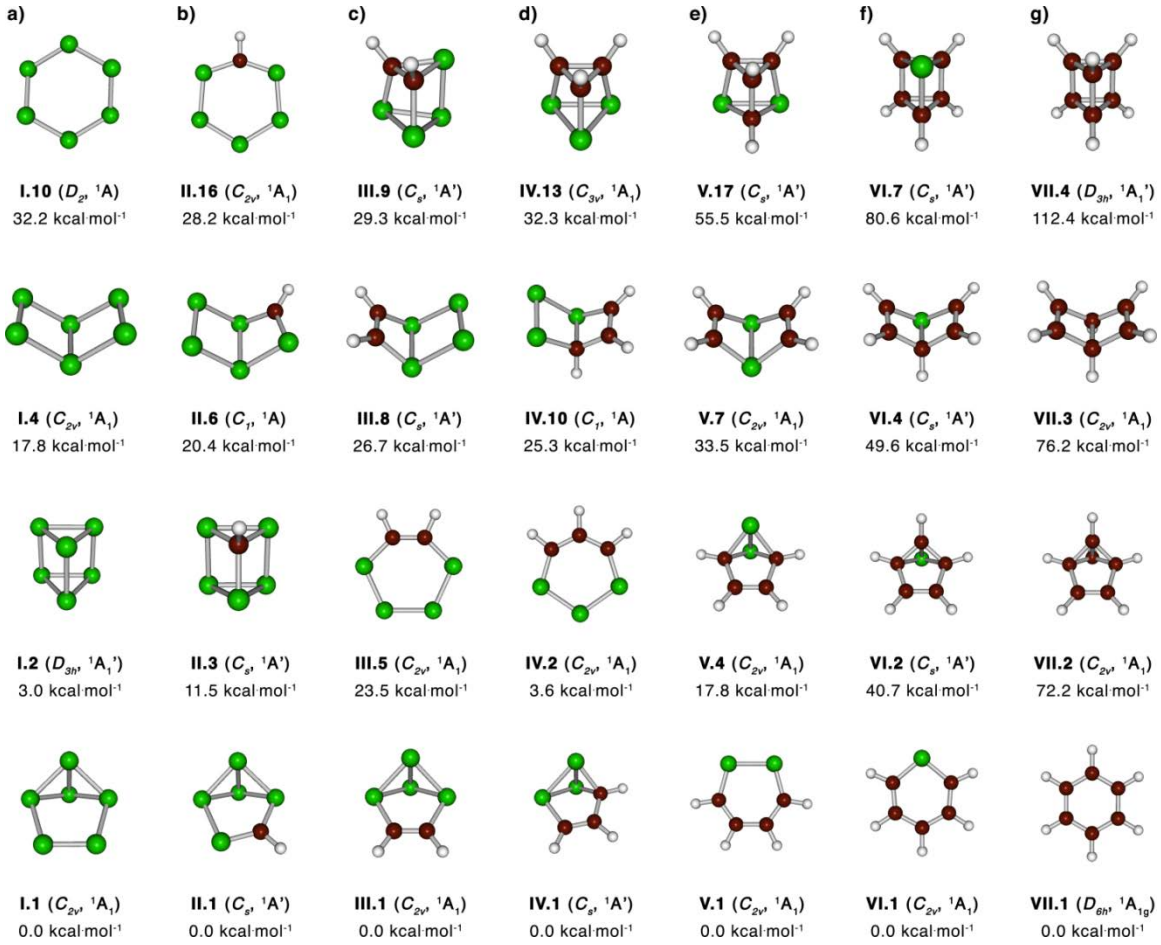

Fig 12-5. The lowest benzvalene, Dewar benzene, prismane and benzene-type isomers of each species in the $C_xH_xP_{6-x}$ (x = 0–6) series, their point group symmetries, spectroscopic states and ZPE corrected (B3LYP/6-311++G**) relative energies (RCCSD(T)/CBS//B3LYP/6-311++G**). The structures are labeled in accordance with Fig. 12-2, 12-4, 12-6 – 12-10.

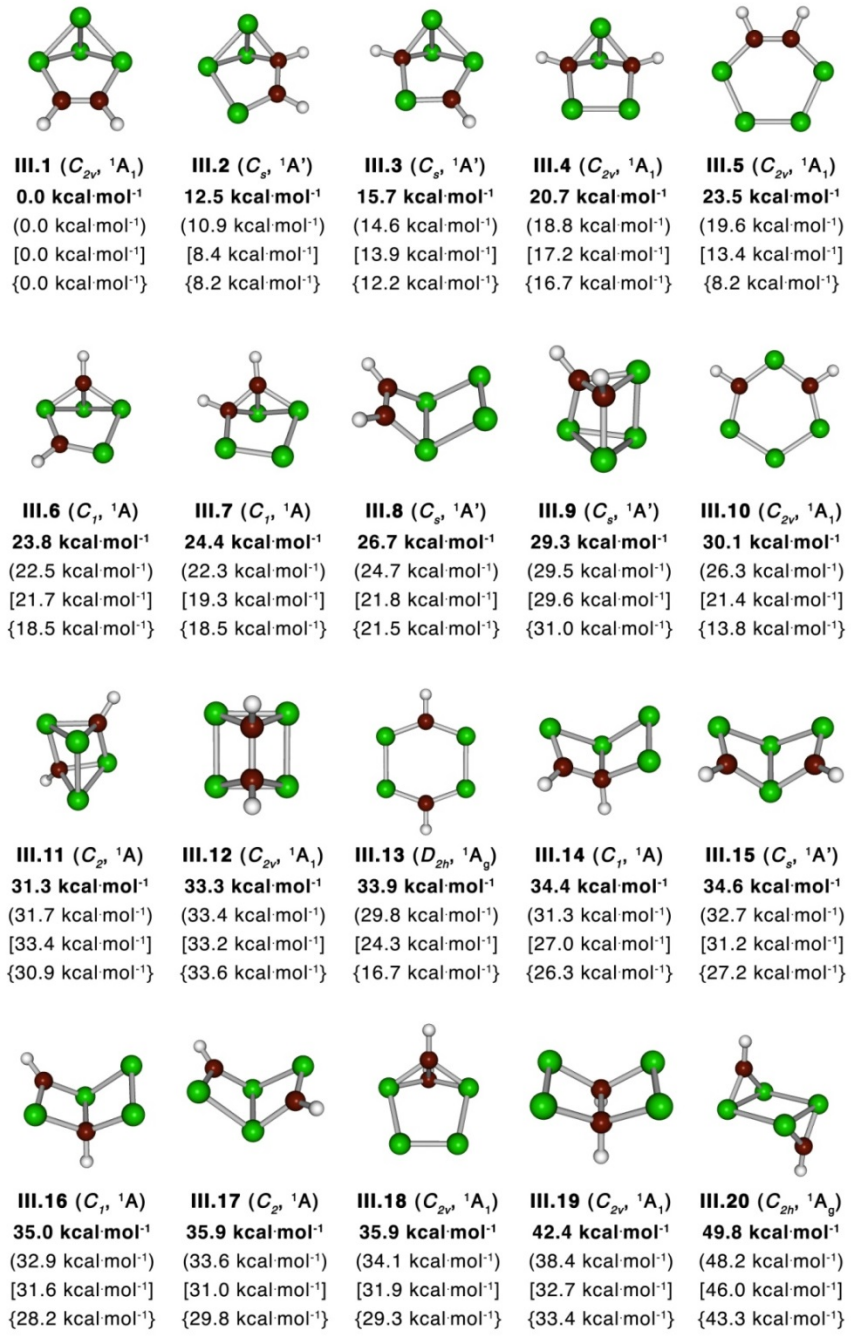

Fig 12-6. Selected structures of $C_2H_2P_4$, their point group symmetries, spectroscopic states and ZPE corrected relative energies. The energies are given at: CCSD(T)/CBS (bold), CCSD(T)/cc-pVTZ (in brackets), CCSD(T)/cc-pVDZ (square brackets), and B3LYP/6-311++G** (curly brackets), all at B3LYP/6-311++G** optimized geometries.

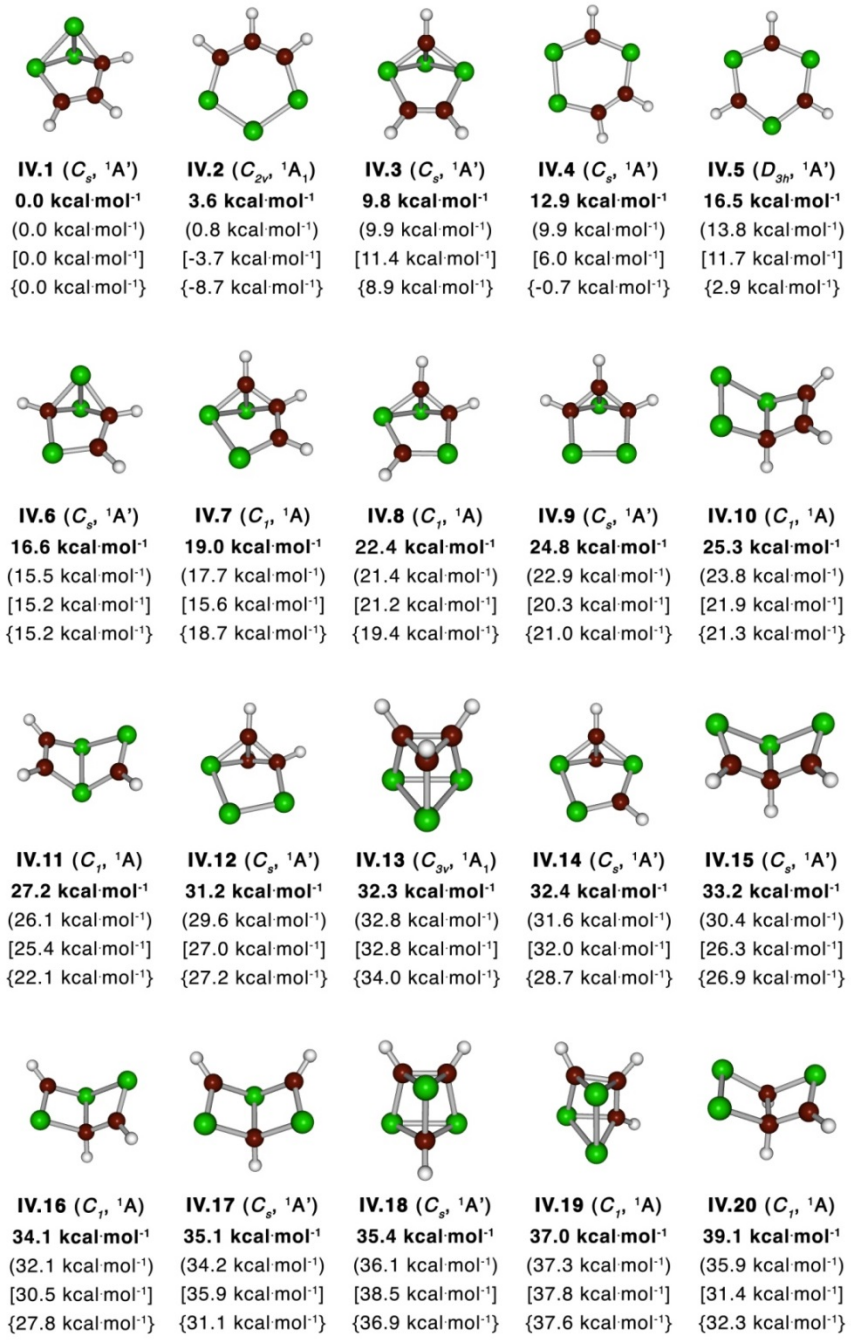

Fig 12-7. Selected isomers of $C_3H_3P_3$, their point group symmetries, spectroscopic states and ZPE corrected relative energies. The energies are given at: CCSD(T)/CBS (bold), CCSD(T)/cc-pVTZ (in brackets), CCSD(T)/cc-pVDZ (square brackets), and B3LYP/6-311++G** (curly brackets), all at B3LYP/6-311++G** optimized geometries.

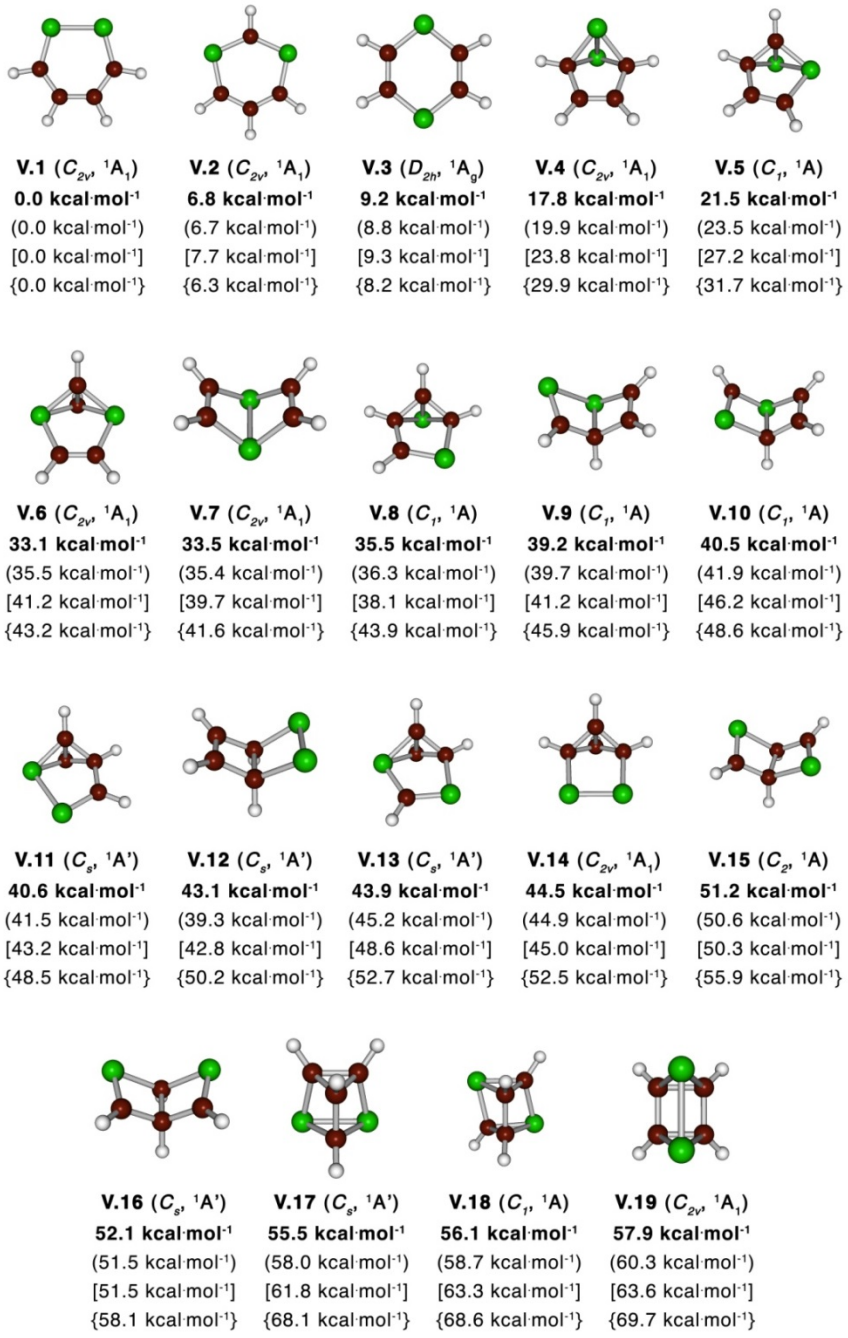

Fig 12-8. Selected isomers of $C_4H_4P_2$, their point group symmetries, spectroscopic states and ZPE corrected relative energies. The energies are given at: CCSD(T)/CBS (bold), CCSD(T)/cc-pVTZ (in brackets), CCSD(T)/cc-pVDZ (square brackets), and B3LYP/6-311++G** (curly brackets), all at B3LYP/6-311++G** optimized geometries.

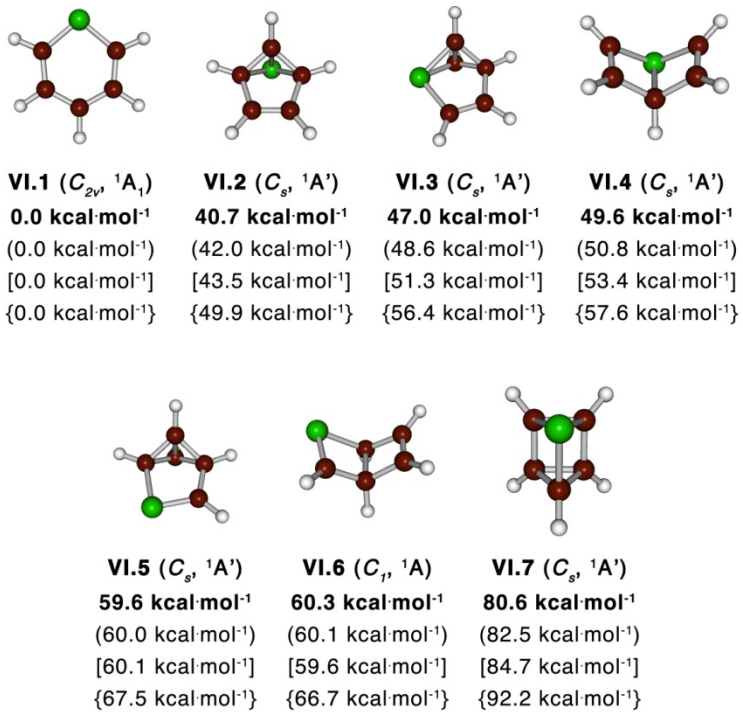

Fig 12-9. Selected isomers of C_6H_6, their point group symmetries, spectroscopic states and ZPE corrected relative energies. The energies are given at: CCSD(T)/CBS (bold), CCSD(T)/cc-pVTZ (in brackets), CCSD(T)/cc-pVDZ (square brackets), and B3LYP/6-311++G** (curly brackets), all at B3LYP/6-311++G** optimized geometries.

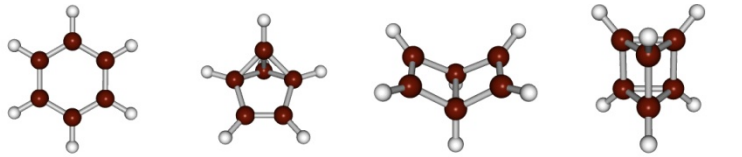

VII.1 (D_{6h}, $^1A_{1g}$)	**VII.2** (C_{2v}, $^1A_1$)	**VII.3** (C_{2v}, $^1A_1$)	**VII.4** (D_{3h}, $^1A_1'$)
0.0 kcal·mol^{-1}	**72.2 kcal·mol^{-1}**	**76.2 kcal·mol^{-1}**	**112.4 kcal·mol^{-1}**
(0.0 kcal·mol^{-1})	(72.5 kcal·mol^{-1})	(76.0 kcal·mol^{-1})	(113.3 kcal·mol^{-1})
[0.0 kcal·mol^{-1}]	[72.8 kcal·mol^{-1}]	[75.6 kcal·mol^{-1}]	[113.6 kcal·mol^{-1}]
{0.0 kcal·mol^{-1}}	{80.1 kcal·mol^{-1}}	{82.8 kcal·mol^{-1}}	{122.2 kcal·mol^{-1}}

Fig 12-10. Selected isomers of C_6H_6, their point group symmetries, spectroscopic states and ZPE corrected relative energies. The energies are given at: CCSD(T)/CBS (bold), CCSD(T)/cc-pVTZ (in brackets), CCSD(T)/cc-pVDZ (square brackets), and B3LYP/6-311++G** (curly brackets), all at B3LYP/6-311++G** optimized geometries.

CHAPTER 13

DECIPHERING THE MYSTERY OF HEXAGON HOLES IN AN ALL-BORON GRAPHENE α-SHEET [*]

Abstract

Boron could be the next element after carbon capable of forming 2D-materials similar to graphene. Theoretical calculations predict that the most stable planar all-boron structure is the so-called α-sheet. The mysterious structure of the α-sheet with peculiar distribution of filled and empty hexagons is rationalized in terms of chemical bonding. We show that the hexagon holes serve as scavengers of extra electrons from the filled hexagons. This work could advance rational design of all-boron nanomaterials.

Recently discovered graphene,[1,2] a one-atom-thick planar sheet of carbon atoms densely packed in a honeycomb crystal lattice, gave us the opportunity to probe properties of 2D-materials. The isolated layers of graphene were found to exhibit high carrier mobilities (>200 000 $cm^2 V^{-1} s^{-1}$ at electron densities of 2×10^{11} cm^{-2}),[3-6] exceptional Young modulus values (>0.5–1 TPa), and large force constants (1–5 Nm^{-1}).[7–9] Due to these properties graphene is attractive for many potential commercial applications such as energy storage,[10] micro- and optoelectronics.[11]

Boron, the light neighbour of carbon in the Periodic Table, is an excellent next candidate for acquiring 2D-structures. Indeed, graphite-like material MgB_2, which

[*] Coauthored by Timur R. Galeev, Qiang Chen, Jin-Chang Guo, Hui Bai, Chang-Qing Miao, Hai-Gang Lu, Alina P. Sergeeva, Si-Dian Li, and Alexander I. Boldyrev. Reproduced from *Phys. Chem. Chem. Phys.* **2011**, *13*, 11575-11578 with permission from the PCCP Owner Societies.

possesses remarkable superconductivity near 40 K,[12] is composed of planar honeycomb crystal lattices of boron atoms with magnesium atoms located above the center of the hexagons between the layers. Thus, each of the all-boron graphite-like sheets in MgB_2 is an example of a 2D-structure composed of boron atoms. However, boron atoms in MgB_2 have a charge of −1 and thus acquire electronic configuration similar to that of carbon. One can construct a honeycomb crystal lattice of a neutral boron sheet assuming that every boron is sp^2-hybridized and forms three two-center-two-electron (2c-2e) σ-bonds. Such a structure was shown to be less stable than the truly remarkable α-sheet structure (Fig. 13-1), computationally predicted by Tang and Ismail-Beigi[13,14] and Yang *et al.*[15] This structure is formed of two types of hexagons: empty hexagons and ones with an additional boron atom at the center. A similar pattern with hexagon holes and filled hexagons was predicted for boron nanotubes.[15,16] All-boron fullerenes with a similar network of filled hexagons and pentagon holes have also attracted significant attention[13,16–27] since Szwacki *et al.* predicted a highly spherical buckyball structure for B_{80}.[28]

The 2D-lattice with hexagon holes and filled hexagon motifs in the α-sheet is puzzling and understanding its chemical bonding pattern could be an important advancement towards future design of all-boron nanostructures. In order to address this issue we performed a chemical bonding analysis for the lattice. To date there is no computational tool capable of analyzing chemical bonding in terms of 2c-2e, 3c-2e or *n*c-2e bonds in general in infinite 2D-lattices, therefore we investigated chemical bonding in fragments of the all-boron α-sheet. For our analysis we chose three α-sheet fragments,

which are shown in Fig. 13-2, 13-3, and 13-4. They were selected in a way to preserve electro neutrality when placed into the 2D-α-sheet. These fragments allowed us to trace all bonding elements in the α-sheet and reduce the influence of the boundary conditions in our fragments upon extension of their size.

Since chemical bonding in the all-boron α-sheet was anticipated to involve delocalized bonding we selected the Adaptive Natural Density Partitioning (AdNDP) method as a tool for our chemical bonding analysis. This method was recently developed by Zubarev and Boldyrev[29] and used to analyze chemical bonding in boron clusters,[29–31] prototypical aromatic organic molecules[32] and gold clusters.[33] The AdNDP method analyzes the first-order reduced density matrix in order to obtain its local block eigenfunctions with optimal convergence properties for electron density description. The obtained local blocks correspond to the sets of *n* atoms (*n* ranging from one to the total number of atoms in the molecule) that are tested for the presence of two-electron objects (*n*-center two electron (*n*c-2e) bonds, including core electrons and lone pairs as a special case of *n* = 1) associated with this particular set of *n* atoms. AdNDP initially searches for core electron pairs and lone pairs (1c-2e), then 2c-2e, 3c-2e,… and finally *n*c-2e bonds. At every step the density matrix is depleted of the density corresponding to the appropriate bonding elements. User-directed form of the AdNDP analysis can be applied to specified molecular fragments and is analogous to the directed search option of the standard Natural Bond Orbital (NBO) code.[34,35]AdNDP accepts only those bonding elements whose occupation numbers (ON) exceed the specified threshold values, which are usually chosen to be close to 2.00 |e|. When all recovered *n*c-2e bonding elements are

superimposed onto the molecular frame the overall pattern always corresponds to the point-group symmetry of the system. Thus, AdNDP recovers both Lewis bonding elements (1c-2e and 2c-2e objects, corresponding to the core electrons and lone pairs, and two-center two-electron bonds) and delocalized bonding elements, which are associated with the concepts of aromaticity and antiaromaticity. From this point of view, AdNDP achieves seamless description of systems featuring both localized and delocalized bonding without invoking the concept of resonance. Essentially, AdNDP is a very efficient and visual approach to interpretation of the molecular orbital-based wave functions.

We performed the AdNDP analysis of the all boron α-sheet fragments with geometric parameters (B–B distance of 1.67 Å) of the predicted lattice structure.[13,15] We used a hybrid density functional method known in the literature as B3LYP with the 6-31G basis set. AdNDP is an extension of the NBO analysis[34,35] and it was shown before[29,36] that AdNDP is not sensitive to the level of theory or the basis set. All calculations were performed using the AdNDP program and the Gaussian 03 software package.[37] Molecular visualization was performed using Molekel 5.4.[38]

First, we analyzed the seven-atom (the filled hexagon) fragment of the α-sheet (Fig. 13-2a). The charge of +7 was selected for the bare B_7 cluster from a few trial AdNDP runs which allowed us to have a symmetric chemical bonding picture with bonding elements, which will be shown later to be present in the 2D α-sheet lattice. The AdNDP analysis revealed six 3c-2e σ-bonds and one 7c-2e π-bond in the B_7^{+7} fragment. In order to reduce external charge we ran AdNDP calculations for the $B_7H_6^+$ cluster. The

analysis revealed the same chemical bonding pattern with additional six 2c-2e B–H σ-bonds (Fig. 13-2b), showing robustness of the chemical bonding picture.

The second model system was chosen in order to understand how the chemical bonding picture changes upon addition of three neighbouring filled hexagons to the B_7 motif (Fig. 13-3a). The AdNDP analysis of the B_{22}^{+16} cluster revealed a 3c-2e σ-bond in every peripheral triangle while a 4c-2e σ-bond was found in every rhombus motif at the junction of two hexagons (Fig. 13-3a). In addition, a 7c-2e π-bond on every filled hexagon was revealed using the user-directed form of the AdNDP method. It will be shown below that the newly found 4c-2e σ-bonds are present in the α-sheet at all junctions of the filled hexagons. Again, in order to test the robustness of this chemical bonding pattern we performed the same analysis for the $B_{22}H_{12}^{+4}$ system (Fig. 13-3b). We found that the bonding picture is the same as that for the B_{22}^{+16}cluster with additional twelve 2c-2e B–H σ-bonds.

The B_{30}^{+16} cluster was chosen as a fragment of the all-boron α-sheet containing a hexagonal hole (Fig. 13-4). The AdNDP analysis revealed twenty-four 3c-2e σ-bonds at the peripheral triangles and triangles bordering upon the hole. Again, a 4c-2e σ-bond was found in every rhombus motif at the junction of two hexagons. Then a 7c-2e π-bond was revealed on every filled hexagon using the user directed AdNDP method as well as the new bonding element in this cluster: a 6c-2e π-bond over the hexagon hole at the center. The analysis of the largest studied fragment allowed us to recover the last missing bonding element – the 6c-2e π-bond over the hexagon hole.

From the chemical bonding analyses of the model fragments we now can propose the following chemical bonding picture (Fig. 13-1b) for the infinite all-boron α-sheet. On every filled hexagon we found three 3c-2e σ-bonds (solid triangles), which are bordering upon the holes, three 4c-2e σ-bonds (solid rhombi) at the junction of two filled hexagons, and one 7c-2e π-bond (circles). With this chemical bonding for each B_7 fragment we have six valence electrons coming from three 3c-2e σ-bonds, three electrons coming from three 4c-2e σ-bonds and two electrons coming from the 7c-2e π-bond with the total number of eleven electrons. On the other hand, if we consider a filled hexagon as a part of the lattice we can calculate the total number of valence electrons as follows: each of the six peripheral boron atoms brings half of its valence electrons (9 electrons in total) and the central atom brings all its valence electrons (3 electrons) resulting in the total of twelve electrons per filled hexagon. Thus, there is one extra electron on each filled hexagon motif not involved in the bonding presented above. As one can see from the whole lattice picture the extra electron on a filled hexagon (an electronic donor) is shared by three hexagonal holes (three electronic acceptors) evenly distributed around it, while each hole is surrounded by six filled hexagons, resulting in two 'extra' electrons per hole. Those two electrons form the 6c-2e π-bond (Fig. 13-1b, circles over hexagon holes), which was revealed in our B_{30}^{+16}model system. It is interesting to notice that, unlike graphene, which contains in-plane 2c-2e C–C σ-bonds, the all-boron graphene α-sheet studied in this work possesses no localized 2c-2e B–B σ-interactions.

Occupation numbers (ONs) revealed for every bonding element are very close to the ideal value of 2.00 |e| (see Fig. 12-2, 12-3, 12-4) giving additional credibility to the presented chemical bonding picture for the all-boron α-sheet.

The AdNDP method revealed a delocalized π-bond on every filled hexagon and every hexagon hole. Each π-bond is responsible for local π-aromaticity in the corresponding fragment. We further probed the revealed π-aromaticity using one of the most popular ways of evaluating aromaticity in planar species, the nuclear independent chemical shift ($NICS_{zz}$), which was introduced by Schleyer and co-workers.[39] In this method negative $NICS_{zz}$ values indicate aromaticity and positive values indicate antiaromaticity. $NICS_{zz}$ calculations were performed above the center of the filled and empty hexagons in the B_{30}^{+16} model system using the B3LYP/6-311+G* level of theory. We also calculated the same set of the $NICS_{zz}$ values for the prototypical aromatic system, benzene, using the B3LYP/6-311++G** level of theory. Results of all the calculations are summarized in Table 13-1.

One can see that the $NICS_{zz}$ values above the filled hexagons and hexagon holes are significantly more negative than the corresponding values of benzene, thus, confirming the presence of local π-aromaticity in the hexagons.

From our overall chemical bonding picture we get a 1/3 ratio for the numbers of valence π- and σ-electrons in the all-boron α-sheet, which was obtained from the fact that out of a total of twelve valence electrons on each filled hexagon motif (including the one it donates to the holes) three form π-bonds and nine form σ-bonds. We would like to stress that this ratio is close to that of the so far largest planar boron clusters studied both

experimentally and theoretically: B_{16}^{2-} (the valence π- to σ-ratio is 0.25)[30] and B_{19}^{-} (the valence π- to σ-ratio is 0.26).[31] The presence of holes as well as their amount relative to the number of filled hexagons in the all-boron α-sheet is determined by this π- to σ-electrons ratio: the holes in the all-boron α-sheet absorb the third π-electron of each filled hexagon, which cannot be accepted by the motif. Interestingly, the ratio of 1/9 between the number of the donated π-electrons (1 electron) and the number of total σ-electrons (9 electrons) in a filled hexagon equals the hexagon hole density of 1/9 in the infinite all-boron α-sheet.[13] This analysis agrees with the proposed chemical bonding pattern demonstrated in Fig. 13-1b for a building block of the α-sheet boron.

Now it is clear why the hypothetical honeycomb crystal lattice of a neutral boron sheet where each boron atom acquires sp^2-hybridization and forms three 2c-2e σ-bonds but no π-bonds is not energetically favourable. In order for the neutral all-boron 2D-structure to be energetically favourable it should have a certain amount of electron density in the π-system. If we transfer some amount of electrons from the 2c-2e σ-bonds in the honeycomb crystal lattice to the π-system it breaks the connectivity in the σ-framework and that makes the whole structure energetically unfavourable. Similarly, the all-boron neutral 2D-structure composed of boron equilateral triangles (or of filled hexagons but with no holes), the so-called triangular sheet, should be unstable too. There are two ways to construct the triangular boron sheet in accordance with our bonding model. First, if one tried to build it with every triangle carrying a 3c-2e σ-bond, there would be not enough electrons even for such σ-bonding, since every boron atom belongs to six triangles and therefore can contribute $3 \times (1/6) = 1/2$ electrons to the triangle with

the total of 1.5 electrons per triangle only. Alternatively, we can construct the neutral all-boron 2D-sheet of filled hexagons with the presence of six 4c-2e σ-bonds (they are shared with the neighbouring hexagons) and six π-orbitals on each filled hexagon. This structure is also unfavourable since the ratio of π- to σ-electrons is 0.5, which was not observed for the lowest energy planar boron clusters.[30,31,40–42]

The unprecedented chemical bonding model presented in the current work widens our understanding of chemical bonding in general and we believe that the presented bonding picture could be an advance toward rational design of future all-boron nanomaterials.

Notes and references

1 K. S. Novoselov, A. K. Geim, S. V. Morozov, D. Jiang, Y. Zhang, S. V. Dubonos, I. V. Grigorieva and A. A. Firsov, *Science*, 2004, **306**, 666.

2 K. S. Novoselov, A. K. Geim, S. V. Morozov, D. Jiang, M. I. Katsnelson, I. V. Grigorieva, S. V. Dubonos and A. A. Firsov, *Nature*, 2005, **438**, 197.

3 S. Unarunotai, Y. Murata, C. E. Chialvo, N. Mason, I. Petrov, R. G. Nuzzo, J. S. Moore and J. A. Rogers, *Adv. Mater.*, 2010, **22**, 1072.

4 K. I. Bolotin, K. J. Sikes, Z. Jiang, M. Klima, G. Gudenberg, J. Hone, P. Kim and H. L. Stormer, *Solid State Commun.*, 2008, **16**, 351.

5 S. V. Morozov, K. S. Novoselov, M. I. Katsnelson, F. Schedin, D. C. Elias, J. A. Jaszcnak and A. K. Geim, *Phys. Rev. Lett.*, 2008, **100**, 016602.

6 X. Du, I. Skachko, A. Barker and E. Y. Andrei, *Nat. Nanotechnol.*, 2008, **3**, 491.

7 I. W. Frank, D. M. Tanenbaum, A. M. van der Zanda and P. L. McEuen, *J. Vac. Sci. Technol., A*, 2007, **25**, 2558.

8 F. Scarpa, S. Adhikari and A. S. Phani, *Nanotechnology*, 2009, **20**, 065709.

9 R. Faccio, P. A. Denis, H. Pardo, C. Goyenola and A. W. Mombru, *J. Phys.: Condens. Matter*, 2009, **21**, 285304.

10 M. D. Stoller, S. Park, Y. Zhu, J. An and R. S. Ruoff, *Nano Lett.*, 2008, **8**, 3498.

11 K. Mullen and J. P. Rabe, *Acc. Chem. Res.*, 2008, **41**, 511.

12 J. Nagamatsu, N. Nakagawa, T. Muranaka, Y. Zenitani and J. Akimitsu, *Nature*, 2001, **410**, 63.

13 H. Tang and S. Ismail-Beigi, *Phys. Rev. Lett.*, 2007, **99**, 115501.

14 H. Tang and S. Ismail-Beigi, *Phys. Rev. B*, 2009, **80**, 134113.

15 X. Yang, Y. Ding and J. Ni, *Phys. Rev. B*, 2008, **77**, 0414402.

16 N. G. Szwacki and C. J. Tymczak, *Chem. Phys. Lett.*, 2010, **494**, 80.

17 G. Gopakumar, M. T. Nguyen and A. Ceulemans, *Chem. Phys. Lett.*, 2008, **450**, 175.

18 T. Baruah, M. R. Pederson and R. R. Zope, *Phys. Rev. B*, 2008, **78**, 045408.

19 A. Sadrzadeh, O. V. Pupysheva, A. K. Singh and B. I. Yakobson, *J. Phys. Chem. A*, 2008.

20 S. Botti, A. Castro, N. N. Lathiotakis, X. Andrade and M. A. L. Marques, *Phys. Chem. Chem. Phys.*, 2009, **11**, 4523.

21 Q. B. Yan, Q. R. Zheng and G. Su, *Phys. Rev. B*, 2008, **77**, 224106.

22 A. Y. Liu, R. R. Zope and M. R. Pederson, *Phys. Rev. B*, 2008, **78**, 155422.

23 N. G. Szwacki, *Nanoscale Res. Lett.*, 2008, **3**, 80.

24 Q. B. Yan, X. L. Sheng, Q. R. Zheng, L. Zhang and G. Su, *Phys. Rev. B*, 2008, **78**, 201401R.

25 R. R. Zope, T. Baruah, K. C. Lau, A. Y. Liu, M. R. Pederson and B. I. Dunlap, *Phys. Rev. B*, 2009, **79**, 161403R.

26 J. Zhao, L. Wang, F. Li and Z. Chen, *J. Phys. Chem. A*, 2010, **114**, 9969.

27 P. Jin, C. Hao, Z. Gao, S. Zhang and Z. Chen, *J. Phys. Chem. A*, 2009, **113**, 11613.

28 N. G. Szwacki, A. Sadrzadeh and B. I. Yakobson, *Phys. Rev. Lett.*, 2007, **98**, 166804.

29 D. Yu. Zubarev and A. I. Boldyrev, *Phys. Chem. Chem. Phys.*, 2008, **10**, 5207.

30 A. P. Sergeeva, D. Yu. Zubarev, H.-J. Zhai, A. I. Boldyrev and L. S. Wang, *J. Am. Chem. Soc.*, 2008, **130**, 7244.

31 W. Huang, A. P. Sergeeva, H.-J. Zhai, B. B. Averkiev, L. S. Wang and A. I. Boldyrev, *Nat. Chem.*, 2010, **2**, 202.

32 D. Yu. Zubarev and A. I. Boldyrev, *J. Org. Chem.*, 2008, **73**, 9251.

33 D. Yu. Zubarev and A. I. Boldyrev, *J. Phys. Chem.*, 2009, **13**, 866.

34 J. P. Foster and F. Weinhold, *J. Am. Chem. Soc.*, 1980, **102**, 7211.

35 F. Weinhold and C. Landis, *Valency and Bonding. A Natural Bond Orbital Donor-Acceptor Perspective*, Cambridge University Press, Cambridge, UK, 2005.

36 A. P. Sergeeva and A. I. Boldyrev, *Comments Inorg. Chem.*, 2010, **31**, 2.

37 M. J. Frisch, G. W. Trucks, H. B. Schlegel, G. E. Scuseria, M. A. Robb, J. R. Cheeseman, J. A. Montgomery, Jr., T. Vreven, K. N. Kudin, J. C. Burant, J. M. Millam, S. S. Iyengar, J. Tomasi, V. Barone, B. Mennucci, M. Cossi, G. Scalmani, N. Rega, G. A. Petersson, H. Nakatsuji, M. Hada, M. Ehara, K. Toyota, R. Fukuda, J. Hasegawa, M. Ishida, T. Nakajima, Y. Honda, O. Kitao, H. Nakai, M. Klene, X. Li, J. E. Knox, H. P. Hratchian, J. B. Cross, V. Bakken, C. Adamo, J. Jaramillo, R. Gomperts, R. E. Stratmann, O. Yazyev, A. J. Austin, R. Cammi, C. Pomelli, J. W. Ochterski, P. Y. Ayala, K. Morokuma, G. A. Voth, P. Salvador, J. J. Dannenberg, V. G. Zakrzewski, S. Dapprich, A. D. Daniels, M. C. Strain, O. Farkas, D. K. Malick, A. D. Rabuck, K. Raghavachari, J. B. Foresman, J. V. Ortiz, Q. Cui, A. G. Baboul, S. Clifford, J. Cioslowski, B. B. Stefanov, G. Liu, A. Liashenko, P. Piskorz, I. Komaromi, R. L. Martin, D. J. Fox, T. Keith, M. A. Al-Laham, C. Y. Peng, A. Nanayakkara, M. Challacombe, P. M. W. Gill, B. Johnson, W. Chen, M. W. Wong, C. Gonzalez and J. A. Pople, *GAUSSIAN 03, (Revision D.01)*, Gaussian, Inc., Wallingford, CT, 2004.

38 U. Varetto, *Molekel 5.4.0.8*, Swiss National Supercomputing Centre, Manno, Switzerland, 2009.

39 P. v. R. Schleyer, C. Maerker, A. Dransfeld, H. Jiao and N. J. R. v. E. Hommes, *J. Am. Chem. Soc.*, 1996, **118**, 6317.

40 A. N. Alexandrova, A. I. Boldyrev, H.-J. Zhai and L. S. Wang, *Coord. Chem. Rev.*, 2006, **250**, 2811.

41 B. Kiran, S. Bulusu, H. J. Zhai, S. Yoo, X. C. Zeng and L. S. Wang, *Proc. Natl. Acad. Sci. U. S. A.*, 2005, **102**, 961.

42 H. J. Zhai, B. Kiran, J. Li and L. S. Wang, *Nat. Mater.*, 2003, **2**, 827.

Table 13-1 Calculated $NICS_{zz}$ values (ppm)

R_z[a]/Å	Filled hexagon[b]	Hexagon hole[b]	Benzene [c]
0.0	—	−51.5	−14.5
0.2	−100.4	−53.0	−16.3
0.4	−75.3	−56.9	−20.6
0.6	−70.8	−61.7	−25.2
0.8	−66.3	−66.1	−28.3
1.0	−60.8	−68.9	−29.2
1.2	−55.2	−69.9	−28.2
1.4	−49.9	−69.0	−26.0
1.6	−45.2	−66.8	−23.2
1.8	−41.0	−63.6	−20.2
2.0	−37.3	−59.8	−17.4

[a] Distance from the hexagon centre.
[b] Calculated at B3LYP/6-311+G*.
[c] Calculated at B3LYP/6-311++G**.

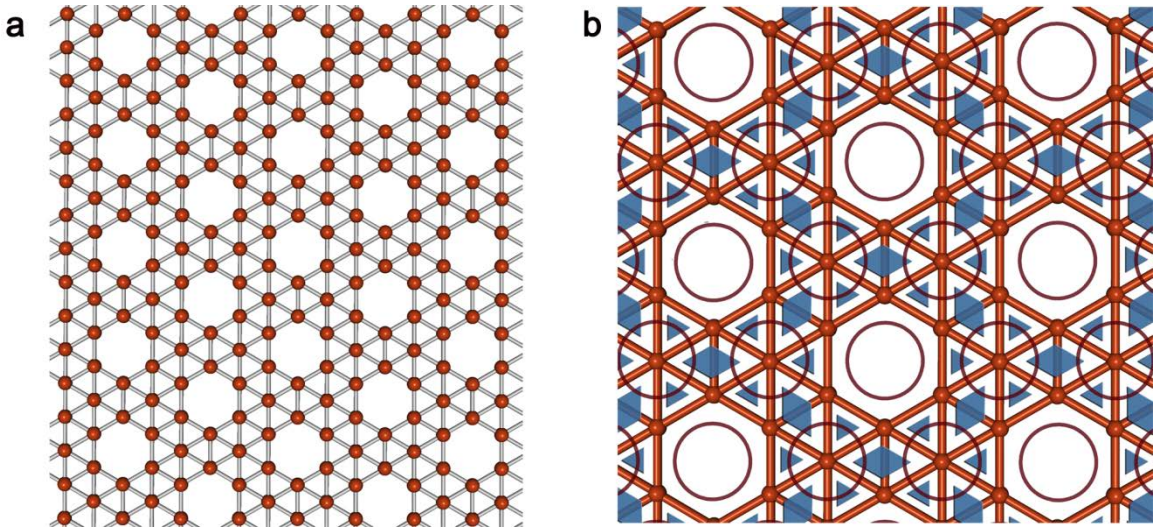

Fig. 13-1 (a) Geometric structure of the all-boron α-sheet. (b) The proposed bonding pattern for the all-boron α-sheet: 3c-2e σ-bonds (solid triangles), 4c-2e σ-bonds (solid rhombi) and delocalized π-bonds (circles).

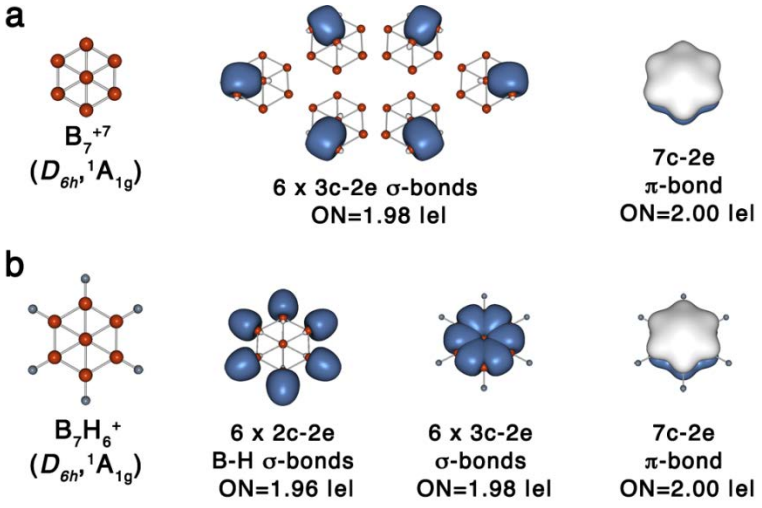

Fig. 13-2 (a) Geometric structure of the B_7^{+7} fragment, six 3c-2e σ-bonds, and one 7c-2e π-bond. (b) Geometric structure of the $B_7H_6^+$ fragment, six 2c-2e B–H σ-bonds superimposed on a single framework, six 3c-2e σ-bonds superimposed on a single framework, and one 7c-2e π-bond.

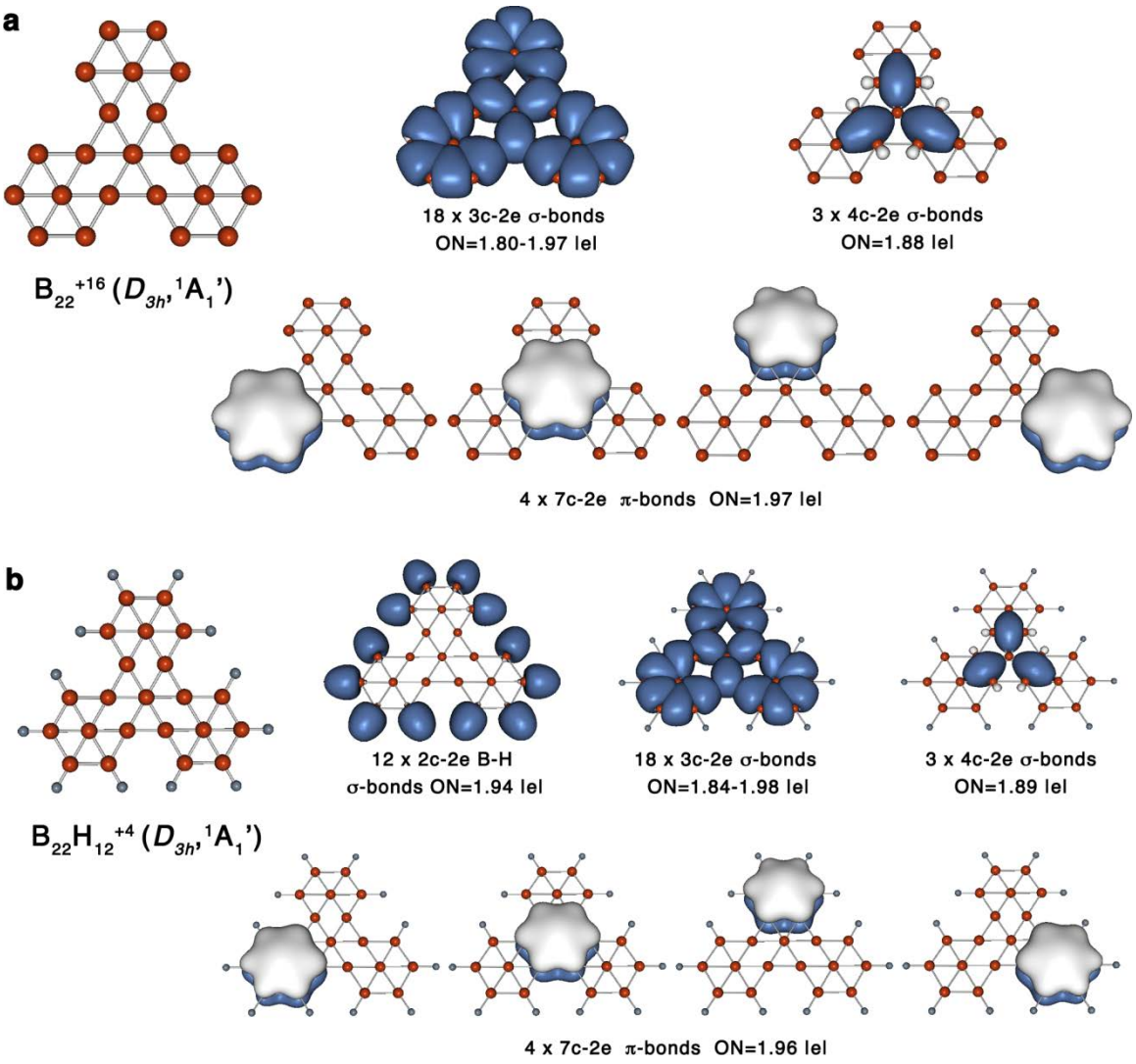

Fig. 13-3 (a) Geometric structure of the B_{22}^{+16} fragment, eighteen 3c-2e σ-bonds (inside of peripheral triangles) superimposed on a single framework, three 4c-2e σ-bonds (inside of rhombus motifs) superimposed on a single framework, and four 7c-2e π-bonds located on filled hexagons. (b) Geometric structure of the $B_{22}H_{12}^{+4}$ fragment, twelve 2c-2e B–H σ-bonds, eighteen 3c-2e σ-bonds superimposed on a single framework, three 4c-2e σ-bonds superimposed on a single framework, and four 7c-2e π-bonds.

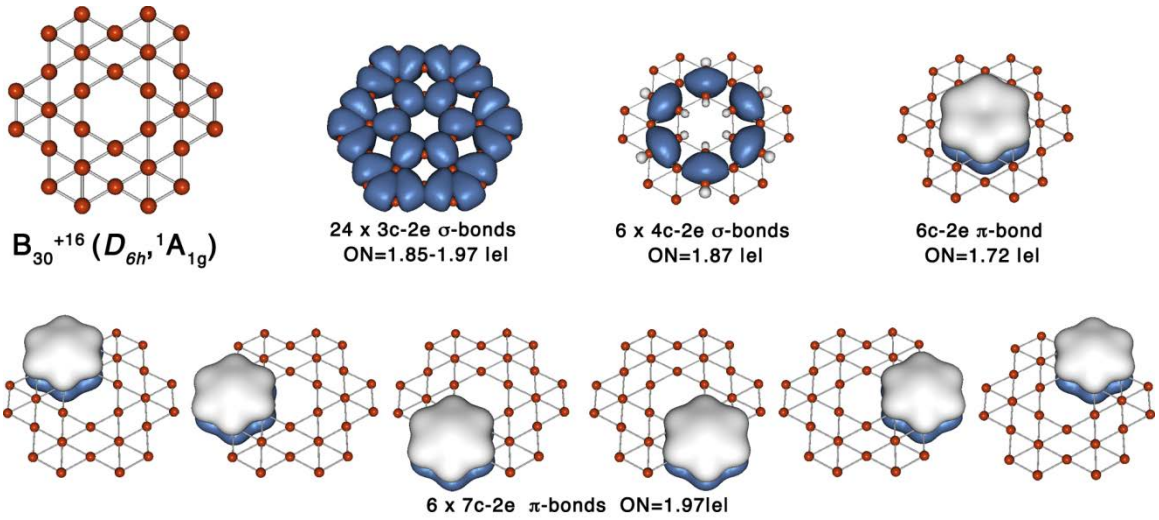

Fig. 13-4 Geometric structure of the B_{30}^{+16} fragment of the α-sheet, twenty-four 3c-2e σ-bonds (inside of peripheral triangles and triangles bordering upon the hole) superimposed on a single framework, six 4c-2e σ-bonds (inside of rhombus motifs) superimposed on a single framework, one 6c-2e π-bond located on the hexagon hole, and six 7c-2e π-bonds located on filled hexagons.

CHAPTER 14

SOLID STATE ADAPTIVE NATURAL DENSITY PARTITIONING: A TOOL FOR DECIPHERING MULTI-CENTER BONDING IN PERIODIC SYSTEMS *

Abstract

A new tool to elucidate chemical bonding in bulk solids, surfaces and nanostructures has been developed. Solid State Adaptive Natural Density Partitioning (SSAdNDP) is a method to interpret chemical bonding in terms of classical lone pairs and two-center bonds, as well as multi-center delocalized bonds. Here we extend the domain of AdNDP to bulk materials and interfaces, yielding SSAdNDP. We demonstrate the versatility of the method by applying it to several systems featuring both localized and many-center chemical bonding, and varying in structural complexity: boron α-sheet, magnesium diboride and the Na_8BaSn_6 Zintl phase.

14-1. Introduction

The lone pairs and two-centered bonds of Lewis structures form the basis of our qualitative understanding of chemical bonding. Due to their simplicity and wide applicability, Lewis structures are widely used and taught throughout chemistry, in spite of their known limitations in describing delocalized interactions. Such limitations can be overcome by using molecular orbital (MO) theory, which provides a more rigorous description of molecules and forms the basic language of much of quantum chemistry.

---

* Coauthored by Timur R. Galeev Benjamin D. Dunnington, J. R. Schmidt, and Alexander I. Boldyrev. Reproduced from *Phys. Chem. Chem. Phys*. **2013**, *15*, 5022-5029 with permission from the PCCP Owner Societies.

However, the resulting canonical molecular orbitals are, in general, delocalized over the whole molecule and thus hard to interpret within the chemically intuitive framework of Lewis theory. As a result, there is a need for techniques to interpret MO calculation results within a localized bonding perspective. While a wide variety of such techniques exist, only a handful are also applicable to systems with periodic symmetry, specifically bulk and surface structures.

Among these existing approaches, delocalization (and corresponding localization) indices (LI/DI) provide one such quantitative description of such multi-center bonding interactions.[1,2] In this approach, electron localization within some predefined volume (LI) and delocalization between different volumes (DI) is quantified *via* analysis of the Fermi hole. The spatial localization of this Fermi hole among one, two, or more atomic centers, often defined in terms of Bader volumes,[3] provides a metric on the delocalization of a bonding pair of electrons, corresponding loosely to lone pairs, two- and multi-center bonding. While not entirely consistent with conventional notions of valency (especially when analyzing polar systems or when electron correlation is accounted for), the LI and DI can be used to inform valency and bond order respectively, giving a quantitative view of bonding interactions. While readily applicable to periodic systems,[4,5] in general, it is difficult to map the results of electron delocalization analysis into an intuitive Lewis-like picture.

An alternative representation of bonding is offered by the crystal orbital overlap population (COOP)[6,7] approach, which is explicitly designed for analysis of bonding in periodic systems. Bonding interactions are identified between defined atomic-like orbitals

on different centers by analyzing the bonding (or anti-bonding) character of a given band $\psi(k)$. The orbital basis allows for the characterization of interactions using chemical concepts such as σ- and π-bonding. However these interactions are described in *reciprocal* space (*k*-space, as opposed to real space) and are therefore delocalized over all space. While COOP found utility in applications such as justifying observed crystal structures,[7] it does not provide a localized, real space description of bonding that is commensurate with conventional Lewis theory.

Localized molecular orbital (LMO) techniques,[8–11] provide another orbital-based approach to analyzing chemical bonding in bulk materials. LMO methods exploit the invariance of the wavefunction under unitary transformation to localize the orbitals under a given metric. However, no unique localization criterion can be defined, and each yields slightly different results and interpretations. Nonetheless, these techniques have found wide utility in studying molecular systems and have been extended to periodic systems *via* maximally localized Wannier functions.[12,13] Although one-, two-, and many-center bonding are inherently treated on an equal footing, the resulting localized orbitals are not rigorously related to bonds involving specific atomic centers. Rather, orbitals are generally localized to some region of space and then (frequently) interpreted in terms of specific bonding interactions or lone pairs – once again, providing no direct mapping to the powerful, intuitive (and often predictive) Lewis-like framework.

In contrast to the above methods, Natural Bond Orbital (NBO) analysis[14–17] constructs an optimal Lewis-like representation of bonding based on the underlying electronic structure calculation. The analysis is “natural” in that the bonding orbitals are

determined directly as eigenvectors of the system's density matrix (or portions thereof). Basing the analysis in the density matrix ensures a rigorous foundation for the orbitals identified. While this limits the bonds to two-electron interactions, it allows for the results to be interpreted within the classical Lewis picture of electron pairing. Additionally, many electron bonding motifs, such as three-center four-electron bonds, can be understood using a resonance representation of two-electron bonds; for a detailed discussion, see ref. 14. In NBO, lone pairs and bonds are constructed as linear combinations of orthogonal hybrid orbitals centered on atoms within the molecule. While traditionally restricted to molecular systems, NBO was recently extended to periodic systems, allowing for the analysis of chemical bonding in bulk materials and interfaces.[18]

While, in principle, the NBO algorithm can be generalized to many-centered bonding, the extension is nontrivial and existing implementations are limited to two- and three-centered bonds. In some cases, this limitation can be partially circumvented by introducing the concept of multiple resonance structures *via* Natural Resonance Theory.[19–21] However, there is a need for an analysis technique capable of explicitly identifying multi-center bonding motifs alongside the traditional Lewis structure elements of lone pairs and bonds, especially in periodic systems where the number of potential resonance structures grows rapidly. Adaptive Natural Density Partioning (AdNDP) is an extension of NBO that offers a natural description of both localized (two-centered) and delocalized (many-centered) bonding.[22] AdNDP has been successfully applied to a variety of molecular systems, including: prototypical organic aromatic

compounds,[23,24] metalloorganic and inorganic complex compounds,[25,26] pure and mixed boron clusters,[27–37] and gold nanoparticles.[38,39]

Here, we present an extension of AdNDP to periodic systems. We demonstrate the scope of the newly developed solid-state AdNDP (SSAdNDP) by applying it to several representative bulk systems featuring both traditional localized and many-center bonds.

14-2. Theory

We begin with a brief review of the standard AdNDP process as applied to molecular systems; complete details can be found elsewhere.[22] AdNDP calculations begin with the real space density matrix, P^{AO}, expressed in a localized atomic orbital (AO) basis set that is obtained from the underlying electronic structure calculation. The density matrix is then transformed into the Natural Atomic Orbital basis, P^{NAO}, which is an *orthogonal* atom-centered basis that is maximally occupied for the given molecular environment. The details of this transformation are given in ref. 16. The density matrix in this basis straightforwardly provides atomic populations in what is known as Natural Population Analysis (NPA).[16]

Bonds are identified by analyzing various atomic subblocks of P^{NAO}. For a given number of centers, n, all possible n-tuples are first enumerated. For each tuple, the corresponding n-atom subblock of P^{NAO} is extracted and the eigenvalues/eigenvectors of this matrix are calculated. Each eigenvector with occupation (eigenvalue) above some pre-determined threshold (usually near two) is identified as an n-center two-electron bond. Contributions from all identified n-center bonds are then removed from the density

matrix to prevent the double counting of their density in higher-center bonds. The process is repeated for n + 1-center bonds and iterated until all electron pairs have been accounted for. This ascending structure guarantees that localized interactions are properly identified. Note that selection of appropriate occupancy cutoffs is extremely important, since the designation of n-center bonds directly affects the classification of n + 1-center bonds. The goal is to obtain the most localized bonds, with occupancy near two and symmetry consistent with that of the system.

The lth bond thus obtained for a given tuple ($ij\ldots k$), $\left|h_l^{(ij\ldots k)}\right\rangle$, can be thought of as a linear combination of hybrids, $\left|\eta_l^{\alpha}\right\rangle$, on each center, α, contained in the tuple, with some coefficients $c_{l,\alpha}$.

$$\left|h_l^{(ij\ldots k)}\right\rangle = \sum_{\alpha}^{(ij\ldots k)} c_{l,\alpha}\left|\eta_l^{\alpha}\right\rangle ,$$

where hybrid $\left|\eta_l^{\alpha}\right\rangle$ is simply the collection of all NAO functions in the bond $\left|h_l^{(ij\ldots k)}\right\rangle$ contained on center α. In AdNDP, unlike the NBO procedure, the hybrids on a given center in different bonds are *not* rigorously orthogonal. Although this leads to a slight overestimation of bond occupancies, relaxing the orthogonality requirement maintains the symmetry of the obtained bonds and ensures that, for a given n, the results are independent of the order in which the tuples are searched.

The extension of AdNDP to periodic systems follows that recently applied to periodic NBO. We focus specifically on the *modifications* required to yield SSAdNDP, with additional details available elsewhere.[18]

The most natural description of the electronic structure of periodic systems is in reciprocal space (*k*-space).[40] The standard output of an electronic structure calculation of a periodic system gives the orbitals represented on a grid of points spanning the Brillouin zone (reciprocal space equivalent of the unit cell), known as *k*-points, yielding a set of density matrices, $\mathrm{P}^{k,AO}$. The AO-to-NAO transformation is now performed in reciprocal space, and the set of $\mathrm{P}^{k,AO}$ are transformed into the corresponding basis, $\mathrm{P}^{k,NAO}$. Details on how this transformation is performed in periodic systems can be found in ref. 18.

The $\mathrm{P}^{k,NAO}$ are not amenable to search for localized bonding orbitals, since the *k*-space picture is inherently delocalized over all of real space. Thus, the corresponding real space density matrices, $\mathrm{P}^{0s,NAO}$, are obtained by an inverse Fourier transform. Under periodic boundary conditions, four index tensors are required to represent a matrix quantity in real space; $\mathrm{P}^{0s}_{\mu\nu}$ represents the density matrix element between basis function μ located in the "central" unit cell 0 and basis function ν located in unit cell s. Due to locality, all relevant interactions can be captured by including all unit cells, relative to the central one, up to some $s_{\max}$, such that $\mathrm{P}^{0s_{\max}}_{\mu\nu} \approx 0$. Additionally, only interactions relative to the central unit cell must be accounted for, since $\mathrm{P}^{0s}_{\mu\nu} = \mathrm{P}^{h(h+s)}_{\mu\nu}$ by translational symmetry.

With the real space density matrix in the NAO basis, the search for bonds can begin. The first step is looking for one-center bonds, or lone pairs. For each atom in the unit cell, i, the atomic subblock $\mathrm{P}^{(i)} = \mathrm{P}^{00,NAO}_{ii}$ is diagonalized, corresponding to all basis functions centered on atom i. Any eigenvectors with eigenvalues above the occupancy

threshold (again close to two) are identified as lone pairs. The density contribution of each accepted lone pair is then depleted from P^{NAO},

$$\tilde{\mathbf{P}}^{00,NAO}_{\bar{i}\bar{i}} = \mathbf{P}^{00,NAO}_{\bar{i}\bar{i}} - N_l^{(i)} \left| h_l^{(i)} \right\rangle \left\langle h_l^{(i)} \right|,$$

where $|h^{(\mathrm{i})}{}_l\rangle$ is the lth eigenvector of $\mathrm{P}^{(i)}$ with eigenvalue, $N_l^{(i)}$, above the lone pair occupancy threshold. Note, for ease of notation, $\tilde{\mathbf{P}}^{NAO}$ will only be used to denote the density matrix as it is actively depleted of the bonds for a given number of centers, n. For the n + 1-center search, P^{NAO} will denote the density matrix depleted of all lower-center bonds; that is $\tilde{\mathbf{P}}^{NAO} \rightarrow \mathbf{P}^{NAO}$ in between the n and n + 1-center search.

Note that in the periodic NBO implementation, projection (rather than depletion) was used to remove the contribution of identified lone pairs. Here depletion is used for consistency with prior AdNDP work and for simplicity when dealing with many-centered bonds in periodic systems (*vide infra*).

The search continues with two-centered bonds. Periodic boundary conditions must now be taken into account when generating all symmetry unique atom pairs, and thus it is necessary to include bonding partners in the surrounding unit cells. Due to translational symmetry only those combinations which contain at least one atom in the central unit cell are necessary. Additionally a bond between an atom j in the central unit cell and atom i in unit cell s is symmetrically equivalent to the bond between atom i in the central unit cell and atom j in $-s$. Thus only one of these combinations must be probed for bonding interactions to properly count the bonds per unit cell. Furthermore, due to locality, we find that it is sufficient to include only bonding partners within the central and immediately adjacent unit cells.

To test for a localized two-center bond between a given pair of atomic centers i and j, in unit cells 0 and *s* respectively, the two-atom subblock $\mathrm{P}^{(ij)}$ is constructed from P^{NAO}

$$\mathrm{P}^{(ij)} = \begin{bmatrix} \mathrm{P}_{ii}^{00,NAO} & \mathrm{P}_{ij}^{0s,NAO} \\ \mathrm{P}_{ji}^{s0,NAO} & \mathrm{P}_{jj}^{ss,NAO} \end{bmatrix} = \begin{bmatrix} \mathrm{P}_{ii}^{00,NAO} & \mathrm{P}_{ij}^{0s,NAO} \\ \mathrm{P}_{ji}^{0(-s),NAO} & \mathrm{P}_{jj}^{00,NAO} \end{bmatrix},$$

where translational symmetry guarantees the second equality. Eigenvectors of this matrix, with corresponding eigenvalue above some designated two-center threshold, correspond to two-center bonds.

Unlike in NBO, the hybrids composing each bond are not orthogonalized to the lone pairs already found. Instead, the bonding orbitals as identified are depleted. Depletion is completed for each atomic block, $\mathrm{P}_{ij}^{0r,NAO}$ with $r \in \{0, s, -s\}$, that was used to construct $\mathrm{P}^{(ij)}$. Using the corresponding hybrids, $\left|\eta_l^i\right\rangle$, that compose the l^{th} bond $\left|h_l^{(ij)}\right\rangle$ with occupancy $N_l^{(ij)}$, above the two-center threshold, we deplete according to

$$\tilde{\mathrm{P}}_{ij}^{0r,NAO} = \mathrm{P}_{ij}^{0r,NAO} - N_l^{(ij)} c_{l,i} c_{l,j}^* \left|\eta_l^i\right\rangle\left\langle\eta_l^j\right|,$$

Note that even though for a particular bond, atom j may be located in unit cell *s*, the $\mathrm{P}_{jj}^{00,NAO}$ subblock will be depleted. Since the goal of SSAdNDP is to account for all electrons within the central unit cell, this is necessary to account for the symmetrically equivalent bond between atom i in unit cell –*s* and atom j in unit cell 0. Identifying both bonds leads to double counting, but the contribution of both hybrids in the central unit cell must be depleted to prevent inclusion of either in an *n* + 1-center bond. In a specific case, a particular bond can span atom i in the central unit cell as well as its periodic

image in a neighboring unit cell, *s*. The contribution of both hybrids must be removed from $\mathrm{P}_{ii}^{00,NAO}$ which is accomplished by the iterative depletion of atomic subblocks contained in $\mathrm{P}^{(ij\ldots k)}$). This situation only becomes likely as the number of centers increases and projection as implemented in ref. 18 was incapable of handling the iterative procedure necessary to account for this.

The process continues in a similar fashion for higher *n*-center bonding. To identify bonds for a given *n*-tuple of atomic centers (*ij*…*k*), $\mathrm{P}^{(ij\ldots k)}$ is constructed as before:

$$\mathrm{P}^{(ij\ldots k)} = \begin{bmatrix} \mathrm{P}_{ii}^{00,NAO} & \mathrm{P}_{ij}^{0s,NAO} & \ldots & \mathrm{P}_{ik}^{0t,NAO} \\ \mathrm{P}_{ji}^{s0,NAO} & \mathrm{P}_{jj}^{ss,NAO} & \ldots & \mathrm{P}_{jk}^{st,NAO} \\ \ldots & \ldots & \ldots & \ldots \\ \mathrm{P}_{ki}^{t0,NAO} & \mathrm{P}_{kj}^{ts,NAO} & \ldots & \mathrm{P}_{kk}^{tt,NAO} \end{bmatrix} = \begin{bmatrix} \mathrm{P}_{ii}^{00,NAO} & \mathrm{P}_{ij}^{0s,NAO} & \ldots & \mathrm{P}_{ik}^{0t,NAO} \\ \mathrm{P}_{ji}^{0(-s),NAO} & \mathrm{P}_{jj}^{00,NAO} & \ldots & \mathrm{P}_{jk}^{0(t-s),NAO} \\ \ldots & \ldots & \ldots & \ldots \\ \mathrm{P}_{ki}^{0(-t),NAO} & \mathrm{P}_{kj}^{0(s-t),NAO} & \ldots & \mathrm{P}_{kk}^{00,NAO} \end{bmatrix}.$$

Eigenvalues of this matrix are again used to identify bonds with occupancy higher than the specified *n*-center cutoff. Depletion is performed as before:

$$\tilde{\mathrm{P}}_{ij}^{0r,NAO} = \mathrm{P}_{ij}^{0r,NAO} - N_l^{(ij\ldots k)} c_{l,i} c_{l,j}^* \left|\eta_l^i\right\rangle\left\langle\eta_l^j\right|.$$

After all *n*-center bonds have been depleted, the search is repeated for $n + 1$ centers, and in general until the number of bonds equals the number of electron pairs per unit cell. As the number of centers increases, the number of possible combinations quickly rises. Testing all such combinations quickly becomes computationally intractable. Using locality, we have implemented a distance cutoff to screen the number of possible *n*-tuples. If any two centers in a combination are further apart than some predetermined threshold (typically some conservative function of the unit cell parameters), the combination is not tested for bonding. Even a very conservative distance

cutoff is capable of large computational cost reduction without affecting the obtained results, as many tuples feature atoms on opposite sides of non-neighboring unit cells and are therefore incapable of forming localized bonds.

Even with these optimizations, a general many-center search can be extremely computationally demanding. To this end we have also implemented a user-directed search, where user defined combinations of atomic centers can be tested for bonding. While this may bias the resulting analysis towards one's preconceived chemical intuition as compared to a general search, it allows the user to obtain chemically meaningful results on a particular fragment of interest.

14-3. Computational methods

Plane-wave DFT calculations were performed using the Vienna *ab initio* simulations package (VASP, version 4.6)[41–44] with PAW pseudopotentials from the VASP database[45,46] and the PBE density functional.[47,48] The default plane-wave cutoff energy of the associated pseudopotential was used. The Brillouin zone was sampled with a Γ-centered Monkhorst–Pack grid.[49]

A projection algorithm is used to obtain a representation of the delocalized PW DFT results in a localized AO basis. As long as an appropriate AO basis set is chosen, projection has been found to result in an accurate density matrix.[18] While technical details of the implementation of the projection have been slightly modified, the general process is the same as that in ref. 18. Standard Gaussian-type atom-centered basis sets were used for the projection, and were trimmed of any functions with angular momentum $l \geq 4$ as well as diffuse functions with exponents <0.1. Basis sets were selected so that on average

less than 1% of the density of each occupied plane wave band was lost in projecting into the AO basis to guarantee that the density matrix used in the SSAdNDP procedure accurately represents the original plane wave results.

The Visualization for Electronic and Structural Analysis software (VESTA, series 3)[50] was used for all visualizations.

14-4. Results and discussion

We have applied SSAdNDP to several periodic systems that range in structural complexity and represent various chemical bonding motifs, featuring both simple Lewis-type lone pairs and two-center two-electron (2c–2e) bonds and "non-ordinary" many-centered bonds.

14-4.1. Boron α-sheet

The α-sheet is the most stable all-boron planar structure predicted computationally thus far.[51–56] Its peculiar geometrical structure of alternating centered hexagons and vacancies has attracted significant interest.[57–60]

A PW DFT calculation was performed on the geometry of the predicted lattice structure[51] using an 11 × 11 × 1 *k*-point grid. The cc-pVTZ AO basis set[61] was used to represent the projected PW density.

We utilize SSAdNDP in conjunction with a general (non-directed) search to elucidate the bonding in the boron sheet. The resulting chemical bonding pattern is presented in 14-1b. There are 8 boron atoms and 24 valence electrons per unit cell, thus we anticipate 12 two-electron bonds. Six three-center two-electron (3c–2e) σ-type bonds with occupation number (ON) of 1.9 |e| were found on every boron triangle bordering a

vacant hexagon. Three 4c–2e σ bonds were revealed in the rhombi connecting two centered hexagons. Thus nine electron pairs were found *via* general search over three and four centers, leaving three more to be accounted for. A further general search became computationally demanding, and frequently yielded bonding motifs that were not commensurate with the symmetry of the underlying lattice. Presumably, linear (resonance) combinations of such symmetry-breaking bonding motifs commensurate with the lattice symmetry could be generated. However, such a complex resonance representative is not easily interpretable within a simple Lewis-like framework. Therefore, a user-directed search was utilized to probe the next smallest tuple which maintains the symmetry of the system – a six-center fragment over the hexagonal hole. We found a π-bond with a ON = 1.5 |e| over this hexagonal vacancy. Similarly, two 7c–2e π-bonds were found *via* directed search over each centered hexagon in the unit cell with ON = 1.6 |e|.

The bonding motifs found in SSAdNDP are in qualitative agreement with those obtained in a previous molecular AdNDP study performed using cluster models.[58] The cluster's multi-center π-bonds had higher ONs (1.72 for the 6c–2e bond and 1.97 |e| for the 7c–2e bonds), which is probably due to the less accurate treatment of boundary conditions. Quantitative comparison is further obscured by the use of a hybrid functional in the cluster study and the charged nature of the clusters.

14-4.2. Magnesium diboride

The structure of MgB_2 consists of hexagonal boron layers alternating with layers of magnesium atoms, located above the center of each boron hexagon (see Fig. 14-2a).[62]

A 9 × 9 × 9 *k*-point grid was used for PW DFT calculations and the results were projected into the 6-31(d) AO basis set.[63,64] The resulting density matrix was analyzed for chemical bonding patterns using the SSAdNDP general search. Since the unit cell contains 8 valence electrons, we anticipate a total of 4 two-electron bonds.

Three 2c–2e B–B σ-bonds were revealed with ON = 1.8 |e| (Fig. 14-2b), leaving one more electron pair to be accounted for. In a completely ionic representation each magnesium atom would donate one electron to a boron atom, making each boron sheet isoelectronic with graphene.[65] This suggests the possibility of a six-centered bond around the boron rings, as obtained in previous cluster model studies of graphene.[58] A directed search reveals such a 6c–2e π bond with ON = 1.4 |e| (Fig. 14-2b). Alternatively, this bond can be represented as an 8c–2e bond, by inclusion of each sandwiching Mg atom, with ON = 1.6 |e| (Fig. 14-2c). The possibility of this six- *versus* eight-center bonding shows that the magnesium atom does not adopt a fully ionic character and donate its two electrons, as further evidenced by the NPA charge +0.9 |e| on Mg. Based on the NPA results and the higher occupancy of the 8c–2e bond, we tend to favor the latter "covalent" perspective over the purely "ionic."

14-4.3. Na_8BaSn_6

A series of isostructural Zintl phases: Na_8BaPb_6, Na_8BaSn_6, and Na_8EuSn_6 were synthesized by Todorov and Sevov.[66] The structures (Fig. 14-3a) contain clearly recognizable five-membered rings of either Pb or Sn. These five-membered rings were interpreted as possessing a charge of −6 and therefore analogues of the organic cyclopentadienyl anion. Prior AdNDP analysis of Sn_5^{6-} rings, both isolated and

embedded in a Zintl phase Na_8BaSn_6 cluster, found such aromatic character, representing the first such species of these heavy metals.[67]

PW DFT calculations were performed on the experimental geometry[66] of Na_8BaSn_6 using a 3 × 9 × 3 *k*-point grid and projected into the def2-QZVP basis set.[68] We include the following electrons in the valence space: Ba, $5s^25p^66s^2$; Na, $3s^1$; Sn, $5s^25p^2$; while the remaining electrons are treated within the PAW pseudopotential approach. With two formula units per unit cell, this results in a total of 42 electron pairs per unit cell (Fig. 14-3a).

The general SSAdNDP search revealed 4 core electron pairs on each Ba atom, ON = 2.0 |e| (not shown), one lone pair on each of the Sn atoms, ON = 1.8–1.9 |e|, and a 2c–2e σ bond between every pair of Sn atoms around the pentagonal rings (Fig. 14-3b), accounting for a total of 30 electron pairs. Three 5c–2e π bonds on each of the Sn_5 moieties were found by directed search with ON = 1.6 |e|, highlighting each ring's aromaticity in agreement with prior cluster-model studies on simple analogues.[67] These six π-bonds bring the total number of electron pairs to 36 within the unit cell.

The remaining six electron pairs could not be localized on the two non-ring Sn atoms, which would satisfy the Sn^{4-} octet configuration of a purely ionic system. However, only the single s-type lone pair was found on each of the two atoms; no p-type lone pairs could be localized, even with low ON thresholds. We believe this is due to the metallic nature of these remaining electrons, making them intrinsically non-localizable, especially within the electron-pair based bonding model of Lewis theory. This interpretation is reinforced by the lack of a full +1 charge on each Na atom, positive

charges ranging from 0.6–0.8 |e| are found on Na atoms in the NPA, which would be required for Sn to assume a pure −4 state. This also indicates that the Na atoms contain some valence electron density to contribute to metallic interactions.

While previous works have indicated the potential presence of identifiable multi-center bonding motifs in metallic systems, such as four-center bonds in the tetrahedral holes of face-centered cubic metals,[13,38] attempts to apply SSAdNDP to (for example) bulk copper have proved problematic. Copper has eleven valence electrons per center. Traditionally ten of these are assigned as occupying d-type orbitals and the remaining electron as s-type. Using a standard fcc unit cell containing four atoms, SSAdNDP recovers the expected five d-lone pairs on each center. There are four s-type electrons remaining, so that two two-electron bonds could be found. However, there are eight equivalent tetrahedral holes contained within the unit cell. Since each atom (or its periodic image) borders each tetrahedron, any biasing to have bonds span two specific holes would be artificial and break the symmetry of the system.[13] One potential solution to this problem is the use of a resonance type picture. Instead of identifying the bonding within only two particular tetrahedral holes, it could be described as the linear combination of equal bonding contributions in all eight holes. This would allow for a representation of multi-center bonding motifs that is consistent with symmetry. A similar situation can be considered in a molecule such as benzene. After the two center search, six electrons remain. From this remaining density, it is possible to assign a π-type three-center bond over neighboring carbon atoms (regardless of occupancy); however, to match the symmetry of the molecule, six such bonds would need to be found, but there are only

three electron pairs yet to be assigned. In such a three-center bonding perspective, a resonance image with each bond weighted by factor of one half would be necessary. Of course, for benzene a single representation of three six-center bonds (with larger ON) can be found,[23] which is preferable to a resonance description. A similar many-center resonance picture is likely also possible for (at least a subset) of metallic systems, but a general SSAdNDP search would be extremely difficult to perform for such a high number of centers, and the associated chemical insight is likely minimal.

14-5. Conclusions

Solid State Adaptive Natural Density Partitioning (SSAdNDP) yields a localized and inherently "chemical" representation of bonding in terms of localized Lewis-type lone pairs and two-center bonds as well as delocalized (multi-center) bonds in periodic systems. Our extension of AdNDP to periodic systems *via* SSAdNDP allows us to elucidate the bonding in bulk materials and interfaces in a natural, chemically-intuitive fashion, yielding insight into the fundamental origins of their structure, properties, and reactivity.

We have applied this newly developed method to several representative systems, featuring both localized and delocalized bonding. In the all-boron α-sheet, SSAdNDP reveals not only prototypical boron 3c–2e σ bonds, but also additional, unexpected bonding: three 4c–2e σ bonds, one 6c–2e and two 7c–2e π bonds per 8 atom unit cell. Analysis of MgB_2 reveals a graphene-like electronic structure of the boron sheet, with three 2c–2e σ-bonds and one delocalized π-bond. The latter is perturbed by the neighboring Mg layers and as such can be represented as either a 6c–2e or an 8c–2e

bond. For Na_8BaSn_6 SSAdNDP reveals a cyclopentadienyl anion like structure, with three delocalized π-bonds on each Sn five-membered ring. The resulting chemical bonding patterns are consistent with symmetry and chemical intuition, providing a useful interpretation of chemical bonding in complex systems.

We anticipate that SSAdNDP will be as helpful in analyzing both localized and multi-center chemical bonding in solids, providing a powerful compliment to standard Natural Bond Orbital analysis in circumstances where non-classical many-center bonding may play a crucial role.

Notes and references

1 R. F. W. Bader, A. Streitwieser, A. Neuhaus, K. E. Laidig and P. Speers, *J. Am. Chem. Soc.*, 1996, **118**, 4959–4965.

2 X. Fradera, M. A. Austen and R. F. W. Bader, *J. Phys. Chem. A*, 1999, **103**, 304–314.

3 R. F. W. Bader, *Atoms in Molecules: A Quantum Theory*, Clarendon Press, Oxford, New York, 1990.

4 G. La Penna, S. Furlan and M. Sola, *Theor. Chem. Acc.*, 2011, **130**, 27–36.

5 A. I. Baranov and M. Kohout, *J. Comput. Chem.*, 2011, **32**, 2064–2076.

6 R. Hoffmann, *Solids and Surfaces: A Chemist's View of Bonding in Extended Structures*, VCH Publishers, New York, 1988.

7 T. Hughbanks and R. Hoffmann, *J. Am. Chem. Soc.*, 1983, **105**, 3528–3537.

8 J. M. Foster and S. F. Boys, *Rev. Mod. Phys.*, 1960, **32**, 300–302.

9 C. Edmiston and K. Ruedenberg, *Rev. Mod. Phys.*, 1963, **35**, 457–464.

10 J. Pipek and P. G. Mezey, *J. Chem. Phys.*, 1989, **90**, 4916–4926.

11 H. Weinstein, R. Pauncz and M. Cohen, *Adv. At. Mol. Phys.*, 1971, **7**, 97–140.

12 N. Marzari and D. Vanderbilt, *Phys. Rev. B: Condens. Matter Mater. Phys.*, 1997, **56**, 12847–12865.

13 I. Souza, N. Marzari and D. Vanderbilt, *Phys. Rev. B: Condens. Matter Mater. Phys.*, 2001, **65**, 035109.

14 F. Weinhold and C. R. Landis, *Valency and Bonding: A Natural Bond Orbital Donor-Acceptor Perspective*, Cambridge University Press, Cambridge, U.K., 2005.

15 J. P. Foster and F. Weinhold, *J. Am. Chem. Soc.*, 1980, **102**, 7211–7218.

16 A. E. Reed, R. B. Weinstock and F. Weinhold, *J. Chem. Phys.*, 1985, **83**, 735–746.

17 A. E. Reed, L. A. Curtiss and F. Weinhold, *Chem. Rev.*, 1988, **88**, 899–926.

18 B. D. Dunnington and J. R. Schmidt, *J. Chem. Theory Comput.*, 2012, **8**, 1902–1911.

19 E. D. Glendening and F. Weinhold, *J. Comput. Chem.*, 1998, **19**, 593–609.

20 E. D. Glendening and F. Weinhold, *J. Comput. Chem.*, 1998, **19**, 610–627.

21 E. D. Glendening, J. K. Badenhoop and F. Weinhold, *J. Comput. Chem.*, 1998, **19**, 628–646.

22 D. Yu. Zubarev and A. I. Boldyrev, *Phys. Chem. Chem. Phys.*, 2008, **10**, 5207–5217.

23 D. Yu. Zubarev and A. I. Boldyrev, *J. Org. Chem.*, 2008, **73**, 9251–9258.

24 I. A. Popov and A. I. Boldyrev, *Eur. J. Org. Chem.*, 2012, 3485–3491.

25 A. P. Sergeeva and A. I. Boldyrev, *Phys. Chem. Chem. Phys.*, 2010, **12**, 12050–12054.

26 P. F. Weck, A. P. Sergeeva, E. Kim, A. I. Boldyrev and K. R. Czerwinski, *Inorg. Chem.*, 2010, **50**, 1039–1046.

27 W. Huang, A. P. Sergeeva, H. J. Zhai, B. B. Averkiev, L. S. Wang and A. I. Boldyrev, *Nat. Chem.*, 2010, **2**, 202–206.

28 A. P. Sergeeva, D. Yu. Zubarev, H. J. Zhai, A. I. Boldyrev and L. S. Wang, *J. Am. Chem. Soc.*, 2008, **130**, 7244–7246.

29 Q. Chen, H. Bai, J.-C. Guo, C.-Q. Miao and S.-D. Li, *Phys. Chem. Chem. Phys.*, 2011, **13**, 20620–20626.

30 C. Romanescu, T. R. Galeev, W. L. Li, A. I. Boldyrev and L. S. Wang, *Angew. Chem., Int. Ed.*, 2011, **50**, 9334–9337.

31 C. Romanescu, A. P. Sergeeva, W. L. Li, A. I. Boldyrev and L. S. Wang, *J. Am. Chem. Soc.*, 2011, **133**, 8646–8653.

32 A. P. Sergeeva, B. B. Averkiev, H. J. Zhai, A. I. Boldyrev and L. S. Wang, *J. Chem. Phys.*, 2011, **134**, 224304–224311.

33 Q. Chen and S. D. Li, *J. Cluster Sci.*, 2011, **22**, 513–523.

34 T. R. Galeev, C. Romanescu, W. L. Li, L. S. Wang and A. I. Boldyrev, *Angew. Chem., Int. Ed.*, 2012, **51**, 2101–2105.

35 L. J. Cheng, *J. Chem. Phys.*, 2012, **136**, 104301.

36 L. Ren, L. J. Cheng, Y. Feng and X. M. Wang, *J. Chem. Phys.*, 2012, **137**, 014309.

37 W. L. Li, C. Romanescu, T. Jian and L. S. Wang, *J. Am. Chem. Soc.*, 2012, **134**, 13228–13231.

38 D. Yu. Zubarev and A. I. Boldyrev, *J. Phys. Chem. A*, 2008, **113**, 866–868.

39 A. P. Sergeeva and A. I. Boldyrev, *J. Cluster Sci.*, 2011, **22**, 321–329.

40 N. W. Ashcroft and N. D. Mermin, *Solid State Physics*, Holt, New York, 1976.

41 G. Kresse and J. Hafner, *Phys. Rev. B: Condens. Matter Mater. Phys.*, 1993, **47**, 558–561.

42 G. Kresse and J. Hafner, *Phys. Rev. B: Condens. Matter Mater. Phys.*, 1994, **49**, 14251–14269.

43 G. Kresse and J. Furthmüller, *Phys. Rev. B: Condens. Matter Mater. Phys.*, 1996, **54**, 11169–11186.

44 G. Kresse and J. Furthmüller, *Comput. Mater. Sci.*, 1996, **6**, 15–50.

45 P. E. Blöchl, *Phys. Rev. B: Condens. Matter Mater. Phys.*, 1994, **50**, 17953–17979.

46 G. Kresse and D. Joubert, *Phys. Rev. B: Condens. Matter Mater. Phys.*, 1999, **59**, 1758–1775.

47 J. P. Perdew, K. Burke and M. Ernzerhof, *Phys. Rev. Lett.*, 1996, **77**, 3865–3868.

48 J. P. Perdew, K. Burke and M. Ernzerhof, *Phys. Rev. Lett.*, 1997, **78**, 1396–1396.

49 H. J. Monkhorst and J. D. Pack, *Phys. Rev. B: Condens. Matter Mater. Phys.*, 1976, **13**, 5188–5192.

50 K. Momma and F. Izumi, *J. Appl. Crystallogr.*, 2011, **44**, 1272–1276.

51 H. Tang and S. Ismail-Beigi, *Phys. Rev. Lett.*, 2007, **99**, 115501.

52 X. Yang, Y. Ding and J. Ni, *Phys. Rev. B: Condens. Matter Mater. Phys.*, 2008, **77**, 041402.

53 I. Boustani, A. Quandt, E. Hernandez and A. Rubio, *J. Chem. Phys.*, 1999, **110**, 3176–3185.

54 M. H. Evans, J. D. Joannopoulos and S. T. Pantelides, *Phys. Rev. B: Condens. Matter Mater. Phys.*, 2005, **72**, 045434.

55 J. Kunstmann and A. Quandt, *Phys. Rev. B: Condens. Matter Mater. Phys.*, 2006, **74**, 035413.

56 K. C. Lau and R. Pandey, *J. Phys. Chem. C*, 2007, **111**, 2906–2912.

57 H. Tang and S. Ismail-Beigi, *Phys. Rev. B: Condens. Matter Mater. Phys.*, 2009, **80**, 134113.

58 T. R. Galeev, Q. Chen, J.-C. Guo, H. Bai, C.-Q. Miao, H.-G. Lu, A. P. Sergeeva, S.-D. Li and A. I. Boldyrev, *Phys. Chem. Chem. Phys.*, 2011, **13**, 11575–11578.

59 E. S. Penev, S. Bhowmick, A. Sadrzadeh and B. I. Yakobson, *Nano Lett.*, 2012, **12**, 2441–2445.

60 X. Wu, J. Dai, Y. Zhao, Z. Zhuo, J. Yang and X. C. Zeng, *ACS Nano*, 2012, 7443–7453.

61 J. T. H. Dunning, *J. Chem. Phys.*, 1989, **90**, 1007–1023.

62 M. E. Jones and R. E. Marsh, *J. Am. Chem. Soc.*, 1954, **76**, 1434–1436.

63 J. D. Dill and J. A. Pople, *J. Chem. Phys.*, 1975, **62**, 2921–2923.

64 M. M. Francl, W. J. Pietro, W. J. Hehre, J. S. Binkley, M. S. Gordon, D. J. DeFrees and J. A. Pople, *J. Chem. Phys.*, 1982, **77**, 3654–3665.

65 I. A. Popov, K. V. Bozhenko and A. I. Boldyrev, *Nano Res.*, 2012, **5**, 117–123.

66 I. Todorov and S. C. Sevov, *Inorg. Chem.*, 2004, **43**, 6490–6494.

67 A. P. Sergeeva and A. I. Boldyrev, in *Aromaticity and Metal clusters*, ed. P. K. Chattaraj, CRC Press, Taylor & Francis Group, Boca Raton, FL, 2010, pp. 55–68.

68 F. Weigend and R. Ahlrichs, *Phys. Chem. Chem. Phys.*, 2005, **7**, 3297–3305.

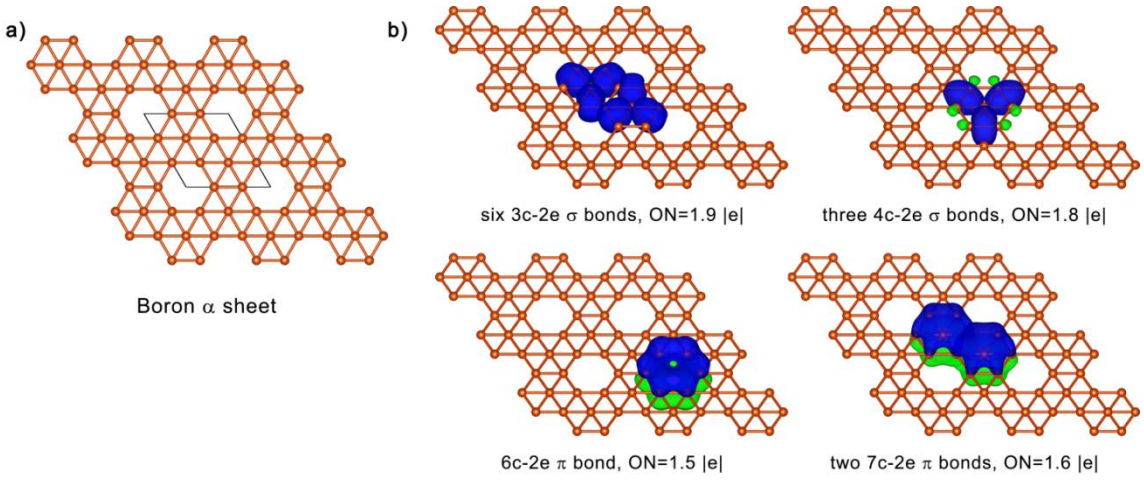

Fig. 14-1 (a) Structure and (b) SSAdNDP chemical bonding pattern of boron α-sheet. The unit cell is shown in black.

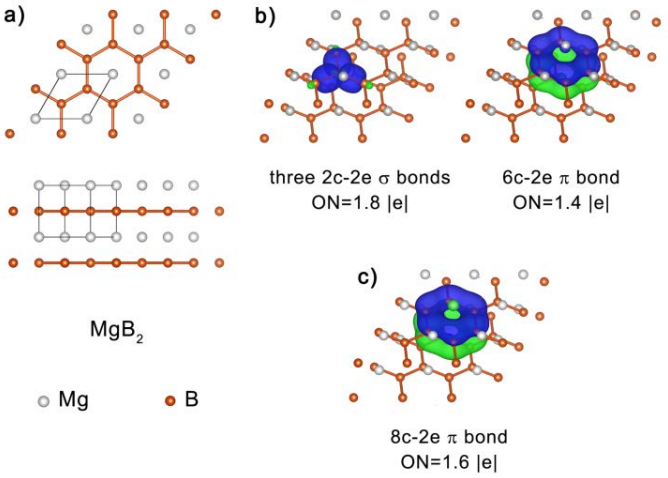

Fig. 14-2 (a) Structure, (b) SSAdNDP chemical bonding pattern and (c) alternative 8c–2e π bond representation of the 6c–2e π bond in magnesium diboride. The unit cell is shown in black.

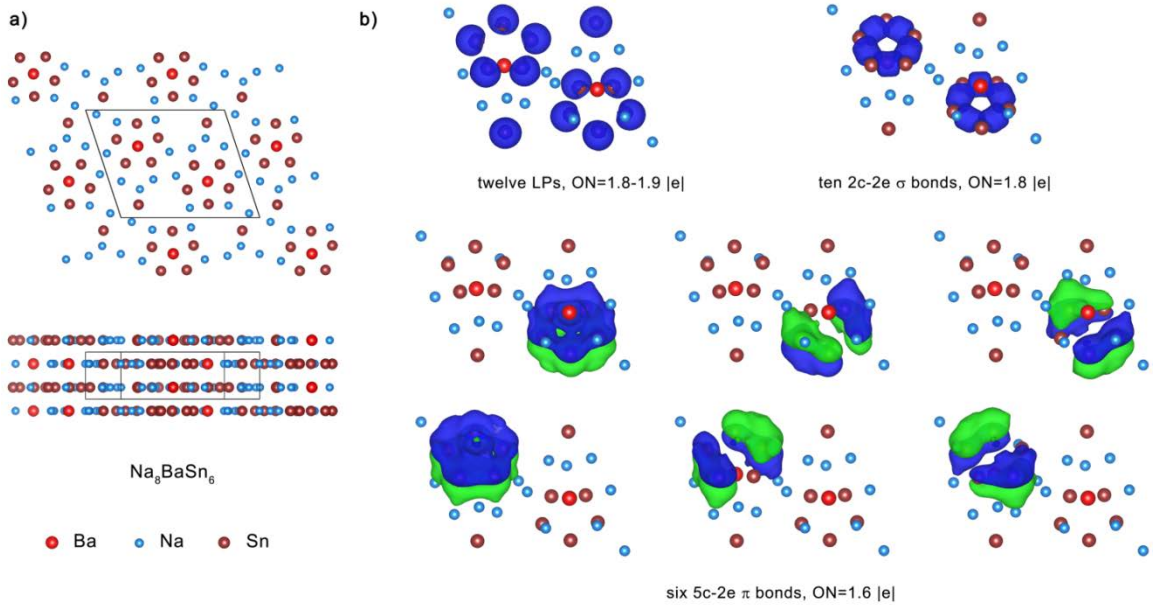

Fig. 14-3 (a) Structure, (b) SSAdNDP chemical bonding pattern for the Na_8BaSn_6 Zintl phase. The unit cell is shown in black.

CHAPTER 15

SUMMARY

A large part of this dissertation reports a series of joint theoretical and experimental studies of doped boron clusters.[1–9] The structures of the clusters obtained in molecular beam[10] by our collaborators (Prof. Lai-Sheng Wang group, Brown University) were established using computational search techniques[11] and modern *ab initio* methods. Theoretically calculated photoelectron spectra were used to verify the established structures by comparing them with the experimentally observed spectral features. A common thread through all of the research projects presented has been an attempt to understand how structure can be interpreted via chemical bonding and to use this understanding to design new chemical species. The former (descriptive or analytic) approach is necessary to gain knowledge to develop models or theories that can be used for the latter (predictive) purpose. The simple electron-counting rule[4,6,12] for construction of stable hypercoordinate transition metal-centered boron clusters presented in this work is an example of the predictive power a chemical bonding model may possess. Paradigms and concepts useful for description of chemical bonding in electron-deficient clusters, such as localized and delocalized (multi-center) bonding, (local) aromaticity and antiaromaticity,[13–19] etc., can be naturally conveyed using the Adaptive Natural Density Partitioning (AdNDP)[20,21] language of *n*c-2e bonds. One of the most important developments of the dissertation is an extension of the AdNDP methodology to periodic systems yielding a new theoretical tool capable of providing a chemically intuitive interpretation of bonding in solid phase materials.

Four anionic carbon-doped boron clusters have been studied experimentally and theoretically: $C_2B_6^-$, $C_3B_5^-$, CB_9^-, and $C_2B_8^-$.[1,8] All of these clusters have planar structures with the carbon atoms preferring peripheral rather than inner positions in agreement with previous studies of mixed carbon-boron clusters.[22–24] Interestingly, increasing the number of carbon atoms in these clusters leads to a decrease of the number of the inner atoms in their structures. A 'wheel' ($C_2B_6^-$, one central boron atom) to 'ring' ($C_3B_5^-$, no central atom) structural transition[1] was observed in $C_xB_{8-x}^-$ (x = 1–3) between x=2 and 3. Similarly, B_{10}^- has two central atoms,[25] whereas CB_9^- and $C_2B_8^-$ have one boron atom in their distorted structures.[8] All four clusters have strong 2c-2e σ bonds between C and B atoms on the peripheral rings and several multi-center σ and π bonds.

The influence of valence isoelectronic substitution in boron clusters by substituting a boron center with aluminum in B_8^-, B_9^-, B_{10}^-, and B_{11}^-, yielding the AlB_7^-, AlB_8^-, AlB_9^-, and AlB_{10}^- clusters, respectively, was a subject of two other studies.[2,3] Only AlB_9^- has a structure (and bonding) similar to that of the B_{10}^- cluster. The structures of the other clusters can be interpreted as stable anionic boron cluster fragments ionically bound to aluminum cations. In AlB_7^- and AlB_8^-, this yields beautiful umbrella-like geometries, where Al^{2+} and Al^+ are coordinated to the doubly aromatic B_7^{3-} and B_8^{2-} anions, respectively.[3] AlB_9^- also represents an interesting example of how addition of an electron to a cluster may significantly alter[26] stabilities of its isomers: for the neutral AlB_9, it was shown[27] that the wheel-type D_{9h} and B_{10}-type[25] isomers are almost equally stable, whereas addition of an electron yielding AlB_9^- leads to a significant destabilization of the wheel-type structure (the electron disturbs its double aromaticity) relative to the B_{10}-type

global minimum structure (where the electron is localized on the peripheral aluminum atom).[2]

Electronic and geometric principles for construction of stable transition metal-centered boron clusters, $M©B_n^{q-}$ have been introduced and applied for n = 8-12 and M = Co and Ru, Rh and Ir, V, Fe, and Nb and Ta.[4–7,9,12] The approach was inspired by the structure and chemical bonding of the first all-boron wheel, B_9^-, discovered previously.[28] The global minimum structure of the B_9^- cluster is a D_{8h} wheel-type structure, $B©B_8^-$, consisting of an octacoordinate central boron atom surrounded by a ring of eight boron atoms. The peripheral boron atoms in all of these clusters are bonded to each other by 2c-2e σ bonds, and the central atom is bound to the outer ring by delocalized σ and π bonds. In the symmetric wheels, the numbers of delocalized σ and π electrons satisfy the $4N$+2 Hückel rule for aromaticity. $Co©B_8^-$, $Ru©B_9$, $Fe©B_9^-$ have highly symmetric planar global minimum structures with octacoordinate Co and nonacoordinate Ru and Fe atoms in the center of boron rings. Decacoordinate Ta and Nb in the lowest energy structures of $Ta©B_{10}^-$ and $Nb©B_{10}^-$ have attracted significant attention[29] owing to the highest known to date coordination number (ten) in planar species. Open-shell RhB_9^- and IrB_9^- clusters are slightly distorted wheels due to the Jahn-Teller effect,[30,31] while their neutrals, $Rh©B_9$ and $Ir©B_9$, are perfectly symmetric. The electronic principle for designing an $M^{(x)}©B_n^{q-}$ transition metal-centered boron wheel requires that the total number of bonding electrons ensures formation of n 2c-2e bonds on the circumference of the cluster and two sets (σ and π) of delocalized bonds satisfying Hückel's rule separately for σ and π electrons. Thus, the formal valency of the metal (x), number of boron atoms

(n) and the negative charge (q) should satisfy $x + n + q = (4N_\sigma + 2) + (4N_\pi + 2)$. The transition metal centered boron molecular wheels represent a new class of aromatic species that have been designed based on a simple chemical bonding model and might potentially be obtained in condensed phase as ligands or building blocks of complex compounds and new materials.

The rest of the projects presented in the dissertation are purely theoretical. A systematic computational study[32] has been performed for the $C_xH_xP_{6-x}$ (x = 0–6) clusters. Starting from P_6 (x = 0) and leading to benzene (x = 6), the relative stabilities of benzvalene-type (global minimum for P_6) and planar ring-type (global minimum for C_6H_6) and several other representative isomers were investigated. The transition from 3D (benzvalene) structure to 2D (planar ring) structure occurs at x = 4 ($C_4H_4P_2$), where benzene-like isomers become significantly more stable than the benzvalene-like structures. Hexaphospha-, pentaphospha- and (the lowest in energy) tetraphosphabenzene are not only high in energy isomers, but also undergo out-of-plane pseudo Jahn-Teller[30,31] distortion. Occupied and unoccupied molecular orbital pairs responsible for the distortions were determined for each cluster based on the symmetry requirements. It was shown that isolobal substitution of the phosphorus atoms with the CH-groups increases the energy gaps between the orbitals leading to complete suppression of the pseudo Jahn-Teller effect starting from $C_3H_3P_3$.

All-boron α-sheet[33,34] was the first periodic structure studied in this dissertation. AdNDP analysis was performed on fragments (cluster models) of the infinite lattice.[35] The analysis revealed 3c-2e σ and 4c-2e σ bonds and 6c-2e and 7c-2e π bonds. The π

bonding is responsible for its local aromaticity and for the presence and arrangement of hexagonal vacancies in its peculiar structure.

A new theoretical method for analysis of chemical bonding in periodic structures, Solid State Adaptive Natural Density Partitioning (SSAdNDP), has been developed.[36] SSAdNDP is an extension of the AdNDP method[20,21] to periodic systems and as such was derived from a periodic implementation of the Natural Bond Orbital Analysis (NBO)[37–40] introduced recently by Dunnington and Schmidt.[41] SSAdNDP allows the interpretation of bonding in solid state in chemically intuitive terms of lone pairs, two-center bonds, and delocalized (multi-center) bonding. The new method has been applied to several representative systems featuring both localized and multi-center bonding elements[36] and has a potential to become an indispensable tool for understanding bonding interactions in bulk solids, surfaces, and low-dimensional materials.

References

(1) Galeev, T. R.; Ivanov, A. S.; Romanescu, C.; Li, W. L.; Bozhenko, K. V.; Wang, L. S.; Boldyrev, A. I. *Phys. Chem. Chem. Phys.* **2011**, *13*, 8805.

(2) Li, W. L.; Romanescu, C.; Galeev, T. R.; Wang, L. S.; Boldyrev, A. I. *J. Phys. Chem. A* **2011**, *115*, 10391–10397.

(3) Galeev, T. R.; Romanescu, C.; Li, W. L.; Wang, L. S.; Boldyrev, A. I. *J. Chem. Phys.* **2011**, *135*, 104301–104301.

(4) Romanescu, C.; Galeev, T. R.; Li, W. L.; Boldyrev, A. I.; Wang, L. S. *Angew. Chem. Int. Ed.* **2011**, *50*, 9334–9337.

(5) Li, W.-L.; Romanescu, C.; Galeev, T. R.; Piazza, Z. A.; Boldyrev, A. I.; Wang, L. S. *J. Am. Chem. Soc.* **2011**, *134*, 165–168.

(6) Galeev, T. R.; Romanescu, C.; Li, W.; Wang, L.; Boldyrev, A. I. *Angew. Chem. Int. Ed.* **2012**, *51*, 2101-2105.

(7) Romanescu, C.; Galeev, T. R.; Sergeeva, A. P.; Li, W. L.; Wang, L. S.; Boldyrev, A. I. *J. Organomet. Chem.* **2012**, *721–722*, 148–154.

(8) Galeev, T. R.; Li, W. L.; Romanescu, C.; Černušák, I.; Wang, L. S.; Boldyrev, A. I. *J. Chem. Phys.* **2012**, *137*, 234306.

(9) Romanescu, C.; Galeev, T. R.; Li, W. L.; Boldyrev, A. I.; Wang, L. S. *J. Chem. Phys.* **2013**, *138*, 134315.

(10) Wang, L. S.; Cheng, H. S.; Fan, J. *J. Chem. Phys.* **1995**, *102*, 9480–9493.

(11) Averkiev, B. B. Geometry and Electronic Structure of Doped Clusters via the Coalescence Kick Method. PhD Dissertation, Utah State University, Logan, UT, 2009.

(12) Romanescu, C.; Galeev, T. R.; Li, W. L.; Boldyrev, A. I.; Wang, L. S. *Acc. Chem. Res.* **2012**.

(13) Li, X.; Kuznetsov, A. E.; Zhang, H. F.; Boldyrev, A. I.; Wang, L. S. *Science* **2001**, *291*, 859–861.

(14) Kuznetsov, A. E.; Birch, K. A.; Boldyrev, A. I.; Li, X.; Zhai, H. J.; Wang, L. S. *Science* **2003**, *300*, 622–625.

(15) Boldyrev, A. I.; Wang, L. S. *Chem. Rev.* **2005**, *105*, 3716–3757.

(16) Zubarev, D. Y.; Averkiev, B. B.; Zhai, H.-J.; Wang, L. S.; Boldyrev, A. I. *Phys. Chem. Chem. Phys.* **2007**, *10*, 257–267.

(17) Sergeeva, A.; Averkiev, B.; Boldyrev, A. In *Metal-Metal Bonding*; Parkin, G., Ed.; Structure and Bonding; Springer: Berlin Heidelberg, 2010; Vol. 136, pp. 275–305.

(18) Galeev, T. R.; Boldyrev, A. I. *Annu Rep Prog Chem Sect C Phys Chem* **2011**, *107*, 124–147.

(19) Galeev, T. R.; Boldyrev, A. I. In *Comprehensive Inorganic Chemistry II (Second Edition)*; Reedijk, J.; Poeppelmeier, K., Eds.; Elsevier: Amsterdam, 2013; pp. 245–275.

(20) Zubarev, D. Y.; Boldyrev, A. I. *Phys. Chem. Chem. Phys.* **2008**, *10*, 5207–5217.

(21) Zubarev D. Yu. Analysis of Chemical Bonding in Clusters by Means of The Adaptive Natural Density Partitioning. PhD Dissertation, Utah State University, Logan, UT, 2008.

(22) Wang, L. M.; Huang, W.; Averkiev, B. B.; Boldyrev, A. I.; Wang, L. S. *Angew. Chem. Int. Ed.* **2007**, *46*, 4550–4553.

(23) Averkiev, B. B.; Zubarev, D. Y.; Wang, L.-M.; Huang, W.; Wang, L. S.; Boldyrev, A. I. *J. Am. Chem. Soc.* **2008**, *130*, 9248–9250.

(24) Averkiev, B. B.; Wang, L. M.; Huang, W.; Wang, L. S.; Boldyrev, A. I. *Phys. Chem. Chem. Phys.* **2009**, *11*, 9840.

(25) Zhai, H. J.; Kiran, B.; Li, J.; Wang, L. S. *Nat. Mater.* **2003**, *2*, 827–833.

(26) Jena, P.; Khanna, S.; Rao, B. K. *Physics and Chemistry of Finite Systems: From Clusters to Crystals*; Kluwer Academic Publishers: Dordreght, 1992; Vol. 1.

(27) Averkiev, B. B.; Boldyrev, A. I. *Russ. J. Gen. Chem.* **2008**, *78*, 769–773.

(28) Zhai, H.-J.; Alexandrova, A. N.; Birch, K. A.; Boldyrev, A. I.; Wang, L.-S. *Angew. Chem. Int. Ed.* **2003**, *42*, 6004–6008.

(29) a) Heine, T.; Merino, G. *Angew. Chem. Int. Ed.* **2012**, *51*, 4275–4276; b) S. K. Ritter, C&EN, 2012, 90, 38; c) D. Bradley, Chemistry World, Feb. 6, 2012

(30) Pearson, R. G. *Proc. Natl. Acad. Sci.* **1975**, *72*, 2104–2106.

(31) Bersuker, I. B. *Chem. Rev.* **2001**, *101*, 1067–1114.

(32) Galeev, T. R.; Boldyrev, A. I. *Phys Chem Chem Phys* **2011**, *13*, 20549–20556.

(33) Tang, H.; Ismail-Beigi, S. *Phys. Rev. Lett.* **2007**, *99*, 115501.

(34) Yang, X.; Ding, Y.; Ni, J. *Phys. Rev. B* **2008**, *77*, 041402.

(35) Galeev, T. R.; Chen, Q.; Guo, J.-C.; Bai, H.; Miao, C.-Q.; Lu, H.-G.; Sergeeva, A. P.; Li, S.-D.; Boldyrev, A. I. *Phys. Chem. Chem. Phys.* **2011**, *13*, 11575.

(36) Galeev, T. R.; Dunnington, B. D.; Schmidt, J. R.; Boldyrev, A. I. *Phys. Chem. Chem. Phys.* **2013**, *15*, 5022–5029.

(37) Foster, J. P.; Weinhold, F. *J. Am. Chem. Soc.* **1980**, *102*, 7211–7218.

(38) Reed, A. E.; Weinhold, F. *J. Chem. Phys.* **1985**, *83*, 1736–1740.

(39) Reed, A. E.; Curtiss, L. A.; Weinhold, F. *Chem. Rev*. **1988**, *88*, 899–926.

(40) Weinhold, F.; Landis, C. R. *Valency and Bonding: A Natural Bond Orbital Donor-Acceptor Perspective*; Cambridge University Press: Cambridge, UK, 2005.

(41) Dunnington, B. D.; Schmidt, J. R. *J. Chem. Theory. Comput.* **2012**, *8*, 1902–1911.

APPENDIX

PERMISSIONS

Molecular wheel to monocyclic ring transition in boron–carbon mixed clusters $C_2B_6^-$ and $C_3B_5^-$

T. R. Galeev, A. S. Ivanov, C. Romanescu, W. Li, K. V. Bozhenko, L. Wang and A. I. Boldyrev, *Phys. Chem. Chem. Phys.*, 2011, **13**, 8805
DOI: 10.1039/C1CP20359B

[Original citation] - Reproduced by permission of the PCCP Owner Societies

- For reproduction of material from PPS:
  [Original citation] - Reproduced by permission of The Royal Society of Chemistry (RSC) on behalf of the European Society for Photobiology, the European Photochemistry Association, and RSC
- For reproduction of material from all other RSC journals:
  [Original citation] - Reproduced by permission of The Royal Society of Chemistry

If you are the author of this article you still need to obtain permission to reproduce the whole article in a third party publication with the exception of reproduction of the whole article in a thesis or dissertation.

Information about reproducing material from RSC articles with different licences is available on our Permission Requests page.

AIP PUBLISHING LLC LICENSE
TERMS AND CONDITIONS

May 12, 2014

All payments must be made in full to CCC. For payment instructions, please see information listed at the bottom of this form.

License Number	3386670814952
Order Date	May 12, 2014
Publisher	AIP Publishing LLC
Publication	Journal of Chemical Physics
Article Title	Photoelectron spectroscopy and ab initio study of boron-carbon mixed clusters: CB9− and C2B8−
Author	Timur R. Galeev,Wei-Li Li,Constantin Romanescu, et al.
Online Publication Date	Dec 18, 2012
Volume number	137
Issue number	23
Type of Use	Thesis/Dissertation
Requestor type	Author (original article)
Format	Print and electronic
Portion	Excerpt (> 800 words)
Will you be translating?	No
Title of your thesis / dissertation	Structure and Multi-center Bonding: from Atomic Clusters to Solid Phase Materials
Expected completion date	Jun 2014
Estimated size (number of pages)	400
Total	0.00 USD

Terms and Conditions

AIP Publishing LLC -- Terms and Conditions: Permissions Uses

AIP Publishing LLC ("AIPP"") hereby grants to you the non-exclusive right and license to use and/or distribute the Material according to the use specified in your order, on a one-time basis, for the specified term, with a maximum distribution equal to the number that you have ordered. Any links or other content accompanying the Material are not the subject of this license.

1. You agree to include the following copyright and permission notice with the reproduction of the Material:"Reprinted with permission from [FULL CITATION]. Copyright [PUBLICATION YEAR], AIP Publishing LLC." For an article, the copyright and permission notice must be printed on the first page of the article or book chapter. For photographs, covers, or tables, the copyright and permission notice may appear with the Material, in a footnote, or in the reference list.
2. If you have licensed reuse of a figure, photograph, cover, or table, it is your responsibility to ensure that the material is original to AIPP and does not contain the copyright of another entity, and that the copyright notice of the figure, photograph, cover, or table does not indicate that it was reprinted by AIPP, with permission, from another source. Under no circumstances does AIPP, purport or intend to grant permission to reuse material to which it does not hold copyright.
3. You may not alter or modify the Material in any manner. You may translate the Material into another language only if you have licensed translation rights. You may not use the Material for promotional purposes. AIPP reserves all rights not specifically granted herein.

4. The foregoing license shall not take effect unless and until AIPP or its agent, Copyright Clearance Center, receives the Payment in accordance with Copyright Clearance Center Billing and Payment Terms and Conditions, which are incorporated herein by reference.
5. AIPP or the Copyright Clearance Center may, within two business days of granting this license, revoke the license for any reason whatsoever, with a full refund payable to you. Should you violate the terms of this license at any time, AIPP, AIP Publishing LLC, or Copyright Clearance Center may revoke the license with no refund to you. Notice of such revocation will be made using the contact information provided by you. Failure to receive such notice will not nullify the revocation.
6. AIPP makes no representations or warranties with respect to the Material. You agree to indemnify and hold harmless AIPP, AIP Publishing LLC, and their officers, directors, employees or agents from and against any and all claims arising out of your use of the Material other than as specifically authorized herein.
7. The permission granted herein is personal to you and is not transferable or assignable without the prior written permission of AIPP. This license may not be amended except in a writing signed by the party to be charged.
8. If purchase orders, acknowledgments or check endorsements are issued on any forms containing terms and conditions which are inconsistent with these provisions, such inconsistent terms and conditions shall be of no force and effect. This document, including the CCC Billing and Payment Terms and Conditions, shall be the entire agreement between the parties relating to the subject matter hereof.

This Agreement shall be governed by and construed in accordance with the laws of the State of New York. Both parties hereby submit to the jurisdiction of the courts of New York County for purposes of resolving any disputes that may arise hereunder.

If you would like to pay for this license now, please remit this license along with your payment made payable to "COPYRIGHT CLEARANCE CENTER" otherwise you will be invoiced within 48 hours of the license date. Payment should be in the form of a check or money order referencing your account number and this invoice number 501300921. Once you receive your invoice for this order, you may pay your invoice by credit card. Please follow instructions provided at that time.

Make Payment To:
Copyright Clearance Center
Dept 001
P.O. Box 843006
Boston, MA 02284-3006

For suggestions or comments regarding this order, contact RightsLink Customer Support: customercare@copyright.com or +1-877-622-5543 (toll free in the US) or +1-978-646-2777.

Gratis licenses (referencing $0 in the Total field) are free. Please retain this printable license for your reference. No payment is required.

AIP PUBLISHING LLC LICENSE
TERMS AND CONDITIONS

May 12, 2014

All payments must be made in full to CCC. For payment instructions, please see information listed at the bottom of this form.

License Number	3386671219824
Order Date	May 12, 2014
Publisher	AIP Publishing LLC
Publication	Journal of Chemical Physics
Article Title	Valence isoelectronic substitution in the B8− and B9− molecular wheels by an Al dopant atom: Umbrella-like structures of AlB7− and AlB8−
Author	Timur R. Galeev,Constantin Romanescu,Wei-Li Li, et al.
Online Publication Date	Sep 8, 2011
Volume number	135
Issue number	10
Type of Use	Thesis/Dissertation
Requestor type	Author (original article)
Format	Print and electronic
Portion	Excerpt (> 800 words)
Will you be translating?	No
Title of your thesis / dissertation	Structure and Multi-center Bonding: from Atomic Clusters to Solid Phase Materials
Expected completion date	Jun 2014
Estimated size (number of pages)	400
Total	0.00 USD
Terms and Conditions	

AIP Publishing LLC -- Terms and Conditions: Permissions Uses

AIP Publishing LLC ("AIPP"") hereby grants to you the non-exclusive right and license to use and/or distribute the Material according to the use specified in your order, on a one-time basis, for the specified term, with a maximum distribution equal to the number that you have ordered. Any links or other content accompanying the Material are not the subject of this license.

1. You agree to include the following copyright and permission notice with the reproduction of the Material:"Reprinted with permission from [FULL CITATION]. Copyright [PUBLICATION YEAR], AIP Publishing LLC." For an article, the copyright and permission notice must be printed on the first page of the article or book chapter. For photographs, covers, or tables, the copyright and permission notice may appear with the Material, in a footnote, or in the reference list.
2. If you have licensed reuse of a figure, photograph, cover, or table, it is your responsibility to ensure that the material is original to AIPP and does not contain the copyright of another entity, and that the copyright notice of the figure, photograph, cover, or table does not indicate that it was reprinted by AIPP, with permission, from another source. Under no circumstances does AIPP, purport or intend to grant permission to reuse material to which it does not hold copyright.
3. You may not alter or modify the Material in any manner. You may translate the Material into another language only if you have licensed translation rights. You may not use the Material for promotional purposes. AIPP reserves all rights not specifically granted

herein.

4. The foregoing license shall not take effect unless and until AIPP or its agent, Copyright Clearance Center, receives the Payment in accordance with Copyright Clearance Center Billing and Payment Terms and Conditions, which are incorporated herein by reference.
5. AIPP or the Copyright Clearance Center may, within two business days of granting this license, revoke the license for any reason whatsoever, with a full refund payable to you. Should you violate the terms of this license at any time, AIPP, AIP Publishing LLC, or Copyright Clearance Center may revoke the license with no refund to you. Notice of such revocation will be made using the contact information provided by you. Failure to receive such notice will not nullify the revocation.
6. AIPP makes no representations or warranties with respect to the Material. You agree to indemnify and hold harmless AIPP, AIP Publishing LLC, and their officers, directors, employees or agents from and against any and all claims arising out of your use of the Material other than as specifically authorized herein.
7. The permission granted herein is personal to you and is not transferable or assignable without the prior written permission of AIPP. This license may not be amended except in a writing signed by the party to be charged.
8. If purchase orders, acknowledgments or check endorsements are issued on any forms containing terms and conditions which are inconsistent with these provisions, such inconsistent terms and conditions shall be of no force and effect. This document, including the CCC Billing and Payment Terms and Conditions, shall be the entire agreement between the parties relating to the subject matter hereof.

This Agreement shall be governed by and construed in accordance with the laws of the State of New York. Both parties hereby submit to the jurisdiction of the courts of New York County for purposes of resolving any disputes that may arise hereunder.

If you would like to pay for this license now, please remit this license along with your payment made payable to "COPYRIGHT CLEARANCE CENTER" otherwise you will be invoiced within 48 hours of the license date. Payment should be in the form of a check or money order referencing your account number and this invoice number 501300931. Once you receive your invoice for this order, you may pay your invoice by credit card. Please follow instructions provided at that time.

Make Payment To:
Copyright Clearance Center
Dept 001
P.O. Box 843006
Boston, MA 02284-3006

For suggestions or comments regarding this order, contact RightsLink Customer Support: customercare@copyright.com or +1-877-622-5543 (toll free in the US) or +1-978-646-2777.

Gratis licenses (referencing $0 in the Total field) are free. Please retain this printable license for your reference. No payment is required.

RightsLink®

Home | Account Info | Help

Title: Aluminum Avoids the Central Position in AlB9− and AlB10−: Photoelectron Spectroscopy and ab Initio Study

Author: Wei-Li Li, Constantin Romanescu, Timur R. Galeev, Lai-Sheng Wang, and Alexander I. Boldyrev

Publication: The Journal of Physical Chemistry A

Publisher: American Chemical Society

Date: Sep 1, 2011

Logged in as:
Timur Galeev
Account #:
3000753113

LOGOUT

PERMISSION/LICENSE IS GRANTED FOR YOUR ORDER AT NO CHARGE

This type of permission/license, instead of the standard Terms & Conditions, is sent to you because no fee is being charged for your order. Please note the following:

- Permission is granted for your request in both print and electronic formats, and translations.
- If figures and/or tables were requested, they may be adapted or used in part.
- Please print this page for your records and send a copy of it to your publisher/graduate school.
- Appropriate credit for the requested material should be given as follows: "Reprinted (adapted) with permission from (COMPLETE REFERENCE CITATION). Copyright (YEAR) American Chemical Society." Insert appropriate information in place of the capitalized words.
- One-time permission is granted only for the use specified in your request. No additional uses are granted (such as derivative works or other editions). For any other uses, please submit a new request.

BACK | CLOSE WINDOW

JOHN WILEY AND SONS LICENSE TERMS AND CONDITIONS

May 12, 2014

This is a License Agreement between Timur R Galeev ("You") and John Wiley and Sons ("John Wiley and Sons") provided by Copyright Clearance Center ("CCC"). The license consists of your order details, the terms and conditions provided by John Wiley and Sons, and the payment terms and conditions.

All payments must be made in full to CCC. For payment instructions, please see information listed at the bottom of this form.

License Number	3386680399606
License date	May 12, 2014
Licensed content publisher	John Wiley and Sons
Licensed content publication	Angewandte Chemie International Edition
Licensed content title	Aromatic Metal-Centered Monocyclic Boron Rings: Co©B8− and Ru©B9−
Licensed copyright line	Copyright © 2011 WILEY-VCH Verlag GmbH & Co. KGaA, Weinheim
Licensed content author	Constantin Romanescu,Timur R. Galeev,Wei-Li Li,Alexander I. Boldyrev,Lai-Sheng Wang
Licensed content date	Aug 31, 2011
Start page	9334
End page	9337
Type of use	Dissertation/Thesis
Requestor type	Author of this Wiley article
Format	Print and electronic
Portion	Full article
Will you be translating?	No
Title of your thesis / dissertation	Structure and Multi-center Bonding: from Atomic Clusters to Solid Phase Materials
Expected completion date	Jun 2014
Expected size (number of pages)	400
Total	0.00 USD
Terms and Conditions	

TERMS AND CONDITIONS

This copyrighted material is owned by or exclusively licensed to John Wiley & Sons, Inc. or one of

its group companies (each a"Wiley Company") or handled on behalf of a society with which a Wiley Company has exclusive publishing rights in relation to a particular work (collectively "WILEY"). By clicking "accept" in connection with completing this licensing transaction, you agree that the following terms and conditions apply to this transaction (along with the billing and payment terms and conditions established by the Copyright Clearance Center Inc., ("CCC's Billing and Payment terms and conditions"), at the time that you opened your Rightslink account (these are available at any time at http://myaccount.copyright.com).

Terms and Conditions

- The materials you have requested permission to reproduce or reuse (the "Wiley Materials") are protected by copyright.

- You are hereby granted a personal, non-exclusive, non-sub licensable (on a stand-alone basis), non-transferable, worldwide, limited license to reproduce the Wiley Materials for the purpose specified in the licensing process. This license is for a one-time use only and limited to any maximum distribution number specified in the license. The first instance of republication or reuse granted by this licence must be completed within two years of the date of the grant of this licence (although copies prepared before the end date may be distributed thereafter). The Wiley Materials shall not be used in any other manner or for any other purpose, beyond what is granted in the license. Permission is granted subject to an appropriate acknowledgement given to the author, title of the material/book/journal and the publisher. You shall also duplicate the copyright notice that appears in the Wiley publication in your use of the Wiley Material. Permission is also granted on the understanding that nowhere in the text is a previously published source acknowledged for all or part of this Wiley Material. Any third party content is expressly excluded from this permission.

- With respect to the Wiley Materials, all rights are reserved. Except as expressly granted by the terms of the license, no part of the Wiley Materials may be copied, modified, adapted (except for minor reformatting required by the new Publication), translated, reproduced, transferred or distributed, in any form or by any means, and no derivative works may be made based on the Wiley Materials without the prior permission of the respective copyright owner. You may not alter, remove or suppress in any manner any copyright, trademark or other notices displayed by the Wiley Materials. You may not license, rent, sell, loan, lease, pledge, offer as security, transfer or assign the Wiley Materials on a stand-alone basis, or any of the rights granted to you hereunder to any other person.

- The Wiley Materials and all of the intellectual property rights therein shall at all times remain the exclusive property of John Wiley & Sons Inc, the Wiley Companies, or their respective licensors, and your interest therein is only that of having possession of and the right to reproduce the Wiley Materials pursuant to Section 2 herein during the continuance of this Agreement. You agree that you own no right, title or interest in or to the Wiley Materials or any of the intellectual property rights therein. You shall have no rights hereunder other than the license as provided for above in Section 2. No right, license or interest to any trademark, trade name, service mark or other branding ("Marks") of WILEY or its licensors is granted

hereunder, and you agree that you shall not assert any such right, license or interest with respect thereto.

- NEITHER WILEY NOR ITS LICENSORS MAKES ANY WARRANTY OR REPRESENTATION OF ANY KIND TO YOU OR ANY THIRD PARTY, EXPRESS, IMPLIED OR STATUTORY, WITH RESPECT TO THE MATERIALS OR THE ACCURACY OF ANY INFORMATION CONTAINED IN THE MATERIALS, INCLUDING, WITHOUT LIMITATION, ANY IMPLIED WARRANTY OF MERCHANTABILITY, ACCURACY, SATISFACTORY QUALITY, FITNESS FOR A PARTICULAR PURPOSE, USABILITY, INTEGRATION OR NON-INFRINGEMENT AND ALL SUCH WARRANTIES ARE HEREBY EXCLUDED BY WILEY AND ITS LICENSORS AND WAIVED BY YOU

- WILEY shall have the right to terminate this Agreement immediately upon breach of this Agreement by you.

- You shall indemnify, defend and hold harmless WILEY, its Licensors and their respective directors, officers, agents and employees, from and against any actual or threatened claims, demands, causes of action or proceedings arising from any breach of this Agreement by you.

- IN NO EVENT SHALL WILEY OR ITS LICENSORS BE LIABLE TO YOU OR ANY OTHER PARTY OR ANY OTHER PERSON OR ENTITY FOR ANY SPECIAL, CONSEQUENTIAL, INCIDENTAL, INDIRECT, EXEMPLARY OR PUNITIVE DAMAGES, HOWEVER CAUSED, ARISING OUT OF OR IN CONNECTION WITH THE DOWNLOADING, PROVISIONING, VIEWING OR USE OF THE MATERIALS REGARDLESS OF THE FORM OF ACTION, WHETHER FOR BREACH OF CONTRACT, BREACH OF WARRANTY, TORT, NEGLIGENCE, INFRINGEMENT OR OTHERWISE (INCLUDING, WITHOUT LIMITATION, DAMAGES BASED ON LOSS OF PROFITS, DATA, FILES, USE, BUSINESS OPPORTUNITY OR CLAIMS OF THIRD PARTIES), AND WHETHER OR NOT THE PARTY HAS BEEN ADVISED OF THE POSSIBILITY OF SUCH DAMAGES. THIS LIMITATION SHALL APPLY NOTWITHSTANDING ANY FAILURE OF ESSENTIAL PURPOSE OF ANY LIMITED REMEDY PROVIDED HEREIN.

- Should any provision of this Agreement be held by a court of competent jurisdiction to be illegal, invalid, or unenforceable, that provision shall be deemed amended to achieve as nearly as possible the same economic effect as the original provision, and the legality, validity and enforceability of the remaining provisions of this Agreement shall not be affected or impaired thereby.

- The failure of either party to enforce any term or condition of this Agreement shall not constitute a waiver of either party's right to enforce each and every term and condition of this Agreement. No breach under this agreement shall be deemed waived or excused by either party unless such waiver or consent is in writing signed by the party granting such waiver or consent. The waiver by or consent of a party to a breach of any provision of this Agreement shall not operate or be construed as a waiver of or consent to any other or subsequent

breach by such other party.

- This Agreement may not be assigned (including by operation of law or otherwise) by you without WILEY's prior written consent.
- Any fee required for this permission shall be non-refundable after thirty (30) days from receipt by the CCC.
- These terms and conditions together with CCC's Billing and Payment terms and conditions (which are incorporated herein) form the entire agreement between you and WILEY concerning this licensing transaction and (in the absence of fraud) supersedes all prior agreements and representations of the parties, oral or written. This Agreement may not be amended except in writing signed by both parties. This Agreement shall be binding upon and inure to the benefit of the parties' successors, legal representatives, and authorized assigns.
- In the event of any conflict between your obligations established by these terms and conditions and those established by CCC's Billing and Payment terms and conditions, these terms and conditions shall prevail.
- WILEY expressly reserves all rights not specifically granted in the combination of (i) the license details provided by you and accepted in the course of this licensing transaction, (ii) these terms and conditions and (iii) CCC's Billing and Payment terms and conditions.
- This Agreement will be void if the Type of Use, Format, Circulation, or Requestor Type was misrepresented during the licensing process.
- This Agreement shall be governed by and construed in accordance with the laws of the State of New York, USA, without regards to such state's conflict of law rules. Any legal action, suit or proceeding arising out of or relating to these Terms and Conditions or the breach thereof shall be instituted in a court of competent jurisdiction in New York County in the State of New York in the United States of America and each party hereby consents and submits to the personal jurisdiction of such court, waives any objection to venue in such court and consents to service of process by registered or certified mail, return receipt requested, at the last known address of such party.

WILEY OPEN ACCESS TERMS AND CONDITIONS

Wiley Publishes Open Access Articles in fully Open Access Journals and in Subscription journals offering Online Open. Although most of the fully Open Access journals publish open access articles under the terms of the Creative Commons Attribution (CC BY) License only, the subscription journals and a few of the Open Access Journals offer a choice of Creative Commons Licenses:: Creative Commons Attribution (CC-BY) license Creative Commons Attribution Non-Commercial (CC-BY-NC) license and Creative Commons Attribution Non-Commercial-NoDerivs (CC-BY-NC-ND) License. The license type is clearly identified on the article.

Copyright in any research article in a journal published as Open Access under a Creative Commons License is retained by the author(s). Authors grant Wiley a license to publish the article and identify itself as the original publisher. Authors also grant any third party the right to use the article freely as long as its integrity is maintained and its original authors, citation details and publisher are identified as follows: [Title of Article/Author/Journal Title and Volume/Issue. Copyright (c) [year] [copyright owner as specified in the Journal]. Links to the final article on Wiley's website are encouraged where applicable.

The Creative Commons Attribution License

The Creative Commons Attribution License (CC-BY) allows users to copy, distribute and transmit an article, adapt the article and make commercial use of the article. The CC-BY license permits commercial and non-commercial re-use of an open access article, as long as the author is properly attributed.

The Creative Commons Attribution License does not affect the moral rights of authors, including without limitation the right not to have their work subjected to derogatory treatment. It also does not affect any other rights held by authors or third parties in the article, including without limitation the rights of privacy and publicity. Use of the article must not assert or imply, whether implicitly or explicitly, any connection with, endorsement or sponsorship of such use by the author, publisher or any other party associated with the article.

For any reuse or distribution, users must include the copyright notice and make clear to others that the article is made available under a Creative Commons Attribution license, linking to the relevant Creative Commons web page.

To the fullest extent permitted by applicable law, the article is made available as is and without representation or warranties of any kind whether express, implied, statutory or otherwise and including, without limitation, warranties of title, merchantability, fitness for a particular purpose, non-infringement, absence of defects, accuracy, or the presence or absence of errors.

Creative Commons Attribution Non-Commercial License

The Creative Commons Attribution Non-Commercial (CC-BY-NC) License permits use, distribution and reproduction in any medium, provided the original work is properly cited and is not used for commercial purposes.(see below)

Creative Commons Attribution-Non-Commercial-NoDerivs License

The Creative Commons Attribution Non-Commercial-NoDerivs License (CC-BY-NC-ND) permits use, distribution and reproduction in any medium, provided the original work is properly cited, is not used for commercial purposes and no modifications or adaptations are made. (see below)

Use by non-commercial users

For non-commercial and non-promotional purposes, individual users may access, download, copy, display and redistribute to colleagues Wiley Open Access articles, as well as adapt, translate, text-

and data-mine the content subject to the following conditions:

- The authors' moral rights are not compromised. These rights include the right of "paternity" (also known as "attribution" - the right for the author to be identified as such) and "integrity" (the right for the author not to have the work altered in such a way that the author's reputation or integrity may be impugned).

- Where content in the article is identified as belonging to a third party, it is the obligation of the user to ensure that any reuse complies with the copyright policies of the owner of that content.

- If article content is copied, downloaded or otherwise reused for non-commercial research and education purposes, a link to the appropriate bibliographic citation (authors, journal, article title, volume, issue, page numbers, DOI and the link to the definitive published version on **Wiley Online Library**) should be maintained. Copyright notices and disclaimers must not be deleted.

- Any translations, for which a prior translation agreement with Wiley has not been agreed, must prominently display the statement: "This is an unofficial translation of an article that appeared in a Wiley publication. The publisher has not endorsed this translation."

Use by commercial "for-profit" organisations

Use of Wiley Open Access articles for commercial, promotional, or marketing purposes requires further explicit permission from Wiley and will be subject to a fee. Commercial purposes include:

- Copying or downloading of articles, or linking to such articles for further redistribution, sale or licensing;

- Copying, downloading or posting by a site or service that incorporates advertising with such content;

- The inclusion or incorporation of article content in other works or services (other than normal quotations with an appropriate citation) that is then available for sale or licensing, for a fee (for example, a compilation produced for marketing purposes, inclusion in a sales pack)

- Use of article content (other than normal quotations with appropriate citation) by for-profit organisations for promotional purposes

- Linking to article content in e-mails redistributed for promotional, marketing or educational purposes;

- Use for the purposes of monetary reward by means of sale, resale, licence, loan, transfer or other form of commercial exploitation such as marketing products

- Print reprints of Wiley Open Access articles can be purchased from: corporatesales@wiley.com

Further details can be found on Wiley Online Library
http://olabout.wiley.com/WileyCDA/Section/id-410895.html

Other Terms and Conditions:

v1.9

If you would like to pay for this license now, please remit this license along with your payment made payable to "COPYRIGHT CLEARANCE CENTER" otherwise you will be invoiced within 48 hours of the license date. Payment should be in the form of a check or money order referencing your account number and this invoice number 501300949. Once you receive your invoice for this order, you may pay your invoice by credit card. Please follow instructions provided at that time.

Make Payment To:
Copyright Clearance Center
Dept 001
P.O. Box 843006
Boston, MA 02284-3006

For suggestions or comments regarding this order, contact RightsLink Customer Support: customercare@copyright.com or +1-877-622-5543 (toll free in the US) or +1-978-646-2777.

Gratis licenses (referencing $0 in the Total field) are free. Please retain this printable license for your reference. No payment is required.

JOHN WILEY AND SONS LICENSE TERMS AND CONDITIONS

May 12, 2014

This is a License Agreement between Timur R Galeev ("You") and John Wiley and Sons ("John Wiley and Sons") provided by Copyright Clearance Center ("CCC"). The license consists of your order details, the terms and conditions provided by John Wiley and Sons, and the payment terms and conditions.

All payments must be made in full to CCC. For payment instructions, please see information listed at the bottom of this form.

License Number	3386681483478
License date	May 12, 2014
Licensed content publisher	John Wiley and Sons
Licensed content publication	Angewandte Chemie International Edition
Licensed content title	Observation of the Highest Coordination Number in Planar Species: Decacoordinated Ta©B10− and Nb©B10− Anions
Licensed copyright line	Copyright © 2012 WILEY-VCH Verlag GmbH & Co. KGaA, Weinheim
Licensed content author	Timur R. Galeev,Constantin Romanescu,Wei-Li Li,Lai-Sheng Wang,Alexander I. Boldyrev
Licensed content date	Feb 1, 2012
Start page	2101
End page	2105
Type of use	Dissertation/Thesis
Requestor type	Author of this Wiley article
Format	Print and electronic
Portion	Full article
Will you be translating?	No
Title of your thesis / dissertation	Structure and Multi-center Bonding: from Atomic Clusters to Solid Phase Materials
Expected completion date	Jun 2014
Expected size (number of pages)	400
Total	0.00 USD
Terms and Conditions	

TERMS AND CONDITIONS

This copyrighted material is owned by or exclusively licensed to John Wiley & Sons, Inc. or one of

its group companies (each a"Wiley Company") or handled on behalf of a society with which a Wiley Company has exclusive publishing rights in relation to a particular work (collectively "WILEY"). By clicking "accept" in connection with completing this licensing transaction, you agree that the following terms and conditions apply to this transaction (along with the billing and payment terms and conditions established by the Copyright Clearance Center Inc., ("CCC's Billing and Payment terms and conditions"), at the time that you opened your Rightslink account (these are available at any time at http://myaccount.copyright.com).

Terms and Conditions

- The materials you have requested permission to reproduce or reuse (the "Wiley Materials") are protected by copyright.

- You are hereby granted a personal, non-exclusive, non-sub licensable (on a stand-alone basis), non-transferable, worldwide, limited license to reproduce the Wiley Materials for the purpose specified in the licensing process. This license is for a one-time use only and limited to any maximum distribution number specified in the license. The first instance of republication or reuse granted by this licence must be completed within two years of the date of the grant of this licence (although copies prepared before the end date may be distributed thereafter). The Wiley Materials shall not be used in any other manner or for any other purpose, beyond what is granted in the license. Permission is granted subject to an appropriate acknowledgement given to the author, title of the material/book/journal and the publisher. You shall also duplicate the copyright notice that appears in the Wiley publication in your use of the Wiley Material. Permission is also granted on the understanding that nowhere in the text is a previously published source acknowledged for all or part of this Wiley Material. Any third party content is expressly excluded from this permission.

- With respect to the Wiley Materials, all rights are reserved. Except as expressly granted by the terms of the license, no part of the Wiley Materials may be copied, modified, adapted (except for minor reformatting required by the new Publication), translated, reproduced, transferred or distributed, in any form or by any means, and no derivative works may be made based on the Wiley Materials without the prior permission of the respective copyright owner. You may not alter, remove or suppress in any manner any copyright, trademark or other notices displayed by the Wiley Materials. You may not license, rent, sell, loan, lease, pledge, offer as security, transfer or assign the Wiley Materials on a stand-alone basis, or any of the rights granted to you hereunder to any other person.

- The Wiley Materials and all of the intellectual property rights therein shall at all times remain the exclusive property of John Wiley & Sons Inc, the Wiley Companies, or their respective licensors, and your interest therein is only that of having possession of and the right to reproduce the Wiley Materials pursuant to Section 2 herein during the continuance of this Agreement. You agree that you own no right, title or interest in or to the Wiley Materials or any of the intellectual property rights therein. You shall have no rights hereunder other than the license as provided for above in Section 2. No right, license or interest to any trademark, trade name, service mark or other branding ("Marks") of WILEY or its licensors is granted

hereunder, and you agree that you shall not assert any such right, license or interest with respect thereto.

- NEITHER WILEY NOR ITS LICENSORS MAKES ANY WARRANTY OR REPRESENTATION OF ANY KIND TO YOU OR ANY THIRD PARTY, EXPRESS, IMPLIED OR STATUTORY, WITH RESPECT TO THE MATERIALS OR THE ACCURACY OF ANY INFORMATION CONTAINED IN THE MATERIALS, INCLUDING, WITHOUT LIMITATION, ANY IMPLIED WARRANTY OF MERCHANTABILITY, ACCURACY, SATISFACTORY QUALITY, FITNESS FOR A PARTICULAR PURPOSE, USABILITY, INTEGRATION OR NON-INFRINGEMENT AND ALL SUCH WARRANTIES ARE HEREBY EXCLUDED BY WILEY AND ITS LICENSORS AND WAIVED BY YOU

- WILEY shall have the right to terminate this Agreement immediately upon breach of this Agreement by you.

- You shall indemnify, defend and hold harmless WILEY, its Licensors and their respective directors, officers, agents and employees, from and against any actual or threatened claims, demands, causes of action or proceedings arising from any breach of this Agreement by you.

- IN NO EVENT SHALL WILEY OR ITS LICENSORS BE LIABLE TO YOU OR ANY OTHER PARTY OR ANY OTHER PERSON OR ENTITY FOR ANY SPECIAL, CONSEQUENTIAL, INCIDENTAL, INDIRECT, EXEMPLARY OR PUNITIVE DAMAGES, HOWEVER CAUSED, ARISING OUT OF OR IN CONNECTION WITH THE DOWNLOADING, PROVISIONING, VIEWING OR USE OF THE MATERIALS REGARDLESS OF THE FORM OF ACTION, WHETHER FOR BREACH OF CONTRACT, BREACH OF WARRANTY, TORT, NEGLIGENCE, INFRINGEMENT OR OTHERWISE (INCLUDING, WITHOUT LIMITATION, DAMAGES BASED ON LOSS OF PROFITS, DATA, FILES, USE, BUSINESS OPPORTUNITY OR CLAIMS OF THIRD PARTIES), AND WHETHER OR NOT THE PARTY HAS BEEN ADVISED OF THE POSSIBILITY OF SUCH DAMAGES. THIS LIMITATION SHALL APPLY NOTWITHSTANDING ANY FAILURE OF ESSENTIAL PURPOSE OF ANY LIMITED REMEDY PROVIDED HEREIN.

- Should any provision of this Agreement be held by a court of competent jurisdiction to be illegal, invalid, or unenforceable, that provision shall be deemed amended to achieve as nearly as possible the same economic effect as the original provision, and the legality, validity and enforceability of the remaining provisions of this Agreement shall not be affected or impaired thereby.

- The failure of either party to enforce any term or condition of this Agreement shall not constitute a waiver of either party's right to enforce each and every term and condition of this Agreement. No breach under this agreement shall be deemed waived or excused by either party unless such waiver or consent is in writing signed by the party granting such waiver or consent. The waiver by or consent of a party to a breach of any provision of this Agreement shall not operate or be construed as a waiver of or consent to any other or subsequent

breach by such other party.

- This Agreement may not be assigned (including by operation of law or otherwise) by you without WILEY's prior written consent.
- Any fee required for this permission shall be non-refundable after thirty (30) days from receipt by the CCC.
- These terms and conditions together with CCC's Billing and Payment terms and conditions (which are incorporated herein) form the entire agreement between you and WILEY concerning this licensing transaction and (in the absence of fraud) supersedes all prior agreements and representations of the parties, oral or written. This Agreement may not be amended except in writing signed by both parties. This Agreement shall be binding upon and inure to the benefit of the parties' successors, legal representatives, and authorized assigns.
- In the event of any conflict between your obligations established by these terms and conditions and those established by CCC's Billing and Payment terms and conditions, these terms and conditions shall prevail.
- WILEY expressly reserves all rights not specifically granted in the combination of (i) the license details provided by you and accepted in the course of this licensing transaction, (ii) these terms and conditions and (iii) CCC's Billing and Payment terms and conditions.
- This Agreement will be void if the Type of Use, Format, Circulation, or Requestor Type was misrepresented during the licensing process.
- This Agreement shall be governed by and construed in accordance with the laws of the State of New York, USA, without regards to such state's conflict of law rules. Any legal action, suit or proceeding arising out of or relating to these Terms and Conditions or the breach thereof shall be instituted in a court of competent jurisdiction in New York County in the State of New York in the United States of America and each party hereby consents and submits to the personal jurisdiction of such court, waives any objection to venue in such court and consents to service of process by registered or certified mail, return receipt requested, at the last known address of such party.

WILEY OPEN ACCESS TERMS AND CONDITIONS

Wiley Publishes Open Access Articles in fully Open Access Journals and in Subscription journals offering Online Open. Although most of the fully Open Access journals publish open access articles under the terms of the Creative Commons Attribution (CC BY) License only, the subscription journals and a few of the Open Access Journals offer a choice of Creative Commons Licenses:: Creative Commons Attribution (CC-BY) license Creative Commons Attribution Non-Commercial (CC-BY-NC) license and Creative Commons Attribution Non-Commercial-NoDerivs (CC-BY-NC-ND) License. The license type is clearly identified on the article.

Copyright in any research article in a journal published as Open Access under a Creative Commons License is retained by the author(s). Authors grant Wiley a license to publish the article and identify itself as the original publisher. Authors also grant any third party the right to use the article freely as long as its integrity is maintained and its original authors, citation details and publisher are identified as follows: [Title of Article/Author/Journal Title and Volume/Issue. Copyright (c) [year] [copyright owner as specified in the Journal]. Links to the final article on Wiley's website are encouraged where applicable.

The Creative Commons Attribution License

The Creative Commons Attribution License (CC-BY) allows users to copy, distribute and transmit an article, adapt the article and make commercial use of the article. The CC-BY license permits commercial and non-commercial re-use of an open access article, as long as the author is properly attributed.

The Creative Commons Attribution License does not affect the moral rights of authors, including without limitation the right not to have their work subjected to derogatory treatment. It also does not affect any other rights held by authors or third parties in the article, including without limitation the rights of privacy and publicity. Use of the article must not assert or imply, whether implicitly or explicitly, any connection with, endorsement or sponsorship of such use by the author, publisher or any other party associated with the article.

For any reuse or distribution, users must include the copyright notice and make clear to others that the article is made available under a Creative Commons Attribution license, linking to the relevant Creative Commons web page.

To the fullest extent permitted by applicable law, the article is made available as is and without representation or warranties of any kind whether express, implied, statutory or otherwise and including, without limitation, warranties of title, merchantability, fitness for a particular purpose, non-infringement, absence of defects, accuracy, or the presence or absence of errors.

Creative Commons Attribution Non-Commercial License

The Creative Commons Attribution Non-Commercial (CC-BY-NC) License permits use, distribution and reproduction in any medium, provided the original work is properly cited and is not used for commercial purposes.(see below)

Creative Commons Attribution-Non-Commercial-NoDerivs License

The Creative Commons Attribution Non-Commercial-NoDerivs License (CC-BY-NC-ND) permits use, distribution and reproduction in any medium, provided the original work is properly cited, is not used for commercial purposes and no modifications or adaptations are made. (see below)

Use by non-commercial users

For non-commercial and non-promotional purposes, individual users may access, download, copy, display and redistribute to colleagues Wiley Open Access articles, as well as adapt, translate, text-

and data-mine the content subject to the following conditions:

- The authors' moral rights are not compromised. These rights include the right of "paternity" (also known as "attribution" - the right for the author to be identified as such) and "integrity" (the right for the author not to have the work altered in such a way that the author's reputation or integrity may be impugned).

- Where content in the article is identified as belonging to a third party, it is the obligation of the user to ensure that any reuse complies with the copyright policies of the owner of that content.

- If article content is copied, downloaded or otherwise reused for non-commercial research and education purposes, a link to the appropriate bibliographic citation (authors, journal, article title, volume, issue, page numbers, DOI and the link to the definitive published version on **Wiley Online Library**) should be maintained. Copyright notices and disclaimers must not be deleted.

- Any translations, for which a prior translation agreement with Wiley has not been agreed, must prominently display the statement: "This is an unofficial translation of an article that appeared in a Wiley publication. The publisher has not endorsed this translation."

Use by commercial "for-profit" organisations

Use of Wiley Open Access articles for commercial, promotional, or marketing purposes requires further explicit permission from Wiley and will be subject to a fee. Commercial purposes include:

- Copying or downloading of articles, or linking to such articles for further redistribution, sale or licensing;

- Copying, downloading or posting by a site or service that incorporates advertising with such content;

- The inclusion or incorporation of article content in other works or services (other than normal quotations with an appropriate citation) that is then available for sale or licensing, for a fee (for example, a compilation produced for marketing purposes, inclusion in a sales pack)

- Use of article content (other than normal quotations with appropriate citation) by for-profit organisations for promotional purposes

- Linking to article content in e-mails redistributed for promotional, marketing or educational purposes;

- Use for the purposes of monetary reward by means of sale, resale, licence, loan, transfer or other form of commercial exploitation such as marketing products

- Print reprints of Wiley Open Access articles can be purchased from: corporatesales@wiley.com

Further details can be found on Wiley Online Library
http://olabout.wiley.com/WileyCDA/Section/id-410895.html

Other Terms and Conditions:

v1.9

If you would like to pay for this license now, please remit this license along with your payment made payable to "COPYRIGHT CLEARANCE CENTER" otherwise you will be invoiced within 48 hours of the license date. Payment should be in the form of a check or money order referencing your account number and this invoice number 501300959. Once you receive your invoice for this order, you may pay your invoice by credit card. Please follow instructions provided at that time.

Make Payment To:
Copyright Clearance Center
Dept 001
P.O. Box 843006
Boston, MA 02284-3006

For suggestions or comments regarding this order, contact RightsLink Customer Support: customercare@copyright.com or +1-877-622-5543 (toll free in the US) or +1-978-646-2777.

Gratis licenses (referencing $0 in the Total field) are free. Please retain this printable license for your reference. No payment is required.

ELSEVIER LICENSE
TERMS AND CONDITIONS

May 12, 2014

This is a License Agreement between Timur R Galeev ("You") and Elsevier ("Elsevier") provided by Copyright Clearance Center ("CCC"). The license consists of your order details, the terms and conditions provided by Elsevier, and the payment terms and conditions.

All payments must be made in full to CCC. For payment instructions, please see information listed at the bottom of this form.

Supplier	Elsevier Limited The Boulevard,Langford Lane Kidlington,Oxford,OX5 1GB,UK
Registered Company Number	1982084
Customer name	Timur R Galeev
Customer address	755 E 700 N, #22A Logan, UT 84321
License number	3386690322883
License date	May 12, 2014
Licensed content publisher	Elsevier
Licensed content publication	Journal of Organometallic Chemistry
Licensed content title	Experimental and computational evidence of octa- and nona-coordinated planar iron-doped boron clusters: Fe©B8and Fe©B9
Licensed content author	Constantin Romanescu,Timur R. Galeev,Alina P. Sergeeva,Wei-Li Li,Lai-Sheng Wang,Alexander I. Boldyrev
Licensed content date	15 December 2012
Licensed content volume number	721–722
Licensed content issue number	None
Number of pages	7
Start Page	148
End Page	154
Type of Use	reuse in a thesis/dissertation
Intended publisher of new work	other
Portion	full article
Format	both print and electronic
Are you the author of this	Yes

Elsevier article?	
Will you be translating?	No
Title of your thesis/dissertation	Structure and Multi-center Bonding: from Atomic Clusters to Solid Phase Materials
Expected completion date	Jun 2014
Estimated size (number of pages)	400
Elsevier VAT number	GB 494 6272 12
Permissions price	0.00 USD
VAT/Local Sales Tax	0.00 USD / 0.00 GBP
Total	0.00 USD
Terms and Conditions	

INTRODUCTION

1. The publisher for this copyrighted material is Elsevier. By clicking "accept" in connection with completing this licensing transaction, you agree that the following terms and conditions apply to this transaction (along with the Billing and Payment terms and conditions established by Copyright Clearance Center, Inc. ("CCC"), at the time that you opened your Rightslink account and that are available at any time at http://myaccount.copyright.com).

GENERAL TERMS

2. Elsevier hereby grants you permission to reproduce the aforementioned material subject to the terms and conditions indicated.

3. Acknowledgement: If any part of the material to be used (for example, figures) has appeared in our publication with credit or acknowledgement to another source, permission must also be sought from that source. If such permission is not obtained then that material may not be included in your publication/copies. Suitable acknowledgement to the source must be made, either as a footnote or in a reference list at the end of your publication, as follows:

"Reprinted from Publication title, Vol /edition number, Author(s), Title of article / title of chapter, Pages No., Copyright (Year), with permission from Elsevier [OR APPLICABLE SOCIETY COPYRIGHT OWNER]." Also Lancet special credit - "Reprinted from The Lancet, Vol. number, Author(s), Title of article, Pages No., Copyright (Year), with permission from Elsevier."

4. Reproduction of this material is confined to the purpose and/or media for which permission is hereby given.

5. Altering/Modifying Material: Not Permitted. However figures and illustrations may be altered/adapted minimally to serve your work. Any other abbreviations, additions, deletions and/or any other alterations shall be made only with prior written authorization of Elsevier Ltd. (Please contact Elsevier at permissions@elsevier.com)

6. If the permission fee for the requested use of our material is waived in this instance, please be advised that your future requests for Elsevier materials may attract a fee.

7. Reservation of Rights: Publisher reserves all rights not specifically granted in the combination of (i) the license details provided by you and accepted in the course of this licensing transaction, (ii) these terms and conditions and (iii) CCC's Billing and Payment terms and conditions.

8. License Contingent Upon Payment: While you may exercise the rights licensed immediately upon issuance of the license at the end of the licensing process for the transaction, provided that you have disclosed complete and accurate details of your proposed use, no license is finally effective unless and until full payment is received from you (either by publisher or by CCC) as provided in CCC's Billing and Payment terms and conditions. If full payment is not received on a timely basis, then any license preliminarily granted shall be deemed automatically revoked and shall be void as if never granted. Further, in the event that you breach any of these terms and conditions or any of CCC's Billing and Payment terms and conditions, the license is automatically revoked and shall be void as if never granted. Use of materials as described in a revoked license, as well as any use of the materials beyond the scope of an unrevoked license, may constitute copyright infringement and publisher reserves the right to take any and all action to protect its copyright in the materials.

9. Warranties: Publisher makes no representations or warranties with respect to the licensed material.

10. Indemnity: You hereby indemnify and agree to hold harmless publisher and CCC, and their respective officers, directors, employees and agents, from and against any and all claims arising out of your use of the licensed material other than as specifically authorized pursuant to this license.

11. No Transfer of License: This license is personal to you and may not be sublicensed, assigned, or transferred by you to any other person without publisher's written permission.

12. No Amendment Except in Writing: This license may not be amended except in a writing signed by both parties (or, in the case of publisher, by CCC on publisher's behalf).

13. Objection to Contrary Terms: Publisher hereby objects to any terms contained in any purchase order, acknowledgment, check endorsement or other writing prepared by you, which terms are inconsistent with these terms and conditions or CCC's Billing and Payment terms and conditions. These terms and conditions, together with CCC's Billing and Payment terms and conditions (which are incorporated herein), comprise the entire agreement between you and publisher (and CCC) concerning this licensing transaction. In the event of any conflict between your obligations established by these terms and conditions and those established by CCC's Billing and Payment terms and conditions, these terms and conditions shall control.

14. Revocation: Elsevier or Copyright Clearance Center may deny the permissions described in this License at their sole discretion, for any reason or no reason, with a full refund payable to you. Notice of such denial will be made using the contact information provided by you. Failure to receive such notice will not alter or invalidate the denial. In no event will Elsevier or Copyright Clearance Center be responsible or liable for any costs, expenses or damage incurred by you as a result of a denial of your permission request, other than a refund of the amount(s) paid by you to Elsevier and/or Copyright Clearance Center for denied permissions.

LIMITED LICENSE

The following terms and conditions apply only to specific license types:

15. **Translation**: This permission is granted for non-exclusive world **English** rights only unless your license was granted for translation rights. If you licensed translation rights you may only translate this content into the languages you requested. A professional translator must perform all translations and reproduce the content word for word preserving the integrity of the article. If this license is to re-use 1 or 2 figures then permission is granted for non-exclusive world rights in all languages.

16. **Posting licensed content on any Website**: The following terms and conditions apply as follows: Licensing material from an Elsevier journal: All content posted to the web site must maintain the copyright information line on the bottom of each image; A hyper-text must be included to the Homepage of the journal from which you are licensing at http://www.sciencedirect.com/science/journal/xxxxx or the Elsevier homepage for books at http://www.elsevier.com; Central Storage: This license does not include permission for a scanned version of the material to be stored in a central repository such as that provided by Heron/XanEdu.

Licensing material from an Elsevier book: A hyper-text link must be included to the Elsevier homepage at http://www.elsevier.com . All content posted to the web site must maintain the copyright information line on the bottom of each image.

Posting licensed content on Electronic reserve: In addition to the above the following clauses are applicable: The web site must be password-protected and made available only to bona fide students registered on a relevant course. This permission is granted for 1 year only. You may obtain a new license for future website posting.

For journal authors: the following clauses are applicable in addition to the above: Permission granted is limited to the author accepted manuscript version* of your paper.

***Accepted Author Manuscript (AAM) Definition:** An accepted author manuscript (AAM) is the author's version of the manuscript of an article that has been accepted for publication and which may include any author-incorporated changes suggested through the processes of submission processing, peer review, and editor-author communications. AAMs do not include other publisher value-added contributions such as copy-editing, formatting, technical enhancements and (if relevant) pagination.

You are not allowed to download and post the published journal article (whether PDF or HTML, proof or final version), nor may you scan the printed edition to create an electronic version. A hyper-text must be included to the Homepage of the journal from which you are licensing at http://www.sciencedirect.com/science/journal/xxxxx. As part of our normal production process, you will receive an e-mail notice when your article appears on Elsevier's online service ScienceDirect (www.sciencedirect.com). That e-mail will include the article's Digital Object Identifier (DOI). This number provides the electronic link to the published article and should be included in the posting of your personal version. We ask that you wait until you receive this e-mail and have the DOI to do any posting.

Posting to a repository: Authors may post their AAM immediately to their employer's

institutional repository for internal use only and may make their manuscript publically available after the journal-specific embargo period has ended.

Please also refer to Elsevier's Article Posting Policy for further information.

18. **For book authors** the following clauses are applicable in addition to the above: Authors are permitted to place a brief summary of their work online only.. You are not allowed to download and post the published electronic version of your chapter, nor may you scan the printed edition to create an electronic version. **Posting to a repository:** Authors are permitted to post a summary of their chapter only in their institution's repository.

20. **Thesis/Dissertation**: If your license is for use in a thesis/dissertation your thesis may be submitted to your institution in either print or electronic form. Should your thesis be published commercially, please reapply for permission. These requirements include permission for the Library and Archives of Canada to supply single copies, on demand, of the complete thesis and include permission for UMI to supply single copies, on demand, of the complete thesis. Should your thesis be published commercially, please reapply for permission.

Elsevier Open Access Terms and Conditions

Elsevier publishes Open Access articles in both its Open Access journals and via its Open Access articles option in subscription journals.

Authors publishing in an Open Access journal or who choose to make their article Open Access in an Elsevier subscription journal select one of the following Creative Commons user licenses, which define how a reader may reuse their work: Creative Commons Attribution License (CC BY), Creative Commons Attribution – Non Commercial - ShareAlike (CC BY NC SA) and Creative Commons Attribution – Non Commercial – No Derivatives (CC BY NC ND)

Terms & Conditions applicable to all Elsevier Open Access articles:

Any reuse of the article must not represent the author as endorsing the adaptation of the article nor should the article be modified in such a way as to damage the author's honour or reputation.

The author(s) must be appropriately credited.

If any part of the material to be used (for example, figures) has appeared in our publication with credit or acknowledgement to another source it is the responsibility of the user to ensure their reuse complies with the terms and conditions determined by the rights holder.

Additional Terms & Conditions applicable to each Creative Commons user license:

CC BY: You may distribute and copy the article, create extracts, abstracts, and other revised versions, adaptations or derivative works of or from an article (such as a translation), to include in a collective work (such as an anthology), to text or data mine the article, including for commercial purposes without permission from Elsevier

CC BY NC SA: For non-commercial purposes you may distribute and copy the article, create extracts, abstracts and other revised versions, adaptations or derivative works of or from an article (such as a translation), to include in a collective work (such as an anthology), to text and data mine the article and license new adaptations or creations under identical terms without permission from Elsevier

CC BY NC ND: For non-commercial purposes you may distribute and copy the article and include it in a collective work (such as an anthology), provided you do not alter or modify the article, without permission from Elsevier

Any commercial reuse of Open Access articles published with a CC BY NC SA or CC BY NC ND license requires permission from Elsevier and will be subject to a fee.

Commercial reuse includes:

- Promotional purposes (advertising or marketing)
- Commercial exploitation (e.g. a product for sale or loan)
- Systematic distribution (for a fee or free of charge)

Please refer to Elsevier's Open Access Policy for further information.

21. **Other Conditions**:

v1.7

If you would like to pay for this license now, please remit this license along with your payment made payable to "COPYRIGHT CLEARANCE CENTER" otherwise you will be invoiced within 48 hours of the license date. Payment should be in the form of a check or money order referencing your account number and this invoice number 501300968. Once you receive your invoice for this order, you may pay your invoice by credit card. Please follow instructions provided at that time.

Make Payment To:
Copyright Clearance Center
Dept 001
P.O. Box 843006
Boston, MA 02284-3006

For suggestions or comments regarding this order, contact RightsLink Customer Support: customercare@copyright.com or +1-877-622-5543 (toll free in the US) or +1-978-646-2777.

Gratis licenses (referencing $0 in the Total field) are free. Please retain this printable license for your reference. No payment is required.

AIP PUBLISHING LLC LICENSE
TERMS AND CONDITIONS

May 12, 2014

All payments must be made in full to CCC. For payment instructions, please see information listed at the bottom of this form.

License Number	3386700359949
Order Date	May 12, 2014
Publisher	AIP Publishing LLC
Publication	Journal of Chemical Physics
Article Title	Geometric and electronic factors in the rational design of transition-metal-centered boron molecular wheels
Author	Constantin Romanescu,Timur R. Galeev,Wei-Li Li, et al.
Online Publication Date	Apr 5, 2013
Volume number	138
Issue number	13
Type of Use	Thesis/Dissertation
Requestor type	Author (original article)
Format	Print and electronic
Portion	Excerpt (> 800 words)
Will you be translating?	No
Title of your thesis / dissertation	Structure and Multi-center Bonding: from Atomic Clusters to Solid Phase Materials
Expected completion date	Jun 2014
Estimated size (number of pages)	400
Total	0.00 USD

Terms and Conditions

AIP Publishing LLC -- Terms and Conditions: Permissions Uses

AIP Publishing LLC ("AIPP"") hereby grants to you the non-exclusive right and license to use and/or distribute the Material according to the use specified in your order, on a one-time basis, for the specified term, with a maximum distribution equal to the number that you have ordered. Any links or other content accompanying the Material are not the subject of this license.

1. You agree to include the following copyright and permission notice with the reproduction of the Material:"Reprinted with permission from [FULL CITATION]. Copyright [PUBLICATION YEAR], AIP Publishing LLC." For an article, the copyright and permission notice must be printed on the first page of the article or book chapter. For photographs, covers, or tables, the copyright and permission notice may appear with the Material, in a footnote, or in the reference list.
2. If you have licensed reuse of a figure, photograph, cover, or table, it is your responsibility to ensure that the material is original to AIPP and does not contain the copyright of another entity, and that the copyright notice of the figure, photograph, cover, or table does not indicate that it was reprinted by AIPP, with permission, from another source. Under no circumstances does AIPP, purport or intend to grant permission to reuse material to which it does not hold copyright.
3. You may not alter or modify the Material in any manner. You may translate the Material into another language only if you have licensed translation rights. You may not use the Material for promotional purposes. AIPP reserves all rights not specifically granted herein.

4. The foregoing license shall not take effect unless and until AIPP or its agent, Copyright Clearance Center, receives the Payment in accordance with Copyright Clearance Center Billing and Payment Terms and Conditions, which are incorporated herein by reference.
5. AIPP or the Copyright Clearance Center may, within two business days of granting this license, revoke the license for any reason whatsoever, with a full refund payable to you. Should you violate the terms of this license at any time, AIPP, AIP Publishing LLC, or Copyright Clearance Center may revoke the license with no refund to you. Notice of such revocation will be made using the contact information provided by you. Failure to receive such notice will not nullify the revocation.
6. AIPP makes no representations or warranties with respect to the Material. You agree to indemnify and hold harmless AIPP, AIP Publishing LLC, and their officers, directors, employees or agents from and against any and all claims arising out of your use of the Material other than as specifically authorized herein.
7. The permission granted herein is personal to you and is not transferable or assignable without the prior written permission of AIPP. This license may not be amended except in a writing signed by the party to be charged.
8. If purchase orders, acknowledgments or check endorsements are issued on any forms containing terms and conditions which are inconsistent with these provisions, such inconsistent terms and conditions shall be of no force and effect. This document, including the CCC Billing and Payment Terms and Conditions, shall be the entire agreement between the parties relating to the subject matter hereof.

This Agreement shall be governed by and construed in accordance with the laws of the State of New York. Both parties hereby submit to the jurisdiction of the courts of New York County for purposes of resolving any disputes that may arise hereunder.

If you would like to pay for this license now, please remit this license along with your payment made payable to "COPYRIGHT CLEARANCE CENTER" otherwise you will be invoiced within 48 hours of the license date. Payment should be in the form of a check or money order referencing your account number and this invoice number 501300987. Once you receive your invoice for this order, you may pay your invoice by credit card. Please follow instructions provided at that time.

Make Payment To:
Copyright Clearance Center
Dept 001
P.O. Box 843006
Boston, MA 02284-3006

For suggestions or comments regarding this order, contact RightsLink Customer Support: customercare@copyright.com or +1-877-622-5543 (toll free in the US) or +1-978-646-2777.

Gratis licenses (referencing $0 in the Total field) are free. Please retain this printable license for your reference. No payment is required.

Planarity takes over in the $C_xH_xP_{6-x}$ (x = 0–6) series at x = 4

T. R. Galeev and A. I. Boldyrev, *Phys. Chem. Chem. Phys.*, 2011, **13**, 20549
DOI: 10.1039/C1CP21959F

- For reproduction of material from PPS:
  [Original citation] - Reproduced by permission of The Royal Society of Chemistry (RSC) on behalf of the European Society for Photobiology, the European Photochemistry Association, and RSC
- For reproduction of material from all other RSC journals:
  [Original citation] - Reproduced by permission of The Royal Society of Chemistry

If you are the author of this article you still need to obtain permission to reproduce the whole article in a third party publication with the exception of reproduction of the whole article in a thesis or dissertation.

Information about reproducing material from RSC articles with different licences is available on our Permission Requests page.

Deciphering the mystery of hexagon holes in an all-boron graphene α-sheet

T. R. Galeev, Q. Chen, J. Guo, H. Bai, C. Miao, H. Lu, A. P. Sergeeva, S. Li and A. I. Boldyrev, *Phys. Chem. Chem. Phys.*, 2011, **13**, 11575
DOI: 10.1039/C1CP20439D

[Original citation] - Reproduced by permission of the PCCP Owner Societies

- For reproduction of material from PPS:
  [Original citation] - Reproduced by permission of The Royal Society of Chemistry (RSC) on behalf of the European Society for Photobiology, the European Photochemistry Association, and RSC
- For reproduction of material from all other RSC journals:
  [Original citation] - Reproduced by permission of The Royal Society of Chemistry

If you are the author of this article you still need to obtain permission to reproduce the whole article in a third party publication with the exception of reproduction of the whole article in a thesis or dissertation.

Information about reproducing material from RSC articles with different licences is available on our Permission Requests page.

Solid state adaptive natural density partitioning: a tool for deciphering multi-center bonding in periodic systems

T. R. Galeev, B. D. Dunnington, J. R. Schmidt and A. I. Boldyrev, *Phys. Chem. Chem. Phys.*, 2013, **15**, 5022
DOI: 10.1039/C3CP50350J

- For reproduction of material from PCCP:
  [Original citation] - Reproduced by permission of the PCCP Owner Societies
- For reproduction of material from PPS:
  [Original citation] - Reproduced by permission of The Royal Society of Chemistry (RSC) on behalf of the European Society for Photobiology, the European Photochemistry Association, and RSC
- For reproduction of material from all other RSC journals:
  [Original citation] - Reproduced by permission of The Royal Society of Chemistry

If you are the author of this article you still need to obtain permission to reproduce the whole article in a third party publication with the exception of reproduction of the whole article in a thesis or dissertation.

Information about reproducing material from RSC articles with different licences is available on our Permission Requests page.

Brown University
Department of Chemistry
324 Brook Street, Box H
Providence, Rhode Island 02912
Tel: (401) 863-3389 Fax: (401) 863-2594
E-mail: Lai-Sheng_Wang@brown.edu
http://casey.brown.edu/chemistry/research/LSWang/

Lai-Sheng Wang
Professor

January 28, 2014

Timur R. Galeev
Utah State University
Logan, Utah

Dear Timur,

This letter is to confirm that you have my permission to use the following papers in part or in full for preparation or presentation of your dissertation.

- "Geometric and electronic factors in the rational design of transition-metal-centered boron molecular wheels" Constantin Romanescu, Timur R. Galeev, Wei-Li Li, Alexander I. Boldyrev, and Lai-Sheng Wang, J. Chem. Phys., 2013, 138, 134315

- "Transition-Metal-Centered Monocyclic Boron Wheel Clusters ($M©B_n$): A New Class of Aromatic Borometallic Compounds" Constantin Romanescu, Timur R. Galeev, Wei-Li Li, Alexander I. Boldyrev, and Lai-Sheng Wang, Acc. Chem. Res., 2013, 46, 350-358

- "Photoelectron spectroscopy and ab initio study of boron-carbon mixed clusters: CB_9^- and $C_2B_8^-$" Timur R. Galeev, Wei-Li Li, Constantin Romanescu, Ivan Černušàk, Lai-Sheng Wang, and Alexander I. Boldyrev, J. Chem. Phys., 2012, 137, 234306

- "Experimental and Computational Evidence of Octa- and Nona-Coordinated Planar Iron-Doped Boron Clusters: $Fe©B_8^-$ and $Fe©B_9^-$" Constantin Romanescu, Timur R. Galeev, Alina P. Sergeeva, Wei-Li Li, Lai-Sheng Wang, and Alexander I. Boldyrev, J. Organomet. Chem., 2012, 721-722, 148-154

- "Observation of the Highest Coordination Number in Planar Species: Decacoordinated $Ta©B_{10}^-$ and $Nb©B_{10}^-$ Anions" Timur R. Galeev, Constantin Romanescu, Wei-Li Li, Lai-Sheng Wang, Alexander I. Boldyrev, Angew. Chem. Int. Ed., 2012, 51, 2101-2105

- "Transition-Metal-Centered Nine-Membered Boron Rings: $M©B_9$ and $M©B_9^-$ (M = Rh, Ir)" Wei-Li Li, Constantin Romanescu, Timur R. Galeev, Zachary Piazza, Alexander I. Boldyrev, and Lai-Sheng Wang, J. Am. Chem. Soc., 2012, 134, 165-168

- "Aluminum Avoids the Central Position in AlB_9^- and AlB_{10}^-: Photoelectron Spectroscopy and ab Initio Study" Wei-Li Li, Constantin Romanescu, Timur R. Galeev, Lai-Sheng Wang, and Alexander I. Boldyrev, J. Phys. Chem. A, 2011, 115, 10391-10397

- "Valence isoelectronic substitution in the B_8^- and B_9^- molecular wheels by an Al dopant atom: Umbrella-like structures of AlB_7^- and AlB_8^-" Timur R. Galeev, Constantin

Romanescu, Wei-Li Li, Lai-Sheng Wang, and Alexander I. Boldyrev, J. Chem. Phys., 2011, 135, 104301

- "Aromatic Metal-Centered Monocyclic Boron Rings: $Co©B_8^-$ and $Ru©B_9^-$" Constantin Romanescu, Timur R. Galeev, Wei-Li Li, Alexander I. Boldyrev, and Lai-Sheng Wang, Angew. Chem. Int. Ed., 2011, 40, 9334-9337

- "Molecular Wheel to Monocyclic Ring Transition in Boron-Carbon Mixed Clusters $C_2B_6^-$ and $C_3B_5^-$" Timur R. Galeev, Alexander S. Ivanov, Constantin Romanescu, Wei-Li Li, Konstantin V. Bozhenko, Lai-Sheng Wang, and Alexander I. Boldyrev, Phys. Chem. Chem. Phys., 2011, 13, 8805-8810

Sincerely,

Lai-Sheng Wang

Chemistry Department

Brown University

324 Brook St, Providence, RI, 02912

Jan 20, 2011

Dear Timur R. Galeev,

This letter is to confirm that you have my permission to use the following papers in part or in full for preparation or presentation of your dissertation.

- "Geometric and electronic factors in the rational design of transition-metal-centered boron molecular wheels" Constantin Romanescu, Timur R. Galeev, Wei-Li Li, Alexander I. Boldyrev, and Lai-Sheng Wang, J. Chem. Phys., 2013, 138, 134315
- "Transition-Metal-Centered Monocyclic Boron Wheel Clusters ($M©B_n$): A New Class of Aromatic Borometallic Compounds" Constantin Romanescu, Timur R. Galeev, Wei-Li Li, Alexander I. Boldyrev, and Lai-Sheng Wang, Acc. Chem. Res., 2013, 46, 350-358
- "Photoelectron spectroscopy and ab initio study of boron-carbon mixed clusters: CB_9^- and $C_2B_8^-$" Timur R. Galeev, Wei-Li Li, Constantin Romanescu, Ivan Černušàk, Lai-Sheng Wang, and Alexander I. Boldyrev, J. Chem. Phys., 2012, 137, 234306
- "Experimental and Computational Evidence of Octa- and Nona-Coordinated Planar Iron-Doped Boron Clusters: $Fe©B_8^-$ and $Fe©B_9^-$" Constantin Romanescu, Timur R. Galeev, Alina P. Sergeeva, Wei-Li Li, Lai-Sheng Wang, and Alexander I. Boldyrev, J. Organomet. Chem., 2012, 721-722, 148-154
- "Observation of the Highest Coordination Number in Planar Species: Decacoordinated $Ta©B_{10}^-$ and $Nb©B_{10}^-$ Anions" Timur R. Galeev, Constantin Romanescu, Wei-Li Li, Lai-Sheng Wang, Alexander I. Boldyrev, Angew. Chem. Int. Ed., 2012, 51, 2101-2105
- "Transition-Metal-Centered Nine-Membered Boron Rings: $M©B_9$ and $M©B_9^-$ (M = Rh, Ir)" Wei-Li Li, Constantin Romanescu, Timur R. Galeev, Zachary Piazza, Alexander I. Boldyrev, and Lai-Sheng Wang, J. Am. Chem. Soc., 2012, 134, 165-168
- "Aluminum Avoids the Central Position in AlB_9^- and AlB_{10}^-: Photoelectron Spectroscopy and ab Initio Study" Wei-Li Li, Constantin Romanescu, Timur R.

Galeev, Lai-Sheng Wang, and Alexander I. Boldyrev, J. Phys. Chem. A, 2011, 115, 10391-10397

- "Valence isoelectronic substitution in the B_8^- and B_9^- molecular wheels by an Al dopant atom: Umbrella-like structures of AlB_7^- and AlB_8^-" Timur R. Galeev, Constantin Romanescu, Wei-Li Li, Lai-Sheng Wang, and Alexander I. Boldyrev, J. Chem. Phys., 2011, 135, 104301
- "Aromatic Metal-Centered Monocyclic Boron Rings: Co©B_8^- and Ru©B_9^-" Constantin Romanescu, Timur R. Galeev, Wei-Li Li, Alexander I. Boldyrev, and Lai-Sheng Wang, Angew. Chem. Int. Ed., 2011, 40, 9334-9337
- ”Molecular Wheel to Monocyclic Ring Transition in Boron-Carbon Mixed Clusters $C_2B_6^-$ and $C_3B_5^-$“ Timur R. Galeev, Alexander S. Ivanov, Constantin Romanescu, Wei-Li Li, Konstantin V. Bozhenko, Lai-Sheng Wang, and Alexander I. Boldyrev, Phys. Chem. Chem. Phys., 2011, 13, 8805-8810

Sincerely,

Weili Li

Constantin Romanescu
217-11 Dervock Cres.
Toronto, ON M2K 1A6
Canada

January 29, 2014

Dear Timur R. Galeev,

This letter is to confirm that you have my permission to use the following papers in part or in full for preparation or presentation of your dissertation.

- "Geometric and electronic factors in the rational design of transition-metal-centered boron molecular wheels" Constantin Romanescu, Timur R. Galeev, Wei-Li Li, Alexander I. Boldyrev, and Lai-Sheng Wang, J. Chem. Phys., 2013, 138, 134315

- "Transition-Metal-Centered Monocyclic Boron Wheel Clusters ($M©B_n$): A New Class of Aromatic Borometallic Compounds" Constantin Romanescu, Timur R. Galeev, Wei-Li Li, Alexander I. Boldyrev, and Lai-Sheng Wang, Acc. Chem. Res., 2013, 46, 350-358

- "Photoelectron spectroscopy and ab initio study of boron-carbon mixed clusters: CB_9^- and $C_2B_8^-$" Timur R. Galeev, Wei-Li Li, Constantin Romanescu, Ivan Černušàk, Lai-Sheng Wang, and Alexander I. Boldyrev, J. Chem. Phys., 2012, 137, 234306

- "Experimental and Computational Evidence of Octa- and Nona-Coordinated Planar Iron-Doped Boron Clusters: $Fe©B_8^-$ and $Fe©B_9^-$" Constantin Romanescu, Timur R. Galeev, Alina P. Sergeeva, Wei-Li Li, Lai-Sheng Wang, and Alexander I. Boldyrev, J. Organomet. Chem., 2012, 721-722, 148-154

- "Observation of the Highest Coordination Number in Planar Species: Decacoordinated $Ta©B_{10}^-$ and $Nb©B_{10}^-$ Anions" Timur R. Galeev, Constantin Romanescu, Wei-Li Li, Lai-Sheng Wang, Alexander I. Boldyrev, Angew. Chem. Int. Ed., 2012, 51, 2101-2105

- "Transition-Metal-Centered Nine-Membered Boron Rings: $M©B_9$ and $M©B_9^-$ (M = Rh, Ir)" Wei-Li Li, Constantin Romanescu, Timur R. Galeev, Zachary Piazza, Alexander I. Boldyrev, and Lai-Sheng Wang, J. Am. Chem. Soc., 2012, 134, 165-168

- "Aluminum Avoids the Central Position in AlB_9^- and AlB_{10}^-: Photoelectron Spectroscopy and ab Initio Study" Wei-Li Li, Constantin Romanescu, Timur R. Galeev, Lai-Sheng Wang, and Alexander I. Boldyrev, J. Phys. Chem. A, 2011, 115, 10391-10397
- "Valence isoelectronic substitution in the B_8^- and B_9^- molecular wheels by an Al dopant atom: Umbrella-like structures of AlB_7^- and AlB_8^-" Timur R. Galeev, Constantin Romanescu, Wei-Li Li, Lai-Sheng Wang, and Alexander I. Boldyrev, J. Chem. Phys., 2011, 135, 104301
- "Aromatic Metal-Centered Monocyclic Boron Rings: $Co©B_8^-$ and $Ru©B_9^-$" Constantin Romanescu, Timur R. Galeev, Wei-Li Li, Alexander I. Boldyrev, and Lai-Sheng Wang, Angew. Chem. Int. Ed., 2011, 40, 9334-9337
- ”Molecular Wheel to Monocyclic Ring Transition in Boron-Carbon Mixed Clusters $C_2B_6^-$ and $C_3B_5^-$“ Timur R. Galeev, Alexander S. Ivanov, Constantin Romanescu, Wei-Li Li, Konstantin V. Bozhenko, Lai-Sheng Wang, and Alexander I. Boldyrev, Phys. Chem. Chem. Phys., 2011, 13, 8805-8810

Sincerely,

Constantin Romanescu

Utah State University

Department of Chemistry and Biochemistry

0300 Old Main Hill

02/25/2014

Dear Timur Galeev,

This letter is to confirm that you have my permission to use the following paper in part or in full for preparation or presentation of your dissertation.

> "Molecular Wheel to Monocyclic Ring Transition in Boron-Carbon Mixed Clusters $C_2B_6^-$ and $C_3B_5^-$" Timur R. Galeev, Alexander S. Ivanov, Constantin Romanescu, Wei-Li Li, Konstantin V. Bozhenko, Lai-Sheng Wang, and Alexander I. Boldyrev, Phys. Chem. Chem. Phys., 2011, 13, 8805-8810 (DOI: 10.1039/C1CP20359B)

Sincerely,

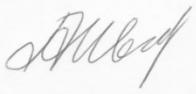

Mr. Alexander Ivanov

Prof. Konstantin V. Bozhenko
E-mail: kbogenko@mail.ru
Department of Physical and Colloidal Chemistry,
Peoples' Friendship University of Russia,
6, Miklukho-Maklaya Street ,
Moscow, Russia,
117198

31.01.2014

Dear Timur R. Galeev,

This letter is to confirm that you have my permission to use the following paper in part or in full for preparation or presentation of your dissertation.

> "Molecular Wheel to Monocyclic Ring Transition in Boron-Carbon Mixed Clusters $C_2B_6^-$ and $C_3B_5^-$" Timur R. Galeev, Alexander S. Ivanov, Constantin Romanescu, Wei-Li Li, Konstantin V. Bozhenko, Lai-Sheng Wang, and Alexander I. Boldyrev, Phys. Chem. Chem. Phys., 2011, 13, 8805-8810.

Sincerely,

K Bozhenko K.V. Bozhenko

COMENIUS UNIVERSITY IN BRATISLAVA
FACULTY OF NATURAL SCIENCES
DEPARTMENT PHYSICAL AND THEORETICAL CHEMISTRY
Prof. RNDr. Ivan Černušák, DrSc.
Mlynská dolina CH1, 842 15 Bratislava 4, SLOVAKIA

Mr.
Timur R. Galeev
Department of Chemistry and Biochemistry
Utah State University
Logan
Utah 84322, USA

Your ref#: sine **Our ref#:** KFZ-7/2014 **Bratislava,** January 29, 2014

Re: Permission to use the paper in your dissertation

Dear Timur R. Galeev,:

This letter is to confirm that you have my permission to use the following paper in part or in full for preparation or presentation of your dissertation:

"Photoelectron spectroscopy and ab initio study of boron-carbon mixed clusters: CB_9^- and $C_2B_8^-$" by Timur R. Galeev, Wei-Li Li, Constantin Romanescu, Ivan Černušák, Lai-Sheng Wang, and Alexander I. Boldyrev, J. Chem. Phys., 2012, 137, 234306.

Sincerely Yours,

UNIVERZITA KOMENSKÉHO V BRATISLAVE
Prírodovedecká fakulta
Katedra fyzikálnej a teoretickej chémie
842 15 Bratislava, Mlynská dolina
1

Prof. RNDr. Ivan Černušák, DrSc.

☎ + 421 2 602 96 429
ID#: 00397865 06
Fax: + 421 2 602 96 231
VAT ID: SK2020845332
✉ cernusak@fns.uniba.sk
Internet: http://www.fns.uniba.sk

Brown University Chemistry Department
Box H
Zachary Piazza
324 Brook Street
Providence, RI 02906

1/28/2014

Dear Timur R. Galeev,

This letter is to confirm that you have my permission to use the following paper in part or in full for preparation or presentation of your dissertation.

- "Transition-Metal-Centered Nine-Membered Boron Rings: M©B_9 and M©B_9^- (M = Rh, Ir)" Wei-Li Li, Constantin Romanescu, Timur R. Galeev, Zachary Piazza, Alexander I. Boldyrev, and Lai-Sheng Wang, J. Am. Chem. Soc., 2012, 134, 165-168

Sincerely,

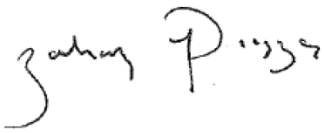

Zachary A. Piazza

Alina P. Sergeeva
Postdoctoral Research Scientist
Honig Lab
Department of Biochemistry and Molecular Biophysics
Center for Computational Biology and Bioinformatics
Howard Hughes Medical Institute
Columbia University
1130 St Nicholas Ave, ICRC
New York, NY, 10032

February 3, 2014

Dear Timur R. Galeev,

This letter is to confirm that you have my permission to use the following papers in part or in full for preparation or presentation of your dissertation.

- "Experimental and Computational Evidence of Octa- and Nona-Coordinated Planar Iron-Doped Boron Clusters: $Fe©B_8^-$ and $Fe©B_9^-$" Constantin Romanescu, Timur R. Galeev, Alina P. Sergeeva, Wei-Li Li, Lai-Sheng Wang, and Alexander I. Boldyrev, J. Organomet. Chem., 2012, 721-722, 148-154

- "Deciphering the mystery of hexagon holes in an all-boron graphene α-sheet" Timur R. Galeev, Qiang Chen, Jin-Chang Guo, Hui Bai, Chang-Qing Miao, Hai-Gang Lu, Alina P. Sergeeva, Si-Dian Li, and Alexander I. Boldyrev, Phys. Chem. Chem. Phys., 2011, 13, 11575-11578

Sincerely,

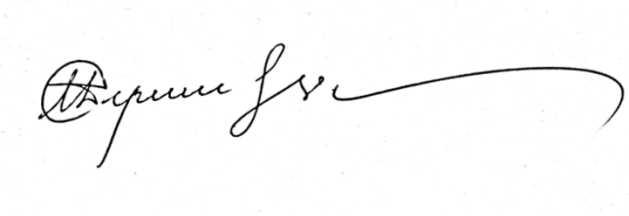

Alina P. Sergeeva

山西大学
SHANXI UNIVERSITY

Institute of Molecular Sciences,

Shanxi University, Taiyuan 030006,

People's Republic of China

February 22, 2014

Dear TimurR. Galeev,

This letter is to confirm that you have my permission to use the following paper in part or in full for preparation or presentation of your dissertation.

- "Deciphering the mystery of hexagon holes in an all-boron graphene α-sheet" Timur R. Galeev, Qiang Chen, Jin-Chang Guo, Hui Bai, Chang-Qing Miao, Hai-Gang Lu, Alina P. Sergeeva, Si-Dian Li, and Alexander I. Boldyrev, Phys. Chem. Chem. Phys., 2011, 13, 11575-11578

Sincerely,

Qiang Chen, Jin-Chang Guo, Hui Bai, Chang-Qiang Miao, Hai-Gang Lu

地　　址：山西省太原市坞城路 92 号
邮　　编：030006
电　　话：0086-351-7010255
传　　真：0086-351-7011981
网　　址：Http://www.sxu.edu.cn
电子信箱：Xiaoban@sxu.edu.cn

Si-Dian Li
Professor of Chemistry
Institute of Molecular Sciences
Shanxi University
Taiyuan 030006
China

Timur R. Galeev
Department of Chemistry and Biochemistry
Utah State University
0300 Old Main Hill
Logan, UT 84322-0300

Dear Timur R. Galeev:

Congratulations! This letter is to confirm that you have my permission to use the following paper in part or in full for preparation or presentation of your dissertation.

"Deciphering the mystery of hexagon holes in an all-boron graphene α-sheet" Timur R. Galeev, Qiang Chen, Jin-Chang Guo, Hui Bai, Chang-Qing Miao, Hai-Gang Lu, Alina P. Sergeeva, Si-Dian Li, and Alexander I. Boldyrev, Phys. Chem. Chem. Phys., 2011, 13, 11575-11578

Sincerely,

Si-Dian Li

Department of Chemistry
University of Wisconsin Madison
1101 University Avenue
Madison, Wisconsin 53706

February 19, 2014

Dear Timur R. Galeev,

This letter is to confirm that you have my permission to use the following paper in part or in full for preparation or presentation of your dissertation.

> "Solid State Adaptive Natural Density Partitioning: A Tool for Deciphering Multi-center Bonding in Periodic Systems" Timur R. Galeev, Benjamin D. Dunnington, J.R. Schmidt, and Alexander I. Boldyrev, Phys. Chem. Chem. Phys., 2013, 15, 5022-5029

Sincerely,

Benjamin Dunnington

JR Schmidt
UW-Madison
Department of Chemistry

January 31, 2014

Dear Timur,

This letter is to confirm that you have my permission to use the following paper in part or in full for preparation or presentation of your dissertation:

"Solid State Adaptive Natural Density Partitioning: A Tool for Deciphering Multi-center Bonding in Periodic Systems" Timur R. Galeev, Benjamin D. Dunnington, J.R. Schmidt, and Alexander I. Boldyrev, Phys. Chem. Chem. Phys., 2013, 15, 5022-5029

Sincerely,

J.R. Schmidt
Assistant Professor
Department of Chemistry
University of Wisconsin-Madison

CURRICULUM VITAE

Timur R. Galeev

(May, 2014)

Deparment of Chemistry and Biochemistry

Utah State University

0300 Old Main Hill, Logan, UT 84322

E-mail: timur.galeev@aggiemail.usu.edu

Webpage: http://www.chem.usu.edu/~boldyrev/timur.php

RESEARCH AND EDUCATIONAL BACKGROUND

2010-2014 Ph.D. Program, Department of Chemistry and Biochemistry, Utah State University, Logan, UT. Advisor: Prof. Alexander I. Boldyrev. Research focus: Theoretical and Physical Chemistry. GPA 4.0.

Fall'12 Visiting Graduate Research Assistant, Prof. B. I. Yakobson's Group, Department of Mechanical Engineering and Materials Science, Rice University, Houston, TX.

Summer'12 Visiting Summer Graduate Student, Prof. JR Schmidt's Group, Department of Chemistry and Theoretical Chemistry Institute, University of Wisconsin-Madison, Madison, WI.

2008-2010 Associate Research Scientist, Chemical Diversity Research Institute (ChemDiv), Khimki, Moscow, Russia

2006-2008 Part-time Research Intern, Lab Technician, Chemical Diversity Research Institute (ChemDiv), Khimki, Moscow, Russia.

2006-2008 M. S. in Organic Chemistry (with Excellence), Department of Science, Peoples' Friendship University of Russia, Moscow, Russia. Advisor: Prof. F. I. Zubkov. Research focus: Synthetic Organic Chemistry.

2002-2006 B. S. in Chemistry (with Excellence), Department of Science, Peoples' Friendship University of Russia, Moscow, Russia. Advisors: Prof. F. I. Zubkov and E. V. Nikitina. Research focus: Synthetic Organic Chemistry.

AWARDS, HONORS, FELLOWSHIPS

2014 University Graduate Researcher of the Year – Robins Award, Utah State University

2014 Marjorie H. Gardner Teaching Award, Deparment of Chemistry and Biochemistry, Utah State University

2013-2014 College of Science PhD Graduate Researcher of the Year, Utah State University

2013-2014 SGS Dissertation Fellowship, Office of Research and Graduate Studies, Utah State University

2013 Outstanding Graduate Student in Chemistry, Department of Chemistry and Biochemistry, Utah State University

2011 Award for Early Research Progress in Chemistry, Department of Chemistry and Biochemistry, Utah State University

2010-2011 Vice President for Research Graduate Fellowship, Utah State University

2008 Best Graduate - 2008 Award, Department of Science, Peoples' Friendship University of Russia

2002-2008 Scholarship for Outstanding Academic Standing, Peoples' Friendship University of Russia

TEACHING EXPERIENCE

Fall 2014 Recitations Instructor, CHEM 1220 – Chemistry Majors. Principles of Chemistry II. Department of Chemistry and Biochemistry, USU

Fall 2011 Laboratory Instructor, CHEM 1225. Principles of Chemistry II. Department of Chemistry and Biochemistry, Utah State University

Spring 2011 Recitations Instructor, CHEM 1220. Principles of Chemistry II. Department of Chemistry and Biochemistry, Utah State University

2008 College-level Chemistry Teaching, Peoples' Friendship University of Russia, 1 semester course

2006 High School-level Chemistry Teaching, Peoples' Friendship University of Russia, 1 semester course, Qualification Certificate

PROFESSIONAL ACTIVITIES

2013 Abstract and Technical Program Manager, International Conference on Chemical Bonding-2013, July 4-8, 2013, Kauai, HI, USA

2011-present Member of the American Chemical Society

PRESENTATIONS AT PROFESSIONAL MEETINGS

Talk Design and observation of transition metal-centered boron wheels $M©B_n^{-/0}$ T. R. Galeev, C. Romanescu, W. L. Li, Z. Piazza, L.-S. Wang, and A. I. Boldyrev 44th Midwest Theoretical Chemistry Conference, June 7-9 2012, Madison, WI

Poster Solid state adaptive natural density partitioning: A tool for deciphering chemical bonding in periodic systems, T. R. Galeev, B. D. Dunnington, J. R. Schmidt, A. I. Boldyrev, 245th National ACS Meeting & Exposition, Division of Computers in Chemistry, April 7-11, 2013, New Orleans, LA.

Poster Novel molecular structural transition: Wheel to monocyclic ring transition in boron carbon mixed clusters $C_2B_6^-$ and $C_3B_5^-$, T. R. Galeev, A. S. Ivanov, C. Romanescu, W. L. Li, K. V. Bozhenko, L.-S. Wang, A. I. Boldyrev, 242nd National ACS Meeting & Exposition, Division of Physical Chemistry, August 28 – Sept. 1, 2011, Denver, CO.

PUBLICATIONS

(May, 2014)

Publications: **18** published papers.

Sum of the times cited: **224**; *h*-index: **10** (Google Scholar)

Utah State University (Advisor: A. I. Boldyrev)

18. Aromaticity and Antiaromaticity in Inorganic Chemistry.

T. R. Galeev and A. I. Boldyrev, *Comprehensive Inorganic Chemistry II (Second Edition),* Editors-in-Chief: Jan Reedijk and Kenneth Poeppelmeier, Amsterdam, 2013, pp 245-275 (Invited Chapter).

17. Geometric and electronic factors in the rational design of transition-metal-centered boron molecular wheels, C. Romanescu, T. R. Galeev, W. L. Li, A. I. Boldyrev, L. S. Wang, *J. Chem. Phys*., 2013, 138, 134315.

16. Solid State Adaptive Natural Density Partitioning: A Tool for Deciphering Multi-center Bonding in Periodic Systems, T. R. Galeev, B. D. Dunnington, J. R. Schmidt, A. I. Boldyrev, *Phys. Chem. Chem. Phys*., 2013, 15, 5022-5029.

15. Transition-Metal-Centered Monocyclic Boron Wheel Clusters (M©B_n): A New Class of Aromatic Borometallic Compounds, C. Romanescu, T. R. Galeev, W. L. Li, A. I. Boldyrev, L. S. Wang, *Acc. Chem. Res.*, 2013, 46, 350-358.

14. Photoelectron spectroscopy and *ab initio* study of boron-carbon mixed clusters: CB_9^- and $C_2B_8^-$, T. R. Galeev, W. L. Li, C. Romanescu, I. Černušàk, L. S. Wang, A. I. Boldyrev, *J. Chem. Phys.*, 2012, 137, 234306.

13. Experimental and Computational Evidence of Octa- and Nona-Coordinated Planar Iron-Doped Boron Clusters: Fe©B_8^- and Fe©B_9^-, C. Romanescu, T. R. Galeev, A. P. Sergeeva, W. L. Li, L. S. Wang, A. I. Boldyrev, *J. Organomet. Chem*., 2012, 721-722, 148-154.

12. Observation of the Highest Coordination Number in Planar Species: Decacoordinated Ta©B_{10}^- and Nb©B_{10}^- Anions, T. R. Galeev, C. Romanescu, W. L. Li, L. S. Wang, A. I. Boldyrev, *Angew. Chem. Int. Ed.*, 2012, 51, 2101-2105.

Highlighted in:

Chemical & Engineering News, 2012, 90, 38

Chemistry World 2012, Feb. 6

Angew. Chem. Int. Ed. 2012, 51, 4275

Utah State Today 2012, Feb. 2

11. Transition-Metal-Centered Nine-Membered Boron Rings: M©B_9 and M©B_9^- (M = Rh, Ir), W. L. Li, C. Romanescu, T. R. Galeev, Z. Piazza, A. I. Boldyrev, L. S. Wang, *J. Am. Chem. Soc.*, 2012, 134, 165-168.

10. Aluminum Avoids the Central Position in AlB_9^- and AlB_{10}^-: Photoelectron Spectroscopy and ab Initio Study, W. L. Li, C. Romanescu, T. R. Galeev, L. S. Wang, A. I. Boldyrev, *J. Phys. Chem. A*, 2011, 115, 10391-10397.

9. Valence isoelectronic substitution in the B_8^- and B_9^- molecular wheels by an Al dopant atom: Umbrella-like structures of AlB_7^- and AlB_8^-, T. R. Galeev, C. Romanescu, W. L. Li, L. S. Wang, A. I. Boldyrev, *J. Chem. Phys.*, 2011, 135, 104301.

Featured on the Cover

8. Aromatic Metal-Centered Monocyclic Boron Rings: Co©B_8^- and Ru©B_9^-, C. Romanescu, T. R. Galeev, W. L. Li, A. I. Boldyrev, and L. S. Wang, *Angew. Chem. Int. Ed.*, 2011, 40, 9334-9337.

7. Planarity takes over in the $C_xH_xP_{6-x}$ (x = 0-6) series at x = 4, T. R. Galeev and A. I. Boldyrev, *Phys. Chem. Chem. Phys.*, 2011, 13, 20549-20556.

6. Deciphering the mystery of hexagon holes in an all-boron graphene α-sheet, T. R. Galeev, Q. Chen, J.-C. Guo, H. Bai, C.-Q. Miao, H.-G. Lu, A. P. Sergeeva, S.-D. Li, A. I. Boldyrev, *Phys. Chem. Chem. Phys*., 2011, 13, 11575-11578.

5. Recent advances in aromaticity and antiaromaticity in transition-metal systems, T. R. Galeev and A. I. Boldyrev, *Annu. Rep. Prog. Chem., Sect. C*, 2011, 107, 124-147 (Review).

4. Molecular Wheel to Monocyclic Ring Transition in Boron-Carbon Mixed Clusters $C_2B_6^-$ and $C_3B_5^-$, T. R. Galeev, A. S. Ivanov, C. Romanescu, W. L. Li, K. V. Bozhenko, L. S. Wang, A. I. Boldyrev, *Phys. Chem. Chem. Phys*., 2011, 13, 8805-8810.

PFUR (Advisor: F. I. Zubkov):

3. General synthetic approach towards annelated 3a,6-epoxyisoindoles by tandem, acylation/IMDAF reaction of furylazaheterocycles. Scope and limitations, F. I. Zubkov, E. V. Nikitina, T. R. Galeev, V. P. Zaytsev, V. N. Khrustalev, R. A. Novikov, A. V. Varlamov, *Tetrahedron,* 2014, 70, 1659-1690.

2. Aromatization of IMDAF Adducts in Aqueous Alkaline Medium, F. I. Zubkov, I. K. Airiyan, J. D. Ershova, T. R. Galeev, V. P. Zaytsev, E. V. Nikitina and A. V. Varlamov, *RSC Adv.*, 2012, 2, 4103-4109.

1. A Simple Preparative Synthesis of Epoxy[1,3]oxazino(or oxazolo)[2,3-a]-isoindoles and Their Thia Analogues via IMDAF, F. I. Zubkov, T. R. Galeev, E. V. Nikitina, I. V. Lazenkova, V. P. Zaytsev, A. V. Varlamov, *Synlett*, 2010, 2063.